Niobium-Mediated Generation of P–P Multiply Bonded Intermediates

by

Nicholas A. Piro

B.S., Chemistry (2004)
California Institute of Technology

Submitted to the Department of Chemistry
in partial fulfillment of the requirements for the degree of

DOCTOR OF PHILOSOPHY

at the

MASSACHUSETTS INSTITUTE OF TECHNOLOGY

June 2009

Author . . . . . .
Department of Chemistry
May 5, 2009

Certified by . . . . . .
Christopher C. Cummins
Professor of Chemistry
Thesis Supervisor

Accepted by . . . . . .
Robert W. Field
Chairman, Department Committee on Graduate Studies

This Doctoral Thesis has been examined by a Committee of the Department of Chemistry as follows:

Professor Jonas C. Peters . . . . . .

W. M. Keck Professor of Energy

Chairman

Professor Christopher C. Cummins . . . . . .

Professor of Chemistry

Thesis Supervisor

Professor Stephen J. Lippard . . . . . .

Arthur Amos Noyes Professor of Chemistry

Committee Member

Niobium-Mediated Generation of P–P Multiply Bonded Intermediates

by

Nicholas A. Piro

Submitted to the Department of Chemistry
on May 5, 2009, in partial fulfillment of the
requirements for the degree of
Doctor of Philosophy in Inorganic Chemistry

Abstract

The diphosphaazide complex (Mes*NPP)Nb(N[$CH_2{}^tBu$]Ar)$_3$, **1** (Mes* = 2,4,6-tri-*tert*-butylphenyl, Ar = 3,5-dimethylphenyl), releases a P_2 unit upon heating to form Mes*NNb(N[$CH_2{}^tBu$]Ar)$_3$, **2**, in a first-order process. The chemistry of the putative P_2 intermediate was probed with a variety of reagents. It was successfully transferred to organic dienes to yield polycyclic diphosphines, and also to terminal phosphide complexes of the general formula P≡M(N[R]Ar)$_3$ to yield *cyclo*-P_3 complexes. Coordination of $W(CO)_5$ to **1** accelerates conversion to **2**, with loss of the $(P_2)W(CO)_5$ fragment, such that this reaction occurs readily at 20 °C. The $(P_2)W(CO)_5$ fragment was transferred to the same substrates listed above, as well as to a low-valent platinum source. In all cases, this transfer occurs in higher yields than for the uncomplexed P_2. Kinetic measurements on the elimination reactions showed them to be first-order in diphosphaazide complex and independent of substrate concentration, consistent with the hypothesis that P_2 and $(P_2)W(CO)_5$ are released into solution as discrete species.

The above reaction chemistry was used to synthesize reactive, anionic *cyclo*-P_3 complexes of niobium with formulas $[\{(OC)_5W\}_n(P_3)Nb(N[CH_2{}^tBu]Ar)_3]^-$ ($n = 0,1,2$). These complexes were shown to react with the electrophiles Ph_3SnCl, Mes*NPCl, and RC(O)Cl to yield coordinated η^2-triphosphirene complexes. The acyltriphosphirene complexes $[(OC)_5W]_2RC(O)P_3Nb(N[CH_2{}^tBu]Ar)_3$ are unstable toward loss of an $RCP_3[W(CO)_5]_2$ fragment and formation of oxoniobium $ONb(N[CH_2{}^tBu]Ar)_3$. The cycloaddition chemistry of the so-generated, putative triphosphacyclobutadiene intermediate was probed through trapping reactions, including with adamantylphosphaalkyne to provide tetraphosphabenzenes complexed to $W(CO)_5$.

Silylphosphinidene complexes of niobium, $R_3SiPNb(N[CH_2{}^tBu]Ar)_3$, were used to transfer phosphinidenes to isocyanates, carbon dioxide, and a terminal phosphorus monoxide complex of molybdenum in O-for-PR metathesis reactions. The latter reaction served as a synthesis of the unique, $3e^-$ donor diphosphenido ligand in the complex $^iPr_3SiPPMo(N[^tBu]Ar)_3$. Also investigated were the syntheses and reaction chemistry of metallacyclic phosphorylphosphinidene complexes, $R_2P(O)PNb(N[CH_2{}^tBu]Ar)_3$.

The niobaziridine hydride complex $HNb(\eta^2\text{-}C_6H_{10}{=}NCy)(NCy_2)_2$ was synthesized as a potential model for N_2 binding, while independently prepared $(\mu\text{-}N_2)[Nb(N[CH_2tBu]Ar)_3$ was reductively cleaved to the anionic terminal nitride complex $[NNb(N[CH_2{}^tBu]Ar)_3]^-$. Activation chemistry of As_4 by $Mo(N[^tBu]Ar)_3$ and $HNb(\eta^2\text{-}^tBuC(H){=}NAr)(N[CH_2{}^tBu]Ar)_2$ was used to synthesize two terminal arsenide complexes. The syntheses of potential AsP- and PN-eliminating complexes are also described.

Thesis Supervisor: Christopher C. Cummins

Title: Professor of Chemistry

ACKNOWLEDGMENTS

The work that went into completing this document would not have been possible without the assistance, guidance, and support of many people. While there are surely more than those I list here, I would like to take this opportunity to thank several of them individually for their contributions to me and this work.

Firstly, I'd like to thank my advisor, Kit. By taking me into his group five years ago he has given me the opportunity to study some fantastic molecules. It is easy to say that making the molecules I've had the chances to make here could not have been done anywhere else. Throughout these explorations, Kit has provided me with a balance of focus and freedom that has served to let my projects develop fruitfully without keeping new, exploratory chemistry off the table. His growing enthusiasm for phosphorus chemistry has allowed us to share in the excitement of making some pretty neat, phosphorus-rich molecules.

Getting to this point certainly would not have been possible without the rest of the Cummins Group. They are graciously acknowledged for the environment they have provided, where there has been a productive exchange of both ideas and materials that have allowed for this work to be accomplished.

When I joined the lab Josh Figueroa showed me the ropes of niobium trisanilide chemistry and left me to inherit this project. It is also Josh who first synthesized the diphosphaazide complex, and realizing its potential P_2 elimination chemistry he affectionately dubbed it "The Eliminator." As this molecule became the basis for much of my thesis work, I owe him an extra thanks.

With me joining the group in 2004 was a collection of three other wonderful chemists: John Curley, Glen Alliger, and Alexander Fox. Having been left as the only members of the group shortly after our joining, together we navigated our way through. Fox's skills as EHS representative have made me feel safe in lab every day. Glen was always there to commiserate with through the past five "dark years" of Yankee baseball, may they be over. John and I have together spent (maybe too much) of the past several years mastering the conversion of countless cups of coffee and hundreds of glasses of wine into two PhD theses. Moreover, not only have we have spent a fair amount of time arguing over points we actually agree on, but we have been pretty good at pointing out each other's ridiculousness when it just goes too far. For this, and for being a good friend, he deserves a special thanks.

While I started with a glovebox pretty much to myself, and enjoyed it, I have since realized that having a boxmate can be very rewarding. Brandi Cossairt joined the group, and team niobium, working in my lab. She has been a terrific labmate and certainly kept this lab functioning. She deserves acknowledgment for putting up with my messes without ever complaining and always being there to bounce ideas off of productively. Moreover, her abilities to locate compounds in the box and to stay happy "85% of the time" are unrivaled. Heather Spinney has also shared our box for a few years, and is thanked for always being up for a chat and a reminder of who is Canadian.

I'd like to acknowledge Jared Silvia for not only leading the Red NO_x on a near-championship run, but also for having masterfully kept our solvents dry. Chris Clough, always ready to fix anything mechanical, is thanked for repairing the blower in my box, solving some early crystal structures, and being just crazy enough to make any situation funny.

There have been may people who have come through the group for shorter periods of time and each of whom have contributed in some way to the completion of this work. To Ivo, Evan, Paresh, Mostafa, Nao, and Boris, thanks. To the recent arrivals, Michael, Matt and Tofan, thanks and good luck.

The Cummins Group is not always the most functional of places, but it is Allison Kelsey who is responsible for the semblance of order around here and she is gratefully acknowledged for this.

I thank Peter Müller, the department crystallographer, for teaching me crystallography both in class and hands on. His keeping of the diffractometers running at all hours and assistance in solving many of the structures that appear herein has made this work possible. His ability to solve any disorder, sense of humor, and willingness to help even when he says he is busy—which he nearly always is—will be missed.

The MIT Department of Chemistry Instrumentation Facility has been the place for the acquisition of nearly all the spectroscopic data that appear in this work. David Bray, Jeff Simpson, Bob Kennedy and Anne Gorham are acknowledged for helpful discussions, assistance in acquiring these data when needed, and for the huge task of keeping the NMR instruments functioning. I'd also like to thank Li Li for the acquisition of mass spectrometric data. I also acknowledge Guy Bernard (University of Alberta), who acquired the solid-state NMR data presented in this work, and who assisted in fitting these data. Scott Speakman of the MIT Center for Materials Science and Engineering is thanked for assistance acquiring powder X-ray diffraction data.

I'd like to thank my thesis chairs, Jonas Peters and Joseph Sadighi, for their input on my thesis work prior to its completion. I'd also like to thank Jonas for being partly responsible for my interest in inorganic chemistry, dating back to our times at Caltech. While at Caltech my interest in chemistry was fostered initially by Prof. Jack Roberts who gave me a chance to work in a chemistry lab as a freshman and to learn something about NMR. When my interests turned to inorganic chemistry, it was Prof. John Bercaw who gave me an opportunity to make some organometallic coordination complexes in his group. I'm grateful to Jonathan Owen for taking the time to show me my way around a lab, a Schlenk line, and a glove box.

Even before I entered college it was pretty clear I was headed for chemistry. This was in no small part due to my high school chemistry teacher, Dr. Joan D'Agostino. Her ability to bring excitement to her teaching of chemistry was truly rewarding. Moreover, I'd also like to thank "Dr. D" for her friendship, mentoring, and a relaxing place to stay in Maine.

On a personal level, completing this work in state of relative happiness and sanity would not have been possible without a great group of friends here in Boston. I'd especially like to thank Ashtu, Casey, Eric, John, Joe, Leah, and Yan.

It is unfathomable that I would be here today without the support and encouragement of my family. I thank them for all they have provided and their interest in what I do, even as a chemist among artists.

Lastly, I'd like to thank Christine, who has been a constant source of love and support. Knowing that she will always be there for me has made everyday just that much better.

Table of Contents

List of Figures

List of Schemes

List of Tables

List of Compounds

1 $(Mes^*NPP)Nb(N[CH_2{}^tBu]Ar)_3$

1-$W(CO)_5$ $(OC)_5W(Mes^*NPP)Nb(N[CH_2{}^tBu]Ar)_3$

2 $Mes^*NNb(N[CH_2{}^tBu]Ar)_3$

3 $[PNb(N[CH_2{}^tBu]Ar)_3]^-$

4 $[(OC)_5WPNb(N[CH_2{}^tBu]Ar)_3]^-$

5 $(OC)_5WP(Me)Nb(N[CH_2{}^tBu]Ar)_3$

6 $P_2(C_6H_8)_2$

7 $(OC)_5WP_2(C_6H_8)_2$

8 $(OC)_5WP_2(C_5H_6)_2$

9 $Mes^*NP(PtPPh_3)_2PNb(N[CH_2{}^tBu]Ar)_3$

10 $(OC)_5W(P_2)[Pt(PPh_3)_2]_2$

11 $PMo(N[{}^iPr]Ar)_3$

12-M $(P_3)M(N[{}^iPr]Ar)_3$ (M = Mo, W)

13 $PW(N[{}^iPr]Ar)_3$

14-M $(OC)_5WP_3M(N[{}^iPr]Ar)_3$ (M = Mo,W)

15 $[(P_3)Nb(N[CH_2{}^tBu]Ar)_3]^-$

16 $[(OC)_5WP_3Nb(N[CH_2{}^tBu]Ar)_3]^-$

17 $[\{(OC)_5W\}_2P_3Nb(N[CH_2{}^tBu]Ar)_3]^-$

18 $AdCP_2Mo(N[{}^iPr]Ar)_3$

19 $(OC)_5W(Ph_3Sn)P_3Nb(N[CH_2{}^tBu]Ar)_3$

20 $Mes^*NP[W(CO)_5]P_3Nb(N[CH_2{}^tBu]Ar)_3$

21 $ONb(N[CH_2{}^tBu]Ar)_3$

22 $AdC(O)P_3Nb(N[CH_2{}^tBu]Ar)_3$

23^R $\{(OC)_5W\}_2RC(O)P_3Nb(N[CH_2{}^tBu]Ar)_3$

24, **25**, **26** $[{}^tBuCP_3[W(CO)_5]_2]_2$

27^R $RCP_3[W(CO)_5]_2$

28 $(Ph_3P)(OC)Pt(P_3C(C_2H_4)Ad)[W(CO)_5]_2$

29 $C_7H_8(P_3CAd)[W(CO)_5]_2$

30 $(AdCP)_2P_2[W(CO)_5]_2$

31 $P_2(CAd)_2P_2[W(CO)_5]_2$

32 $Me_3SiPNb(N[CH_2{}^tBu]Ar)_3$

33 $^iPr_3SiPNb(N[CH_2{}^tBu]Ar)_3$

34 $(PhO)_2P(O)PNb(N[CH_2{}^tBu]Ar)_3$

35 $(Me_2N)_2P(O)PNb(N[CH_2{}^tBu]Ar)_3$

36 $(Me_2N)_2P(OAlCl_3)PNb(N[CH_2{}^tBu]Ar)_3$

37 $OPMo(N[{}^tBu]Ar)_3$

38 $^iPr_3SiPPMo(N[{}^tBu]Ar)_3$

39 $PMo(N[{}^tBu]Ar)_3$

40 $(^iPr_3SiP)_3$

41 $(^iPr_3Si)_2P_3P(Si^iPr_3)_2$

42 $^iPr_3SiPPSi^iPr_3$

43 $NMo(N[{}^tBu]Ar)_3$

44 $[NNb(N[CH_2{}^tBu]Ar)_3]^-$

45 $HNb(\eta^2\text{-}C_6H_{10}{=}NCy)(NCy_2)_2$

46 $HNb(\eta^2\text{-}{}^tBuCH{=}NAr)(N[CH_2{}^tBu]Ar)_2$

47 $(\mu\text{-}N_2)[Nb(N[CH_2{}^tBuAr)_3]_2$

48 $AsMo(N[{}^tBu]Ar)_3$

49 $(\mu\text{-}As_2)[Nb(N[CH_2{}^tBuAr)_3]_2$

50 $[AsNb(N[CH_2{}^tBu]Ar)_3]^-$

51 $Mes^*NPNNb(N[CH_2{}^tBu]Ar)_3$

52 $Mes^*NPAsNb(N[CH_2{}^tBu]Ar)_3$

53 $(TfO)_2Nb(N[CH_2{}^tBu]Ar)_3$

54 $Mes^*NP(C_6H_{10})PNb(N[CH_2{}^tBu]Ar)_3$

CHAPTER 1

Diphosphaazide Complexes in the Generation of P_2 Intermediates

Contents

Reproduced in part with permission from:
Piro, N. A.; Figueroa, J. S.; McKellar, J. T.; Cummins, C. C. *Science*, **2006**, *313*, 1276–1279; AAAS.
Piro, N. A.; Cummins, C. C. *Inorg. Chem.* **2007**, *46*, 7387–7393; Copyright 2007 American Chemical Society.
Piro, N. A.; Cummins, C. C. *J. Am. Chem. Soc.* **2008**, *130*, 9524–9535; Copyright 2008 American Chemical Society.

1.1 INTRODUCTION

P-Block Multiple Bonds

The generation and reactivity of multiple bonds between the heavier p-block elements is a field of considerable modern interest.[1–5] Underlying this intrigue is the diminished propensity of these elements to engage in such bonding, relative to their lighter congeners.[6] As an example of this dichotomy consider the stable allotropes of nitrogen and oxygen compared to those of phosphorus and sulfur: Although the allotropes of the lighter elements, N_2 and O_2, have triple and double bonds, respectively, the common molecular allotropes of the 3p elements are P_4 and S_8, each constructed exclusively with single bonds.[7] The equilibrium $P_4 \rightleftharpoons 2\,P_2$ becomes important only at temperatures greater than 1100 K.[7]

The source of this dichotomy can be traced to the unusually low-energy π bonds formed by elements of the first-row. As we descend the periodic table, the more diffuse p-orbitals and longer bond lengths do not give rise to appreciable stabilization of π bonding orbitals.[8,9] This can be seen when comparing the molecular orbitals of N_2 and P_2, Figure 1.1. The contrast in strength of the π bonds results in the fact that, whereas N_2 has one of the strongest bonds in nature (D_e = 226 kcal/mol), the triple bond in P_2 is considerably weaker (D_e = 117 kcal/mol).

The weak nature of π bonding between two heavier p-block elements translates into the observation that molecules containing such bonds are often high-energy and very reactive. This makes the synthesis of these molecules a persistent synthetic challenge. For example, the first isolable "phosphobenzene" did not appear until 1981 with the report of bis(2,4,6-tri-*tert*-butylphenyl)diphosphene, 125 years after the synthesis of azobenene.[10,11] Here, and in reports since, the use of steric protection has been a key strategy. When such multiple bonds lack the requisite steric protection such molecules can still be accessed, but often these species must be studied as reactive intermediates.

As one example of a multiply-bonded intermediate, Sekiguchi and coworkers pioneered the chemistry of triply-bonded silicon with the generation of dimethyldisilyne and characterized this

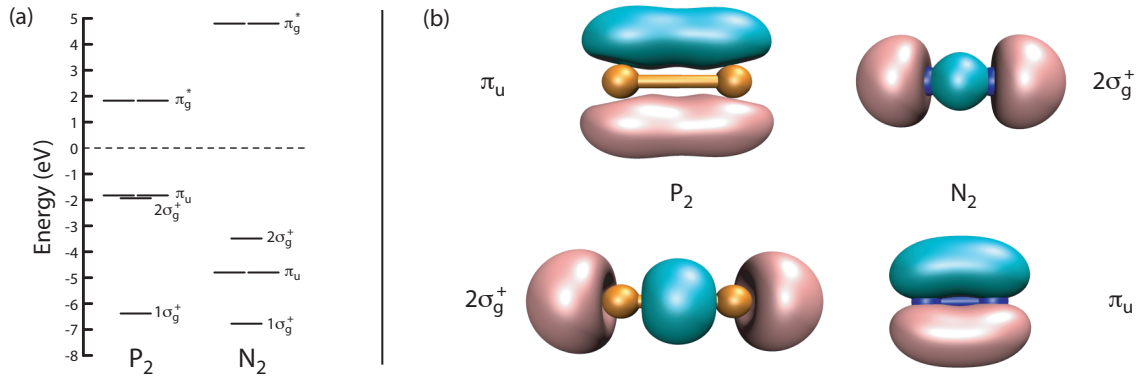

Figure 1.1. (a) A comparison of the molecular orbital diagrams of P_2 and N_2, as determined by DFT (the zero level is arbitrarily assigned as the energy midpoint between π and π* orbitals) (b) A visualization of the occupied frontier orbitals for P_2 and N_2; orbitals are shown at an isosurface value of 0.09.

intermediate by its *in situ* reactivity with a variety of reagents.[12] In this example, the driving force for generation of the high-energy intermediate was provided by aromatization of a ring, and the intermediacy was suggested by identifying products resulting from cycloaddition reactions of the disilyne, Scheme 1.1. Eventually, through the use of a steric protection strategy, the synthesis of an isolable disilyne was achieved.[13]

The strategy of steric protection, however, cannot be applied to diatomic molecules, which necessarily have the most accessible of π bonds. Take the case of sulfur, where the unstable, multiply-bonded allotrope, singlet S_2, has been studied as a synthetic intermediate.[14–22] S_2 has been invoked in a variety of reactions, including one system where S_2 is reportedly formed through the fragmentation of 9,10-epidithio-9,10-dihydroanthracene. In this reaction it is the aromatization of anthracene upon S_2 extrusion that serves as a driving force, Scheme 1.1.[21,22] In this case, as with many others, the intermediacy of singlet S_2 has been probed through trapping reactions, such as the reaction of the putative S_2 intermediate with dienes to form disulfides. Reactive S_2 intermediates present an attractive sulfur-containing synthon and have even found a use in drug synthesis.[23] The question still remains, however, as to whether S_2 itself is always the intermediate in these reactions.[24]

Another intriguing heavier diatomic molecule is P_2. Although this species has been a subject of significant astrophysical interest, its study in the laboratory has been limited to high-temperature gas-phase or matrix isolation studies.[25–31] High temperature, gas-phase studies have shown that P_2 and P_4 exist in equilibrium[25] and that streams of hot P_2 condense on cold surfaces to an unstable brown allotrope of phosphorus.[32] Experiments in argon matrices were used to characterize the mixtures of phosphorus oxides produced from reactions between P_2 and ozone or dioxygen.[27–29] However, a solution-phase source of this diatomic molecule accessible under mild laboratory conditions has remained elusive.

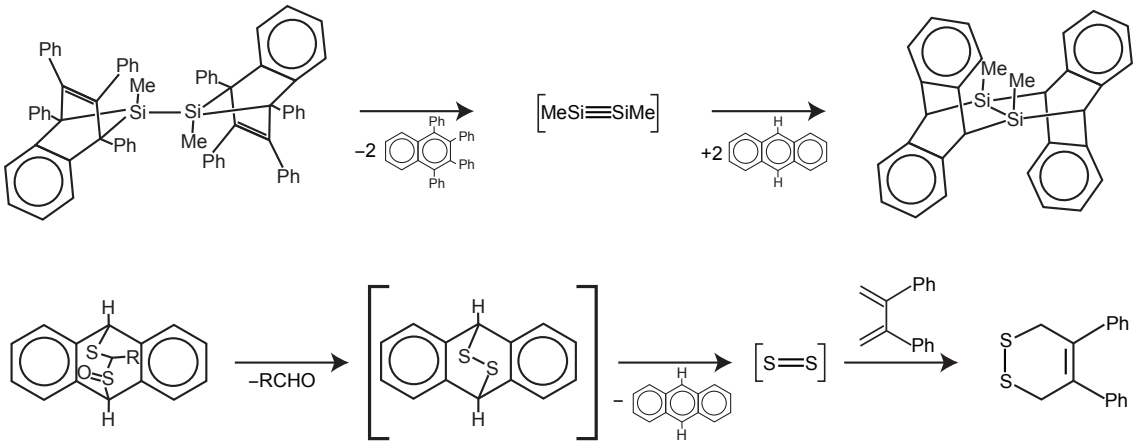

Scheme 1.1. MeSi≡SiMe and S_2, formed by reactions that aromatize a ring, can be generated and trapped *in situ* through cycloaddition reactions.

The energetic costs of generating molecules with multiple bonds between heavy p-block elements must be offset thermodynamically. In the examples mentioned above, the driving forces for multiple bond formation include the aromatization of anthracene and naphthalenes, as illustrated in Scheme 1.1. An alternate, powerful driving force is the formation a strong metal-ligand multiple bond.[33]

Strong Bonds and Niobium Trisanilide

In 1995, Laplaza and Cummins reported reductive scission of the N≡N bond in N_2 by two equivalents of the three-coordinate molybdenum compound $Mo(N[^tBu]Ar)_3$ (Ar = 3,5-dimethylphenyl).[34] This remarkable cleavage of one of the strongest bonds in nature put the the Mo≡N bond strength at at least 113 kcal/mol and provided an early testament to the strength of the bonds between second row, early metal trisamide fragments and electronegative, monoatomic ligands. Later work showed the true Mo≡N bond strength to be significantly higher, 155(3) kcal/mol.[35]

The molybdenum trisanilide species $Mo(N[^tBu]Ar)_3$ is readily prepared in good yield from $MoCl_3(THF)_3$, but access to an analogous niobium species was not as straightforward. Reduction of $ClNb(N[^tBu]Ar)_3$ afforded a dimeric niobium(IV) arylimido, suggesting that the d^2 niobium trisanilide species, $Nb(N[^tBu]Ar)_3$, is unstable toward ^{t}Bu radical ejection.[36,37] Subsequent work by Mindiola targeted the cyclometallated species $HNb(\eta^2\text{-}(CH_3)_2C{=}NAr)(N[^iPr]Ar)_2$, an analogy to the molybdenum complex $HMo(\eta^2\text{-}(CH_3)_2C{=}NAr)(N[^iPr]Ar)_2$, which serves as a solution source of the three-coordinate Mo(III) fragment.[38,39] Evidence for the intermediacy of the desired niobaziridine hydride was obtained, but the compound itself was unstable and underwent bimolecular decomposition.

By increasing the steric protection around the metal, while conserving the ability to cyclometallate, Figueroa and Cummins were able to shut down dimerization and thus synthesize and isolate the niobaziridine hydride complex HNb(η^2-^{t}Bu(H)C=NAr)(N[CH$_2{}^t$Bu]Ar)$_2$.[40] This molecule displays some reactivity consistent with its Nb(V) hydride functionality, but also has demonstrated the ability to serve as a synthon for the niobium(III) trisanilide fragment, Nb(N[CH$_2{}^t$Bu]Ar)$_3$. Much like the molybdenum trisanilide platform, this niobium fragment has demonstrated a propensity toward forming very strong multiple bonds to electronegative fragments. For example, it was shown that the niobaziridine hydride complex deoxygenates triphenylphosphine oxide to form the oxoniobium complex, ONb(N[CH$_2{}^t$Bu]Ar)$_3$.[40] Quantum chemical calculations on this process were used to estimate the Nb≡O bond strength as being greater than 164 kcal/mol.[41]

In another example of HNb(η^2-^{t}BuCH=NAr)(N[CH$_2{}^t$Bu]Ar)$_2$ behaving as a Nb(N[CH$_2{}^t$Bu]Ar)$_3$ synthon, the niobaziridine hydride complex reacts with P_4 to afford the $\mu^2;\eta^2,\eta^2$-P_2 complex (μ-P_2)[Nb(N[CH$_2{}^t$Bu]Ar)$_3$]$_2$. A $2e^-$ reduction of this complex yields two equivalents of the anionic terminal phosphide complex, [PNb(N[CH$_2{}^t$Bu]Ar)$_3$]$^-$. Figueroa uncovered a rich chemistry of this phosphide complex, in particular with regard to its ability to act as a nucleophile in reactions that afford new phosphorus-element bonds.[42–45] By exploiting this reactivity in conjunction with the driving force of Nb≡O bond formation, a synthesis of phosphaalkynes from P_4 and acid chlorides was developed, Scheme 1.2. This reaction sequence demonstrated the synthetic potential of using the formation of strong metal-ligand multiple bonds to drive reactions that form element-phosphorus multiple bonds.

In the sections and chapters that follow, the driving forces of niobium-oxo and niobium-imido bond formation atop the Nb(N[CH$_2{}^t$Bu]Ar)$_3$ platform have been exploited for the synthesis of several species with reactive P–P π bonds.

1.2 A Diphosphaazide Complex

The first isolable transition-metal complexes of organic azides were reported independently in 1995 by Cummins and Bergman for vanadium and tantalum, respectively.[46,47] These complexes eliminate N_2 upon thermolysis to afford metal imidos. The chemistry of azide complexes and the azide-to-imido reaction has undergone much development since then.[48–59] However, this is not the case for heavier analogues of azides, such as those incorporating P atoms ($RN_{3-n}P_n$), which have remained rare.[60–64] Drawing upon the analogy to N_2-eliminating azide complexes, a diphosphaazide ligand complexed to a reducing niobium trisamide fragment was seen as a potential source of the diatomic molecule P_2.

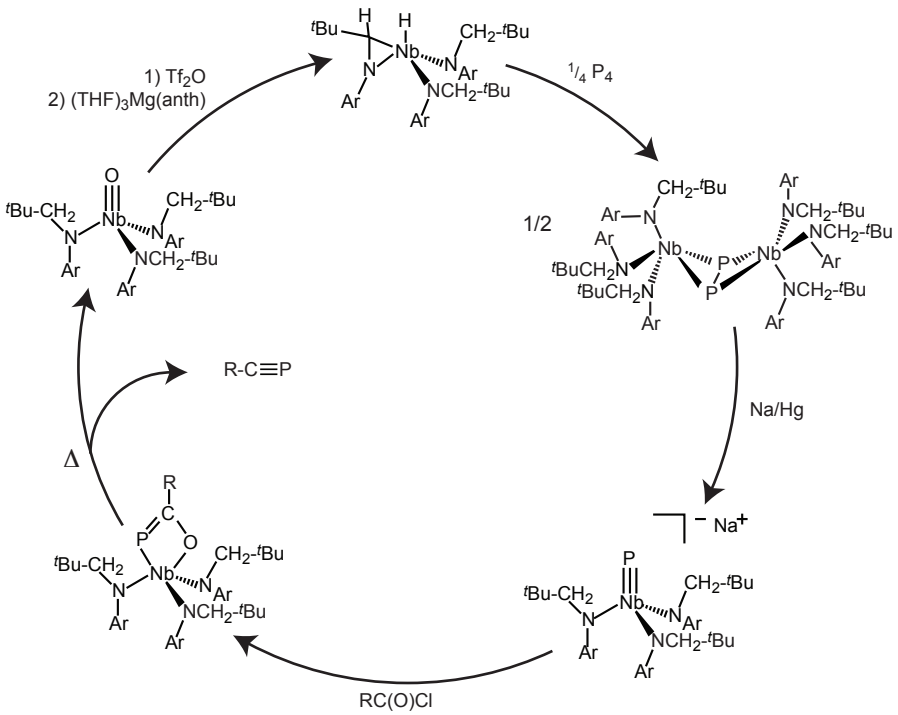

Scheme 1.2. A synthetic cycle for the niobium-mediated synthesis of phosphaalkynes from P_4 and acid chlorides.[42]

1.2.1 Synthesis and Structure

Figueroa demonstrated that the niobium phosphide complex $[PNb(N[CH_2{}^tBu]Ar)_3]^-$ reacts with Niecke's chloroiminophosphane, Mes*NPCl (Mes* = 2,4,6-tri-*tert*-butylphenyl), to afford a Mes*NPP ligand coordinated to the niobium trisanilide platform in the complex (Mes*NPP)-$Nb(N[CH_2{}^tBu]Ar)_3$, **1**, Scheme 1.3.[45,65] This diphosphaazide complex was structurally characterized to reveal an η^2-PP binding mode of the diphosphaazide ligand to the formally d^2 Nb center, Figure 1.2. This structure determination revealed a short P–P bond (2.0173(8) Å), short N–P bond (1.5565(19) Å), and relatively long bonds from Nb to P, consistent with the η^2 binding mode: 2.5653(6) Å to P_α and 2.4673(6) Å to P_β. Several possible resonance structures for this molecule are depicted in Scheme 1.4.

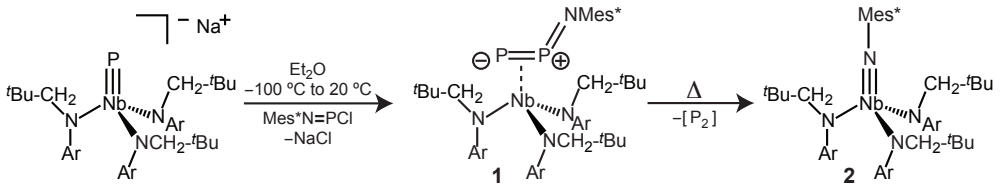

Scheme 1.3. Synthesis and fragmentation of (Mes*NPP)$Nb(N[CH_2{}^tBu]Ar)_3$ (**1**).

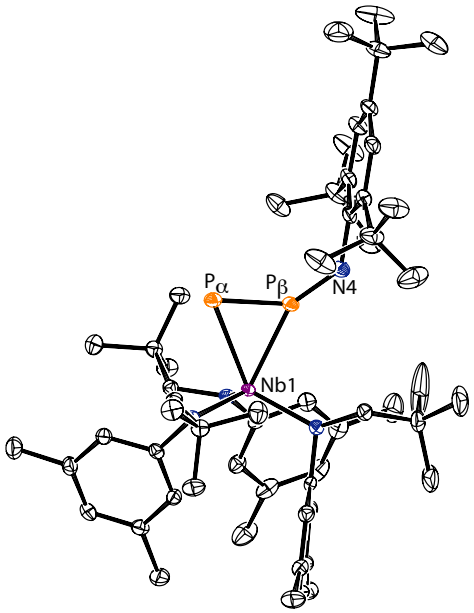

Figure 1.2. Thermal ellipsoid plot (50% probability) of **1** with hydrogen atoms omitted for clarity.

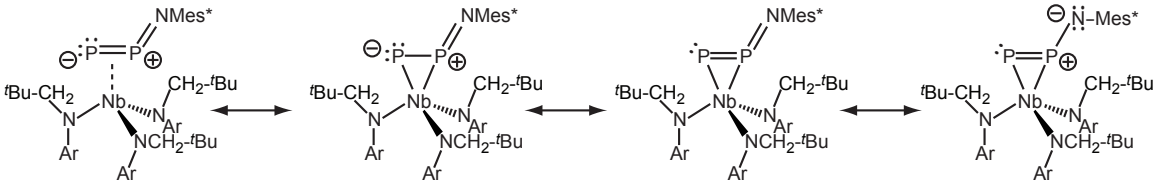

Scheme 1.4. Resonance structures of **1**.

Initial studies on the diphosphaazide complex **1** revealed that upon gentle thermolysis (*e.g.* 60 °C, 45 min) the P_2 fragment is lost to yield a niobium imido, $Mes^*NNb(N[CH_2{}^tBu]Ar)_3$, **2**. This process was intriguing because it suggested that **1** might be serving as a solution-phase source of the diatomic molecule P_2. Before the P_2 elimination chemistry is discussed further, an analysis of the NMR spectrum of **1** is presented.

1.2.2 Solid-state NMR Spectra of $(Mes^*NPP)Nb(N[CH_2{}^tBu]Ar)_3$

The solution-state ^{31}P NMR spectrum of **1** in benzene at 20 °C consists of a pair of doublets, J_{PP} = 650 Hz, at 335 and 315 ppm. The large coupling constant is indicative of a high degree of multiple bonding, but the similarity in chemical shift of these two nuclei makes the assignment of the resonances between P_α (the phosphorus with no bond to N) and P_β (the phosphorus bound to N) difficult. Given that the electronic environments of the two phosphorus nuclei in **1** are expected to be very different, it was hoped that the solid-state ^{31}P NMR spectrum of **1** could aid in the assignment. Furthermore, the solid-state NMR spectrum of **1** could be used to help confirm that the solution-phase structure is the same as the structure determined in the solid state by X-ray crystallography.

The isotropic chemical shift of a nucleus, δ_{iso}, can be measured easily in solution by NMR spectroscopy. However, solution methods do not provide information about the individual components of the chemical shift tensor, which can contain information on electronic structure. The principal components of the chemical shift tensor, δ_{11}, δ_{22}, and δ_{33}, can be experimentally determined through solid-state NMR methods. In particular, these data can often be extracted from the intensities of the spinning sidebands when the NMR experiment is conducted with magic angle spinning (MAS).[66] Such data were obtained on **1** at the University of Alberta in the laboratory of Prof. Roderick Wasylishen by Dr. Guy Bernard and coworkers using samples provided by the author. The ^{31}P MAS NMR spectrum obtained on **1** is shown in Figure 1.3a. As in the solution spectrum, the solid-state spectrum reveals two doublet resonances, one broad and one sharp. In the solid-state MAS spectrum, each is accompanied by a manifold of spinning sidebands. The isotropic signals, inlaid and marked with an asterisk in Figure 1.3a, are at chemical shifts very near to the values found in solution NMR spectra. This observation supports the conclusion that the solution and solid-state structures are very similar.

The difference in electronic environments between P_α and P_β becomes immediately evident from the solid-state data: the spinning side bands for the sharp set of resonances span a very wide chemical shift range (*ca.* 1000 ppm to –500 ppm), while the broad resonances show a much smaller span (*ca.* 600 ppm to 200 ppm). The large span for the sharp resonances is indicative of a large chemical shift anisotropy (CSA), *i.e.* $\delta_{11} \gg \delta_{33}$. Such a property can be expected for a very low-coordinate phosphorus nucleus. For example, the CSAs of the terminal phosphide ligands in the complexes $PMo(N[^tBu]Ar)_3$ and $PMo([Me_3SiNCH_2CH_2]_3N)$ are remarkably large, being greater than 2300 ppm.[67] Accordingly, the sharp set of signals in the spectrum of **1** are assigned to P_α, and this assignment was corroborated by DFT calculations (*vide infra*).

Table 1.1. Experimental (least squares best fit) chemical shielding parameters[a] for **1** and calculated[b] parameters for **1m**

	P_α		P_β	
Parameter	Best-fit	Calculated	Best-fit	Calculated
δ_{iso}	310	331	313	309
Ω	1255	1595	359	367
κ	-0.03	0.01	0.18	0.13
δ_{11}	918	1138	524	517
δ_{22}	350	313	250	261
δ_{33}	–337	–457	165	149

[a] Values are in ppm. [b] Parameters are based on values for absolute shielding calculated by DFT using the ADF program. Chemical shifts are determined by comparison to a computational reference molecule, (OP)Mo(N[^{t}Bu]Ar)$_3$, at 270 ppm.

To allow for a quantitative fit of the experimental spectrum it was desirable to separate the signals of P_α from those of P_β. This was accomplished using a specialized pulse sequence that makes use of a hyperbolic secant (HS) pulse applied to a sideband attributed to only one of the nuclei.[68] When this pulse was applied at 750 ppm, the entire manifold of sidebands arising from P_α was caused to collapse, leaving only signals for P_β, Figure 1.3b. Subtracting this latter spectrum from the one obtained without the HS pulse then provides a view of only the resonances and sidebands for P_α, Figure 1.3c. Having isolated the signals of P_α and P_β, they can be fit individually.

The principal components of the P_α chemical shift tensor were extracted from the intensities of the sidebands in Figure 1.3c by the method of Herzfeld and Berger using the program HBA.[66,69] A least squares analysis yielded the values for the span (Ω) and skew (κ) listed in Table 1.1; these values correspond to the principal components also in the table. A Herzfeld-Berger analysis of the heights of the broad spinning sidebands presented by P_β in Figure 1.3b was similarly used to estimate values for the principal components of the shielding of this nucleus. In this case, however, the residual dipolar interactions that result in the broadening of the signals also interfere with the accuracy of this analysis. Moreover, the relatively small number of spinning sidebands results in a low data-to-parameter ratio for the fit. As a result, the best fit parameters listed in Table 1.1 for P_β are best viewed only as a rough estimate. A more accurate numerical treatment of the simulation will be necessary to more effectively extract the chemical shift parameters as well as parameters of the dipolar couplings and quadrupolar interactions.

Having extracted estimated parameters for the principal components of the chemical shielding tensors of **1** it was desirable to relate these to their electronic origins. To this end, chemical shielding calculations were carried out on an optimized structure of the model complex (2,6-

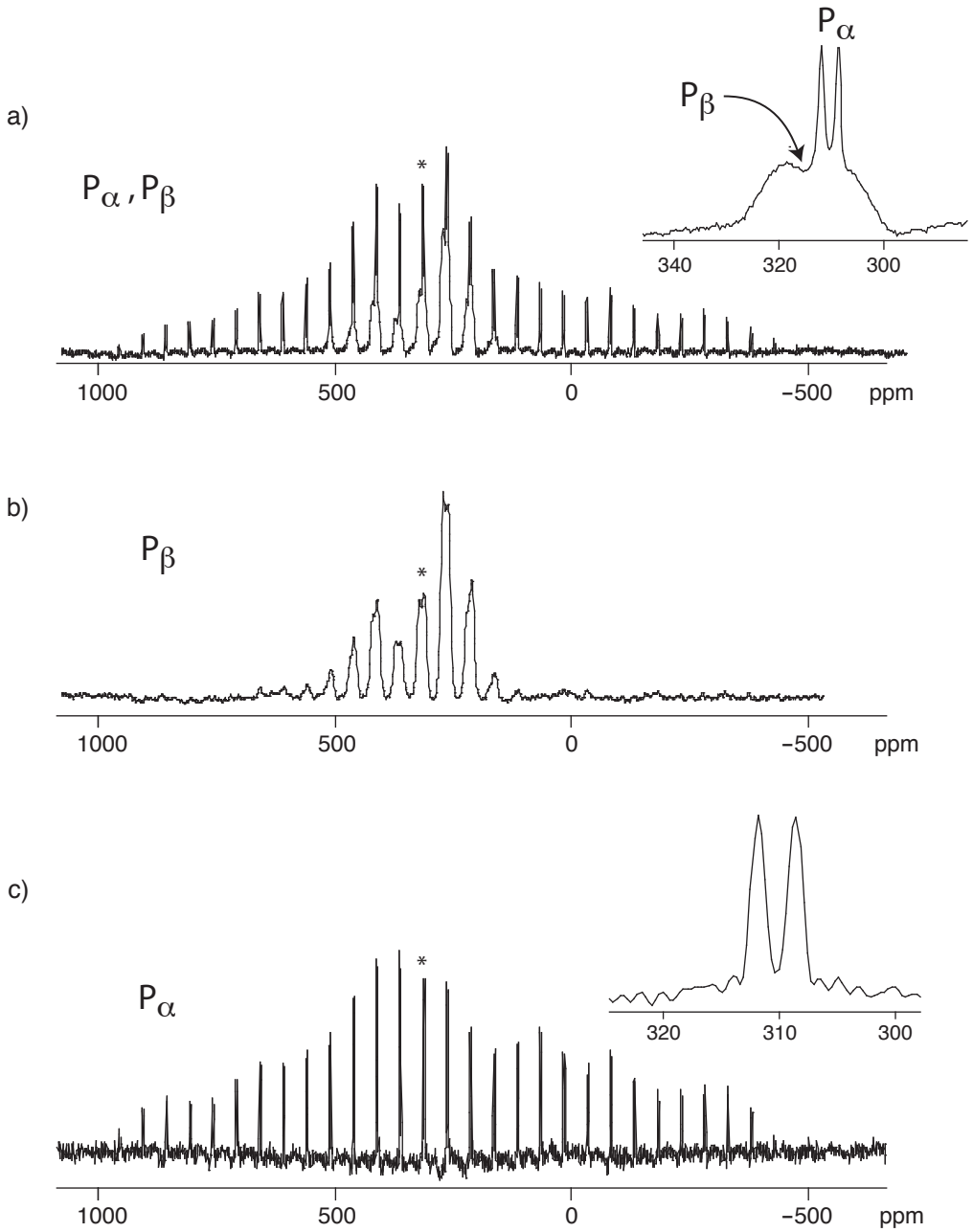

Figure 1.3. Solid-state ^{31}P NMR spectra of **1** taken at 11.75 T and a MAS frequency of 10 kHz. The top spectrum shows broad resonances for the β phosphorus and sharp doublets for the α phosphorus. The middle spectrum is taken with a hyperbolic secant pulse applied at 750 ppm to isolate the signals from P_β. The bottom spectrum is a difference spectrum, showing the signals corresponding to P_α. Isotropic signals are marked with an asterisk and shown inlaid.

Table 1.2. Calculated coupling constants[a] for (2,6-$^{t}Bu_2C_6H_3NPP$)Nb(N[Me]Ph)$_3$ (**1m**)

	Nb	N	P_α	P_β
P_α	–69	–11	–	–696
P_β	351	–147	–696	–

[a] Values are in Hz and are calculated for ^{93}Nb, ^{14}N, and ^{31}P nuclei by DFT using the ADF program.

$^{t}Bu_2C_6H_3NPP$)Nb(N[Me]Ph)$_3$, **1m**, using the ADF package.[70,71] In addition, dipolar couplings between the phosphorus atoms, the phosphorus atoms and niobium, and the phosphorus atoms and the imino nitrogen were calculated. These data are presented in Tables 1.1 and 1.2, and the orientations of the principal components to the chemical shielding tensor of P_α are shown in Figure 1.4. The calculated shielding components and CSAs confirm the assignments of P_α and P_β. The coupling constant data also provide an explanation for the very broad nature of the P_β resonance. This broadness can be attributed to strong interactions between P_β and the quadrupolar ^{93}Nb and ^{14}N nuclei; both nuclei couple to P_α less strongly than P_β, and hence the resonance for P_α is found to be sharper. These larger couplings are consistent with the expected higher degree of *s* character in the bonds to P_β, which has no formal lone pair. It is also noteworthy that the bond from Nb to P_β is shorter than the distance to P_α by *ca*. 0.1 Å.

Based on the DFT calculations, we can attribute the large magnitude of δ_{11}^{α} to a large and negative value for the paramagnetic contribution to σ_{11}. This arises from a coupling of occupied and virtual orbitals in the applied magnetic field. Figure 1.5 shows that orbitals at P_α have strong contributions to both the HOMO and LUMO, and that they are related by a rotation axis aligned along the vector $\vec{\sigma}_1$. The resulting occupied-virtual coupling of these two orbitals thus contributes to the large paramagnetic deshielding along this axis.

1.2.3 Solution-state NMR Spectra of (Mes*NPP)Nb(N[CH$_2$^{t}Bu]Ar)$_3$

The very similar solid-state chemical shifts observed for the two ^{31}P nuclei of **1** prevented its application to a definitive assignment for the solution-phase ^{31}P NMR spectrum. In order to make this assignment, an ^{15}N labeling of **1** at the iminophosphane nitrogen was was carried out. The ^{15}N label was introduced starting from the reaction between Na^{15}NNN and Mes*COOH. Following a Curtius rearrangement, *in situ* hydrolysis of the intermediate isocyanate afforded the aniline, Mes*$^{14/15}$NH$_2$ (^{15}N δ = 66 ppm), with the label introduced to one half of the molecules.[72] From

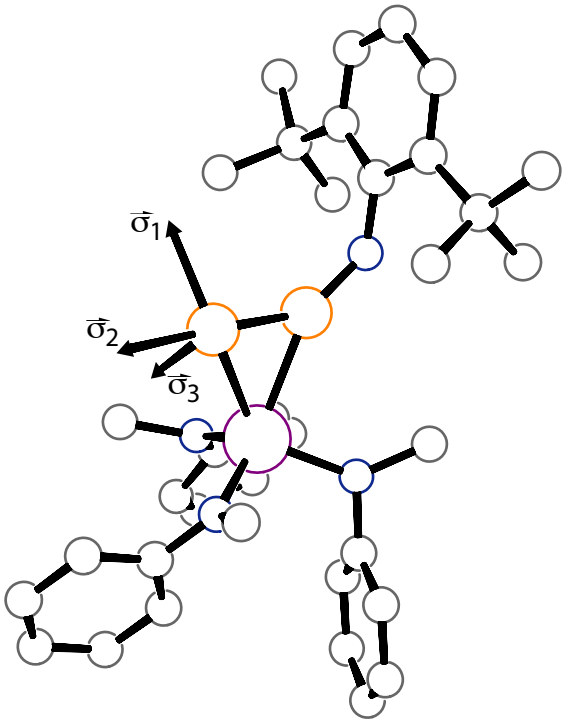

Figure 1.4. The principal components of the chemical shielding tensor for P_α calculated for **1m** and superimposed on the molecular frame.

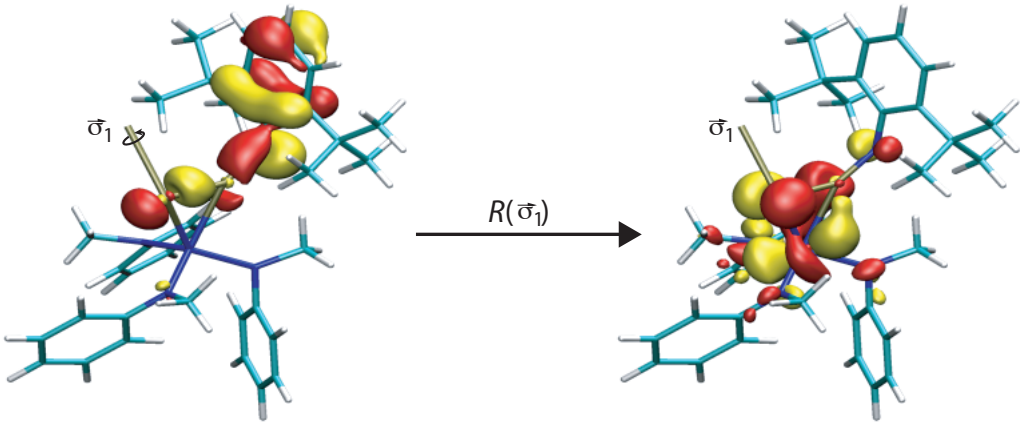

Figure 1.5. Strong occupied-virtual orbital coupling between the HOMO and LUMO is mediated by an applied magnetic field along the principal axis $\vec{\sigma}_1$. Rotation of the HOMO about this axis would cause significant overlap with the LUMO at P_α, giving rise to a large δ_{11}.

this labeled aniline, the synthesis of **1** was carried out according to the procedure for the unlabeled compound by first synthesizing Mes*$^{14/15}$NPCl (J_{PN} = 73 Hz).

The ^{15}N NMR spectrum of **1**-$^{15/14}$N consists of a doublet (J_{PN} = 153 Hz) at 250 ppm versus $NH_{3\,(l)}$. The ^{31}P NMR spectrum of **1**-$^{15/14}$N is presented in Figure 1.6, along with that of the unlabeled compound.[i] From these data, the downfield resonance is observed to be coupled more strongly to ^{15}N and is consequently assigned as P_β. The magnitude of the observed coupling, 153 Hz, is in good agreement with that obtained from DFT calculations, 147 Hz, Table 1.2. Notably, however, if the assignment of these two resonances was made solely on the basis of calculated chemical shielding values, the *opposite* assignment would have been made.

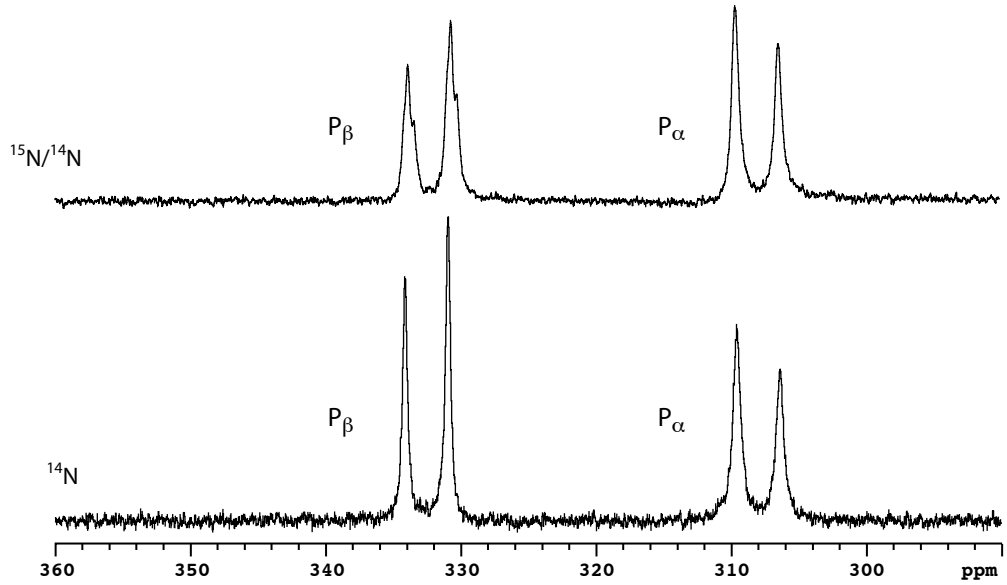

Figure 1.6. ^{31}P NMR spectra (202.5 MHz, toluene) of **1**-$^{15/14}$N (above) and **1** (below) at *ca.* –15 °C.

1.3 Mechanism of Putative P_2 Elimination

1.3.1 Eyring Analysis

The observed transformation of **1** into the niobium(V) imido **2** with loss of the P_2 fragment is a unique reaction, though it is reminiscent of reactions in which a complexed azide ligand loses N_2 and forms a metal imido.[46–48,51,53] Proulx and Bergman have studied the mechanism of N_2 extrusion from the group 5 metal complexes $Cp_2(Me)Ta(N_3R)$ (Cp = C_5H_5, R = *p*-C_6H_4X) and based on kinetic and Hammet analyses have proposed a mechanism for N_2 extrusion that proceeds through a four-membered metallacycle.[53] Higher-order pathways have also been implicated in azide-to-imido

[i]This spectrum was taken at *ca.* –15 °C because at this temperature the resonances of both P_α and P_β are relatively sharp, allowing the ^{15}N splitting to be more easily observed.

reactions on group 5 metals. Mechanistic work by Fickes *et al*. suggested a more complicated mechanism for the transformation of a mesityl azide complex to its imido atop a vanadium bisanilide iodide platform.[37,47]

To probe the mechanism of P_2 loss from **1**, the kinetic profile of this reaction was investigated by ^{1}H NMR spectroscopy in C_6D_6. The integral for the methylene resonance of **1** was fit to a first-order decay model to provide rate constants for the P_2 elimination reaction over the temperature range 30 °C to 80 °C. Representative data are depicted in Figure 1.7. The first-order rate constants over these temperatures range from $3.3(2) \times 10^{-5}$ s^{-1} to $3.8(6) \times 10^{-3}$ s^{-1}. These data are shown as a linear Eyring plot in Figure 1.8, and based on an Eyring analysis correspond to $\Delta H^{\ddagger} = 19.6(2)$ kcal/mol and $\Delta S^{\ddagger} = -14.2(5)$ eu.[73] The negative and relatively large magnitude of the entropy of activation is indicative of a highly ordered transition state and is consistent with rearrangement to a sterically congested metallacycle being the rate-limiting step to imido formation, Figure 1.9 (right side). Similar activation parameters have been reported by Waterman and Hillhouse for the analogous reaction of an η^2-azide complex losing N_2 and forming an imido at a sterically crowded nickel center.[51]

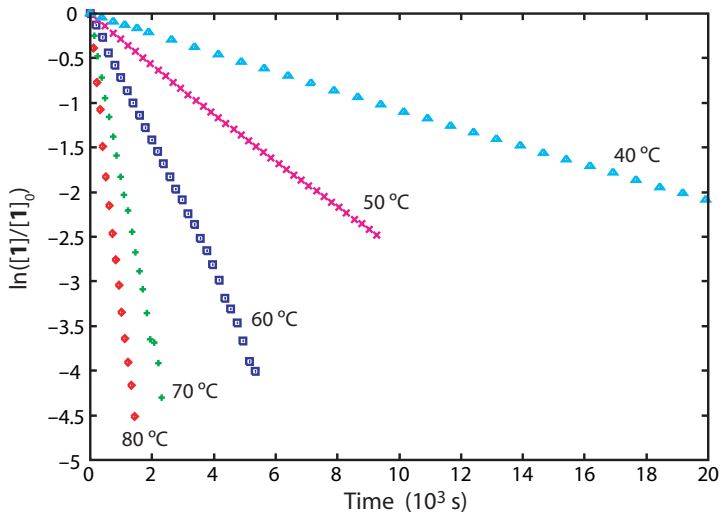

Figure 1.7. Representative kinetic data for the first-order thermal fragmentation of **1** at temperatures between 40 °C and 80 °C in C_6D_6.

1.3.2 DFT Calculations

As a supplement to the Eyring analysis, quantum chemical calculations on the model complex (2,6-^{t}Bu$_2$C$_6$H$_3$NPP)Nb(N[Me]Ph)$_3$, **1m**, were used to investigate two possible pathways for P_2 elimination from complex **1**. The mechanistic pathways investigated are presented in Figure 1.9. One possible mechanism proceeds through a "slippage" reaction to form **1a**, wherein the terminal P-

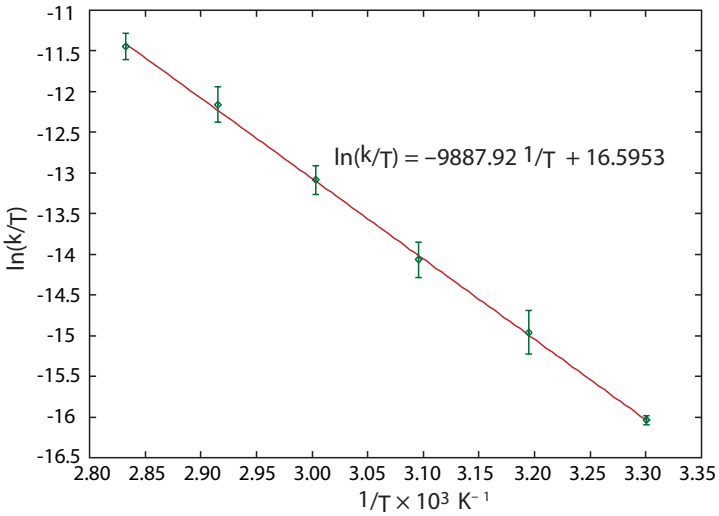

Figure 1.8. An Eyring plot for the thermal fragmentation of **1** (error bars shown at the 95% confidence interval) estimates the activation parameters as $\Delta H^{\ddagger} = 19.6(2)$ kcal/mol and $\Delta S^{\ddagger} = -14.2(5)$ eu.

atom of the diphosphaazide ligand has de-coordinated from the metal center and a new Nb−N bond has formed. The dangling P-atom in this structure would be expected to give rise to a high-energy intermediate, and the DFT analysis supports this hypothesis: isomer **1a** lies 28 kcal/mol above **1m**. From **1a**, extrusion of the P_2 molecule affords **2m** to complete the elimination reaction which is calculated to be near thermoneutral. The calculated energy of the intermediate **1a** suggests that this pathway would have an energy barrier that is inconsistent with the observed rates of formation for **2**.

A potential alternate pathway for P_2 loss from complex **1** proceeds through a 4-membered metallacycle intermediate similar to the mechanism envisioned by Proulx and Bergman.[53] The NbPPN metallacycle structure would also be analogous to that of the isolable, NbPCO metallacycle intermediates that are on the path to phosphaalkyne generation atop the same niobium platform.[42,ii] The first elementary step, involving an η^2 to η^1 isomerization, was calculated to be only slightly uphill and is expected to have a small activation energy. In fact, it may be that the isomers corresponding to **1m** and **1b** are in an unobserved equilibrium in solution. Proceeding from **1b** with an inversion at N, rotation around the P−P bond, and N coordination to the metal delivers metallacycle **1c**, the immediate precursor to P_2 elimination. Inversion at the sp^2 imino nitrogen is perhaps the most concerning of these steps, but inversions at iminophosphanes are known to have low barriers.[74–77] In contrast, the alternate pathway whereby a simple inversion at the β phosphorus affords metallacycle **1c** directly is expected to be higher in energy based on the significant barrier to inversion at sp^2 phosphorus centers.[78,79] In any case, the metallacycle isomer **1c** is found to lie 19 kcal/mol uphill from **1m** and its formation is likely rate-limiting. Though **1c** corresponds to a local energy minimum by DFT, it is noteworthy that its energy relative to **1m** agrees well with the

[ii] Related NbPPO metallacycles have also been synthesized as model complexes, but only molecules having pentavalent phosphorus in the β position have been accessed (see Section 3.3).

experimental value of $\Delta H^{\ddagger}$ such that the transition state is likely nearby.[iii] That formation of the NbPPN metallacycle **1c**, and not P_2 extrusion from **1c**, is rate-limiting is supported by comparing the entropy of activation for this process to that in which ^{t}BuC≡P is generated from a preformed NbPCO metallacycle. In the latter reaction, $\Delta S^{\ddagger}$ was found to be +2 eu; this is consistent with a transition state in which bond-breaking ensues on route to the formation of two molecules.[73] For the reaction of **1** a large and negative value for $\Delta S^{\ddagger}$ is observed, consistent with the ordering process of metallacycle formation as the rate-limiting step. Once at the metallacycle, the geometry is poised to eliminate the P_2 molecule into solution with concomitant formation of a strong Nb≡N imido bond.

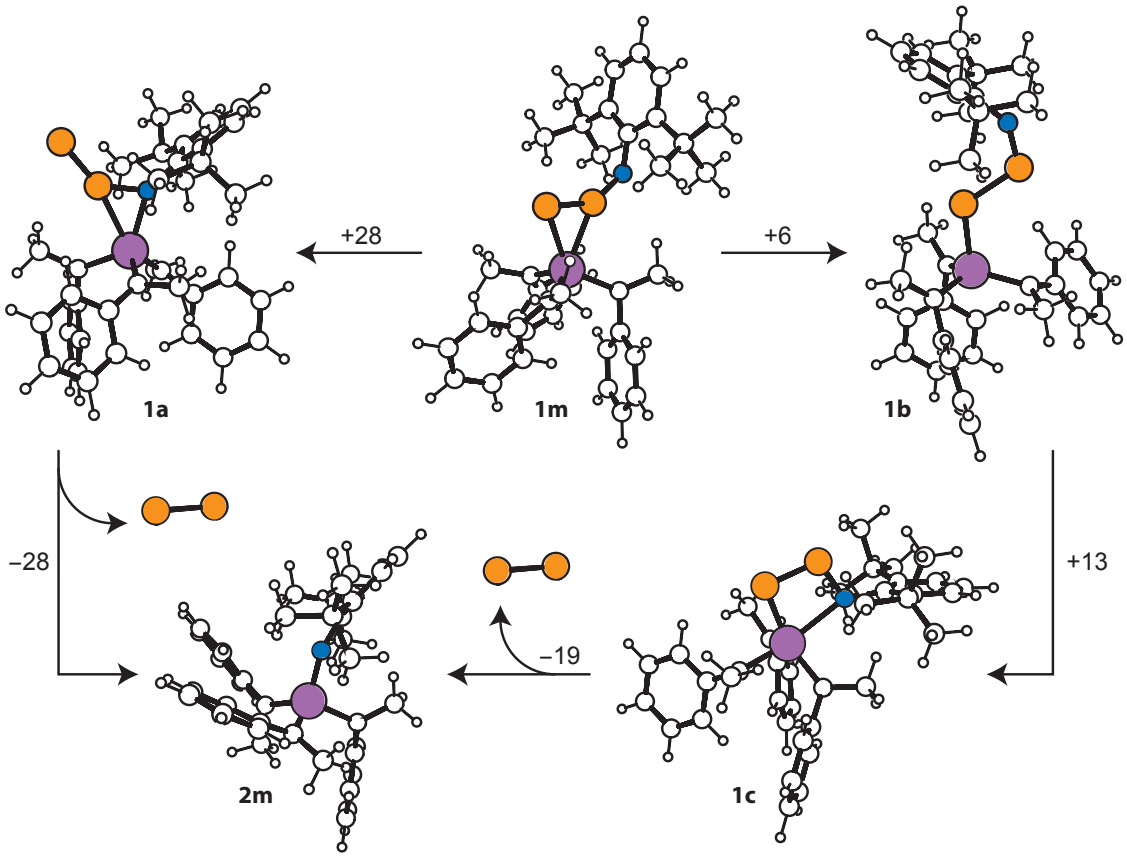

Figure 1.9. Proposed pathways to P_2 elimination from **1m**. Based on quantum chemical calculations and kinetic data, the pathway on the right is preferred. Electronic energies associated with each isomerization are shown for each step in kcal/mol.

[iii]The large size of the model precluded the frequencies calculations necessary to definitively assign these structures as local minima, though they were found to meet default convergence criteria. Analogous structures with smaller ligand sets were found to have similar geometries and were identified as energy minima with no negative vibrational frequencies.

1.4 Elimination of $(P_2)W(CO)_5$ from a Doubly-Coordinated Diphosphaazide Ligand

The reaction of diphosphaazide **1** to form imido **2** suggests the loss of the P_2 molecule. It was thought that by stabilizing the P_2 molecule via complexation to a metal center it might be possible to observe this species, or to better control its reactivity. Metal pentacarbonyl groups, and in particular $W(CO)_5$, have been used in low-coordinate phosphorus chemistry to avoid unwanted side reactions while still allowing for reactions to occur at P–P π bonds.[9] In one example, Scheer and co-workers have used $M(CO)_5$ (M = W, Cr) to impart kinetic stability to the triply bonded phosphorus ligand of the terminal phosphide complex $P{\equiv}W(O^tBu)_3$.[80,81] Moreover, Esterhuysen and Frenking have considered the molecule $(P_2)W(CO)_5$ theoretically and predicted that it should be possible to obtain such a complex with the P_2 molecule bound in an η^2 fashion to the tungsten center.[82] This isomer was calculated to be *ca.* 7 kcal/mol more stable than that with the P_2 bound in the η^1, end-on complexation mode.

Preliminary studies indicated that addition of $(THF)W(CO)_5$ to solutions of diphosphaazide complex **1** formed a $W(CO)_5$ complex of **1** and accelerated the conversion to imido **2**. For synthetic ease, however, an alternate entry point to this potential $(P_2)W(CO)_5$ eliminating system was sought.

1.4.1 $W(CO)_5$-Capping of a Terminal Phosphide

Synthesis and Structure

The sodium salt of the nucleophilic niobium phosphide complex, $[PNb(N[CH_2{}^tBu]Ar)_3]^-$, **3**, was found to react with $W(CO)_6$ in THF at 22 °C over several hours to displace a CO ligand and afford $[(OC)_5WPNb(N[CH_2{}^tBu]Ar)_3]^-$, **4**, Scheme 1.5. The product was then isolated as a *n*-pentane insoluble orange powder by precipitation from Et_2O in 70% yield. This reaction is in contrast to the majority of CO displacement reactions at $W(CO)_6$, which typically require heat, photolysis, or sonication.[83–88] It is unknown what mechanism gives rise to the facile the reaction of **3** and $W(CO)_6$, but because it was observed to proceed in the absence of light it is speculated that the reaction is either catalyzed by electron transfer reactions or proceeds through a nucleophilic attack at a CO ligand.[iv] The capped phosphide complex **4** can alternatively be synthesized by the addition of photochemically generated $(THF)W(CO)_5$ solutions to **3**, but the addition of exactly one equivalent of the photo-generated reagent can be more difficult to control. The ^{31}P NMR spectrum of **4** displays a single broad resonance at 588 ppm. This is in the range expected for a metal phosphinidene complex and significantly upfield of the resonance for the uncapped **3**. An analogous dramatic upfield shift was observed by Scheer upon going from $P{\equiv}W(O^tBu)_3$ to $(OC)_5W{-}P{\equiv}W(O^tBu)_3$.[81]

[iv] It is worth noting that nucleophilic attack by the niobium phosphide on a CO ligand to generate a Fischer carbene was the original impetus for treating **3** with $W(CO)_6$.

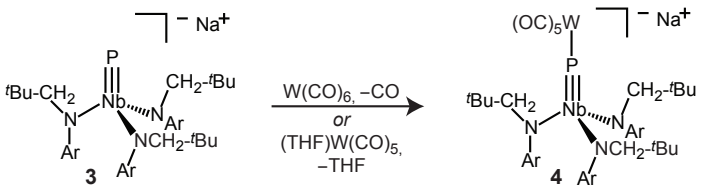

Scheme 1.5. Synthesis of $[(OC)_5WPNb(N[CH_2{}^tBu]Ar)_3]^-$ (**4**).

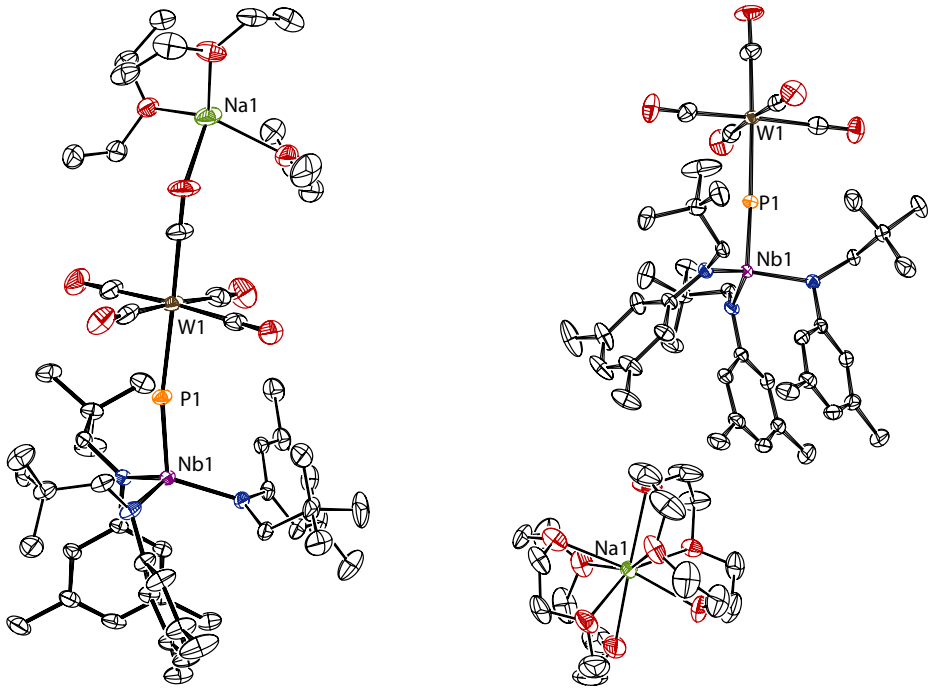

Figure 1.10. (a) Thermal ellipsoid plot (30% probability) of $[(Et_2O)_3Na][\mathbf{4}]$ with hydrogen atoms omitted for clarity. (b) Thermal ellipsoid plot (50% probability) of $[(12\text{-crown-}4)_2Na][\mathbf{4}]$ with hydrogen atoms omitted for clarity.

A red crystal of $[(Et_2O)_3Na][\mathbf{4}]$ grown from Et_2O at –35 °C was subjected to an X-ray diffraction study. The crystals belong to the space group $P2_1/c$ and contain one molecule per asymmetric unit, Figure 1.10a. This study revealed that the core of the molecule possesses the expected geometry of a near linear Nb−P−W linkage with a short Nb−P bond, 2.2035(10) Å, Table 1.3.[81,89,90] The sodium cation resides coordinated to the axial carbonyl ligand, and its tetrahedral coordination sphere is completed by three molecules of Et_2O. Unfortunately, the Et_2O molecules and two of the anilide ligands show disorders over the lattice, which were refined with the help of similarity restraints.

Alternatively, treatment of $[(Et_2O)Na][\mathbf{4}]$ with 2 equivalents of 12-crown-4 in Et_2O yields the bis(12-crown-4)sodium salt of **4** as a red precipitate. Diffraction quality crystals of this compound in the space group $P2_12_12_1$ were grown from a mixture of THF and Et_2O at –35 °C. The metric parameters of the core were similar to that of the compound without the sequestering 12-crown-4

Table 1.3. Selected bond lengths (Å) and angles (°) for **4**

	$[(Et_2O)_3Na][\mathbf{4}]$	$[(12\text{-c-}4)_2Na][\mathbf{4}]$
Nb1–P1	2.2035(10)	2.2005(8)
W1–P1	2.5324(9)	2.5394(8)
Nb1–P1–W1	169.37(6)	170.79(4)

molecules. While the 12-crown-4 linkages were themselves disordered, this disorder was removed from the vicinity of the anion allowing for a better refinement. The structure of the anion is shown in Figure 1.10b and selected metrical parameters of the two structures are listed in Table 1.3.

Nucleophilicity of the $W(CO)_5$-Capped Phosphide Complex

Nucleophilic substitution reactions of the anionic terminal phosphide complex **3** constitute a valuable route for formation of phosphorus–element bonds atop the niobium trisanilide platform. It was initially unclear as to whether the $W(CO)_5$-capped phosphide anion would display the same nucleophilicity as the terminal phosphide anion. Not only does the $W(CO)_5$ unit provide a steric shield for the phosphorus atom, but it also could serve to delocalize the negative charge on the complex over several carbonyl groups. Nevertheless, **4** was found to engage cleanly in rapid nucleophilic substitution reactions with MeOTf and MeOTs ($OTf^- = CF_3SO_3^-$, $OTs^- = p\text{-}MeC_6H_4SO_3^-$) to generate the $W(CO)_5$-coordinated methyl phosphinidene complex, $(OC)_5WP(Me)Nb(N[CH_2{}^tBu]Ar)_3$, **5**. This compound was characterized by an X-ray diffraction study that confirmed its identity, Figure 1.11. The structure revealed a Nb−P bond distance of 2.3599(11) Å and a W−P distance of 2.5407 Å, consistent with the formulation as a doubly-bonded niobium phosphinidene coordinated to a Lewis acidic $W(CO)_5$ fragment. These reactions demonstrate that the capped niobium phosphide anion **4** retains its nucleophilicity at the phosphide ligand. It is also noteworthy that the reaction of **4** with the potent electrophile MeOTf was found to be significantly cleaner than the analogous reaction of the very reducing and reactive **3**.

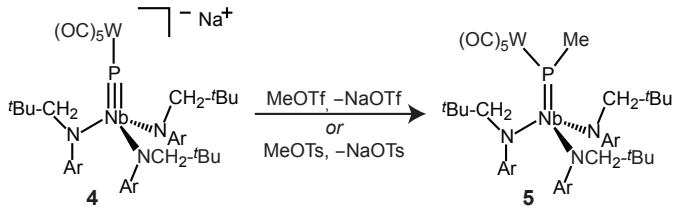

Scheme 1.6. Synthesis of $(OC)_5WP(Me)Nb(N[CH_2{}^tBu]Ar)_3$ (**5**).

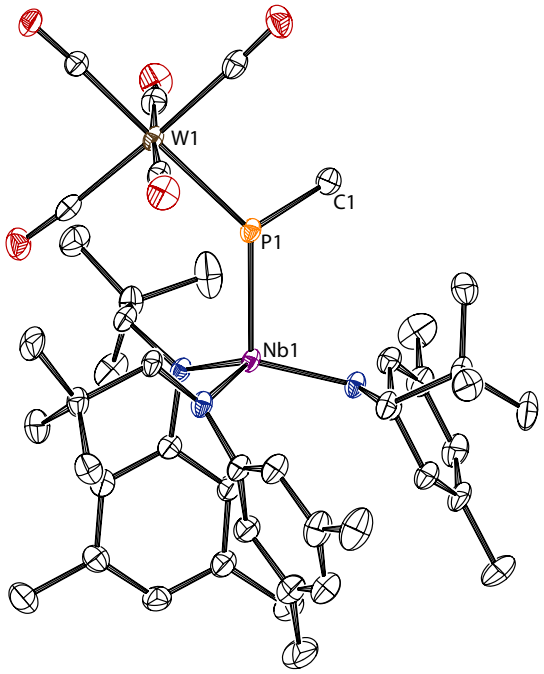

Figure 1.11. Thermal ellipsoid plot (50% probability) of **5** with hydrogen atoms omitted for clarity.

1.4.2 Synthesis of $(OC)_5W(Mes^*NPP)Nb(N[CH_2{}^tBu]Ar)_3$

As a route to a potential $(P_2)W(CO)_5$-eliminating complex, a synthesis analogous to that for generating **1** from **3** was investigated. The sodium salt of **4** was found to react cleanly with Mes^*NPCl to generate the $W(CO)_5$-coordinated niobium diphosphaazide complex $(OC)_5W$-$(Mes^*NPP)Nb(N[CH_2{}^tBu]Ar)_3$, **1**-$W(CO)_5$. This complex displays two strongly coupled resonances in its ^{31}P NMR spectrum at 285 and 247 ppm. The coupling constant of 730 Hz indicates that the P–P multiple bonding present in **1** is maintained. Red crystals of **1**-$W(CO)_5$ were grown from Et_2O at –35 °C and subjected to an X-ray diffraction experiment from which a low-resolution solution structure could be determined. The connectivity was as predicted, with $W(CO)_5$ coordinated to the α phosphorus of an η^2 bound diphosphaazide ligand. Unfortunately, anisotropic refinement was problematic without the use of heavy restraints, precluding a full discussion of metrical parameters. Using the X-ray structure solution as the basis for a starting geometry, the structure of the model complex $(OC)_5W(2,6\text{-}{}^tBu_2C_6H_3NPP)Nb(N[Me]Ph)_3$ was optimized. This structure and selected metrical parameters for this computational model are presented in Figure 1.12. The calculated ^{31}P chemical shifts of 297 ppm (P_α) and 271 ppm (P_β) were also found to be in good agreement with the observed chemical shifts.

The bimetallic diphosphaazide complex **1**-$W(CO)_5$ is thermally unstable and affords **2** with a half-life of *ca.* 20 min at 20 °C. This facile elimination of the $(P_2)W(CO)_5$ unit from **1**-$W(CO)_5$ implies a stabilization of the transition state for the reaction to form imido, relative to that for

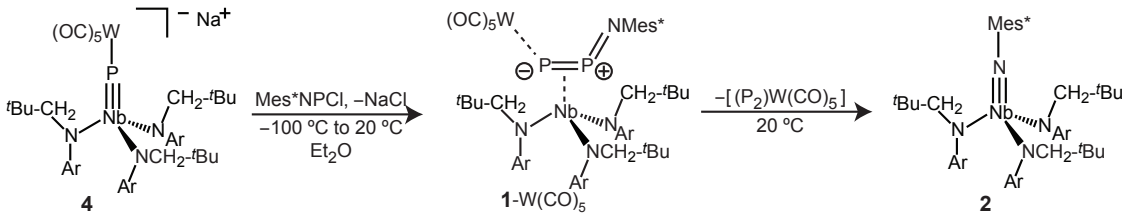

Scheme 1.7. Synthesis and fragmentation of $(OC)_5W(Mes^*NPP)Nb(N[CH_2{}^tBu]Ar)_3$ (**1**-$W(CO)_5$).

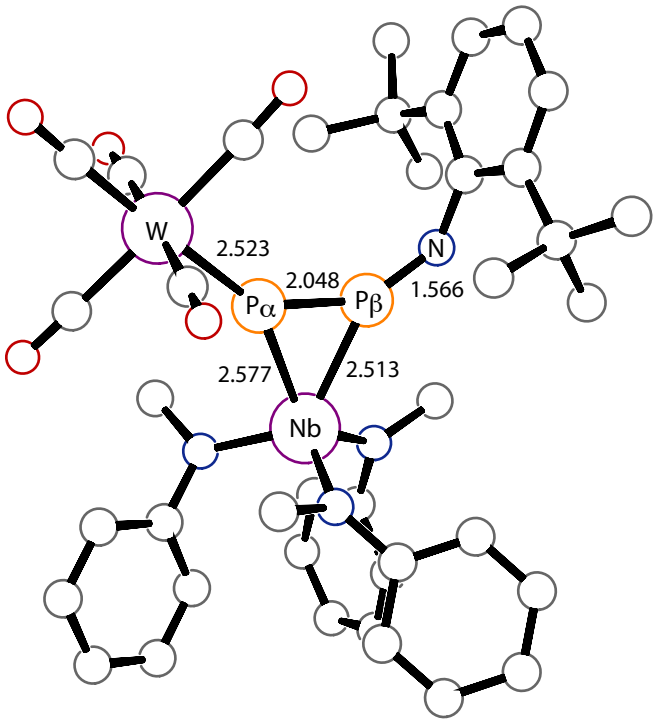

Figure 1.12. DFT optimized structure of $(OC)_5W(2,6\text{-}{}^tBu_2C_6H_3NPP)Nb(N[Me]Ph)_3$. Selected bond lengths are indicated in Å.

1. Taken one step further, the ready elimination of $(P_2)W(CO)_5$ from **1**-$W(CO)_5$ suggests that the products have been successfully stabilized by complexation to $W(CO)_5$. The mechanism for $(P_2)W(CO)_5$ extrusion from **1**-$W(CO)_5$, however, need not proceed through the same sort of metallacycle invoked for **1**. The alternate, "slippage" pathway discussed in Section 1.3.2 is likely stabilized by coordination of $W(CO)_5$ at P_α relative to its energy in the $W(CO)_5$-free reaction and may be operative. In any case, while **1**-$W(CO)_5$ is able to lose a formal equivalent of $(P_2)W(CO)_5$ under mild conditions, this product was not observed in solution or able to be isolated. As a result, this $(P_2)W(CO)_5$-eliminating complex has been studied alongside the P_2-eliminating complex **1**. Also, because **1**-$W(CO)_5$ is thermally unstable, its chemistry has been pursued principally using samples generated *in situ* from **4** and Mes*NPCl .

1.5 Organic Dienes as Probes for P_2- and $(P_2)W(CO)_5$-Elimination Chemistry

1.5.1 Trapping the Putative P_2 Intermediate

The HOMO and LUMO of the diatomic P_2 molecule are both of π symmetry, the HOMO is relatively high in energy, and the HOMO-LUMO gap is small. As such, if P_2 were in fact being produced as an intermediate from the fragmentation of **1**, it was expected to be trapped by suitable reagents that exploit the reactivity of the frontier π systems. One class of such compounds that could react with P_2 in cycloaddition reactions is organic dienes. The P=P double bonds of diphosphenes are well known to react with dienes in $[4+2]$-cycloaddition reactions.[2,8,9] Correspondingly, a double diene addition to the two π bonds of a P_2 unit might be expected. Certain dienes have the added advantage of being volatile liquids that could additionally serve as solvent for the reaction, thus providing a very high concentration of potential trap for a short-lived P_2 intermediate. Indeed, heating a solution of **1** in neat 1,3-cyclohexadiene to 65 °C for 3 h afforded **2** together with a single phosphorus-containing product, Scheme 1.8 (top). This new product, **6**, is characterized by a singlet in the ^{31}P NMR spectrum at –80 ppm. This diphosphine product was isolated in 33% yield as a colorless solid by filtration through a plug of alumina, extraction from the column, and selective crystallization. This double Diels-Alder adduct of P_2 crystallizes on a mirror plane in the space group $P2_1/m$ and its structure was determined crystallographically, Figure 1.13. The tetracyclic structure of **6** exhibits a cofacial pair of C=C π bonds and is analogous to oligocondensed bicyclo[2.2.2]octenes that have been studied as examples of laticyclic conjugation.[91,92] It is speculated that this conjugation results in the observed stereoselectivity of the trapping reaction.[93] This reaction likely occurs in two steps: (1) transfer of P_2 to the first 1,3-cyclohexadiene molecule generating unobserved intermediate 2,3-diphosphabicyclo[2.2.2]octa-2,5-diene, and (2) $[4+2]$ cycloaddition of this intermediate to the second molecule of 1,3-

cyclohexadiene with *endo* stereoselectivity.[94,95] The trapping can also be carried out with 2,3-dimethylbutadiene to afford a bicyclic diphosphine with a ^{31}P NMR chemical shift of –52 ppm.[96]

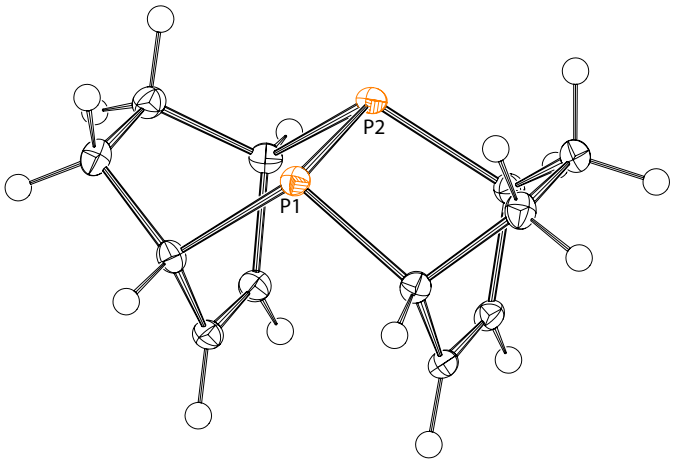

Figure 1.13. Thermal ellipsoid plot (50% probability) of **6**.

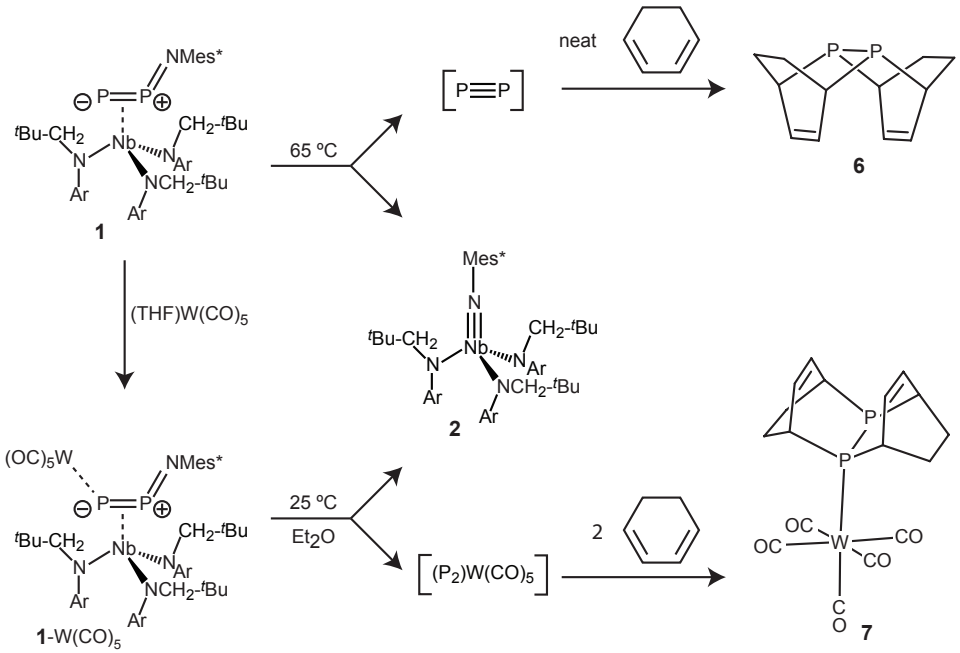

Scheme 1.8. The putative P_2 and $(P_2)W(CO)_5$ intermediates can be trapped with cyclohexadiene. The reaction with the $(P_2)W(CO)_5$ species requires only stoichiometric diene, while trapping the unsupported P_2 fragment proceeds efficiently only in neat diene solvent.

1.5.2 Kinetics of P_2 Elimination in the Presence of Diene

The product diphosphine isolated by thermolysis of **1** in 1,3-cyclohexadiene is consistent with the proposed mechanism wherein P_2 is eliminated into solution before reaction with the diene. If

this mechanism is operative, then there should be no effect of diene concentration on the rate of elimination from **1**. While initial studies suggested that there was a non-productive equilibrium reaction between **1** and 1,3-cyclohexadiene at very high concentrations of diene, it now appears that this was the result of a reaction with impurities in the diene (see Appendix B). Using freshly and carefully distilled 1,3-cyclohexadiene, **1** can be dissolved in diene without any signs of a new product by ^{31}P or ^{1}H NMR. The kinetics for the first-order decomposition of **1** were measured in C_6D_6 over a range of 1,3-cyclohexadiene concentrations from 0 M to 9.6 M (neat) at 50 °C using ^{1}H NMR spectroscopy. At each concentration, first-order behavior was maintained and the rate constants show no dependence on the diene concentration, Figure 1.14. This observation is consistent with elimination of P_2 into solution prior to reaction with diene. However, a rate-determining, unimolecular rearrangement of **1** prior to a bimolecular reaction with diene cannot be ruled out.

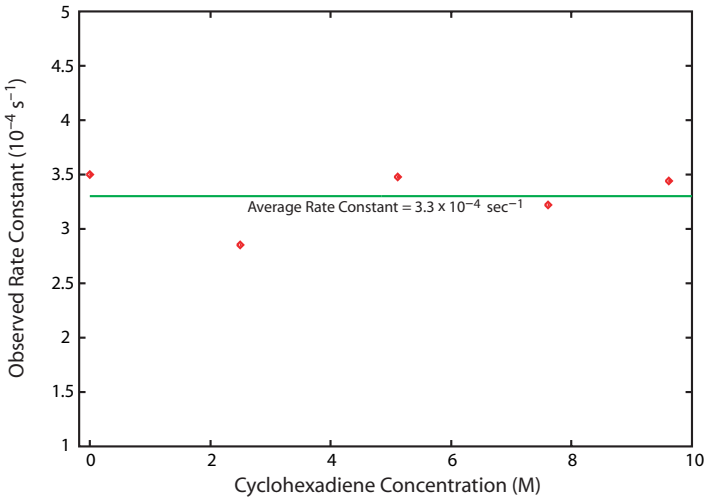

Figure 1.14. Observed rate constants for P_2 loss from **1** at 50 °C over a range of 1,3-cyclohexadiene concentrations with C_6D_6 as co-solvent.

1.5.3 Reactions of Cyclohexadiene and Cyclopentadiene with the Putative $(P_2)W(CO)_5$ Intermediate

The above results demonstrated that **1** serves as a source of P_2 synthons in the synthesis of polycyclic diphosphines from dienes. This suggested the possibility that **1**-$W(CO)_5$ might similarly serve as a source of $(P_2)W(CO)_5$ synthons. Additionally, the stabilizing effect of coordinating the reactive P_2 molecule to a metal fragment was expected to give $(P_2)W(CO)_5$ a longer lifetime in solution than P_2. This property could then make $(P_2)W(CO)_5$ more amenable to trapping in high yields.

When a stoichiometric amount of cyclohexadiene was added to an Et_2O solution of *in situ* generated **1**-$W(CO)_5$, fragmentation of the latter proceeded as normal at 22 °C. Accompanying

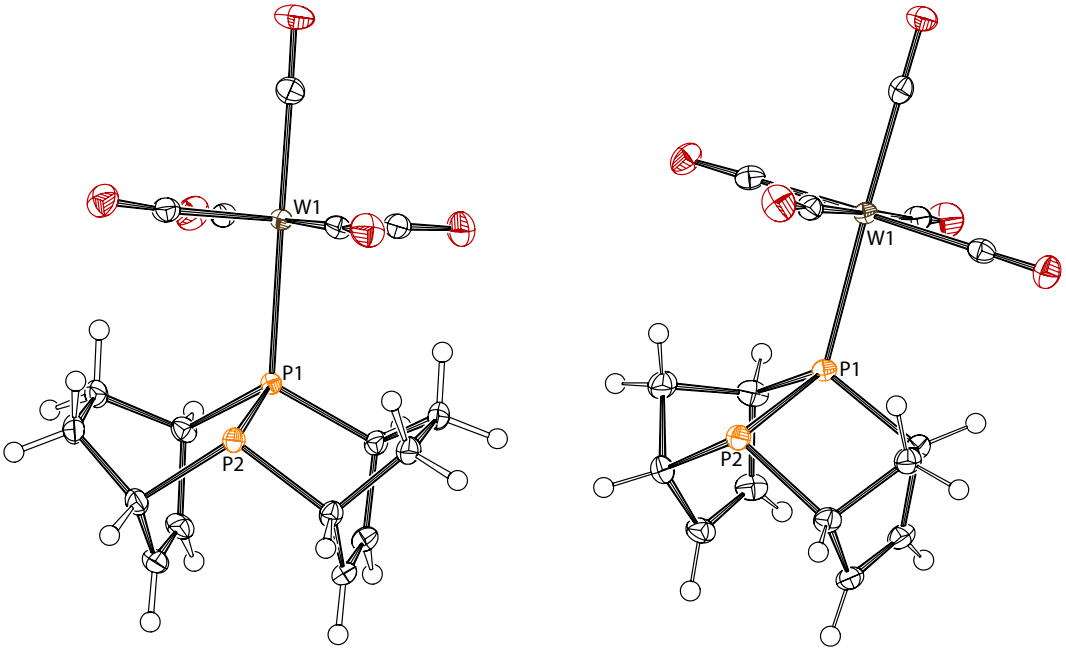

(a) (b)

Figure 1.15. Thermal ellipsoid plots (50% probability) of (a) **7** and (b) **8**.

the production of imido **2** was the product of $(P_2)W(CO)_5$ uptake by 2 equivalents of the diene, $(OC)_5W(P_2)(C_6H_8)_2$, **7**, Scheme 1.8 (bottom). This product displays two ^{31}P NMR resonances, at –34 and –84 ppm, each a doublet with $^1J_{PP}$ = 340 Hz. The downfield resonance also displays ^{183}W satellites with $^1J_{WP}$ = 230 Hz, indicating that this nucleus bears the $W(CO)_5$ group. The conditions used to generate **7** differ from those used for the P_2 trapping described above not only in the lower temperature required, but also in the fact that mere stoichiometric amounts of diene suffice for efficient trapping; this is in contrast to the neat solutions in diene that are required for trapping the unstabilized P_2. Given the more mild conditions that can be employed to release the $(P_2)W(CO)_5$ fragment, the easily dimerized cyclopentadiene could also be used to capture this intermediate and generate $(OC)_5W(P_2)(C_5H_6)_2$, **8**. X-ray diffraction studies on both **7** and **8** revealed polycyclic structures with cofacial π bonds, consistent with the secondary orbital interactions discussed in Section 1.5.1. These structures are depicted in Figure 1.15.

In characterizing the products of trapping $(P_2)W(CO)_5$ with dienes, electron-impact mass spectral data were obtained. The data show a rich fragmentation pattern for $(OC)_5WP_2(C_6H_8)_2$ that is displayed in Figure 1.16. Present in this mass spectrum are ions that correspond to loss of one and two equivalents of diene, as well as successive loss of carbonyl units from $W(CO)_5$. Included prominently among the fragments is the cation $[(P_2)W(CO)_5]^+$.

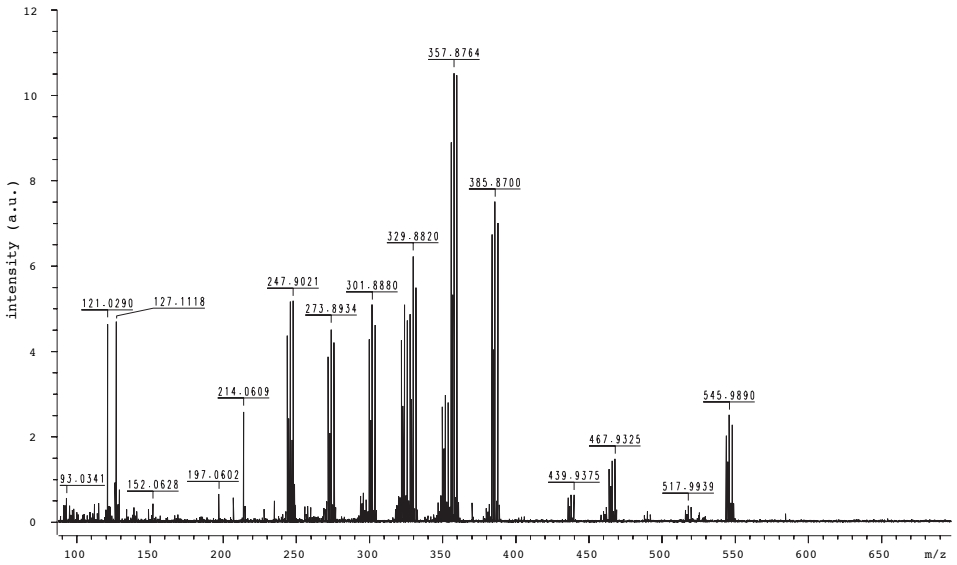

Figure 1.16. The electron impact mass spectrum of $(OC)_5WP_2(C_6H_8)_2$ reveals many fragments. Ion, m/z: $[(OC)_5WP_2(C_6H_8)_2]^+$, 545.998; $[(OC)_4WP_2(C_6H_8)_2]^+$, 518.00; $[(OC)_5WP_2(C_6H_8)]^+$, 565.94; $[(OC)_4WP_2(C_6H_8)]^+$, 437.94; $[(P_2)W(CO)_5]^+$, 385.87; $[(P_2)W(CO)_4]^+$, 357.87; $[(P_2)W(CO)_3]^+$, 329.88; $[W(CO)_5]^+$, 323.92; $[(P_2)W(CO)_2]^+$, 301.89; $[(P_2)W(CO)]^+$, 273.89; $[(P_2)W]^+$, 245.90 amu/*e*.

1.5.4 Kinetics of $(P_2)W(CO)_5$ Loss in the Presence of 1,3-Cyclohexadiene

To test the hypothesis that $(P_2)W(CO)_5$ is in fact an intermediate in the reactions that generate **7** and **8** from **1**-$W(CO)_5$, the kinetics of $(P_2)W(CO)_5$ loss from **1**-$W(CO)_5$ were measured. According to the mechanism implied by Scheme 1.8, the transformation of **1**-$W(CO)_5$ to **2** is expected to be first-order in **1**-$W(CO)_5$ and independent of the concentration of 1,3-cyclohexadiene. Figure 1.17 shows a representative kinetic trace of this transformation monitored at 10 °C, as measured by ^{1}H NMR integration of the methylene resonances for **1**-$W(CO)_5$ and **2**. These data are consistent with a first-order process with rate constant $k = 2 \times 10^{-4}$ s^{-1}. The rate constant was also measured as a function of diene concentration over a wide range, and the observed rate constants display no trend over a concentration range of 0 to *ca*. 3 M cyclohexadiene, Figure 1.18.

1.6 Probing Diphosphorus Chemistry with Ethylenebis(triphenylphosphine)platinum

While the solution-phase chemistry of P_2 is rare, the P_2 unit is a relatively common ligand in coordination complexes.[97] In probing the chemistry of a potential P_2 intermediate, metal complexes of P_2 are thus attractive targets. The availability of ethylenebis(triphenylphosphine)platinum has made this complex an attractive reagent for facile reactions with element-phosphorus π bonds, such as those in diphosphenes and phosphaalkynes.[98–101] As a trap for the P_2-containing

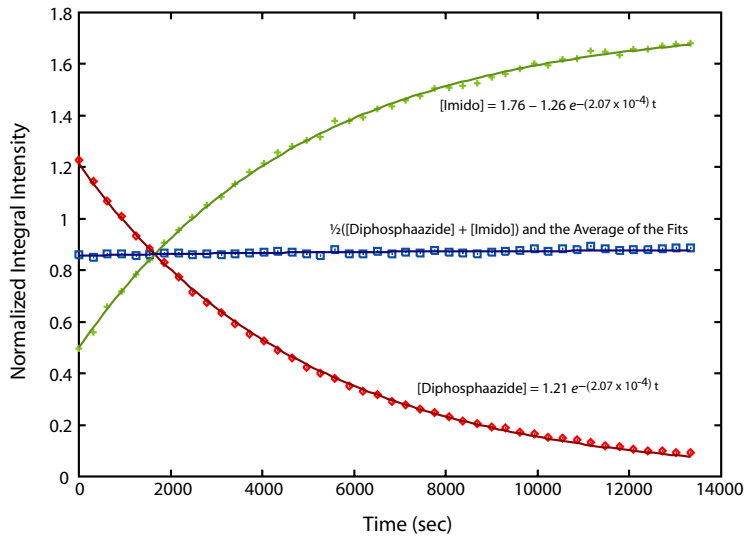

Figure 1.17. Kinetic profile for $(P_2)W(CO)_5$ loss at 10 °C in toluene-d_8. Best-fit lines and equations are provided, along with the average concentration of the two species.

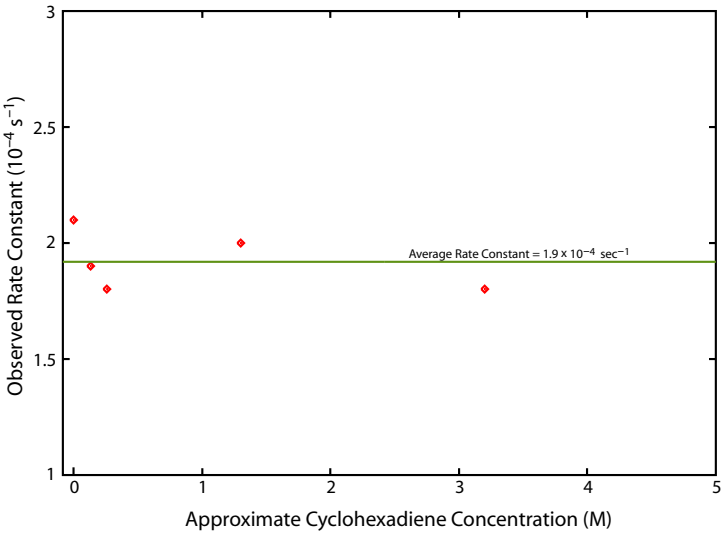

Figure 1.18. Observed rate constants for $(P_2)W(CO)_5$ loss from **1**-$W(CO)_5$ at 10 °C over a range of 1,3-cyclohexadiene concentrations with toluene-d_8 as co-solvent.

intermediates generated from diphosphaazide complexes **1** and **1**-$W(CO)_5$, this reagent was expected to afford species analogous to the diphosphorus complexes of Ni and Pt bisphosphines that are unsupported by a metal-metal bond. These complexes have previously been synthesized from tetrakis(trimethylsilyl)diphosphine by elimination of Me_3SiCl from metal dichloride precursors, Scheme 1.9.[102,103] It is noteworthy that the reaction between $(C_2H_4)Pt(PPh_3)_2$ and P_4 has also been studied and that it does not generate the diphosphorus complex.[104]

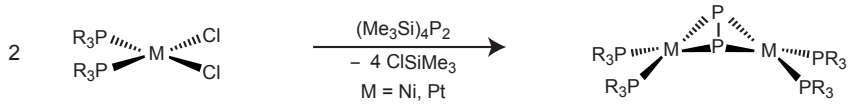

Scheme 1.9. Synthesis of $(P_2)[M(PR_3)_2]_2$ (M = Ni, Pt) from tetrakis(trimethylsilyl)diphosphine as reported by Schäfer.[102,103]

1.6.1 Platinum Insertion into the P−P Bond of (Mes*NPP)Nb(N[$CH_2{}^tBu$]Ar)$_3$

In an attempt to trap as a platinum complex the unstabilized P_2 molecule that is hypothesized to be formed in the thermal fragmentation of **1**, a one-to-one mixture of **1** and the low-valent platinum species $(C_2H_4)Pt(PPh_3)_2$ was prepared in benzene at 22 °C. However, upon mixing an immediate color change from red-orange to a dark maroon-brown ensued. Analysis by ^1H and ^{31}P NMR spectroscopy revealed that PPh_3 and a new product, **9**, are generated with half an equivalent of **1** remaining. Addition of a second equivalent of $(C_2H_4)Pt(PPh_3)_2$ to the reaction mixture resulted in complete conversion to **9**, Scheme 1.10. Based on the stoichiometry of this reaction it was inferred that two equivalents of Pt had coordinated to the diphosphaazide ligand, which likely took on an η^1 geometry based on the large downfield chemical shift of 543 ppm observed for one of the phosphorus nuclei, Figure 1.20. Also identified by its chemical shift, as well as its distant ^{195}Pt satellites, was a Pt-bound PPh_3 ligand: δ = 30.8 ppm, J_{PtP} = 5574 Hz. The remaining multiplet resonance at 337 ppm was attributed to the Mes*NP-derived phosphorus. To determine the exact nature of **9**, a single-crystal X-ray diffraction study was performed on a triclinic crystal of this complex. This structural study revealed that the P−P bond in **1** had been cleaved, with formation of a bond between two three-coordinate Pt centers in a planar Pt_2P_2 diamond core, Figure 1.19. The two phosphorus atoms that comprise this core are both 3-coordinate, distinguishing this structure from other P-bridged Pt(I)–Pt(I) bonded species which contain 4-coordinate, tetrahedral phosphinido (R_2P) bridges.[103,105–107] The Pt−Pt bond length of 2.6490(13) Å and the planarity at each Pt center—the sum of the angles are 358.7° around Pt1 and 359.8° around Pt2—are consistent with the assignment as a Pt(I)/Pt(I) bond. The Nb−P bond length of 2.2704(29) Å is consistent with formulation of this unit as a multiply-bonded niobium phosphinidene.[43,108] The occurrence of this

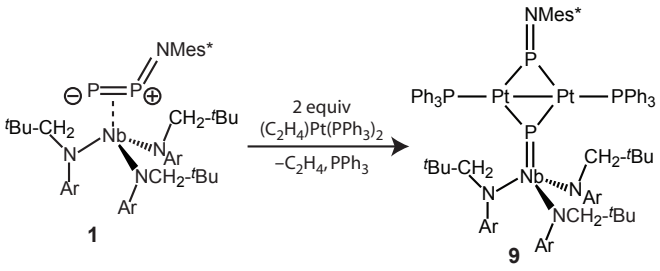

Scheme 1.10. Synthesis of $Mes^{*}NP(PtPPh_3)_2PNb(N[CH_2{}^tBu]Ar)_3$ (**9**).

direct reaction between **1** and the platinum ethylene complex precluded further use of the latter as a probe for the putative P_2 intermediate.

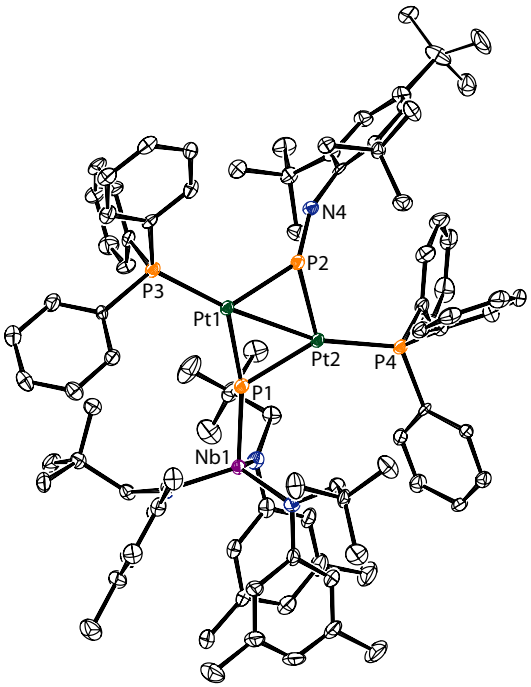

Figure 1.19. Thermal ellipsoid plot (50% probability) of **9** with hydrogen atoms omitted for clarity.

1.6.2 Electrochemistry of a Pt−Pt Bond

The Pt−Pt bond of **9** was probed electrochemically in 0.2 M THF solutions of $[Bu_4N][PF_6]$. The cyclic voltammogram of **9** shows no active electrochemical species upon the first cathodic scan out to –1800 mV (vs. Fc/Fc^{+}, $Fc = Fe(C_5H_5)_2$). The reverse anodic scan results in an irreversible oxidation at E_{pa} = 670 mV. Following this oxidation event and scanning cathodically, an irreversible reduction event is observed at E_{pc} = –1180 mV, Figure 1.21a. The species with events at 670 and –1180 mV are both observed upon repeated scanning from this point, and increasing the scan rate

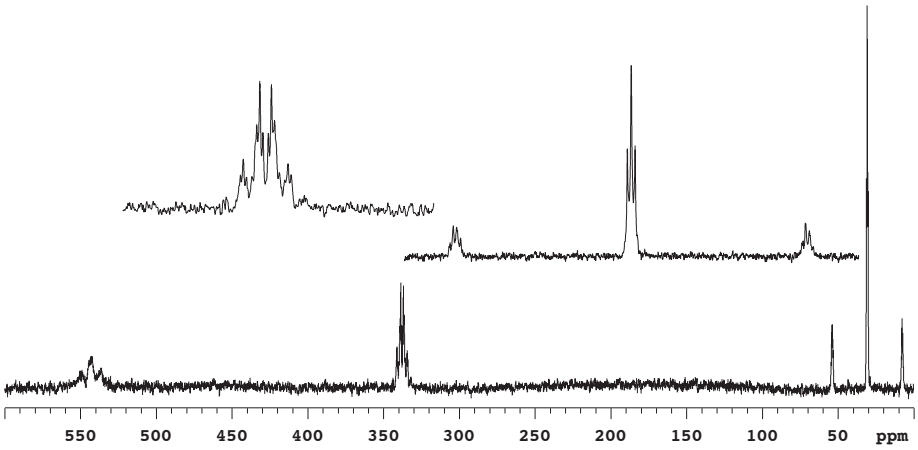

Figure 1.20. ^{31}P NMR spectrum (C_6D_6, 121.5 MHz, 20 °C) of **9**.

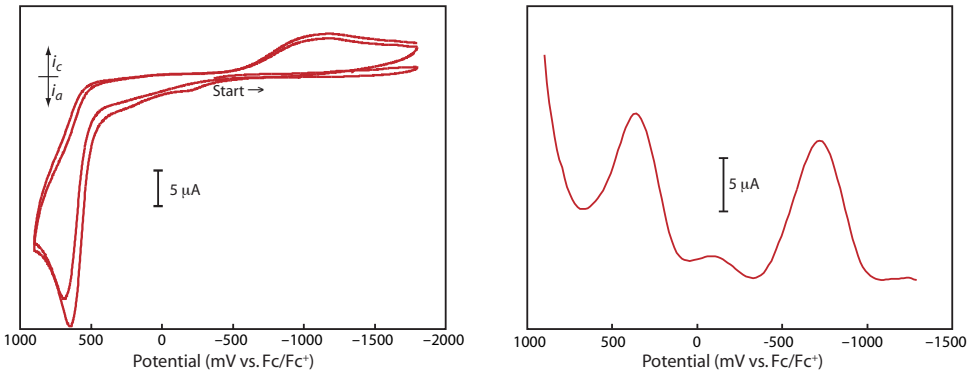

(a) Cyclic voltammogram of **9** **(b)** Differential pulse voltammogram of **9**

Figure 1.21. Electrochemical data on **9** in 0.2 M $[Bu_4N][PF_6]$ in THF as supporting electrolyte. (a) The CV of **9** is consistent with oxidative cleavage and reductive reformation of the Pt−Pt bond. (b) The two events in the DPV corroborate the CV data.

does not change the irreversibility of either process. The differential pulse voltammogram shows the same two redox events when the scan is started at 900 mV and continued through –1300 mV, Figure 1.21b. If the pulse sequence is instead started at –1300 mV and continued in the anodic direction, only the oxidation event is observed. All of the behavior is consistent with electrochemical oxidative cleavage of the Pt−Pt bond by the removal of two electrons, resulting in a species that can be reduced back to the Pt−Pt bonded complex by the sequential reinsertion of two electrons. The broadness of the reduction wave can be attributed to slow electron transfer kinetics that likely result from the bond-forming process. Similar reactions have recently been modeled by Geiger and co-workers studying formation and cleavage of the Re−Re bond in $[Cp(CO)_3Re]_2^{2+}$, though in this case the bonds are cleaved upon reduction.[109]

1.6.3 Synthesis of $(OC)_5W(P_2)[Pt(PPh_3)_2]_2$

The direct reaction of **1** with $(C_2H_4)Pt(PPh_3)_2$ precluded its use as a probe for the intermediacy of P_2 generated from **1**. The insertion reaction to form **9** presumably stems from the coordinating ability of **1**. Accordingly, insertion chemistry leading to products analogous to **9** was not expected to be a problem for **1**-$W(CO)_5$: the coordination of $W(CO)_5$ to the α phosphorus should shut down the pathway for direct reaction with $(C_2H_4)Pt(PPh_3)_2$. Accordingly, addition of $(C_2H_4)Pt(PPh_3)_2$ to an *in situ* generated solution of **1**-$W(CO)_5$ affords no rapid reaction between the starting materials, as observed by NMR spectroscopy. After stirring the mixture for 2 h, over which time **1**-$W(CO)_5$ converts to **2**, analysis by ^{31}P NMR spectroscopy revealed the formation of a new product, Scheme 1.11. This new complex, **10**, displays multiplet ^{31}P NMR resonances at 25.0 ppm and 27.3 ppm, each with ^{195}Pt satellites, Figure 1.23a. The ^{195}Pt NMR spectrum displays a triplet of triplets at –4963 ppm with J_{PtP} = 3510 and 340 Hz. These data are consistent with the formation of the product in Scheme 1.11 if migration of the $W(CO)_5$ unit between termini of the P_2 bridge allows for C_{2v} symmetry on the NMR timescale (*vide infra*).

The structure of **10** was determined by X-ray diffraction using a crystal grown from toluene and 2.5 equivalents of toluene were found to co-crystallize with **10** in the monoclinic $P2_1/n$ lattice. The structure of **10** displays the expected "butterfly" geometry with the $(P_2)W(CO)_5$ unit bridging two Pt centers in a $\mu^2;\eta^2$, η^2-fashion; the remainder of each square planar Pt coordination sphere is occupied by two triphenylphosphine ligands, Figure 1.22. In the solid state, the $W(CO)_5$ unit binds to a single phosphorus atom at a distance of 2.6235(7) Å. The P−P bond length of 2.1222(10) Å is considerably shorter than a P−P single bond (*cf.* 2.21 Å in P_4), indicating that a significant degree of multiple bonding remains despite coordination by two reducing metal centers. The average Pt−P−Pt angle across the bridge is 91° and the angle between the two PtP_2 planes is 106°, consistent with complexation by Pt to the set of orthogonal π-systems in $(P_2)W(CO)_5$.

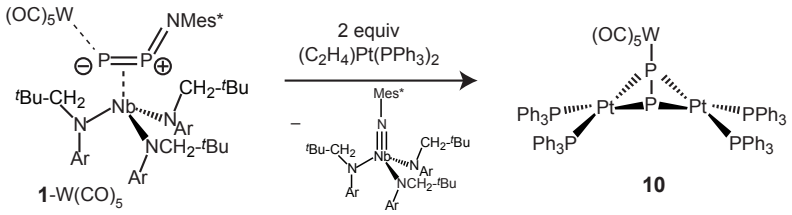

Scheme 1.11. Synthesis of **10** via trapping of the putative $(P_2)W(CO)_5$ intermediate.

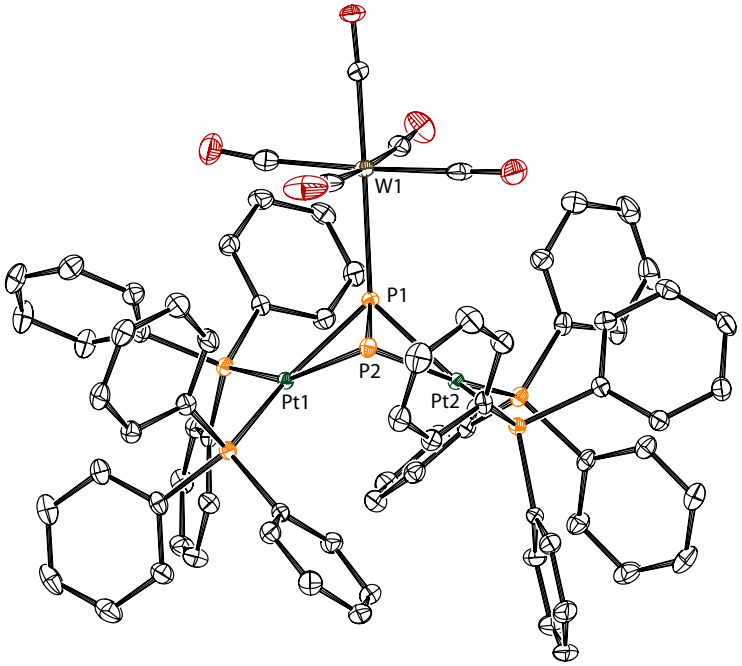

Figure 1.22. Thermal ellipsoid plot (50% probability) of **10** with hydrogen atoms omitted for clarity.

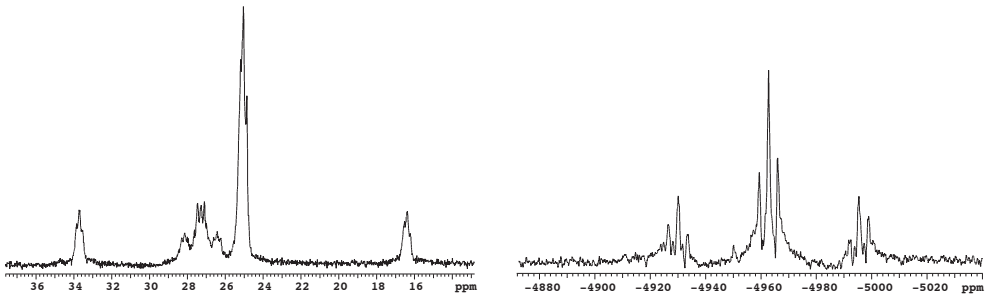

Figure 1.23. (a) ^{31}P NMR spectrum (C_6D_6, 202 MHz, 20 °C) of **10** displays only two phosphorus environments. (b) ^{195}Pt NMR spectrum (C_6D_6, 195 MHz, 20 °C) of **10** displays a triplet of triplets, consistent with bonding to two sets of two equivalent phosphorus nuclei on the NMR timescale.

1.6.4 Mobility of $W(CO)_5$ units across the P−P bond of $(OC)_5WP_2[Pt(PPh_3)_2]_2$

The observation of only two ^{31}P resonances in the NMR spectrum of **10** can be explained by a fluxional process in which the $W(CO)_5$ unit moves back and forth between the two phosphorus atoms of the diphosphorus ligand at room temperature. This process would result in C_{2v} symmetry on the NMR timescale and give chemical equivalence to the two atoms of the P_2 unit, and also to all four PPh_3 ligands. A variable-temperature ^{31}P NMR experiment showed that at low temperatures (< 200 K) the motion of the $W(CO)_5$ unit could be frozen out, resulting in two sets of PPh_3 resonances and two signals with a large PP coupling constant (J_{PP} = 450 Hz) attributed to the μ-$P_2(WO)_5$ unit. Dynamic motion of a $W(CO)_5$ moiety between termini of a μ-P_2 ligand has been observed previously for $W_2Cp_2(CO)_4[\mu;\eta^2$-$P_2W(CO)_5]$.[110] Two possible mechanisms for this isomerization are:

(A) De-coordination of the phosphorus from the $W(CO)_5$ followed by inter- or intra-molecular trapping, or

(B) Migration of the $W(CO)_5$ along the incompletely reduced π bond in the diphosphorus unit and onto the adjacent phosphorus.

Mechanism B is favored based in part on the fact that an analogous isomerization does not occur for Diels-Alder adducts of P_2, where the diene can be considered to have completely reduced the P−P π bond. Mechanism A is also disfavored because this isomerization is observed even in weakly-coordinating solvents (*e.g.*, C_6D_6) that would afford little stabilization to a free $W(CO)_5$ intermediate. Moreover, addition of excess PPh_3 to a benzene solution of **10** does not result in scavenging of the $W(CO)_5$ unit and formation of $(\mu$-$P_2)[Pt(PPh_3)_2]_2$. Mechanism A is also inconsistent with the observation that substitution reactions of phosphine ligands on $M(CO)_5$ fragments are in general only facile under photolytic conditions.[83,111] These combined facts suggest that intramolecular mechanism B is the operative pathway for exchange of the $W(CO)_5$ group.

1.6.5 Kinetics of $(P_2)W(CO)_5$ Trapping by $(C_2H_4)Pt(PPh_3)_2$

The kinetics of the reaction forming **2** from **1** in the presence of $(C_2H_4)Pt(PPH_3)_2$ to generate **10** were also investigated. The decomposition of **1**-$W(CO)_5$ in the presence of $(C_2H_4)Pt(PPh_3)_2$ was monitored by ^1H NMR spectroscopy at 10 °C in the presence of 2.5 equivalents of the platinum ethylene complex. This first-order process was found to have the same rate constant, 2×10^{-4} s^{-1}, as observed previously for the decomposition of **1**-$W(CO)_5$ either by itself or in the presence of cyclohexadiene, Figure 1.24. This finding supports the hypothesis that the fragmentation of **1**-$W(CO)_5$ to release $(P_2)W(CO)_5$ occurs prior to any interactions between platinum (or diene) and the diphosphorus unit.

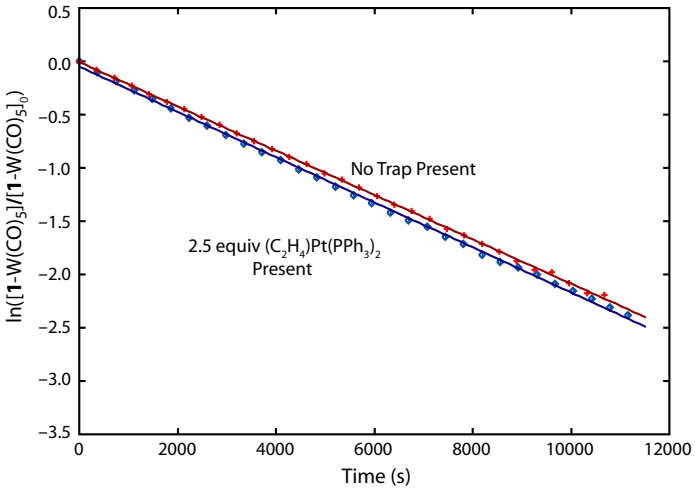

Figure 1.24. First order kinetic traces for the loss of $(P_2)W(CO)_5$ from **1**-$W(CO)_5$ in the presence and absence of $(C_2H_4)Pt(PPh_3)_2$ in toluene-d_8 at 10 °C.

1.6.6 Attempted Mixed Trapping of $(P_2)W(CO)_5$

It was seen that $(P_2)W(CO)_5$ will take up two equivalents of either an organic diene or a platinum(0) bisphosphine fragment. These observations suggest the possibility of generating a mixed trapping product where $(P_2)W(CO)_5$ reacts with one equivalent of platinum and one equivalent of diene to form a coordinated cyclic *Z*-diphosphene. In an attempted synthesis of such a molecule, **1**-$W(CO)_5$ was allowed to fragment in the presence of (1,3-cyclohexadiene)$Pt(PPh_3)_2$: no products incorporating the diene were observed in the NMR spectra of the product mixture. In an additional experiment, **1**-$W(CO)_5$ was allowed to fragment in the presence of 0.75 equivalents of $(C_2H_4)Pt(PPh_3)_2$ and 10 equivalents of 1,3-cyclohexadiene. This procedure resulted in nearly exclusive formation of the known products **6** and **10**; additional resonances in the ^{31}P NMR spectrum of the crude reaction mixture were very minor. These results can be explained by very rapid reactions of the intermediates $(P_2)W(CO)_5$ and $(OC)_5W(P_2)Pt(PPh_3)_2$ with $(C_2H_4)Pt(PPh_3)_2$ relative to any reactions with 1,3-cyclohexadiene. The bis-diene trapping product **6** is then formed only after the platinum ethylene complex is consumed. This observation implies that $(P_2)W(CO)_5$ has a discerning reactivity that could be exploited in future work to learn about its properties and perhaps even address its existence as a discrete intermediate.

1.7 Addition of P_2 to Neutral Terminal Phosphide Complexes

The efforts to define a solution-phase chemistry of P_2-containing intermediates under readily achieved laboratory conditions have been hindered by the large excess required of the trapping reagent, or by direct reactions between potential trapping reagents and the P_2-eliminating complex. To further test the mechanistic hypothesis that P_2 and $(P_2)W(CO)_5$ are reactive, transient

intermediates in the reactions that form imido **2** from diphosphaazide complexes **1** and **1**-$W(CO)_5$, a reactant class for trapping the putative P_2 and $(P_2)W(CO)_5$ intermediates was targeted that was capable of fulfilling the following criteria:

(A) The trap should not react directly with **1** or **1**-$W(CO)_5$

(B) **1** and **1**-$W(CO)_5$ should exhibit unimolecular fragmentation rate constants that are independent of the identity or concentration of the trap

(C) The trap should be an efficient one, such that it could be employed in stoichiometric quantities

(D) The trap should be capable of reacting to completion with P_2 in a 1:1 ratio

Satisfying these criteria would present an important contrast with the diene traps and with the $(C_2H_4)Pt(PPh_3)_2$ molecule, which have complicated the kinetic analysis, reacted directly with **1**, or had to be used in large excess for efficient P_2 incorporation into the double Diels-Alder product in the cases where the supporting $W(CO)_5$ fragment was absent.

It was expected that terminal metal phosphide complexes, as exemplified by $P{\equiv}Mo(N[^iPr]Ar)_3$, **11**, would satisfy the four criteria A–D articulated above. Such species were attractive candidates because the reaction between P_2 and $P{\equiv}ML_n$ was expected to afford MP_3 tetrahedra, or viewed in another way, the *cyclo*-P_3 moiety as a complexed ligand. Terminal metal phosphides were expected to engage in such reactivity with the ostensible P_2 intermediate because of the paired, high-lying, orthogonal π-orbitals and low-lying π* orbitals of the M≡P bond.[67] The organometallic analog of this transformation is the reaction between a terminal alkylidyne and an alkyne, which, in addition to forming metallacyclobutadienes,[112–114] can sometimes result in the formation of η^3-cyclopropenyl complexes.[115–118] Notably, the trapping of P_2 by M≡P triple bonds has been considered as a possible mechanism for *cyclo*-P_3 complex formation in the course of P_4 activation by metal complexes (see also Section 2.6).[119]

Additionally, several *cyclo*-P_3 complexes have been reported in the literature and they are often thermally stable. Most of these were synthesized via white phosphorus (P_4) activation;[120–130] a few have also been assembled from the reactions between bridging-P_2 complexes and the P_1 synthons PCl_3 and PCl_5.[131] A cluster with a terminal (*cyclo*-P_3)Fe unit has been isolated from the reaction of $FeCl_2$, $LiCp^*$ and $P_7(SiMe_3)_3$.[132] The retrosynthetic analysis of *cyclo*-P_3 complexes outlined above suggests that the simple combination of a P≡P triple bond with an M≡P triple bond would provide a synthesis of these species that is complementary to those previously explored.[133]

However, terminal metal phosphides remain rare, with well-characterized examples reported only for the metals W, Mo, and Nb.[43,90,134–139] Of these, both a terminal phosphide and a *cyclo*-P_3 complex with the same ancillary ligands exist only for one system, namely, the terminal phosphide $P{\equiv}Mo(N[^iPr]Ar)_3$, **11**, and its related *cyclo*-P_3 complex $(P_3)Mo(N[^iPr]Ar)_3$, **12**-Mo.[119,137] The specific choice of supporting ligands with which the latter two molecules are decorated, while bulky enough to support a terminal phosphide complex, provides a steric accessibility that allows for the

formation of the pseudo-octahedral *cyclo*-P_3 complex. As a reaction partner for P_2, this terminal phosphide **11** thus seemed ideal.

1.7.1 P_2 Trapping by P≡Mo(N[^{i}Pr]Ar)$_3$ and P≡W(N[^{i}Pr]Ar)$_3$

When the molybdenum terminal phosphide **11** and the diphosphaazide complex **1** are mixed at 20 °C, no direct reaction is observed by ^{31}P and ^{1}H NMR spectroscopies. However, when diphosphaazide complex **1** was thermolyzed at 75 °C in the presence of 1.7 equivalents of **11** and the reaction mixture was assayed by ^{31}P and ^{1}H NMR spectroscopy, signatures attributed to the *cyclo*-P_3 complex **12**-Mo were observed (*e.g.*, ^{31}P NMR, δ = –185 ppm), Scheme 1.12. Under these conditions the trapping is efficient, giving *ca.* 75% yield of the *cyclo*-P_3 complex. Moreover, owing to its poor solubility in alkane solvents, **12**-Mo was readily isolated from reaction mixtures containing only 1 equivalent of **11** in 37% yield. This is the first reaction in which a stoichiometric amount of trapping reagent has been sufficient for efficient P_2 transfer from **1** to a substrate molecule.

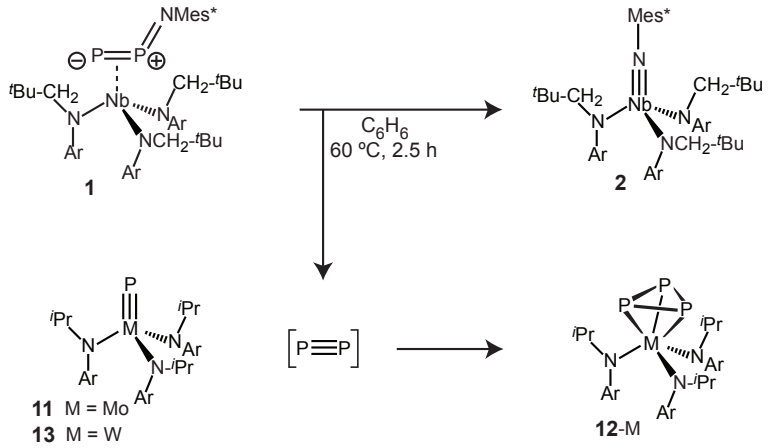

Scheme 1.12. Synthesis of *cyclo*-P_3 complexes (P_3)M(N[^{i}Pr]Ar)$_3$ (**12**-M) via trapping of the putative P_2 intermediate.

The efficient solution-phase transfer of P_2 from **1** to the molybdenum phosphide complex **11** as a synthesis of the *cyclo*-P_3 complex **12**-Mo served as proof of principle for this methodology. To expand this methodology to previously unknown *cyclo*-P_3 complexes, the molecule (P_3)W(N[^{i}Pr]Ar)$_3$ was targeted.[v] This particular *cyclo*-P_3 complex had not been obtained previously in part due to the fact that a potential precursor, W(N[^{i}Pr]Ar)$_3$, has remained elusive. Using P_2 trapping chemistry, the recently reported P≡W(N[^{i}Pr]Ar)$_3$, **13**, could serve as the precursor complex.[138] Indeed, **13** reacts in an analogous fashion to the molybdenum complex **11**:

[v]It should be noted that under conditions similar to those that proved successful for *cyclo*-P_3 formation atop the isopropyl anilide platforms, the terminal phosphide of molybdenum with a more sterically encumbering *tert*-butyl anilide ligand set, P≡Mo(N[^{t}Bu]Ar)$_3$, does not yield a *cyclo*-P_3 complex. Lack of *cyclo*-P_3 complex formation in this case is attributed to prohibitive steric constraints.

when 1 equivalent of **13** was heated with **1** at 65 °C for 2 h, $(P_3)W(N[^iPr]Ar)_3$, **12**-W, was produced in *ca.* 35% yield, as judged by ^{31}P and ^1H NMR spectroscopy, Scheme 1.12. Unfortunately, **12**-W was not able to be efficiently separated from residual $P{\equiv}W(N[^iPr]Ar)_3$ starting material and the co-product niobium imido **2**. The ^{31}P NMR chemical shift for**12**-W is located at –230 ppm, 50 ppm upfield of that for the molybdenum analogue. This shift is consistent with both the better back-bonding ability of the more reducing W center and with spin-orbit effects.[140] Similar trends in chemical shift have been observed upon going from Rh to Ir and from Pd to Pt for [(*cyclo*-P_3)M(triphos)]$^{n+}$ (n = 0 or 1; triphos = $H_3CC(CH_2PPh_2)_3$) complexes.[141]

1.7.2 Kinetics of P_2 Capture by Phosphide Complexes

The rate constant for the fragmentation of **1** was measured in the presence and absence of **11** and found to be independent of the concentration of **11**, remaining constant at $2.5(5) \times 10^{-4}$ s^{-1} at 50 °C in C_6D_6, Figure 1.25. These data are consistent with the working hypothesis that intramolecular fragmentation of **1** is rate-determining and leads to free P_2 as a reactive transient in solution, thus making it available for trapping by suitable reagents.

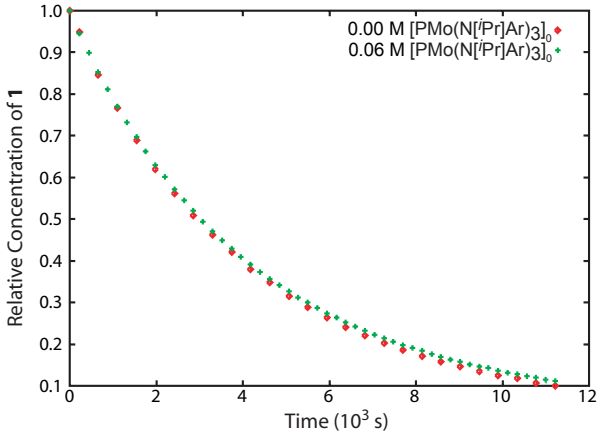

Figure 1.25. The kinetic profile of P_2 elimination in the presence of $PMo(N[^iPr]Ar)_3$ is identical to that in the absence of the bulky phosphide complex at 50 °C in C_6D_6.

1.7.3 $(P_2)W(CO)_5$ Trapping by $P{\equiv}Mo(N[^iPr]Ar)_3$ and $P{\equiv}W(N[^iPr]Ar)_3$

The reactions between the putative $(P_2)W(CO)_5$ intermediate and the M≡P triple bonds of terminal metal phosphides were also investigated as a potential rational, well-defined, and high-yield route to $W(CO)_5$-coordinated *cyclo*-P_3 complexes. When **1**-$W(CO)_5$ was allowed to fragment at 20 °C in the presence of **11** or **13**, formation of the red complexes $(OC)_5W(P_3)M(N[^iPr]Ar)_3$ (M = Mo, W), **14**-M, resulted. These complexes were isolated by repeated recrystallization from Et_2O/*n*-pentane at –35 °C in 50–60% yield; several crystallizations are necessary to afford complete separation from

co-product **2**, thus resulting in a decreased yield relative to the *ca*. 95% yield at which they are formed.

At 20 °C, molecules **14**-M (M = Mo, W) display magnetically equivalent P nuclei as a broadened signal in their ^{31}P NMR spectra. The presence of only one signal is attributed to a rapid migration of the $W(CO)_5$ unit around the *cyclo*-P_3 ring. A variable-temperature ^{31}P NMR experiment was used to confirm this assignment, and at low temperatures three inequivalent ^{31}P environments are observed for **14**-W, Figure 1.26.[vi] That the $W(CO)_5$ unit does not dissociate from the P_3 ring in these molecules was supported by the presence of a quartet ($^2J_{CP}$ = 12 Hz) for the axial carbonyl in the ^{13}C NMR spectrum of $(OC)_5W(P_3)Mo(N[^i Pr]Ar)_3$ at 20 °C. Similar migratory behavior has been studied thoroughly in the systems of $(OC)_5M'P_3M$(triphos).[142,143] In that work, a metallotropic shift along a P–P edge, as opposed to across the P_3 face, was invoked based on orbital considerations, calculations, and mechanistic studies. This migration can also be regarded as a 1,3-sigmatropic shift. This migratory $W(CO)_5$ behavior is related to the behavior observed for the μ-P_2 platinum complex **10**, and seems general to $W(CO)_5$ moieties complexed to P atoms engaged in π bonds that are not completely reduced by their complexation to one or more other metal centers.

The structure of **14**-W was determined by X-ray crystallography using a red, triclinic crystal grown from an Et_2O/*n*-pentane solution. The molecular structure exhibits the expected geometry, with a *cyclo*-P_3 ring η^3-coordinated to the tungsten trisanilide platform (W1) and η^1 to the $W(CO)_5$ unit (W2), Figure 1.27. The distance from W1 to the centroid of the P_3 ring is 2.167 Å, with individual W1–P distances of 2.4648(16), 2.5158(16) and 2.5201(16) Å, where the shortest distance is that to P1, which also bears the pendant $W(CO)_5$ unit. The P–P interatomic distances within the ring that include P1 are also shorter, 2.151(2) and 2.150(2) Å, than the one that does not, 2.182(2) Å. The shorter bonds to P1 are consistent with the rehybridization at P1 caused by its being 4-coordinate and resulting in more *s* character in all of its bonds.

1.7.4 Kinetics of $(P_2)W(CO)_5$ Elimination

The first-order rate constant for fragmentation of **1**-$W(CO)_5$ was measured in the presence of terminal phosphide complex **11** and was found to match that measured in the presence of either no trap, 1,3-cyclohexadiene, or ethylenebis(triphenylphosphine)platinum. These data all are consistent with the interpretation that $(P_2)W(CO)_5$ is released into solution prior to being consumed by M≡P triple bonds.

[vi] Three ^{31}P environments are observed instead of the two expected for a C_s-symmetric $(P_3)W(CO)_5$ moiety because at low temperature a C_3, propeller-like conformation of the anilide ligands is locked out. The combination of the C_3- and C_s-symmetric components yields a C_1-symmetric structure.

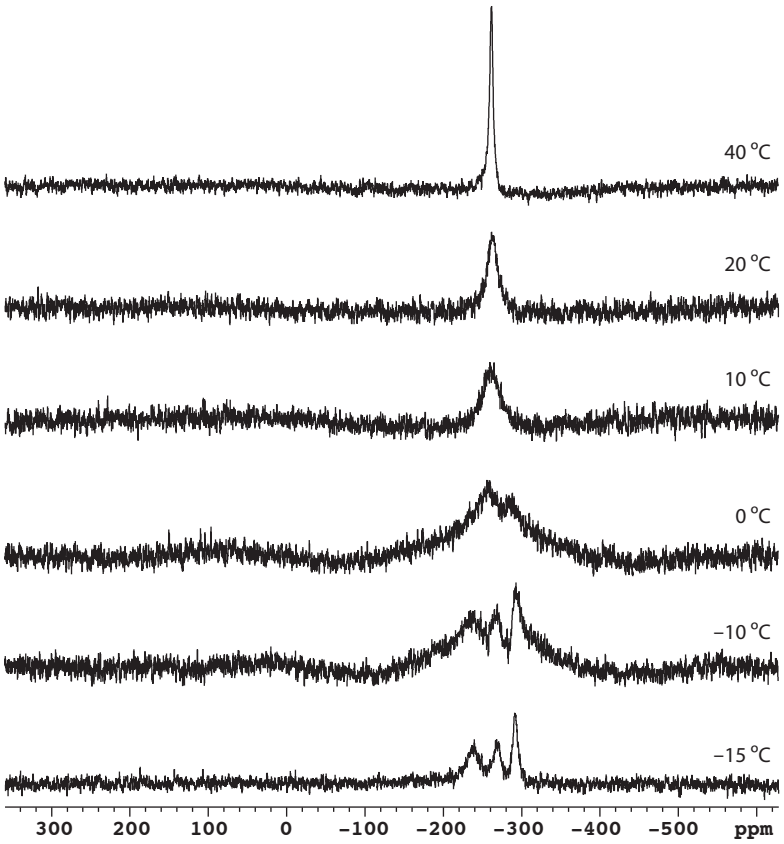

Figure 1.26. Variable-temperature ^{31}P NMR spectra of **14**-W showing the locking out of $W(CO)_5$ migration below 0 °C.

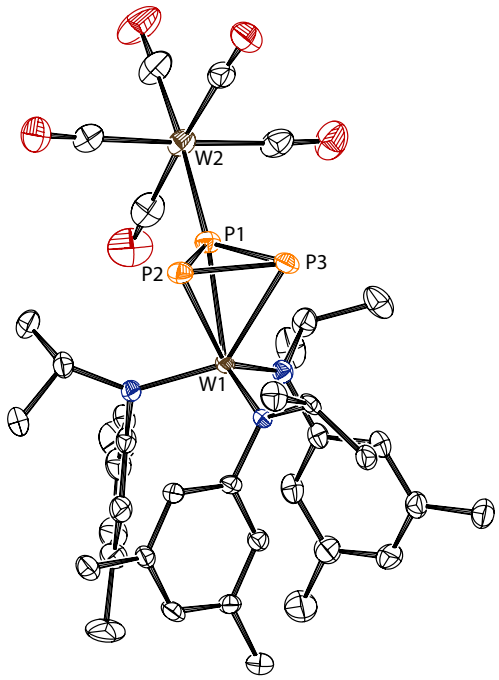

Figure 1.27. Thermal ellipsoid plot (50% probability) of **14**-W with hydrogen atoms omitted for clarity.

1.8 Addition of P_2 to Anionic Niobium Phosphide Complexes

1.8.1 P_2 and $(P_2)W(CO)_5$ Trapping by $[P{\equiv}Nb(N[CH_2{}^tBu]Ar)_3]^-$

The above section focused on the transfer of P_2 to terminal phosphide complexes **11** and **13** as a probe for the intermediacy of P_2 and $(P_2)W(CO)_5$, as well as for the synthesis of novel *cyclo*-P_3 complexes. The reactivity of the anionic niobium terminal phosphide is rich compared to the neutral molybdenum and tungsten species, and so there was also interest in synthesizing anionic *cyclo*-P_3 complexes to study their potentially rich chemistry. Correspondingly, the transfer of P_2 from **1** to the anionic niobium terminal phosphide $[P{\equiv}Nb(N[CH_2{}^tBu]Ar)_3]^-$, **3**, was pursued. Here the thermal sensitivity of **3** results in less clean reaction mixtures, but co-thermolysis of **1** and $[(Et_2O)Na][$**3**$]$ at 50 °C results in formation of $[(P_3)Nb(N[CH_2{}^tBu]Ar)_3]^-$, **15**, which was identified by its upfield ^{31}P NMR chemical shift of –223 ppm. Addition of 2 equivalents of 12-crown-4 to the reaction mixture precipitates this product as its bis(12-crown-4)sodium salt, which can be isolated following addition of *n*-pentane in 32% yield. This compound has a remarkably sharp ^{31}P resonance (δ = –183 ppm, $\Delta\nu_{\frac{1}{2}}$ = 10 Hz) for a niobium-bound phosphorus, a property that can be attributed to low *s*-character in the Nb−P bonds, consistent with a π-complexation model for the P_3 unit binding to the metal center.[141] This observation is also in agreement with the very small couplings to ^{183}W, ^{195}Pt, and ^{103}Rh observed for other *cyclo*-P_3 complexes.[126,141] Higher-order effects, such as a highly symmetrical charge distribution around niobium, may also be partly responsible.[144]

The synthesis of $W(CO)_5$-capped *cyclo*-P_3 complexes was also expanded to the anionic phosphide **3**. The sodium salt of **3** was added to an Et_2O solution of *in situ* generated **1**-$W(CO)_5$ and the mixture was allowed to stir for several hours. After this time the anionic, $W(CO)_5$-coordinated *cyclo*-P_3 complex $[(OC)_5W(P_3)Nb(N[CH_2{}^tBu]Ar)_3]^-$, **16**, was identified in the reaction mixture by NMR spectroscopy. The solubility properties of this compound proved a hindrance to its isolation, so it too was converted to its bis(12-crown-4)Na salt, which displayed limited solubility in *n*-pentane and allowed for the isolation of $[(12\text{-crown-4})_2Na][(OC)_5W(P_3)Nb(N[CH_2{}^tBu]Ar)_3]$ in 75% yield by precipitation from Et_2O/*n*-pentane. As for the neutral complexes **12**-M, only one broad, upfield ^{31}P NMR resonance (δ = –203 ppm) is observed for **16** at 20 °C.

1.8.2 $(P_2)W(CO)_5$ Trapping by $[(OC)_5WP{\equiv}Nb(N[CH_2{}^tBu]Ar)_3]^-$

The $W(CO)_5$-capped niobium phosphide anion, **4**, retains many of the properties of the terminal phosphide itself and can act as a terminal phosphide surrogate. One example of its role in this capacity is in the generation of **1**-$W(CO)_5$ through its nucleophilic reactivity. Metal phosphide complexes that are coordinated to $W(CO)_5$ through their phosphido ligands have also been seen to retain their ability to engage in cycloaddition reactions at the M≡P bond (see also Section 1.10).[80,81] The ability of the Nb≡P triple bond in **4** to act as a trap for the ostensible $(P_2)W(CO)_5$ intermediate was investigated in an operationally simple experiment: addition of Mes*NPCl to *two*

equivalents of **4**. The first equivalent of **4** would serve to generate **1**-$W(CO)_5$, which at 20 °C generates the $(P_2)W(CO)_5$ molecule that in turn is trapped by the second equivalent of **4**. This preparation does generate the doubly $W(CO)_5$-coordinated, anionic, *cyclo*-P_3 complex of niobium $[\{(OC)_5W\}_2(P_3)Nb(NCH_2[^t Bu]Ar)_3]^-$, **17**, which can be isolated as its sodium salt in 83% yield following simple workup and extraction of the neutral by-products, Scheme 1.13. The ^{31}P NMR spectrum again shows a single broad, upfield resonance (δ = –216 ppm), indicating dynamic behavior of the two $W(CO)_5$ units.

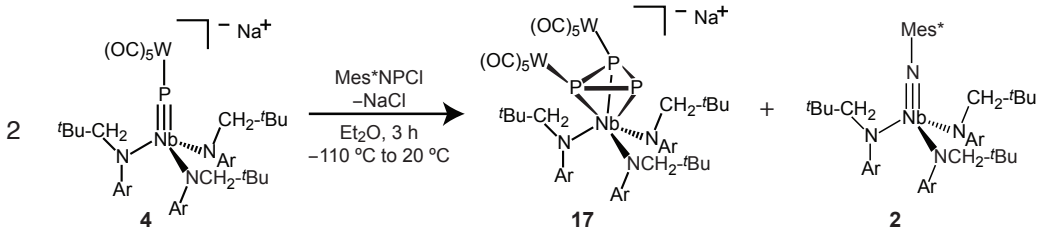

Scheme 1.13. Synthesis of **17** via trapping of the putative $(P_2)W(CO)_5$ intermediate by the anionic phosphide complex $[(OC)_5WPNb(N[CH_2{}^t Bu]Ar)_3]^-$.

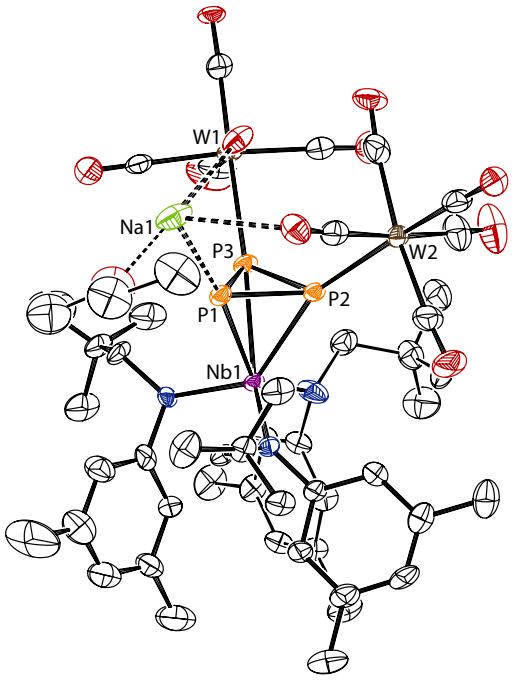

Figure 1.28. Thermal ellipsoid plot (50% probability) of $[(Et_2O)Na][\mathbf{17}]$ with hydrogen atoms omitted for clarity. The coordination sphere of sodium is completed by intermolecular contacts to a carbonyl unit from each of two adjacent molecules of **17** (shown in Figure 1.29).

The structure of $[(Et_2O)Na][\{(OC)_5W\}_2(P_3)Nb(N[CH_2{}^t Bu]Ar)_3]$ was determined by X-ray crystallography from a red-orange, triclinic crystal grown from benzene solution at 22 °C in the presence of trace Et_2O. The solid-state structure shows the expected geometry for the NbP_3 core,

with a closely associated sodium cation. The structure of the anionic core with an included sodium ion is presented in Figure 1.28. The distance from Nb1 to the centroid of the P_3 ring is 2.278 Å, and the individual Nb1–P distances vary from 2.560(2) to 2.665(2) Å. The lengthening of the M−P bond relative to those in $(OC)_5W(P_3)W(N[^iPr]Ar)_3$ can be attributed to anionic nature of **17**. The P−P interatomic distances around the ring vary from 2.164(2) to 2.188(2) Å, and the sodium ion resides at a distance of 3.026(4) Å from P1. The coordination sphere of the sodium ion is made up of the uncapped phosphorus of the *cyclo*-P_3 unit, two intramolecular carbonyl oxygen contacts, one carbonyl oxygen contact involving each of two neighboring molecules, and a molecule of Et_2O. This coordination results in an extended 1D chain that runs through the crystal, with benzene molecules of crystallization filling voids in the lattice, Figure 1.29. This tendency to form a coordination polymer is likely responsible for the favorable solubility properties that allow for easy isolation of [Na][**17**].

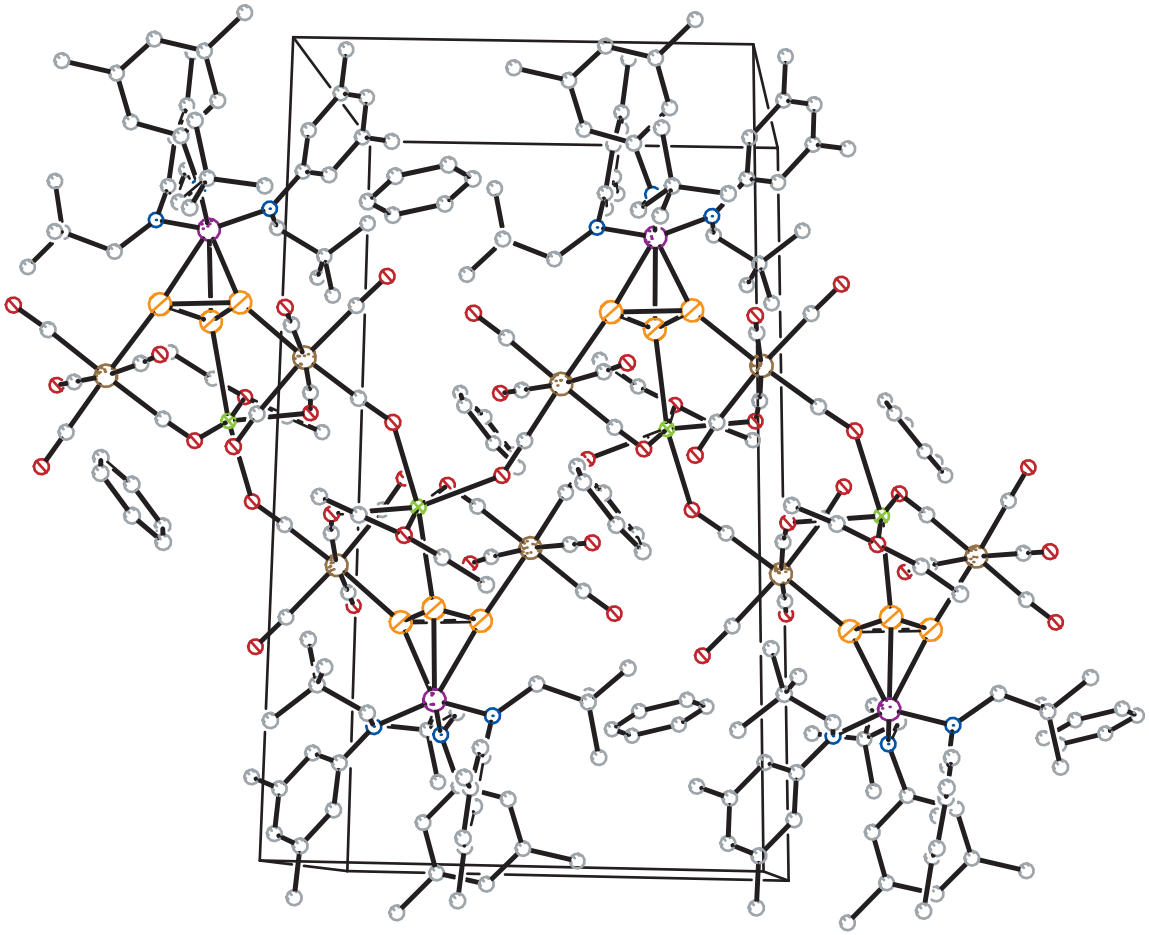

Figure 1.29. A packing diagram shows that in the solid state molecules of **17** form an extended 1-D chain. This chain is linked by etherated sodium ions and gaps in the lattice are filled with benzene molecules. Atoms are colored as follows: niobium, violet; phosphorus, orange, tungsten, brown; oxygen, red; nitrogen, blue; carbon, gray; sodium, green.

1.9 On the Mechanism of *cyclo*-P_3 Formation

The formation of *cyclo*-P_3 complexes from the ostensible reaction of a P≡P triple bond with an M≡P triple bond is related to the organometallic analog, where metallacyclobutadiene complexes form from alkylidynes and alkynes as intermediates in alkyne metathesis reactions.[112–114] There is a contrast, however, in that for phosphorus *cyclo*-P_3 isomers are preferred over triphosphametallacyclobutadienes. Notably, Stephan and co-workers have reported the only example of a metallatriphosphacyclobutadiene complex, the anionic $[Cp^*_2Zr(\kappa^2\text{-}P_3)]^-$, while *cyclo*-$P_3$ complexes are far more common.[145–147] The direct formation of a *cyclo*-P_3 complex could proceed in concerted fashion along an idealized C_s reaction coordinate with orthogonal approach of the two triple bonds, though this is an orbital symmetry forbidden process. Alternatively, a potentially lower energy pathway can be considered wherein a triphosphametallacyclobutadiene intermediate is formed through a more facile suprafacial $[2+2]$ cycloaddition that is made symmetry allowed by the symmetry of the *d* orbitals involved in the bonding. This latter reaction could then be followed by a rapid intramolecular isomerization to yield the transition-metal *cyclo*-P_3 complex. Interestingly, Schrock and co-workers have shown that the introduction of a base to certain metallacyclobutadiene complexes can cause their isomerization to *cyclo*-propenyl complexes.[117,118]

These two pathways have been considered computationally for the analogous organometallic reaction and one such study predicts the suprafacial $[2+2]$ addition to be the lower energy route.[148] Mechanisms for the interconversion of the two isomers have also been considered on a variety of metal platforms for the organometallic analog and similar principles will apply to the P_3 systems.[149] The relative thermodynamic stabilities of metallacyclobutadiene and metallatetrahedrane (*cyclo*-propenyl) complexes have also been studied, but the phosphorus analogs have been neglected.[150,151]

Quantum chemical calculations were carried out on the κ^2 and η^3 isomers of the model complex $(P_3)Mo(N[Me]Ph)_3$ to better understand the relative energies of the two isomers and the reactants, $PMo(N[Me]Ph)_3$ and P_2. Optimized geometries and the energies of the *cyclo*-P_3 and triphosphametallacyclobutadiene isomers relative to free P_2 and the terminal metal phosphide are shown in Figure 1.30. The optimized geometry of the metallacyclic isomer displays a distorted square-pyramidal geometry at the metal and a planar triphosphametallacyclobutadiene ring with distances indicative of alternating single and double bonds. The optimized distances are: Mo1–P1, 2.254 Å; P1–P2, 2.211 Å; P2–P3 2.030 Å, P3–Mo1, 2.542 Å. It is easy to envisage how this structure might result from the in-plane approach of the P2–P3 and Mo1–P1 vectors. In fact, this square pyramidal structure is quite reminiscent of structures along the reaction path calculated by Zeigler and co-workers for the analogous organometallic reaction.[148] The bond length alternation seen here was not present in the minimum energy structure for the organometallic analogue, but was rather seen along the reaction pathway. This is consistent with the general observation that delocalized π bonding is less preferred as we descend the periodic table.[6]

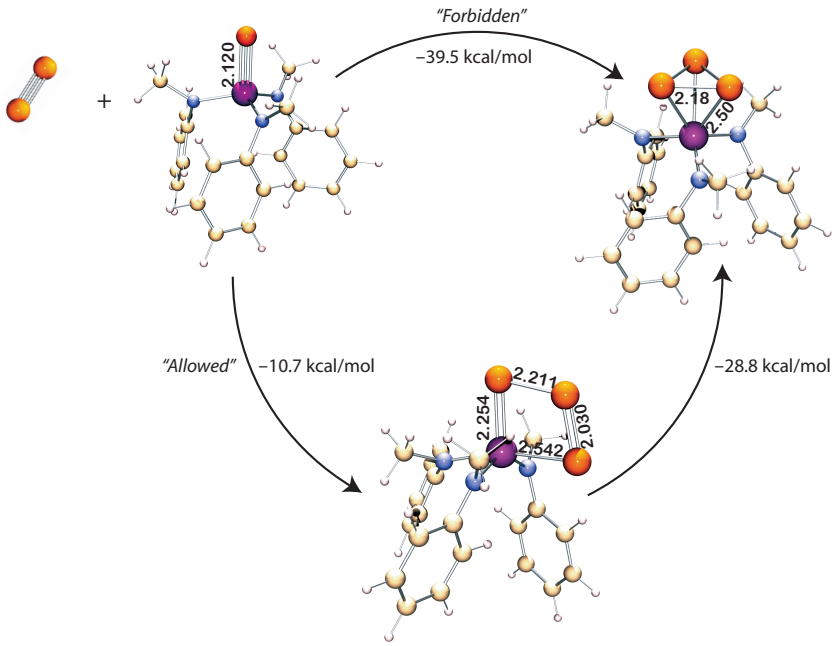

Figure 1.30. Two limiting mechanisms for the formation of a *cyclo*-P_3 complex are illustrated with the model complex $(P_3)Mo(N[Me]Ph)_3$. The top pathway proceeds through a formally "forbidden" cycloaddition with a perpendicular approach of the P≡P bond to the M≡P bond, while the bottom pathway goes first through a formally allowed cycloaddition where the P≡P and M≡P bonds are parallel. Key distances are indicated in Å. Atoms are colored as follows: molybdenum; violet; phosphorus, orange; nitrogen, blue; carbon, tan; hydrogen, pink.

Based on these geometries, energies, and the same orbital symmetry arguments that hold for the organometallic system, it is tempting to suggest that triphosphametallacyclobutadienes are formed as intermediates in the capture of solution-phase P_2. This would then be followed by a rearrangement at the metal to form the *cyclo*-P_3 complex with release of *ca.* 30 kcal/mol of energy. We cannot, however, rule out the direct formation of the *cyclo*-P_3 complex via the perpendicular approach of P_2 to the M≡P bond, and despite the higher barrier expected for this latter reaction, it may be the preferred pathway.[148]

1.10 Phosphaalkynes as a P_2 Model: Synthesis of a *cyclo*-CP_2 Complex

In the previous sections, triply bonded P_2 is invoked as a likely intermediate in the *cyclo*-P_3 forming reactions. An experimental model for this process could be provided by a reaction in which a terminal phosphide complex combines with an established and directly observable triply-bonded phosphorus molecule. Phosphorus has been dubbed the "carbon copy" because of similarities in the reactivity of molecules where RC units are replaced by the isolobal P atom.[9] Thus, a phosphaalkyne could serve in the role of P_2 as a reaction partner for a metal terminal phosphide to yield a *cyclo*-CP_2 complex. In 1985, Becker *et al.* reported evidence for the reaction between ^{t}BuCP and *in situ* generated (^{t}BuO)$_3$W≡P, and this work was followed up by Scheer and co-workers.[80,81,152] In these reactions, the initial products of a simple cycloaddition are unobserved, having reacted further via a 1,3-alkoxide migration to yield the diphosphametallacyclobutadiene complexes (^{t}BuO)P_2C(R)W(O^{t}Bu)$_2$.

At 60 °C in C_6D_6, the molybdenum terminal phosphide **11** and AdC≡P (Ad = 1-adamantyl) react over the course of 3 h to give a new compound with a ^{31}P NMR signal at –249 ppm as the major product. This upfield chemical shift compares well to the analogous *cyclo*-P_3 complex, **12**-Mo, and is consistent with the formation of (AdCP_2)Mo(N[^{i}Pr]Ar)$_3$, **18**, Scheme 1.14. Also present in the reaction mixture was a minor product that displays a pair of doublet ^{31}P resonances at –121 and +571 ppm (J_{PP} = 450 Hz). These signals are consistent with a ligand migration product analogous to those of Scheer and Becker, namely the complex (Ar[^{i}Pr]N)P_2C(Ad)Mo(N[^{i}Pr]Ar)$_2$. The observation that the anilide ligands on the Mo(N[^{i}Pr]Ar)$_3$ platform migrate less readily than the alkoxides of the W(O^{t}Bu)$_3$ moiety is not unexpected.[153,154]

The product **18** was crystallized from toluene/*n*-pentane at –35 °C and an X-ray diffraction study confirmed the formation of the *cyclo*-CP_2 complex, Figure 1.31. The Mo1–P1 and Mo1–P2 distances are 2.4838(8) and 2.4691(7) Å, respectively, while C1 lies 2.1830(19) Å from the metal. The P1–C1 and P2–C1 distances are 1.798(2) and 1.810(2) Å and the P1–P2 distance is 2.1374(9) Å. The relatively short P−P distance can be attributed to the geometric constraints of having a small carbon atom in the three-membered ring. The formation of this product provides clear evidence that

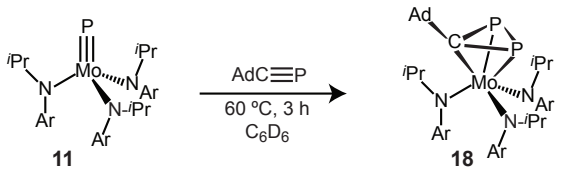

Scheme 1.14. The reaction of AdCP with **11** proceeds analogously to the putative P_2 trapping reaction to afford a *cyclo*-CP_2 complex (**18**).

terminal phosphide complexes are capable of reacting with phosphorus triple bonds to smoothly form the corresponding metallatetrahedrane.

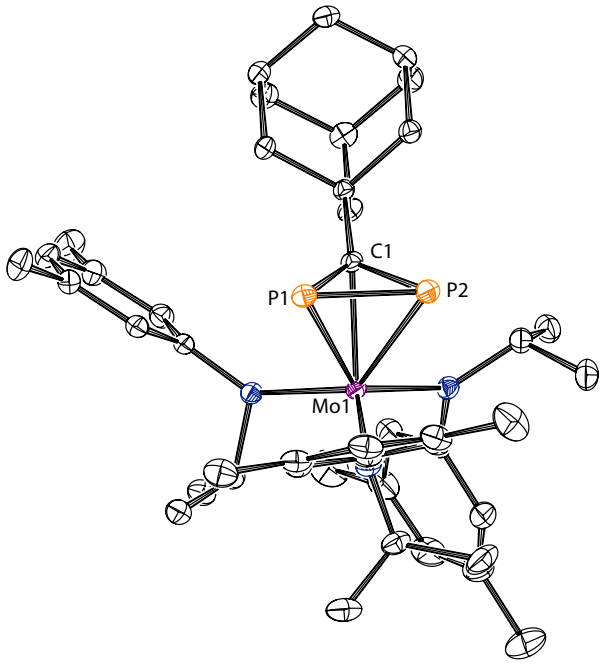

Figure 1.31. Thermal ellipsoid plot (50% probability) of **18** with hydrogen atoms omitted for clarity.

1.11 Conclusions

In this work, strong metal-ligand multiple bonds were used to provide the driving force for the generation of reactive, multiply-bonded intermediates. In particular, the diphosphaazide complex (Mes*NPP)Nb(N[$CH_2{}^t$Bu]Ar)$_3$ has been used as a solution-phase synthon for the diatomic molecule P_2, with the energy requirements being provided by formation of a niobium imido bond. The related $(OC)_5$W(Mes*NPP)Nb(N[$CH_2{}^t$Bu]Ar)$_3$ provides a source of $(P_2)W(CO)_5$ in an analogous reaction. Mechanistic studies suggest that P_2 and $(P_2)W(CO)_5$ may be serving as discrete intermediates in these processes, though neither has been observed directly. Instead, the chemistry of these intermediates has been probed through trapping reactions in which they have served as the P_2 source

in the synthesis of polycyclic diphosphines, μ-P_2 coordination complexes, and *cyclo*-P_3 complexes. In each of these cases, it is the putative $(P_2)W(CO)_5$ intermediate that provides higher yields of the trapping products. The observed higher trapping yields can be attributed to $(P_2)W(CO)_5$ being a longer-lived, less promiscuous intermediate than is the free and unstabilized P_2 molecule.

It is hoped that the methodologies employed here can be applied to related systems for the generation of other reactive species. For example, the generation of AsP containing species has recently been achieved using this method, but the goal of providing a solution-phase source of PN remains outstanding (see Section 4.3).[155] Furthermore, a reengineering of P_2-eliminating molecules that eliminate P_2 from a solid support could be used to provide unambiguous evidence for a free, diatomic intermediate through a "three-phase test."[156]

Independent of whether P_2 and $(P_2)W(CO)_5$ are in fact discrete intermediates, by treating the molecules **1** and **1**-$W(CO)_5$ as synthons for these fragments the syntheses of some interesting P_2-containing molecules were derived. These include polycyclic diphosphines, which represent a potential new class of phosphine ligands for use in organometallic catalysts. As the diene trapping products can be obtained in higher yield when protected by the $W(CO)_5$ group, established deprotection strategies may yet provide more practical routes to uncomplexed diphosphine products.[157,158] Moreover, a rich chemistry for the niobium *cyclo*-P_3 complexes derived from P_2 and $(P_2)W(CO)_5$ has emerged and is the subject of the following chapter.

1.12 Experimental Details

1.12.1 General Considerations

All manipulations were performed in a Vacuum Atmospheres model MO-40M glove box under an atmosphere of purified dinitrogen. Solvents were obtained anhydrous and oxygen-free from a Contour Glass Solvent Purification System, or by analogous methods.[159] Celite 435 (EM Science), 4 Å molecular sieves (Aldrich), and alumina (EM Science) were dried by heating at 200 °C under dynamic vacuum for at least 24 hours prior to use. All glassware was oven-dried at temperatures greater than 170 °C prior to use. Deuterated solvents for NMR spectroscopy were purchased from Cambridge Isotope Labs. Benzene-d_6 and toluene-d_8 were degassed and stored over molecular sieves for at least 2 days prior to use. $CDCl_3$ was distilled off of CaH_2 and stored over molecular sieves. The compounds $PMo(N[^iPr]Ar)_3$,[137] Mes*NPCl,[65] and $(C_2H_4)Pt(PPh_3)_2$[160] were prepared according to literature procedures. $[(Et_2O)Na][PNb(N[CH_2{}^tBu]Ar)_3]$ was prepared by modifications to literature procedures that are described in Appendix A.[42] The complex $PW(N[^iPr]Ar)_3$ was provided by A. R. Fox.[138] Dienes were purchased from Aldrich, distilled from $NaBH_4$, and stored over molecular sieves prior to use. (1,3-cyclohexadiene)$Pt(PPh_3)_2$ was prepared by a modification of a literature procedure reported for (1,3-butadiene)$Pt(PPh_3)_2$.[161] AdCP (Fluka) and $W(CO)_6$ (Strem) were purchased and used as received. ^{15}N labeled Mes*NH_2 (50%^{14}N/50%

^{15}N) was prepared from Na^{15}NNN (Cambridge Isotopes) by the appropriate modification to a literature procedure.[72] NMR spectra were obtained on Varian Mercury 300 or Varian Inova 500 instruments equipped with Oxford Instruments superconducting magnets. ^{1}H NMR spectra were referenced to residual C_6D_5H (7.16 ppm), $CHCl_3$ (7.27 ppm) or C_5D_4HN (8.74 ppm). ^{13}C NMR spectra were referenced to C_6D_6 (128.39 ppm), $CDCl_3$ (77.23 ppm), or C_5D_5N (150.35 ppm). ^{31}P NMR spectra were referenced externally to 85% H_3PO_4 (0 ppm), ^{195}Pt NMR spectra were referenced externally to K_2PtCl_4 in D_2O (–1624 ppm), and ^{15}N NMR spectra were referenced externally to ^{15}NMo(N[^{t}Bu]Ar)$_3$ (845 ppm relative to NH_3 at 0 ppm) in C_6D_6. Elemental analyses were performed by Midwest Microlab, LLC (Indianapolis, Indiana).

1.12.2 Preparation of (η^2-Mes*NPP)Nb(N[CH$_2$^{t}Bu]Ar)$_3$ (1)

This preparation is a modification of one reported previously:[45,96] To a stirring, thawing Et_2O/THF solution (15 mL/2 mL) of [(Et_2O)Na][PNb(NCH$_2$^{t}Bu]Ar)$_3$] (800 mg, 1.0 mmol), a thawing solution of Mes*NPCl (315 mg, 0.97 mmol, 0.97 eq) in Et_2O (3 mL) was added dropwise . Halfway through the addition the solutions were refrozen and the addition was completed upon re-thawing. The reaction mixture was allowed to stir while warming to room temperature over 30 min. Filtration through Celite followed by drying *in vacuo* left a dark red residue, which was extracted with *n*-pentane and filtered through Celite again. This solution was concentrated to *ca*. 3 mL and stored at −35 °C to yield red-orange solids that were collected in several crops (600 mg, 0.60 mmol, 60% yield). ^{1}H NMR (C_6D_6, 500 MHz, 20 °C): δ 7.73 (s, 2H, *m*-Mes*), 6.59 (s, 9H, *o*-, *p*-Ar), 4.11 (s, 6H, NCH_2), 2.12 (s, 18H, ArCH_3), 1.92 (s, 18H, *o*-Mes*), 1.47 (s, 9H, *p*-Mes*), 0.82 (s, 27H, ^{t}Bu) ppm. ^{31}P{^{1}H} NMR (C_6D_6, 121.5 MHz, 20 °C): δ 334 (br d, J_{PP} = 650 Hz), 315 (br d, J_{PP} = 650 Hz) ppm. ^{13}C{^{1}H} NMR (C_6D_6, 125.8 MHz, 20 °C): δ 152.3 (*ipso*-aryl), 150.6 (d, J_{CP} = 35.6 Hz, *ipso*-Mes*), 142.6 (d, J_{CP} = 5.2 Hz, *m*-Mes*), 139.8 (d, J_{CP} = 12.1 Hz, *o*-Mes*), 138.6 (*m*-Ar), 127.6 (*p*-Ar), 124.1 (*o*-Ar), 122.7 (d, J_{CP} = 4.0 Hz, *p*-Mes*), 73.6 (d, J_{CP} = 7 Hz, NCH_2), 37.3 (*o*-*C*(CH$_3$)$_3$ Mes*) 37.1 (CH$_2$*C*(CH$_3$)$_3$), 35.2 (*p*-*C*(CH$_3$)$_3$ Mes*), 33.3 (*o*-C(*C*H$_3$)$_3$ Mes*), 32.4 (*p*-C(*C*H$_3$)$_3$ Mes*), 30.1 (CH$_2$C(*C*H$_3$)$_3$), 21.8 (Ar*C*H$_3$) ppm. Elem. Anal. Calcd for $C_{57}H_{89}N_4NbP_2$: C, 69.49; H, 9.11; N, 5.69. Found: C, 69.26; H, 8.95; N, 5.26. For the ^{15}N-labeled variant: ^{15}N NMR (C_6D_6, 50.6 MHz, 20 °C): δ 250 ($^{1}J_{PN}$= 153 Hz) ppm.

1.12.3 Preparation of [(Et_2O)Na][(CO)$_5$WPNb(N[CH$_2$^{t}Bu]Ar)$_3$] (4)

[(Et_2O)Na][PNb(N[CH$_2$^{t}Bu]Ar)$_3$] (900 mg, 1.13 mmol) and W(CO)$_6$ (400 mg, 1.13 mmol, 1 eq) were mixed as solids, dissolved in THF (5 mL), and stirred together for 18 h. The solvent was removed *in vacuo* and the residue was extracted with Et_2O and filtered through Celite. Recrystallization of the filtrate from Et_2O at −35 °C yielded orange flakes of the product (850 mg, 0.76 mmol, 67% yield). ^{1}H NMR (C_6D_6, 500 MHz, 20 °C): δ 6.87 (s, 6H, *o*-Ar), 6.41 (s, 3H, *p*-Ar), 4.09 (s, 6H, NCH_2), 3.23 (q, 4H, Et_2O), 2.14 (s, 18H, ArCH_3), 1.10 (s, 27H, ^{t}Bu), 1.09 (t,

6H, Et_2O) ppm. $^{13}C\{^1H\}$ NMR (C_6D_6, 125.8 MHz, 20 °C): δ 204.3 (*ax*-CO), 200.8 (*eq*-CO, $^2J_{CW}$ = 120 Hz), 157.8 (*ipso*-Ar), 139.1 (*m*-Ar), 124.0 (*p*-Ar), 121.8 (*o*-Ar), 75.3 (NCH_2), 66.2 (Et_2O), 36.4 ($C(CH_3)_3$), 29.8 ($C(CH_3)_3$), 21.9 ($ArCH_3$), 15.8 (Et_2O) ppm. $^{31}P\{^1H\}$ NMR (C_6D_6, 121.5 MHz, 20 °C): δ 588 (br) ppm. IR (C_6H_6, KBr): $\tilde{\nu}$ 2059, 1982, 1934, 1602 cm^{-1}. Elem. Anal. Calcd for $C_{48}H_{70}N_3NaNbO_6P$: C, 51.67; H, 6.32; N, 3.77. Found (average of 2 runs): C, 51.66; H, 6.42; N, 3.22.

1.12.4 Generation of $(OC)_5W(Mes^*NPP)Nb(N[CH_2{}^tBu]Ar)_3$ (1-$W(CO)_5$)

To a thawing solution of $[(Et_2O)Na][(CO)_5WPNb(N[CH_2{}^tBu]Ar)_3]$ (50 mg, 0.045 mmol) in Et_2O (3 mL) was added a thawing Et_2O (2 mL) solution of Mes*NPCl (14 mg, 0.045 mmol, 1 eq). This solution was stirred for 2 min before the solvent was removed *in vacuo*. The residue was extracted with 1 mL of C_6D_6 and frozen for transport to an NMR probe. ^1H NMR (C_6D_6, 300 MHz, 20 °C): δ 7.67 (s, 2H, *m*-Mes*), 6.60 (s, 3H, *p*-Ar), 6.58 (s, 6H, *o*-Ar), 4.21 (s, 6H, NCH_2), 2.12 (s, 18H, $ArCH_3$), 1.84 (s,18H, *o*-Mes*), 1.50 (s, 9H, *p*-Mes*), 0.81 (s, 27H, ^{t}Bu) ppm. $^{31}P\{^1H\}$ NMR (C_6D_6, 121.5 MHz, 20 °C): δ 285 (br d, $^1J_{PP}$ = 730 Hz), 247 (br d, $^1J_{PP}$ = 730) ppm. The crystal used for the X-ray diffraction study was obtained in an analogous manner, but the extraction was performed with Et_2O and the solution so-obtained was chilled to –35 °C for several days to afford red crystals.

1.12.5 Alternate Generation of $(OC)_5W(Mes^*NPP)Nb(N[CH_2{}^tBu]Ar)_3$

A THF solution (4 mL) of tungsten hexacarbonyl (15 mg, 0.043 mmol) was irradiated with UV light in a Rayonet photoreactor equipped with 16 RPR-2540 bulbs (λ_{max} = 254 nm) for 2 h in a sealed Pyrex tube (50 mL) under static vacuum. The tube was degassed and irradiation was continued for another 24 h. This yellow solution of $(THF)W(CO)_5$ was degassed, cooled to −35 °C and added dropwise to a cold (−35 °C) solution of $(Mes^*NPP)Nb(N[CH_2{}^tBu]Ar)_3$ (40 mg, 0.041 mmol) in THF (2 mL). This solution was immediately dried *in vacuo* and taken up in C_6D_6. Analysis by ^1H and ^{31}P NMR spectroscopy revealed $(OC)_5W(Mes^*NPP)Nb(N[CH_2{}^tBu]Ar)_3$, identified by its spectroscopic features indicated above, in addition to some residual $(Mes^*NPP)Nb(N[CH_2{}^tBu]Ar)_3$ and P_2 elimination product $Mes^*NNb(N[CH_2{}^tBu]Ar)_3$. The ^{31}P NMR spectrum also indicated very small amounts of a separate unidentified product with doublets at −147 and +380 ppm (J_{PP} = 110 Hz).

1.12.6 Preparation of $P_2(C_6H_8)_2$ (*endo, endo*-2,7-diphosphatetracyclo[6.2.2.$2^{3,6}$.$0^{2,7}$]-tetradeca-4,9-diene, 6)

$(Mes^*NPP)Nb(N[CH_2{}^tBu]Ar)_3$ (200 mg, 0.20 mmol) was dissolved in 1,3-cyclohexadiene (2.5 g, 31.2 mmol) and the resulting dark red solution was heated to 65 °C for 3 h. The diene was removed

in vacuo and the residue taken up in *n*-hexane and run down a 7 × 1 cm column of alumina. The column was then washed with CH_2Cl_2 to liberate the diphosphine as a mixture with Mes^*NH_2 and $HN[CH_2{}^tBu]Ar$, both of which were removed by successive extractions from the diphosphine with thawing *n*-pentane and cold hexamethyldisiloxane. Extraction with Et_2O and filtration through Celite removed polycyclohexadiene to yield the diphosphine as an off-white powder upon drying (15 mg, 0.067 mmol, 33% yield). ^{1}H NMR (C_6D_6, 500 MHz, 20 °C): δ 5.12 (m, 2H), 2.69 (m, 2H), 1.08 (m, 2H), 1.33 (m, 2H) ppm. $^{31}P\{^1H\}$ NMR (C_6D_6, 121.5 MHz, 20 °C): δ −80 (s) ppm. $^{13}C\{^1H\}$ NMR (125.8 MHz, C_6D_6, 20 °C): δ 121.5 (*C*=*C*), 28.7 (*pseudo* t, J_{CP} = 18 Hz, *C*P), 24.4 (*pseudo* t, J_{CP} = 11 Hz, *C*H_2) ppm. HRMS-ESI Calcd for $[C_{12}H_{16}P_2 + H^+]$: m/z 223.0807; Found: 223.0807 amu/*e*. Also present in the mass spectrum is a peak at 143.0179 amu/*e* corresponding to loss of one equivalent of cyclohexadiene, $[C_6H_8P_2 + H^+]$.

1.12.7 Preparation of $(OC)_5WP_2(C_6H_8)_2$ (7)

To a thawing solution of $[(Et_2O)Na][(CO)_5WPNb(N[CH_2{}^tBu]Ar)_3]$ (220 mg, 0.195 mmol) in Et_2O (5 mL) was added a thawing Et_2O solution (3 mL) of Mes^*NPCl (64 mg, 0.195 mmol, 1 eq) dropwise. After the addition was complete and precipitate was visible, 1,3-cyclohexadiene (45 μL, 0.46 mmol, 2.2 eq) was added via syringe. Upon stirring for 2 h the color faded from dark red to dark yellow. Removal of the solvent, extraction with toluene and filtration through Celite removed the NaCl by-product. Re-extraction of the product with *n*-hexane and filtration through a 7 × 1 cm column of alumina afforded the niobium imido **2** as a yellow solution. The column was then washed with THF and the washings were dried under dynamic vacuum. The residue was suspended in *n*-pentane, frozen, and upon thawing the desired diphosphine was collected on a frit as an off-white powder in several crops (60 mg, 0.11 mmol, 65% yield). ^{1}H NMR (C_6D_6, 500 MHz, 20 °C): δ 5.19 (td, *J* = 7.8, 4.2 Hz, 1H), 4.80 (td, *J* = 7.7, 3.0 Hz, 1H), 2.53 (m, 1H), 2.33 (m, *J* = 6 Hz, 1H), 1.79 (q, *J* = 11 Hz, 1H), 1.32 (m, 1H), 1.06 (m, 1H) 0.89 (m, 1H) ppm. $^{13}C\{^1H\}$ NMR (C_6D_6, 125.8 MHz, 20 °C): δ 199.1 (dd, $^2J_{CP}$ = 24 Hz, $^3J_{CP}$ = 3 Hz, *ax*-CO), 197.5 (dd, $^2J_{CP}$ = 6.5 Hz, $^3J_{CP}$ = 3 Hz, $^1J_{CW}$ = 125 Hz, *eq*-CO), 125.4 (dd, $^2J_{CP}$ = 9.4 Hz, $^3J_{CP}$ = 2.6 Hz, *C*H), 125.1 (dd,$^2J_{CP}$ = 9.1 Hz, $^3J_{CP}$ = 3.4 Hz, *C*H), 34.0 (s, *C*H_2), 29.5 (dd, $^1J_{CP}$ = 37.0 Hz, $^2J_{CP}$ = 3.5 Hz, P*C*H), 25.6 (d, $^2J_{CP}$ = 7.3 Hz, C*H*$_2$), 23.0 (dd, $^1J_{CP}$ = 21.0 Hz, $^2J_{CP}$ = 3.9 Hz, P*C*H) ppm. $^{31}P\{^1H\}$ NMR (C_6D_6, 121.5 MHz, 20 °C): δ −34 (d, $^1J_{PP}$ = 340 Hz, $^1J_{WP}$ = 230 Hz), −84 (d, $^1J_{PP}$ = 340 Hz) ppm. IR (C_6D_6 solution, KBr plates): $\tilde{\nu}$ 3043 (w), 2937 (w), 2866 (w), 2066 (s) 1972 (m), 1933 (vs) cm^{-1}. HRMS-EI Calcd for $M^{+\cdot}$: m/z 545.998; Found: 545.999. Also present: 465.937, $[W(CO)_5P_2(C_6H_8)]^{+\cdot}$; 385.874, $[W(CO)_5P_2]^{+\cdot}$; 357.889, $[W(CO)_4P_2]^{+\cdot}$; 329.884, $[W(CO)_3P_2]^{+\cdot}$; 323.947, $[W(CO)_5]^{+\cdot}$ amu/*e*; and others, see Figure 1.16.

1.12.8 Preparation of $(OC)_5WP_2(C_5H_6)_2$ (8)

Using a procedure similar to that described above for $(OC)_5WP_2(C_6H_8)_2$, but with cyclopentadiene in place of cyclohexadiene, $(OC)_5WP_2(C_5H_6)_2$ was isolated as off-white crystals following recrystallization from Et_2O/*n*-pentane. ^{1}H NMR (C_6D_6, 500 MHz, 20 °C): δ 4.47 (m, 2H, *H*C=), 4.15 (m, 2H, *H*C=), 2.84 (dm, J_{HP} = 15.4 Hz, 2H, *H*CP), 2.56 (dm, 2H, J_{HP} = 33 Hz), 1.37 (m, 2H, CH_2), 1.03-1.18 (m, 2H, CH_2), ppm. ^{31}P{^{1}H} NMR (C_6D_6, 121.5 MHz, 20 °C): δ −21 (d, $^1J_{PP}$ = 354 Hz, $^1J_{PW}$ = 220 Hz), −97 (d, $^1J_{PP}$ = 354 Hz) ppm. ^{13}C{^{1}H} NMR (125.8 MHz, C_6D_6, 20 °C): δ 197.9 (d, $^2J_{CP}$ = 5.0 Hz, *eq*-CO), 124.1 (m, olefinic), 120.5 (dd, $^2J_{CP}$ = 11.0 Hz, $^3J_{CP}$ = 3.5 Hz, olefinic), 53.5 (d, J_{CP} = 9.4 Hz), 49.7 (t, J_{CP} = 11.5 Hz), 46.8 (dd, $^1J_{CP}$ = 46.5 Hz, $^2J_{CP}$ = 3.6 Hz, H*C*). Note: The *axial* CO residue was not located in the ^{13}C NMR spectrum due to its weak intensity.

1.12.9 Preparation of $Mes^*NP(PtPPh_3)_2PNb(N[CH_2{}^tBu]Ar)_3$ (9)

A red-orange Et_2O solution (7 mL) of $(Mes^*NPP)Nb(N[CH_2{}^tBu]Ar)_3$ (200 mg, 0.20 mmol, 1 eq) was added at 20 °C to an off-white, Et_2O suspension (3 mL) of $(C_2H_4)Pt(PPh_3)_2$ (304 mg, 0.40 mmol, 2.0 eq). The solution rapidly acquired a deep maroon hue and mild gas evolution was observed. Solid precipitate (PPh_3) was observed in the reaction mixture. The solution was allowed to stir for 20 min and then it was filtered through a bed of Celite to remove the precipitate. The maroon filtrate was stripped of solvent *in vacuo*. To the oily residue was added *n*-hexane (5 mL), which was then removed *in vacuo*. The newly formed residue was extracted with *n*-hexane (8 mL) and filtered through Celite to remove residual PPh_3. The dark maroon solution was stored at −35 °C to precipitate the desired product as a brown solid. A small amount of product (20 mg) was isolated by filtration on a frit from this solution. The filtrate was dried, dissolved in toluene and layered with $O(SiMe_3)_2$. After storing at −35 °C for several days, a larger crop (100 mg) was isolated by filtration atop a frit. Subsequent crops were isolated from −35 °C solutions in *n*-pentane/Et_2O. The combined solids were dried *in vacuo* to give a dark maroon-orange powder (220 mg, 0.116 mmol, 58% yield). ^{1}H NMR (C_6D_6, 500 MHz, 20 °C): δ 7.93 (m, 12H, *o*-Ph), 7.38 (s, 2H, *m*-Mes*), 7.06 (m, 18H, *m*,*p*-Ph), 6.67 (s, 6H, *o*-Ar), 6.43 (s, 3H, *p*-Ar), 4.75 (s, 6H, NCH_2), 2.14 (s, ArCH_3), 1.38 (s, 9H, *p*-Mes*), 1.34 (s, 18H, *o*-Mes*), 0.98 (s, 27H, ^{t}Bu) ppm. ^{31}P{^{1}H} NMR (C_6D_6, 202.5 MHz, 20 °C): δ 543 (br pseudo t, Nb*P*), 337 (m, Mes*N*P*), 30.8 (J_{PtP} = 5574 Hz, Pt*P*Ph_3) ppm. ^{13}C{^{1}H} NMR (C_6D_6, 125.8 MHz, 20 °C): δ 152.2 (*ipso*-Ar), 141.7 (d, J_{CP} = 35 Hz, *ipso*-Mes*), 138.2 (*m*-Ar), 137.4 (m, *ipso*-Ph, Mes*), 135.7 (Mes*), 135.3 (Ph), 130.5 (Ph), 129.0 (Ph), 125.2 (*p*-Ar), 121.9 (Mes*), 121.6 (*o*-Ar), 79.6 (NCH_2), 37.7 ($CH_2C(CH_3)_3$), 36.8 (*o*-Mes*), 35.2 (*p*-Mes*), 32.3 (Mes*), 31.9 (Mes*), 30.7 ($CH_2C(CH_3)_3$), 22.2 (ArCH_3) ppm. Elem. Anal. Calcd for $C_{93}H_{119}N_4NbP_4Pt_2$: C, 58.79; H, 6.31; N, 2.95. Found: C, 59.28; H, 6.33; N, 2.44.

1.12.10 Preparation of $(OC)_5W(P_2)[Pt(PPh_3)_2]_2$ (10)

To a thawing, dark orange Et_2O solution (4 mL) of $[(Et_2O)Na][(CO)_5WPNb(N[CH_2{}^tBu]Ar)_3]$ (200 mg, 0.18 mmol) was added dropwise a thawing Et_2O solution (2 mL) of Mes*NPCl (58 mg, 0.18 mmol, 1 eq), affording an immediate color change to dark red. This mixture was allowed to stir for 1 min, and then to it was added a pale yellow THF solution (6 mL) of $(C_2H_4)Pt(PPh_3)_2$ (275 mg, 0.37 mmol, 2.05 eq). This mixture was allowed to stir for 135 min at 22 °C. After this time the solvent was removed *in vacuo* and the residue was extracted with 25 mL of a 2:1 toluene/benzene mixture and filtered through Celite to remove NaCl. The yellow filtrate was dried and then suspended in a 1:1 toluene:*n*-hexane mixture and stored at −35 °C to precipitate the desired product. This yellow powder was isolated on a sintered glass frit and dried *in vacuo* to constant mass (198 mg, 0.11 mmol, 60% yield). ^{1}H NMR ($CDCl_3$, 300 MHz, 20 °C): δ 7.20 (t, J = 9.0 Hz, 12H), 7.06 (t, J = 7.5 Hz, 12H), 6.88 (t, J = 7.5 Hz, 24H) ppm. $^{31}P\{^1H\}$ NMR (toluene-d_8, 202.5 MHz, 20 °C): δ 27.3 (m, J_{PtP} = 340 Hz), 25.0 (m, J_{PtP} = 3510 Hz) ppm. $^{13}C\{^1H\}$ NMR ($CDCl_3$, 75.4 MHz, 20 °C): δ 203.2 (*ax*-CO), 200.1 (*eq*-CO), 135.4 (d, J_{CP} = 43 Hz, *ipso*-Ph), 134.4 (d, J_{CP} = 10 Hz, *o*-Ph), 129.4 (s, *p*-Ph), 127.8 (d, J_{CP} = 10 Hz, *m*-Ph) ppm. $^{195}Pt\{^1H\}$ NMR (THF, 107.1 MHz, 20 °C):δ −4963 (tt, $^1J_{PtPPh_3}$ = 3510 Hz, $^1J_{PtP_2}$ = 340 Hz) ppm. IR (C_6D_6, KBr): $\tilde{\nu}$ 2057, 1924, 1885, 1620 cm^{-1}. Elem. Anal. Calcd for $C_{77}H_{60}O_5P_6Pt_2W$: C, 50.67; H, 3.31. Found: C, 50.84; H, 3.46.

1.12.11 Attempted Displacement of $W(CO)_5$ by PPh_3

$(OC)_5W(P_2)[Pt(PPh_3)_2]_2$ (15 mg, 0.0082 mmol) and PPh_3 (10 mg, 0.038 mmol, 4.6 eq) were dissolved together in a mixture of C_6D_6 (0.5 mL) and CH_2Cl_2 (0.5 mL). A ^{31}P NMR spectrum was acquired and only starting materials were visible. There was no resonance attributable to the P_2 unit in $(\mu\text{-}P_2)[Pt(PPh_3)_2]_2$, which is reported by Schäfer and Binder to be at 99 ppm.[103]

1.12.12 Attempted Mixed Trappings

An Et_2O solution (1 mL) of $[(Et_2O)Na][(CO)_5WPNb(N[CH_2{}^tBu]Ar)_3]$ (20 mg, 0.018 mmol) was frozen and to it was added dropwise a thawing Et_2O solution (1 mL) of Mes*NPCl (5.8 mg, 0.018 mmol, 1.0 eq), affording a color change to dark red. After stirring for 1 min, an orange benzene solution (1 mL) of (1,3-cyclohexadiene)$Pt(PPh_3)_2$, (15 mg, 0.018 mmol, 1. eq) was added, and the resulting mixture was allowed to stir at 22 °C for 1.5 h. After this time, the mixture was filtered through Celite, and the Celite was then washed with benzene (1 mL). The filtrate was stripped to dryness. *n*-Hexane was added and then removed under dynamic vacuum. An NMR in C_6D_6 revealed the presence of imido **2** and phenyl residues, but no olefinic resonances. The ^{31}P NMR showed only some triphenylphosphine and the known **10**.

A thawing Et_2O solution (2 mL) of Mes*NPCl (15 mg, 0.046 mmol, 1.0 eq) was added to a thawing Et_2O solution (3 mL) of $[(Et_2O)Na][(CO)_5WPNb(N[CH_2{}^tBu]Ar)_3]$ (52 mg, 0.046 mmol,

1.0 eq). The mixture immediately took on a dark red hue. A 2:1 Et_2O/C_6H_6 solution (3 mL) of $(C_2H_4)Pt(PPh_3)_2$ (26 mg, 0.023 mmol, 0.75 eq) and 1,3-cyclohexadiene (45 μL, 36 mg, 0.46 mmol, 10 eq) was added to the reaction mixture after 30 s. The mixture was allowed to stir for 2 h at 22 °C, after which time the solvent was removed from the yellow-brown solution *in vacuo*. The resulting solids were dissolved in C_6D_6 and filtered into an NMR tube and spectra were acquired. The ^{31}P NMR spectrum showed mostly **10**, **6**, and free triphenylphosphine; other components present were minor.

1.12.13 Preparation of $(P_3)Mo(N[^iPr]Ar)_3$ (12-Mo)

Solid (Mes*NPP)Nb$(N[CH_2{}^tBu]Ar)_3$ (176 mg, 0.18 mmol, 1 eq) and $PMo(N[^iPr]Ar)_3$ (110 mg, 0.18 mmol, 1 eq) were mixed and to them was added benzene (2 g). The resulting solution was transferred to a teflon-stoppered sealable tube, which was subsequently heated to 65 °C for 3.5 h. The color remained a dark red over this time. Upon cooling, pale fibrous solids precipitated from the solution. *n*-Hexane was added and the solution was chilled to −35 °C to facilitate precipitation of the product. The solids were then collected atop a sintered glass frit and washed with *n*-hexane to yield an off-white fibrous solid, which was dried *in vacuo* to constant mass (45 mg, 0.067 mmol, 37% yield). ^1H NMR ($CDCl_3$, 300 MHz, 20 °C): δ 6.83 (s, 3H, *p*-Ar), 6.33 (s, 6H, *o*-Ar), 4.60 (septet, 3H, $HC(CH_3)_2$), 2.28 (s, 18H, $ArCH_3$), 0.92 (d, 18H, $C(CH_3)_2$) ppm. $^{31}P\{^1H\}$ NMR ($CDCl_3$, 121.5 MHz, 20 °C): δ −185 (br s, $\Delta\nu_{\frac{1}{2}}$ = 350 Hz) ppm. Microanalysis and ^{13}C NMR data have appeared elsewhere on independently prepared samples.[119]

1.12.14 Preparation of $(OC)_5W(P_3)Mo(N[^iPr]Ar)_3$ (14-Mo)

To a thawing Et_2O solution (7 mL) of $[(Et_2O)Na][(OC)_5WPNb(N[CH_2{}^tBu]Ar)_3]$ (365 mg, 0.33 mmol, 1 eq) was added dropwise a thawing Et_2O solution (3 mL) of Mes*NPCl (106 mg, 0.33 mmol, 1.0 eq), affording a color change to deep red. The reaction mixture was allowed to stir for *ca*. 1 min, then a 22 °C, Et_2O solution (4 mL) of $PMo(N[^iPr]Ar)_3$ (220 mg, 0.36 mmol, 1.1 eq) was added. This solution was stirred for three hours at 22 °C, taking on an orange hue over this time. The reaction mixture was then filtered through a bed of Celite to remove salts and concentrated to dryness *in vacuo*. The resulting red powder was slurried in *n*-hexane (10 mL) and the solvent was removed once more. At this point the product mixture was slurried in *n*-pentane and then chilled to −35 °C. The desired product was collected by filtration atop a sintered-glass frit as a brick-red powder. The filtrate was concentrated and this procedure was repeated several times using successively less solvent until the yellow imido and red desired product could not be separated further. The several fractions of red powder were combined and dried *in vacuo* (205 mg). This material is >90% pure by NMR spectroscopy with some Mes*NNb$(N[CH_2{}^tBu]Ar)_3$ impurity. The material was further purified by storing a *n*-pentane suspension at −35 °C and extracting away the undesired imido to give pure $(OC)_5W(P_3)Mo(N[^iPr]Ar)_3$ as a red powder (180 mg, 0.180 mmol,

57% yield). Crystallization from toluene/Et_2O affords analytically pure red crystals. ^{1}H NMR (C_6D_6, 500 MHz, 20 °C): δ 6.69 (s, 3H, *p*-Ar), 6.24 (br s, 6H, *o*-Ar), 4.90 (septet, 3H, $HC(CH_3)_2$), 2.10 (s, 18H, $ArCH_3$), 0.92 (br d, 18H, $C(CH_3)_2$) ppm. $^{31}P\{^1H\}$ NMR (C_6D_6, 202.5 MHz, 50 °C): δ −212 (br s, $\Delta\nu_{\frac{1}{2}}$ = 290 Hz) ppm. $^{13}C\{^1H\}$ NMR (C_6D_6, 125.8 MHz, 20 °C): δ 202.3 (quartet, $^2J_{CP}$ = 12 Hz, *ax*-CO), 197.6 ($^1J_{CW}$ = 128 Hz, *eq*-CO), 148.1 (*ipso*-Ar), 138.1 (*m*-Ar), 129.5 (*p*-Ar), 128.9 (br, *o*-Ar), 64.3 (br, $CH(CH_3)_2$), 22.6 (br, $CH(CH_3)_2$), 21.7 ($ArCH_3$) ppm. IR (C_6D_6, KBr): $\tilde{\nu}$ 2973, 2927, 2869, 2076 (s, sharp), 1942 (vs), 1920 (s), 1600, 1586, 1153, 1113 cm^{-1}. Elem. Anal. Calcd for $C_{38}H_{48}N_3O_5P_3MoW$: C, 45.66; H, 4.84; N, 4.20. Found: C, 46.14; H, 4.90; N, 4.24.

1.12.15 Preparation of $(OC)_5W(P_3)W(N[^iPr]Ar)_3$ (14-W)

To a thawing Et_2O solution (7 mL) of $[(Et_2O)Na][(OC)_5WPNb(N[CH_2{}^tBu]Ar)_3]$ (320 mg, 0.29 mmol, 1 eq) was added dropwise a thawing Et_2O solution (3 mL) of Mes*NPCl (95 mg, 0.29 mmol, 1.0 eq), affording a color change to deep red. The reaction mixture was allowed to stir for *ca.* 1 min, then a 22 °C Et_2O solution (4 mL) of $PW(N[^iPr]Ar)_3$ (220 mg, 0.32 mmol, 1.1 eq) was added. This solution was stirred for 3 h at 22 °C, taking on an orange hue over this time. The reaction mixture was then filtered through a bed of Celite to remove salts and concentrated to dryness *in vacuo*. The resulting reddish powder was slurried in *n*-hexane (10 mL) and dried once more. At this point the reaction mixture was suspended in *n*-hexane and chilled to −35 °C for 24 h. The brick-red precipitate was collected on a sintered-glass frit and dried *in vacuo* (160 mg, 0.15 mmol, 51% yield). ^{1}H NMR (toluene-d_8, 500 MHz, 40 °C): δ 6.66 (s, 3H, *p*-Ar), 6.06 (br s, 6H, *o*-Ar), 4.95 (septet, 3H, $HC(CH_3)_2$), 2.09 (s, 18H, $ArCH_3$), 0.80 (br d, 18H, $C(CH_3)_2$) ppm. $^{31}P\{^1H\}$ NMR (toluene-d_8, 202.5 MHz, 40 °C): δ −262 (br s, $\Delta\nu_{\frac{1}{2}}$ = 960 Hz) ppm. $^{13}C\{^1H\}$ NMR (toluene-d_8, 125.8 MHz, 40 °C): δ 199.2 (m, *ax*-CO), 198.1 (*eq*-CO), 147.2 (*ipso*-Ar), 138.1 (*m*-Ar), 129.5 (*p*-Ar), 128.8 (br, *o*-Ar), 65.8 (br, $CH(CH_3)_2$), 22.3 (br, $CH(CH_3)_2$), 21.7 ($ArCH_3$) ppm. IR (thin film, KBr): $\tilde{\nu}$ 2066, 1933, 1917 cm^{-1}. Elem. Anal. Calcd for $C_{38}H_{48}N_3O_5P_3W_2$: C, 41.97; H, 4.45; N, 3.86. Found: C, 42.77; H, 5.07; N, 3.78.

1.12.16 Preparation of $[(12\text{-crown-}4)_2Na][(P_3)Nb(N[CH_2{}^tBu]Ar)_3]$ (15)

As solids, $(Mes^*NPP)Nb(N[CH_2{}^tBu]Ar)_3$ (405 mg, 0.41 mmol) and $[(Et_2O)Na][PNb(N[CH_2{}^tBu]Ar)_3]$ (325 mg, 0.41 mmol, 1 eq) were mixed and dissolved in benzene (5 g). The resulting red solution was sealed in a teflon-stoppered tube and heated to 55 °C for 2.5 h. The resulting dark-orange solution was then dried *in vacuo* and dissolved in *n*-pentane (5 mL). To this solution was added 12-crown-4 (150 mg, 0.85 mmol, 2.1 eq) as an Et_2O solution (3 mL). A precipitate formed and the solution was allowed to stir for 15 min. After this time the suspension was concentrated to dryness *in vacuo*, the residue was dissolved in THF (2.5 mL), and the resulting solution was filtered through a plug of Celite. The filtered solution was layered with Et_2O (2 mL) and *n*-pentane (3 mL) and then cooled to −35 °C for several days. The resulting orange powder was collected on a sintered

glass frit, washed with *n*-pentane and dried *in vacuo* (135 mg, 0.12 mmol, 30% yield). ^{1}H NMR (C_5D_5N, 500 MHz, 20 °C): δ 7.01 (s, 6H, *o*-Ar), 6.61 (s, 3H, *p*-Ar), 4.22 (s, 6H, NCH_2), 3.59 (s, 32H, crown), 2.35 (s, 18H, ArCH_3), 1.13 (s, 27H, ^{t}Bu) ppm. ^{31}P{^{1}H} NMR (C_5D_5N, 121.5 MHz, 20 °C): δ −183 (s, $\Delta\nu_{\frac{1}{2}}$ = 10 Hz) ppm. ^{13}C{^{1}H} NMR (C_5D_5N, 125.8 MHz, 20 °C): δ 160.2 (*ipso*-Ar), 137.1 (*m*-Ar), 124.5 (*p*-Ar), 122.9 (*o*-Ar), 71.9 (N*C*H$_2$), 67.1 (crown), 36.5 (*C*(CH$_3$)$_3$), 30.5 (C(*C*H$_3$)$_3$), 22.4 (Ar*C*H$_3$) ppm. Elem. Anal. Calcd for $C_{55}H_{92}N_3O_8P_3NaNb$: C, 58.35; H, 8.19; N, 3.71. Found: C, 58.03; H, 8.24; N, 3.73.

1.12.17 Preparation of [(12-crown-4)$_2$Na][(OC)$_5$W(P$_3$)Nb(N[CH$_2$^{t}Bu]Ar)$_3$] (16)

To a thawing Et_2O solution (7 mL) of [(Et_2O)Na][(OC)$_5$WPNb(N[CH$_2$^{t}Bu]Ar)$_3$] (304 mg, 0.27 mmol) was added dropwise a thawing Et_2O solution (3 mL) of Mes*NPCl (88 mg, 0.27 mmol, 1.0 eq), affording a color change to deep red. The reaction mixture was allowed to stir for *ca*. 1 min, and then a 22 °C, Et_2O solution (4 mL) of [(Et_2O)Na][PNb(N[CH$_2$^{t}Bu]Ar)$_3$] (233 mg, 0.29 mmol, 1.1 eq) was added. This solution was stirred for 3 h at 22 °C, remaining red over this time. The reaction mixture was then filtered through a bed of Celite to remove salts and the filtrate was concentrated to dryness *in vacuo*. The resulting red powder was dissolved in *n*-hexane (10 mL) and dried once more. A 1:1 benzene:*n*-pentane solution (10 mL) of the residue was prepared, and to it was added an Et_2O solution (2 mL) of 12-crown-4 (160 mg, 0.91 mmol, 3.3 eq). After stirring for 5 min, the solution was evaporated to dryness and the resulting powder was slurried in *n*-pentane/Et_2O (15 ml/5 mL). A light orange powder (265 mg) was collected atop a sintered glass frit and the dark red filtrate was dried *in vacuo*. The resulting residue was dissolved in *n*-pentane/THF (20 mL total) and stored at −35 °C to precipitate another crop of orange powder, which was collected on a frit and washed with *n*-pentane. The combined orange solids were dried *in vacuo* to constant mass (295 mg, 0.203 mmol, 75% yield). ^{1}H NMR (C_5D_5N, 500 MHz, 20 °C): δ 6.74 (s, 6H, *o*-Ar), 6.69 (s, 3H, *p*-Ar), 4.18 (br s, 6H, NCH_2), 3.58 (s, 32H, crown), 2.30 (s, 18H, ArCH_3), 1.04 (s, 27H, ^{t}Bu) ppm. ^{31}P{^{1}H} NMR (C_5D_5N, 202.5 MHz, 20 °C): δ −203 (br s, $\Delta\nu_{\frac{1}{2}}$ = 520 Hz) ppm. ^{13}C{^{1}H} NMR (C_5D_5N, 125.8 MHz, 20 °C): δ 203.8 (br, *ax*-CO), 201.7 ($^1J_{CW}$ = 126 Hz, *eq*-CO), 157.7 (*ipso*-Ar), 137.5 (*m*-Ar), 124.9 (*p*-Ar), 124.6 (*o*-Ar), 73.2 (br, N*C*H$_2$), 66.2 (crown), 36.7 (*C*(CH$_3$)$_3$), 30.4 (C(*C*H$_3$)$_3$), 22.2 (Ar*C*H$_3$) ppm. IR (thin film, KBr): $\tilde{\nu}$ 2917 (m) 2051 (s), 1917 (vs), 1874 (s), 1602 (m), 1098 (s) cm^{-1}. Elem. Anal. Calcd for $C_{60}H_{92}N_3O_{13}P_3NaNbW$: C, 49.49; H, 6.37; N, 2.89. Found: C, 49.44; H, 6.63; N, 3.05.

1.12.18 Preparation of Na[{(OC)$_5$W}$_2$(P$_3$)Nb(N[CH$_2$^{t}Bu]Ar)$_3$] (17)

To a thawing Et_2O solution (100 mL) of [(THF)$_3$Na][(OC)$_5$WPNb(N[CH$_2$^{t}Bu]Ar)$_3$] (3.0 g, 2.38 mmol, 2.0 eq) was added dropwise a thawing Et_2O solution (12 mL) of Mes*NPCl (390 mg, 1.19 mmol, 1 eq). This solution was stirred for 4 h at 22 °C before the reaction mixture was filtered through a bed of Celite and the filtrate was concentrated to dryness *in vacuo*. To the resulting

red powder was added Et_2O, forming a red solution that contained some undissolved yellow solids, Mes*NNb(N[$CH_2{}^t$Bu]Ar)$_3$. The solution was then filtered through Celite and the yellow solids were washed with minimal Et_2O until the washings were no longer red. The yellow solids were discarded and the red filtrate was dried *in vacuo* to give a red powder, which was slurried in *n*-hexane/benzene (10 mL each) before the mixture was stripped to dryness once more. The resulting solids were slurried in *n*-hexane/benzene (25 mL/10 mL) and the suspended fine red powder was collected atop a sintered glass frit, washed with *n*-pentane until the washings were colorless, and then dried *in vacuo* (1.41 g, 0.99 mmol, 83% yield). ^{1}H NMR (C_5D_5N, 500 MHz, 20 °C): δ 6.83 (s, 6H, *o*-Ar), 6.73 (s, 3H, *p*-Ar), 4.11 (s, 6H, NCH_2), 2.36 (s, 18H, ArCH_3), 0.97 (s, 27H, ^{t}Bu) ppm. ^{31}P{^{1}H} NMR (C_5D_5N, 202.5 MHz, 20 °C): δ −216 (br s, $\Delta\nu_{\frac{1}{2}}$ = 120 Hz) ppm. ^{13}C{^{1}H} NMR (C_5D_5N, 125.8 MHz, 20 °C): δ 202.3 (m, *ax*-CO), 199.9 ($^1J_{CW}$ = 126 Hz, *eq*-CO), 156.3 (*ipso*-Ar), 137.7 (*m*-Ar), 125.8 (*p*-Ar), 124.6 (*o*-Ar), 72.2 (br, NCH_2), 36.5 (C(CH_3)$_3$), 30.3 (C(CH_3)$_3$), 22.1 (ArCH_3) ppm. IR (Et_2O, KBr): $\tilde{\nu}$ 2089 (s), 2066 (s), 2060 (s), 1984 (s), 1975 (s), 1949 (vs), 1921 (vs), 1898 (vs), 1803 (s), 1602 (m), 1586 (m) cm^{-1}. Elem. Anal. Calcd for $C_{49}H_{60}N_3O_{10}P_3NaNbW_2$: C, 41.23; H, 4.23; N, 2.94. Found: C, 41.13; H, 4.53; N, 2.94.

1.12.19 Preparation of (AdCP$_2$)Mo(N[^{i}Pr]Ar)$_3$ (18)

Solid AdCP (31 mg, 0.17 mmol, 1.0 eq) and PMo(N[^{i}Pr]Ar)$_3$ (110 mg, 0.18 mmol, 1.05 eq) were mixed and dissolved in C_6D_6 (2 mL). The resulting solution was heated to 60 °C for 3 h. After this time the ^{1}H and ^{31}P NMR spectra showed consumption of AdCP and the presence of the desired product as the predominant species. Extraction with *n*-pentane and crystallization from toluene/*n*-pentane at −35 °C afforded pure (AdCP$_2$)Mo(N[^{i}Pr]Ar)$_3$ as red crystals (68 mg, 0.086 mmol, 51% yield). ^{1}H NMR (C_6D_6, 500 MHz, 20 °C): δ 6.76 (s, 6H, *o*-Ar), 6.73 (s, 3H, *p*-Ar), 4.75 (septet, 3H, CH(CH_3)$_2$), 2.21 (s, 18H, ArCH_3), 1.96 (m, 3H, Ad), 1.82 (m, 6H, Ad), 1.68 (m, 6H, Ad), 1.12 (d, 18H, CH(CH_3)$_2$) ppm. ^{31}P{^{1}H} NMR (C_6D_6, 202.5 MHz, 20 °C): δ −249 (br s) ppm. ^{13}C{^{1}H} NMR (C_6D_6, 125.8 MHz, 20 °C): δ 149.9 (*ipso*-Ar), 137.3 (*m*-Ar), 129.7 (*p*-Ar), 126.0 (*o*-Ar), 103.6 (t, J_{CP} = 79 Hz, CP_2), 58.3 (CH(CH_3)$_2$), 50.5 (Ad), 37.6 (Ad), 31.4 (Ad), 25.9 (Ad), 23.9 (CH(CH_3)$_2$), 21.8 (ArCH_3) ppm.

1.12.20 Kinetics on the Fragmentation of (Mes*NPP)Nb(N[$CH_2{}^t$Bu]Ar)$_3$

Eyring analysis

Stock solutions containing (Mes*NPP)Nb(N[$CH_2{}^t$Bu]Ar)$_3$ (135 mg) and ONb(N[$CH_2{}^t$Bu]Ar)$_3$ (30 mg, used as an internal standard) were prepared in C_6D_6 (*ca.* 5 mL) and stored at −35 °C between uses. An aliquot of this solution was transferred to a sealable (J. Young) NMR tube, which was then inserted into a pre-warmed NMR probe. The temperature of the probe was verified by an ethylene glycol NMR thermometer before each run. Two- or four-scan ^{1}H NMR spectra were collected over a period of 3–5 half-lives. The integral of the methylene resonance of (Mes*NPP)Nb(N[$CH_2{}^t$Bu]Ar)$_3$

Table 1.4. Rate constants[a] for degradation of **1** at various temperatures.

T	303 K	313 K	323 K	333 K	343 K	353 K
Run 1	0.326	1.12	2.46	7.17	19.2	37.1
Run 2	0.329	0.93	2.51	7.19	18.5	40.4
Run 3	–	0.93	2.11	6.33	16.2	35.6
Average	0.328	0.99	2.51	6.90	18.0	37.7
Std Dev	0.002	0.10	0.35	0.49	1.57	2.46

[a] Values are in units of 10^{-4} sec^{-1}

as a function of time, corrected versus the internal standard, was fit to the first-order rate equation, $I(t) = Ae^{-kt} + b$, using the automated routine of *Gnuplot* to extract k, Table 1.4. Three runs were performed at each temperature (except for 30 °C where two runs were performed) and the error bars were calculated at the 95% confidence level. The Eyring fit was performed using the error-weighted least squares regression analysis of *Gnuplot*.[162]

Kinetics in the presence of PMo(N[^{i}Pr]Ar)$_3$

A solution of (Mes*NPP)Nb(N[$CH_2{}^t$Bu]Ar)$_3$ (30 mg, 0.030 mmol) and PMo(N[^{i}Pr]Ar)$_3$ (0 or 37 mg) was prepared using 1 g of C_6D_6 and transferred to a sealable (J. Young) NMR tube, which was then inserted into an NMR probe pre-warmed to 50 °C. Two-scan ^{1}H NMR spectra were collected every 220 s for 3 h. The integral of the methylene resonance of (Mes*NPP)Nb(N[$CH_2{}^t$Bu]Ar)$_3$ as a function of time, corrected versus residual Et_2O, was fit to the first-order rate equation, $I(t) = Ae^{-kt} + b$, using the automated routine of *Gnuplot*. A rate constant of $k = 2.5 \times 10^{-4}$ s^{-1} was obtained in the presence or absence of PMo(N[^{i}Pr]Ar)$_3$.

1.12.21 Kinetics on the Fragmentation of (OC)$_5$W(Mes*NPP)Nb(N[$CH_2{}^t$Bu]Ar)$_3$

Kinetics in the presence of cyclohexadiene

As a general procedure, a thawing solution of Mes*NPCl (14 mg, 0.045 mmol) was added to a thawing solution of [(Et_2O)Na][(CO)$_5$WPNb(N[$CH_2{}^t$Bu]Ar)$_3$] (50 mg, 0.045 mmol) in Et_2O. This solution was stirred for 1 min before the solvent was removed *in vacuo*. The residue was extracted with *ca.* 0.8 mL of C_7D_8 that was pre-spiked via syringe with varying equivalents of 1,3-cyclohexadiene. Either ($Me_3Si)_2O$ or ferrocene (to be used as an internal standard) was added to the solution and it was filtered through Celite into a sealable (J.Young) NMR tube, which was then frozen for transport to an NMR probe pre-cooled to 10 °C. Single-scan ^{1}H NMR spectra were collected every 2–5 min for 2–4 h. The integral of the methylene resonance of (OC)$_5$W(Mes*NPP)Nb(N[$CH_2{}^t$Bu]Ar)$_3$as a function of time, corrected versus the standard, was

fit to the first-order rate equation, $I(t) = Ae^{-kt} + b$, using the automated routine of *Gnuplot*. Rate constants at various 1,3-cyclohexadiene concentrations are presented in Figure 1.18.

Kinetics in the presence of PMo(N[^{i}Pr]Ar)$_3$

A thawing solution (1 mL) of Mes*NPCl (14 mg, 0.045 mmol, 1 eq) was added to a thawing Et_2O solution (2 mL) of [(THF)$_3$Na][(CO)$_5$WPNb(N[CH$_2{}^t$Bu]Ar)$_3$] (55 mg, 0.044 mmol). This solution was stirred for 30 s before the solvent was removed *in vacuo*. The residue was extracted with a toluene-d_8 (1.0 g) solution of PMo(N[^{i}Pr]Ar)$_3$ (37 mg, 0.060 mmol, 1.3 eq) and ferrocene (4 mg, 0.02 mmol, used as an internal standard). The resulting extract was filtered cold through Celite into a sealable (J. Young) NMR tube, which was then frozen for transport to an NMR probe pre-cooled to 10 °C. Four-scan ^{1}H NMR spectra were collected every 248 s for 3 h. The integral of the methylene resonance of (OC)$_5$W(Mes*NPP)Nb(N[CH$_2{}^t$Bu]Ar)$_3$as a function of time, corrected versus the ferrocene standard, was fit to the first-order rate equation, $I(t) = Ae^{-kt} + b$, using the automated routine of *Gnuplot*. A rate constant $k = 2.1 \times 10^{-4}$ s^{-1} was found.

1.12.22 X-Ray Structure Determinations

Diffraction quality crystals of [(Et$_2$O)$_3$Na][**4**] were grown from Et$_2$O/*n*-pentane at –35 °C, and of [(12-crown-4)$_2$Na][**4**] from Et$_2$O/THF at –35 °C. Crystals of **5** and **9** were grown from O(SiMe$_3$)$_2$ at –35 °C. The products **6**, **7** and **8** were crystallized from Et$_2$O at –35 °C. Crystals of **10** were grown from toluene at 22 °C. The *cyclo* products **12**-W and **18** were crystallized from Et$_2$O. The complex [(Et$_2$O)Na][**17**] was crystallized from benzene at 22 °C in the presence of trace Et$_2$O. All crystals were mounted in hydrocarbon oil on a nylon loop or a glass fiber. Low-temperature (100 K) data were collected on a Siemens Platform three-circle diffractometer coupled to a Bruker-AXS Smart Apex CCD detector with graphite-monochromated Mo Kα radiation (λ = 0.71073 Å) performing ϕ- and ω-scans. A semi-empirical absorption correction was applied to the diffraction data using SADABS.[163] All structures were solved by direct or Patterson methods using SHELXS[164,165] and refined against F^2 on all data by full-matrix least squares with SHELXL-97.[165,166] All non-hydrogen atoms were refined anisotropically. All hydrogen atoms were included in the model at geometrically calculated positions and refined using a riding model. The isotropic displacement parameters of all hydrogen atoms were fixed to 1.2 times the U_{eq} value of the atoms they are linked to (1.5 times for methyl groups). In structures where disorders were present, the disorders were refined within SHELXL with the help of rigid bond restraints as well as similarity restraints on the anisotropic displacement parameters for neighboring atoms and on 1,2- and 1,3-distances throughout the disordered components.[167] The relative occupancies of disordered components were refined freely within SHELXL. Further details are provided in Tables 1.5 – 1.8, on Reciprocal Net,[168] and in the form of cif files available from the CCDC.[169]

1.12.23 Computational Studies

All calculations were carried out using ADF 2004.01 or ADF 2007.01 from Scientific Computing and Modeling (http://www.scm.com) on an eight-processor Quantum Cube workstation from Parallel Quantum Solutions (http://www.pqs-chem.com).[70,71,170] In all cases the LDA functional employed was that of Vosko, Wilk, and Nusair (VWN) while the GGA part was handled using the functionals of Becke and Perdew (BP86).[171–173] In addition, all calculations were carried out using the Zero Order Regular Approximation (ZORA) for relativistic effects.[174–177] For energetics related to the elimination of P_2 from **1**, the basis sets were triple-zeta with two polarization functions (TZ2P) as supplied with ADF. Frozen core approximations were utilized according to the following atom types: N and C: 1s frozen; P: core frozen through and including 2p; Nb: core frozen through and including 4p. For NMR calculations related to the solid-state NMR of **1**, basis sets were quadruple-zeta with four polarization functions (QZ4P) for Nb and P, triple-zeta with two polarization for N, and double-zeta with one polarization for C and H; frozen core approximations were made for made only for C (1s). Geometries were optimized to default convergence criteria and energies are uncorrected for zero-point energies.

Chemical shielding tensors were calculated for the ^{31}P nuclei in the optimized structures by the GIAO method using the ADF package.[178–181] The functionals, basis sets and relativistic approximations used were the same as described above, with the exception that for models **1m**, **1a**, **1b** and **1c**, frozen core approximations were not made. Diamagnetic and paramagnetic contributions were included in the absolute chemical shielding calculations. The total isotropic shielding value was converted to a chemical shift (downfield of 85% phosphoric acid) by comparison to calculated shieldings and experimental chemical shifts for PH_3 or $OPMo(N[^tBu]Ar)_3$.[182,183]

Table 1.5. Crystal Data for $WCO)_5$-coordinated Niobium Phosphide **4** and the Related Phosphinidene **5**

	[$(Et_2O)_3$Na][**4**]	[(12-crown-4)$_2$Na][**4**]	**5**
Reciprocal Net code	05226	05124	05194
Empirical formula	$C_{59}H_{90}N_3NaNbO_8PW$	$C_{60}H_{92}N_3NaNbO_{13}PW$	$C_{51}H_{81}N_3NbO_6PSi_2W$
Formula weight	1264.03	1394.09	1196.10
Temperature	100(2) K	100(2) K	100(2) K
Wavelength	0.71073 Å	0.71073 Å	0.71073 Å
Crystal system	Monoclinic	Orthorhombic	Triclinic
Space group	$P2_1/c$	$P2_12_12_1$	$P\bar{1}$
Unit cell dimensions	$a = 18.1028(7)$ Å, $\alpha = 90°$	$a = 13.297(3)$	$a = 11.6135(6)$ Å, $\alpha = 82.166(2)°$
	$b = 20.7179(8)$ Å, $\beta = 98.7880(10)°$	$b = 19.6681(7)$	$b = 15.4021(10)$ Å, $\beta = 80.988(2)°$
	$c = 16.9850(7)$ Å, $\gamma = 90°$	$c = 25.3876(8)$	$c = 16.9877(11)$ Å, $\gamma = 72.089(2)°$
Volume	6295.5(4) Å^3	6639.6(3) Å^3	2843.1(3) Å^3
Z	4	4	2
Density (calculated)	1.334 Mg/m^3	1.395 Mg/m^3	1.397 Mg/m^3
Absorption coefficient	2.089 mm^{-1}	1.993 mm^{-1}	2.339 mm^{-1}
$F(000)$	2608	2872	1228
Crystal size	$0.30 \times 0.20 \times 0.05$ mm^3	$0.30 \times 0.16 \times 0.14$ mm^3	$0.30 \times 0.12 \times 0.04$ mm^3
Theta range for collection	1.56 to 29.13°	1.60 to 28.37°	1.76 to 29.57°
Index ranges	$-24 \leq h \leq 24$, $-28 \leq k \leq 28$,	$-17 \leq h \leq 17$, $0 \leq k \leq 26$,	$-16 \leq h \leq 16$, $-21 \leq k \leq 21$,
	$-23 \leq l \leq 22$	$0 \leq l \leq 33$	$-23 \leq l \leq 23$
Reflections collected	128574	137847	61792
Independent reflections	16954 [R(int) = 0.0711]	16551 [R(int) = 0.0479]	15874 [R(int) = 0.0471]
Completeness to θ_{max}	99.9%	99.8%	99.4%
Absorption correction	Semi-empirical from equivalents	Semi-empirical from equivalents	Semi-empirical from equivalents
Max. and min. transmission	0.9028 and 0.5730	0.7677 and 0.5862	0.9122 and 0.5404
Refinement method	Full-matrix least-squares on F^2	Full-matrix least-squares on F^2	Full-matrix least-squares on F^2
Data / restraints / parameters	16954 / 1102 / 953	16551 / 2186 / 954	15874 / 0 / 593
Goodness-of-fit[a]	1.035	1.048	1.076
Final R indices[b] [$I > 2\sigma(I)$]	$R_1 = 0.0445$, $wR_2 = 0.0903$	$R_1 = 0.0283$, $wR_2 = 0.0668$	$R_1 = 0.0445$, $wR_2 = 0.1129$
R indices[b] (all data)	$R_1 = 0.0771$, $wR_2 = 0.1033$	$R_1 = 0.0304$, $wR_2 = 0.0676$	$R_1 = 0.0521$, $wR_2 = 0.1174$
Largest diff. peak and hole	1.964 and -1.663 e Å^{-3}	2.126 and -0.385 e Å^{-3}	5.179 and -1.796 e Å^{-3}

[a] GooF = $\left[\frac{\Sigma[w(F_o^2-F_c^2)^2]}{(n-p)}\right]^{\frac{1}{2}}$ [b] $R_1 = \frac{\Sigma||F_o|-|F_c||}{\Sigma|F_o|}$; $wR_2 = \left[\frac{\Sigma[w(F_o^2-F_c^2)^2}{\Sigma[w(F_o^2)^2]}\right]^{\frac{1}{2}}$; $w = \frac{1}{\sigma^2(F_o^2)+(aP)^2+bP}$; $P = \frac{2F_c^2+\max(F_o^2,0)}{3}$

Table 1.6. Crystal Data for Diene Adducts of P_2 and $(P_2)W(CO)_5$

	6	**7**	**8**
Reciprocal Net code	06023	06039	05260
Empirical formula	$C_{12}H_{16}P_2$	$C_{17}H_{16}O_5P_2W$	$C_{15}H_{12}O_5P_2W$
Formula weight	222.19	546.09	518.04
Temperature	100(2) K	100(2) K	100(2) K
Wavelength	0.71073 Å	0.71073 Å	0.71073 Å
Crystal system	Monoclinic	Triclinic	Monoclinic
Space group	$P2_1/m$	$P\bar{1}$	$P2_1/n$
Unit cell dimensions	$a = 6.1614(7)$ Å, $\alpha = 90°$	$a = 6.8867(2)$ Å, $\alpha = 82.3400(10)°$	$a = 6.8952(3)$ Å, $\alpha = 90°$
	$b = 15.5500(18)$ Å, $\beta = 118.925(3)°$	$b = 9.8188(2)$ Å, $\beta = 87.1830(10)°$	$b = 13.6235(6)$ Å, $\beta = 93.5700(10)°$
	$c = 6.3346(10)$ Å, $\gamma = 90°$	$c = 13.5113(3)$ Å, $\gamma = 85.3310(10)°$	$c = 17.4775(6)$ Å, $\gamma = 90°$
Volume	531.21(12) Å^3	901.79(4) Å^3	1638.59(12) Å^3
Z	2	2	4
Density (calculated)	1.389 Mg/m^3	2.011 Mg/m^3	2.100 Mg/m^3
Absorption coefficient	0.364 mm^{-1}	6.606 mm^{-1}	7.265 mm^{-1}
$F(000)$	236	524	984
Crystal size	$0.25 \times 0.25 \times 0.04$ mm^3	$0.40 \times 0.36 \times 0.18$ mm^3	$0.30 \times 0.20 \times 0.20$ mm^3
Theta range for collection	1.31 to 29.12°	2.10 to 30.03°	1.90 to 30.03°
Index ranges	$-8 \le h \le 8$, $-21 \le k \le 21$,	$-9 \le h \le 9$, $-13 \le k \le 13$,	$-9 \le h \le 9$, $-19 \le k \le 19$,
	$-8 \le l \le 8$	$-18 \le l \le 19$	$-24 \le l \le 24$
Reflections collected	11566	20685	37027
Independent reflections	1480 [R(int) = 0.0506]	5246 [R(int) = 0.0228]	4800 [R(int) = 0.0279]
Completeness to θ_{max}	99.8%	99.6%	100.0%
Absorption correction	Semi-empirical from equivalents	Semi-empirical from equivalents	Semi-empirical from equivalents
Max. and min. transmission	0.9856 and 0.9144	0.3826 and 0.1775	0.3244 and 0.2192
Refinement method	Full-matrix least-squares on F^2	Full-matrix least-squares on F^2	Full-matrix least-squares on F^2
Data / restraints / parameters	1480 / 0 / 68	5246 / 0 / 226	4800 / 0 / 208
Goodness-of-fit[a]	1.055	1.065	1.061
Final R indices[b] [$I > 2\sigma(I)$]	$R_1 = 0.0335$, $wR_2 = 0.0796$	$R_1 = 0.0149$, $wR_2 = 0.0371$	$R_1 = 0.0165$ $wR_2 = 0.0399$
R indices[b] (all data)	$R_1 = 0.0377$, $wR_2 = 0.0821$	$R_1 = 0.0155$, $wR_2 = 0.0374$	$R_1 = 0.0180$, $wR_2 = 0.0405$
Largest diff. peak and hole	0.397 and -0.252 e Å^{-3}	1.139 and -0.693 e Å^{-3}	1.238 and -0.461 e Å^{-3}

[a] GooF = $\left[\frac{\Sigma[w(F_o^2-F_c^2)^2]}{(n-p)}\right]^{\frac{1}{2}}$ [b] $R_1 = \frac{\Sigma||F_o|-|F_c||}{\Sigma|F_o|}$; $wR_2 = \left[\frac{\Sigma[w(F_o^2-F_c^2)^2}{\Sigma[w(F_o^2)^2]}\right]^{\frac{1}{2}}$; $w = \frac{1}{\sigma^2(F_o^2)+(aP)^2+bP}$; $P = \frac{2F_c^2+\max(F_o^2,0)}{3}$

Table 1.7. Crystal Data for Platinum-Containing Products **9** and **10**

	9	**10**
Reciprocal Net code	06231	07018
Empirical formula	$C_{104.5}H_{140.5}N_4NbO_{0.75}P_4Pt_2Si_{1.50}$	$C_{94.50}H_{80}O_5P_6Pt_2W$
Formula weight	2113.81	2055.44
Temperature	100(2) K	100(2) K
Wavelength	0.71073 Å	0.71073 Å
Crystal system	Triclinic	Monoclinic
Space group	$P\bar{1}$	$P2_1/n$
Unit cell dimensions	$a = 12.404(6)$ Å, $\alpha = 109.101(8)^\circ$	$a = 14.4491(7)$ Å, $\alpha = 90^\circ$
	$b = 21.068(10)$ Å, $\beta = 93.589(9)^\circ$	$b = 23.0682(11)$ Å, $\beta = 100.5930(10)^\circ$
	$c = 22.997(11)$ Å, $\gamma = 96.043(8)^\circ$	$c = 25.2132(12)$ Å, $\gamma = 90^\circ$
Volume	5617(4) Å^3	8260.7(7) Å^3
Z	2	4
Density (calculated)	1.250 Mg/m^3	1.653 Mg/m^3
Absorption coefficient	2.700 mm^{-1}	4.937 mm^{-1}
$F(000)$	2159	4028
Crystal size	$0.15 \times 0.15 \times 0.02$ mm^3	$0.50 \times 0.50 \times 0.30$ mm^3
Theta range for collection	1.83 to 23.26°	1.52 to 30.03°
Index ranges	$-13 \le h \le 13$, $-23 \le k \le 23$,	$-20 \le h \le 20$, $-32 \le k \le 32$,
	$-25 \le l \le 25$	$-35 \le l \le 35$
Reflections collected	78645	220793
Independent reflections	16144 [R(int) = 0.1198]	24155 [R(int) = 0.0379]
Completeness to θ_{max}	100.0%	99.9%
Absorption correction	Semi-empirical from equivalents	Semi-empirical from equivalents
Max. and min. transmission	0.9480 and 0.6875	0.3190 and 0.1915
Refinement method	Full-matrix least-squares on F^2	Full-matrix least-squares on F^2
Data / restraints / parameters	16144 / 235 / 1194	24155 / 570 / 1108
Goodness-of-fit[a]	1.042	1.211
Final R indices[b] [$I > 2\sigma(I)$]	$R_1 = 0.0503$, $wR_2 = 0.1118$	$R_1 = 0.0257$, $wR_2 = 0.0538$
R indices[b] (all data)	$R_1 = 0.0994$, $wR_2 = 0.1315$	$R_1 = 0.0309$, $wR_2 = 0.0555$
Largest diff. peak and hole	1.616 and -1.000 e Å^{-3}	1.827 and -0.929 e Å^{-3}

[a] GooF = $\left[\frac{\Sigma[w(F_o^2-F_c^2)^2]}{(n-p)}\right]^{\frac{1}{2}}$ [b] $R_1 = \frac{\Sigma||F_o|-|F_c||}{\Sigma|F_o|}$; $wR_2 = \left[\frac{\Sigma[w(F_o^2-F_c^2)^2}{\Sigma[w(F_o^2)^2]}\right]^{\frac{1}{2}}$; $w = \frac{1}{\sigma^2(F_o^2)+(aP)^2+bP}$; $P = \frac{2F_c^2+\max(F_o^2,0)}{3}$

Table 1.8. Crystal Data for *cyclo*-P_3 and *cyclo*-CP_2 Complexes

	12-W	$[(Et_2O)Na][$**17**$]$	**18**
Reciprocal Net code	06209	06215	08049
Empirical formula	$C_{43}H_{60}N_3O_5P_3W_2$	$C_{59}H_{76}N_3NaO_{11}P_3W_2$	$C_{51}H_{71}MoN_3P_2$
Formula weight	1159.55	1579.74	883.99
Temperature	100(2) K	100(2) K	100(2) K
Wavelength	0.71073 Å	0.71073 Å	0.71073 Å
Crystal system	Triclinic	Triclinic	Monoclinic
Space group	$P\bar{1}$	$P\bar{1}$	$C2/c$
Unit cell dimensions	$a = 11.350(2)$ Å, $\alpha = 77.231(3)^\circ$	$a = 12.145(3)$ Å, $\alpha = 106.235(4)^\circ$	$a = 41.125(11)$ Å, $\alpha = 90^\circ$
	$b = 14.150(3)$ Å, $\beta = 75.225(3)^\circ$	$b = 13.565(3)$ Å, $\beta = 91.068(4)^\circ$	$b = 11.457(3)$ Å, $\beta = 93.174(5)^\circ$
	$c = 16.557(3)$ Å, $\gamma = 67.525(3)^\circ$	$c = 22.695(6)$ Å, $\gamma = 94.536(4)^\circ$	$c = 19.976(5)$ Å, $\gamma = 90^\circ$
Volume	2352.9(8) Å^3	3575.5(15) Å^3	9256(4) Å^3
Z	2	2	8
Density (calculated)	1.637 Mg/m^3	1.467 Mg/m^3	1.269 Mg/m^3
Absorption coefficient	5.031 mm^{-1}	3.491 mm^{-1}	0.390 mm^{-1}
$F(000)$	1144	1568	3760
Crystal size	$0.15 \times 0.10 \times 0.03$ mm^3	$0.20 \times 0.10 \times 0.02$ mm^3	$0.28 \times 0.22 \times 0.15$ mm^3
Theta range for collection	1.89 to 29.13°	1.89 to 26.02°	0.99 to 29.57°
Index ranges	$-15 \le h \le 15$, $-19 \le k \le 19$,	$-14 \le h \le 14$, $-16 \le k \le 16$,	$-56 \le h \le 56$, $-15 \le k \le 15$,
	$-21 \le l \le 22$	$-28 \le l \le 28$	$-27 \le l \le 27$
Reflections collected	44584	62023	120360
Independent reflections	12603 [R(int) = 0.0457]	14086 [R(int) = 0.0962]	12977 [R(int) = 0.0776]
Completeness to θ_{max}	99.4%	100.0%	100.0%
Absorption correction	Semi-empirical from equivalents	Semi-empirical from equivalents	Semi-empirical from equivalents
Max. and min. transmission	0.8637 and 0.5191	0.9335 and 0.5419	0.9439 and 0.8987
Refinement method	Full-matrix least-squares on F^2	Full-matrix least-squares on F^2	Full-matrix least-squares on F^2
Data / restraints / parameters	12603 / 135 / 560	14086 / 797 / 935	12977 / 0 / 526
Goodness-of-fit[a]	1.095	1.033	1.036
Final R indices[b] [$I > 2\sigma(I)$]	$R_1 = 0.0420$, $wR_2 = 0.0914$	$R_1 = 0.0515$, $wR_2 = 0.1186$	$R_1 = 0.0365$, $wR_2 = 0.0796$
R indices[b] (all data)	$R_1 = 0.0621$, $wR_2 = 0.0994$	$R_1 = 0.0970$, $wR_2 = 0.1383$	$R_1 = 0.0542$, $wR_2 = 0.0890$
Largest diff. peak and hole	2.462 and -3.862 e Å^{-3}	1.933 and -1.718 e Å^{-3}	0.615 and -0.801 e Å^{-3}

[a] GooF = $\left[\frac{\Sigma[w(F_o^2-F_c^2)^2]}{(n-p)}\right]^{\frac{1}{2}}$ [b] $R_1 = \frac{\Sigma||F_o|-|F_c||}{\Sigma|F_o|}$; $wR_2 = \left[\frac{\Sigma[w(F_o^2-F_c^2)^2}{\Sigma[w(F_o^2)^2]}\right]^{\frac{1}{2}}$; $w = \frac{1}{\sigma^2(F_o^2)+(aP)^2+bP}$; $P = \frac{2F_c^2+\max(F_o^2,0)}{3}$

1.13 REFERENCES

[1] Rivard, E.; Power, P. P. *Inorg. Chem.* **2007**, *46*, 10047–10064.

[2] Weber, L. *Chem. Rev.* **1992**, *92*, 1839–1906.

[3] Power, P. P. *Chem. Commun.* **2003**, 2091–2101.

[4] Power, P. P. *Chem. Rev.* **1999**, *99*, 3463–3503.

[5] Norman, N. C. *Polyhedron* **1993**, *12*, 2431–2446.

[6] Burdett, J. K. *Chemical Bonds: A Dialog*; Wiley: New York, 1997.

[7] Greenwood, N. N.; Earnshaw, A. *Chemistry of the Elements*, 2nd ed.; Butterworth-Heinemann: Oxford, 1997.

[8] Regitz, M.; Scherer, O. J. *Multiple Bonds and Low Coordination in Phosphorus Chemistry*; Thieme: Stuttgart, 1990.

[9] Dillon, K. B.; Mathey, F.; Nixon, J. F. *Phosphorus: The Carbon Copy*; Wiley: Chichester, 1998.

[10] Yoshifuji, M.; Shima, I.; Inamoto, N.; Hirotsu, K.; Higuchi, T. *J. Am. Chem. Soc.* **1981**, *103*, 4587–4589.

[11] Noble, A. *Ann. Chem. Pharm.* **1856**, *98*, 253–256.

[12] Sekiguchi, A.; Zigler, S. S.; West, R.; Michl, J. *J. Am. Chem. Soc.* **1986**, *108*, 4241–4242.

[13] Sekiguchi, A.; Kinjo, R.; Ichinohe, M. *Science* **2004**, *305*, 1755–1757.

[14] Rakitin, O. A.; Rees, C. W.; Vlasova, O. G. *Tetrahedron Lett.* **1996**, *37*, 4589–4592.

[15] Gilchrist, T. L.; Wood, J. E. *J. Chem. Soc., Chem. Commun.* **1992**, 1460–1461.

[16] Steliou, K.; Salama, P.; Brodeur; Gareau, Y. *J. Am. Chem. Soc.* **1987**, *109*, 926–927.

[17] Steliou, K.; Gareau, Y.; Harpp, D. N. *J. Am. Chem. Soc.* **1984**, *106*, 799–801.

[18] Harpp, D. N. *Phosphorus, Sulfur Silicon Relat. Elem.* **1997**, *120*, 41–59.

[19] Okuma, K.; Kuge, S.; Koga, Y.; Shioji, K.; Wakita, H.; Machiguchi, T. *Heterocycles* **1998**, *48*, 1519–1522.

[20] Harpp, D. N.; MacDonald, J. G. *J. Org. Chem.* **1988**, *53*, 3812–3814.

[21] Ando, W.; Sonobe, H.; Akasaka, T. *Tetrahedron* **1990**, *46*, 5093–5100.

[22] Ando, W.; Sonobe, H.; Akasaka, T. *Tetrahedron Lett.* **1987**, *28*, 6653–6656.

[23] Steliou, K.; Gareau, Y.; Milot, G.; Salama, P. *Phosphorus, Sulfur Silicon Relat. Elem.* **1989**, *43*, 209–241.

[24] Micallef, A. S.; Bottle, S. E. *Tetrahedron Lett.* **1997**, *38*, 2303–2306; The method of using butadiene and norbornene to assert the intermediacy of disulfur should be treated with caution.

[25] Stevenson, D. P.; Yost, D. M. *J. Chem. Phys.* **1941**, *9*, 403–408.

[26] Bock, H.; Müller, H. *Inorg. Chem.* **1984**, *23*, 4365–4368.

[27] Andrews, L.; McCluskey, M.; Mielke, Z.; Withnall, R. *J. Mol. Struct.* **1990**, *222*, 95–108.

[28] Mielke, Z.; McCluskey, M.; Andrews, L. *Chem. Phys. Lett.* **1990**, *165*, 146–154.

[29] McCluskey, M.; Andrews, L. *J. Phys. Chem.* **1991**, *95*, 2988–2994.

[30] Kornath, A.; Kaufmann, A.; Torheyden, M. *J. Chem. Phys.* **2002**, *116*, 3323–3326.

[31] Solouki, B.; Bock, H.; Haubold, W.; Keller, W. *Angew. Chem., Int. Ed.* **1990**, *29*, 1044–1046.

[32] Rice, F. O.; Potocki, R.; Gosselin, K. *J. Am. Chem. Soc.* **1953**, *75*, 2003–2004.

[33] Nugent, W. A.; Mayer, J. M. *Metal-Ligand Multiple Bonds: The Chemistry of Transition Metal Complexes Containing Oxo, Nitrido, Imido, Alkylidene, or Alkylidyne Ligands*; John Wiley & Sons, Inc.: New York, 1988.

[34] Laplaza, C. E.; Cummins, C. C. *Science* **1995**, *268*, 861–863.

[35] Cherry, J.-P. F.; Johnson, A. R.; Baraldo, L. M.; Tsai, Y.-C.; Cummins, C. C.; Kryatov, S. V.; Rybak-Akimova, E. V.; Capps, K. B.; Hoff, C. D.; Haar, C. M.; Nolan, S. P. *J. Am. Chem. Soc.* **2001**, *123*, 7271–7286.

[36] Fickes, M. G.; Odom, A. L.; Cummins, C. C. *Chem. Commun.* **1997**, 1993–1994.

[37] Fickes, M. G.; Ph.D. thesis; Massachusetts Institute of Technology; 1998.

[38] Tsai, Y.-C.; Johnson, M. J. A.; Mindiola, D. J.; Cummins, C. C.; Klooster, W. T.; Koetzle, T. F. *J. Am. Chem. Soc.* **1999**, *121*, 10426–10427.

[39] Mindiola, D. J.; Cummins, C. C. *Organometallics* **2001**, *20*, 3626–3628.

[40] Figueroa, J. S.; Cummins, C. C. *J. Am. Chem. Soc.* **2003**, *125*, 4020–4021.

[41] Cummins, C. C.; Personal communication.

[42] Figueroa, J. S.; Cummins, C. C. *J. Am. Chem. Soc.* **2004**, *126*, 13916–13917.

[43] Figueroa, J. S.; Cummins, C. C. *Angew. Chem., Int. Ed.* **2004**, *43*, 984–988.

[44] Figueroa, J. S.; Cummins, C. C. *Angew. Chem., Int. Ed.* **2005**, *44*, 4592–4596.

[45] Figueroa, J. S.; Ph.D. thesis; Massachusetts Institute of Technology; 2005.

[46] Proulx, G.; Bergman, R. G. *J. Am. Chem. Soc.* **1995**, *117*, 6382–6383.

[47] Fickes, M. G.; Davis, W. M.; Cummins, C. C. *J. Am. Chem. Soc.* **1995**, *117*, 6384–6385.

[48] Cenini, S.; Gallo, E.; Caselli, A.; Ragaini, F.; Fantauzzi, S.; Pianiolino, C. *Coord. Chem. Rev.* **2006**, *250*, 1234–1253.

[49] Thyagarajan, S.; Shay, D. T.; Incarvito, C. D.; Rheingold, A. L.; Theopold, K. H. *J. Am. Chem. Soc.* **2003**, *125*, 4440–4441.

[50] Castro-Rodriguez, I.; Olsen, K.; Gantzel, P.; Meyer, K. *J. Am. Chem. Soc.* **2003**, *125*, 4565–4571.

[51] Waterman, R.; Hillhouse, G. L. *J. Am. Chem. Soc.* **2008**, *130*, 12628–12629.

[52] Hanna, T. E.; Keresztes, I.; Lobkovsky, E.; Bernskoetter, W. H.; Chirik, P. J. *Organometallics* **2004**, *23*, 3448–3458.

[53] Proulx, G.; Bergman, R. G. *Organometallics* **1996**, *15*, 684–692.

[54] Guillemot, G.; Solari, E.; Floriani, C.; Rizzoli, C. *Organometallics* **2001**, *20*, 607–615.

[55] Dias, H. V. R.; Polach, S. A.; Goh, S.-K.; Archibong, E. F.; Marynick, D. S. *Inorg. Chem.* **2000**, *39*, 3894–3901.

[56] Bart, S. C.; Lobkovsky, E.; Bill, E.; Chirik, P. J. *J. Am. Chem. Soc.* **2006**, *128*, 5302–5303.

[57] Abu-Omar, M. M.; Shields, C. E.; Edwards, N. Y.; Eikey, R. A. *Angew. Chem., Int. Ed.* **2005**, *44*, 6203–6207.

[58] Jenkins, D. M.; Betley, T. A.; Peters, J. C. *J. Am. Chem. Soc.* **2002**, *124*, 11238–11239.

[59] Brown, S. D.; Betley, T. A.; Peters, J. C. *J. Am. Chem. Soc.* **2003**, *125*, 322–323.

[60] Weber, L. *Angew. Chem., Int. Ed.* **2007**, *46*, 830–832.

[61] Rahmoune, M.; Yeung Lam Ko, Y. Y. C.; Carrie, R. *New J. Chem.* **1989**, *13*, 891–898.

[62] Brask, J. K.; Fickes, M. G.; Sangtrirutnugul, P.; Durà-Vilà, V.; Odom, A. L.; Cummins, C. C. *Chem. Commun.* **2001**, 1676–1677.

[63] Brask, J. K.; Chivers, T.; Krahn, M. L.; Parvez, M. *Inorg. Chem.* **1999**, *38*, 290–295.

[64] Barth, A.; Huttner, G.; Fritz, M.; Zsolnai, L. *Angew. Chem., Int. Ed. Engl.* **1990**, *29*, 929–931.

[65] Niecke, E.; Nieger, M.; Reichert, F. *Angew. Chem., Int. Ed. Engl.* **1988**, *27*, 1715.

[66] Herzfeld, J.; Berger, A. E. *J. Chem. Phys.* **1980**, *73*, 6021–6030.

[67] Wu, G.; Rovnyak, D.; Johnson, M. J. A.; Zanetti, N. C.; Musaev, D. G.; Morokuma, K.; Schrock, R. R.; Griffin, R. G.; Cummins, C. C. *J. Am. Chem. Soc.* **1996**, *118*, 10654–10655.

[68] Nakashima, T. T.; Teymoori, R.; Wasylishen, R. E. *Magn. Reson. Chem.* **2009**.

[69] Eichele, K.; Wasylishen, R. E. *HBA*; 1.6; University of Alberta and Universität Tübingen, 2009.

[70] te Velde, G.; Bickelhaupt, F. M.; Baerends, E. J.; Fonseca Guerra, C.; van Gisbergen, S. J. A.; Snijders, J. G.; Ziegler, T. *J. Comput. Chem.* **2001**, *22*, 931–967.

[71] *ADF*; 2007.01; Scientific Computing & Modeling: Theoretical Chemistry, Vrije Universiteit, Amsterdam, The Netherlands, 2007. `http://www.scm.com`.

[72] Rundel, W. *Chem. Ber.* **1978**, *111*, 3510–3513.

[73] Anslyn, E. V.; Dougherty, D. A. *Modern Physical Organic Chemistry*; University Science Books: Sausalito, 2006.

[74] Niecke, E.; Gudat, D. *Angew. Chem., Int. Ed. Engl.* **1991**, *30*, 217–237.

[75] Schoeller, W. W.; Busch, T.; Niecke, E. *Chem. Ber.* **1990**, *123*, 1653–1654.

[76] Nguyen, M.-T.; McGinn, M. A.; Hegarty, A. F. *J. Am. Chem. Soc.* **1985**, *107*, 8029–8033.

[77] Trinquier, G. *J. Am. Chem. Soc.* **1982**, *104*, 6969–6977.

[78] Schmidt, M. W.; Gordon, M. S. *Inorg. Chem.* **1986**, *25*, 248–254.

[79] Allen, T. L.; Scheiner, A. C.; Yamaguchi, Y.; Schaefer, H. F. *J. Am. Chem. Soc.* **1986**, *108*, 7579–7588.

[80] Scheer, M.; Schuster, K.; Budzichowski, T. A.; Chisholm, M. H.; Streib, W. E. *J. Chem. Soc., Chem. Commun.* **1995**, 1671–1672.

[81] Scheer, M.; Kramkowski, P.; Schuster, K. *Organometallics* **1999**, *18*, 2874–2883.

[82] Esterhuysen, C.; Frenking, G. *Chem. Eur. J.* **2003**, *2003*, 3518–3529.

[83] Darensbourg, D. J. *Mechanistic Pathways for Metal Substitution Pathways in Metal Carbonyls*; Stone, F. G. A.; West, R., Eds.; Advances In Organometallic Chemistry, Vol. 21; Academic Press: New York, 1982; pp 113–150.

[84] Magee, T. A.; Matthews, C. N.; Wang, T. S.; Wotiz, J. H. *J. Am. Chem. Soc.* **1961**, *83*, 3200–3203.

[85] Strohmeier, W.; von Hobe, D. *Chem. Ber.* **1961**, *94*, 761–765.

[86] Strohmeier, W. *Angew. Chem., Int. Ed. Engl.* **1964**, *3*, 730–737.

[87] Angelici, R. J.; Malone, S. M. D. *Inorg. Chem.* **1967**, *6*, 1731–1736.

[88] Suslick, K. S.; Goodale, J. W.; Schubert, P. F.; Wang, H. H. *J. Am. Chem. Soc.* **1983**, *105*, 5781–5785.

[89] Johnson, B. P.; Balázs, G.; Scheer, M. *Coord. Chem. Rev.* **2006**, *250*, 1178–1195.

[90] Scheer, M.; Müller, J.; Häser, M. *Angew. Chem., Int. Ed. Engl.* **1996**, *35*, 2492–2496.

[91] Goldstein, M. J.; Hoffmann, R. *J. Am. Chem. Soc.* **1971**, *93*, 6193–6204.

[92] Grimme, W.; Wortmann, J.; Frowein, D.; Lex, J.; Chen, G.; Gleiter, R. *J. Chem. Soc., Perkin Trans. 2* **1998**, 1893–1900.

[93] Chou, T.-C.; Jiang, T.-S.; Hwang, J.-T.; Lin, K.-J.; Lin, C.-T. *J. Org. Chem.* **1999**, *64*, 4874–4883.

[94] Martin, J.; Hill, R. *Chem. Rev.* **1961**, *61*, 537–562.

[95] Hoffmann, R.; Woodward, R. *J. Am. Chem. Soc.* **1965**, *87*, 4388–4389.

[96] Piro, N. A.; Figueroa, J. S.; McKellar, J. T.; Cummins, C. C. *Science* **2006**, *313*, 1276–1279.

[97] Scherer, O. J. *Acc. Chem. Res.* **1999**, *32*, 751–762.

[98] Jutzi, P.; Meyer, U.; Opiela, S.; Neumann, B.; Stammler, H. G. *J. Organomet. Chem.* **1992**, *439*, 279–301.

[99] Phillips, I. G.; Ball, R.; Cavell, R. G. *Inorg. Chem.* **1992**, *31*, 1633–1641.

[100] Pietschnig, R.; Niecke, E. *Organometallics* **1996**, *15*, 891–893.

[101] Burckett-St.Laurent, J. C. T. R.; Hitchcock, P. B.; Kroto, H. W.; Nixon, J. F. *J. Chem. Soc., Chem. Commun.* **1981**, 1141–1143.

[102] Schäfer, H.; Binder, D.; Fenske, D. *Angew. Chem., Int. Ed. Engl.* **1985**, *24*, 522–524.

[103] Schäfer, H.; Binder, D. *Z. Anorg. Allg. Chem.* **1988**, *560*, 65–79.

[104] Scheer, M.; Dargatz, M.; Rufińska, A. *J. Organomet. Chem.* **1992**, *440*, 327–334.

[105] Taylor, N. J.; Chieh, P. C.; Carty, A. J. *J. Chem. Soc., Chem. Commun.* **1975**, 448–449.

[106] Petz, W.; Kutschera, C.; Neumüller, B. *Organometallics* **2005**, *24*, 5038–5043.

[107] Gallo, V.; Latronico, M.; Mastrorilli, P.; Nobile, C. F.; Suranna, G. P.; Ciccarella, G.; Englert, U. *Eur. J. Inorg. Chem.* **2005**, 4607–4616.

[108] Cowley, A. H. *Acc. Chem. Res.* **1997**, *30*, 445–451.

[109] Chong, D.; Laws, D. R.; Nafady, A.; Costa, P. J.; Rheingold, A. L.; Calhorda, M. J.; Geiger, W. E. *J. Am. Chem. Soc.* **2008**, *130*, 2692–2703.

[110] Davies, J. E.; Mays, M. J.; Raithby, P. R.; Shields, G. P.; Tompkin, P. K.; Woods, A. D. *J. Chem. Soc., Dalton Trans.* **2000**, 1925–1930.

[111] Dahlgren, R. M.; Zink, J. I. *Inorg. Chem.* **1977**, *16*, 3154–3161.

[112] Freudenberger, J. H.; Schrock, R. R.; Churchill, M. R.; Rheingold, A. L.; Ziller, J. W. *Organometallics* **1984**, *3*, 1563–1573.

[113] Churchill, M. R.; Ziller, J. W.; Freudenberger, J. H.; Schrock, R. R. *Organometallics* **1984**, *3*, 1554–1562.

[114] Pedersen, S. F.; Schrock, R. R.; Churchill, M. R.; Wasserman, H. J. *J. Am. Chem. Soc.* **1982**, *104*, 6808–6809.

[115] Schrock, R. R.; Murdzek, J. S.; Freudenberger, J. H.; Churchill, M. R.; Ziller, J. W. *Organometallics* **1986**, *5*, 25–33.

[116] Schrock, R. R.; Pedersen, S. F.; Churchill, M. R.; Ziller, J. W. *Organometallics* **1984**, *3*, 1574–1583.

[117] Churchill, M. R.; Fettinger, J. C.; McCullough, L. G.; Schrock, R. R. *J. Am. Chem. Soc.* **1984**, *106*, 3356–3357.

[118] Churchill, M. R.; Ziller, J. W.; Pedersen, S. F.; Schrock, R. R. *J. Chem. Soc., Chem. Commun.* **1984**, 485–486.

[119] Stephens, F. H.; Johnson, M. J. A.; Cummins, C. C.; Kryatova, O. P.; Kryatov, S. V.; Rybak-Akimova, E. V.; McDonough, J. E.; Hoff, C. D. *J. Am. Chem. Soc.* **2005**, *127*, 15191–15200.

[120] Di Vaira, M.; Sacconi, L. *Angew. Chem., Int. Ed. Engl.* **1982**, *21*, 330–342.

[121] Di Vaira, M.; Midollini, S.; Sacconi, L. *J. Am. Chem. Soc.* **1979**, *101*, 1757–1763.

[122] Di Vaira, M.; Ghilardi, C. A.; Midollini, S.; Sacconi, L. *J. Am. Chem. Soc.* **1978**, *100*, 2550–2551.

[123] Dapporto, P.; Sacconi, L.; Stoppioni, P.; Zanobini, F. *Inorg. Chem.* **1981**, *20*, 3834–3839.

[124] Scherer, O. J.; Sitzmann, H.; Wolmershäuser, G. *J. Organomet. Chem.* **1984**, *268*, C9–C12.

[125] Scherer, O. J.; Sitzmann, H.; Wolmershäuser, G. *Angew. Chem., Int. Ed. Engl.* **1985**, *24*, 351–353.

[126] Chisholm, M. H.; Huffman, J. C.; Pasterczyk, J. W. *Inorg. Chim. Acta.* **1987**, *133*, 17–18.

[127] Scherer, O. J.; Schwalb, J.; Swarowsky, H.; Wolmershäuser, G.; Kaim, W.; Gross, R. *Chem. Ber.* **1988**, *121*, 443–449.

[128] Goh, L. Y.; Chu, C. K.; Wong, R. C. S.; Hambley, T. W. *J. Chem. Soc., Dalton Trans.* **1989**, 1951–1956.

[129] Scherer, O. J.; Braun, J.; Wolmershäuser, G. *Chem. Ber.* **1990**, *123*, 471–475.

[130] Cossairt, B. M.; Diawara, M.-C.; Cummins, C. C. *Science* **2009**, *323*, 602.

[131] Umbarkar, S.; Sekar, P.; Scheer, M. *J. Chem. Soc., Dalton Trans.* **2000**, 1135–1137.

[132] Ahlrichs, R.; Fenske, D.; Fromm, K.; Krautscheid, H.; Krautscheid, U.; Treutler, O. *Chem. Eur. J.* **1996**, *2*, 238–244.

[133] Corey, E. J.; Cheng, X.-M. *The Logic of Chemical Synthesis*; John Wiley & Sons, Inc.: New York, 1995.

[134] Balázs, G.; Gregoriades, L. J.; Scheer, M. *Organometallics* **2007**, *26*, 3058–3075.

[135] Laplaza, C. E.; Davis, W. M.; Cummins, C. C. *Angew. Chem., Int. Ed. Engl.* **1995**, *34*, 2042–2044.

[136] Zanetti, N. C.; Schrock, R. R.; Davis, W. M. *Angew. Chem., Int. Ed. Engl.* **1995**, *34*, 2044–2046.

[137] Cherry, J.-P. F.; Stephens, F. H.; Johnson, M. J. A.; Diaconescu, P. L.; Cummins, C. C. *Inorg. Chem.* **2001**, *40*, 6860–6862.

[138] Fox, A. R.; Clough, C. R.; Piro, N. A.; Cummins, C. C. *Angew. Chem., Int. Ed.* **2007**, *46*, 973–976.

[139] Hirsekorn, K. F.; Veige, A. S.; Wolczanski, P. T. *J. Am. Chem. Soc.* **2006**, *128*, 2192–2193.

[140] Kaupp, M.; Malkina, O. L.; Malkin, V. G.; Pyykkö, P. *Chem. Eur. J.* **1998**, *4*, 118–126.

[141] Di Vaira, M.; Sacconi, L.; Stoppioni, P. *J. Organomet. Chem.* **1983**, *250*, 183–195.

[142] Di Vaira, M.; Ehses, M. P.; Stoppioni, P.; Peruzzini, M. *Inorg. Chem.* **2000**, *39*, 2199–2205.

[143] Di Vaira, M.; Ehses, M. P.; Peruzzini, M.; Stoppioni, P. *J. Organomet. Chem.* **2000**, *593-594*, 127–134.

[144] Labinger, J. A. In *Comprehensive Organometallic Chemistry*; Wilkinson, G.; Stone, F. G. A.; Abel, E. W., Eds.; Pergamon Press: New York, 1982; Vol. 3, pp 707–708.

[145] Fermin, M. C.; Ho, J. W.; Stephan, D. W. *J. Am. Chem. Soc.* **1994**, *116*, 6033–6034.

[146] Fermin, M. C.; Ho, J. W.; Stephan, D. W. *Organometallics* **1995**, *14*, 4247–4256.

[147] Whitmore, K. H. *Main-Group Transition Metal Cluster Compounds of the Group 15 Elements*; Stone, F. G. A.; West, R., Eds.; Advances in Organometallic Chemistry, Vol. 42; Academic Press: San Diego, 1998; pp 1–145.

[148] Woo, T.; Folga, E.; Ziegler, T. *Organometallics* **1993**, *12*, 1289–1298.

[149] Jemmis, E. D.; Hoffmann, R. *J. Am. Chem. Soc.* **1980**, *102*, 2570–2575.

[150] Anslyn, E. V.; Bursich, M. J.; Goddard, I., W. A. *Organometallics* **1988**, *7*, 98–105.

[151] Lin, Z.; Hall, M. B. *Organometallics* **1994**, *13*, 2878–2884.

[152] Becker, G.; Becker, W.; Knebl, R.; Schmidt, H.; Weeber, U.; Westerhausen, M. *Nova Acta Leopold.* **1985**, *59*, 55–67.

[153] Bradley, D. C.; Mehrotra, R.; Rothwell, I.; Singh, A. *Alkoxo and Aryloxo Derivatives of Metals*; Academic Press: San Diego, 2001.

[154] Jamison, G. M.; Saunders, R. S.; Wheeler, D. R.; McClain, M. D.; Loy, D. A.; Ziller, J. W. *Organometallics* **1996**, *15*, 16–18.

[155] Spinney, H. A.; Piro, N. A.; Cummins, C. C. *In preparation.* **2009**.

[156] Rebek, J.; Gavina, F. *J. Am. Chem. Soc.* **1974**, *96*, 7112–7114.

[157] Marinetti, A.; Mathey, F.; Fishcer, J.; Mitschler, A. *J. Chem. Soc., Chem. Commun.* **1984**, 45–46.

[158] van Eis, M. J.; Zappey, H.; de Kanter, F. J. J.; de Wolf, W. H.; Lammertsma, K.; Bickelhaupt, F. *J. Am. Chem. Soc.* **2000**, *122*, 3386–3390.

[159] Pangborn, A. B.; Giardello, M. A.; Grubbs, R. H.; Rosen, R. K.; Timmers, F. J. *Organometallics* **1996**, *15*, 1518–1520.

[160] Hartley, F. R. *Organomet. Chem. Rev. A* **1970**, *6*, 119–137.

[161] Sen, A.; Halpern, J. *Inorg. Chem.* **1980**, *19*, 1073–1075.

[162] Williams, T.; Kelley, C. *Gnuplot*; 3.8j, 2002. `http://www.gnuplot.info`.

[163] Sheldrick, G. M. *SHELXTL*; Bruker AXS, Inc.: Madison, WI (USA), 2005–2008.

[164] Sheldrick, G. M. *Acta Crystallogr., Sect. A: Fundam. Crystallogr.* **1990**, *46*, 467–473.

[165] Sheldrick, G. M. *Acta Crystallogr., Sect. A: Fundam. Crystallogr.* **2008**, *64*, 112–122.

[166] Sheldrick, G. M. *SHELXL-97: Program for crystal structure determination*; University of Göttingen, 1997.

[167] Müller, P.; Herbst-Irmer, R.; Spek, A. L.; Schneider, T. R.; Sawaya, M. R. *Crystal Structure Refinement: A Crystallographer's Guide to SHELXL*; Müller, P., Ed.; IUCr Texts on Crystallography; Oxford University Press: Oxford, 2006.

[168] The Reciprocal Net Site Network is a distributed database for crystallographic information, supported by the National Science Digital Library, and is run by participating crystallography labs across the world. Crystallographic data for complexes in this chapter are available under the identification codes listed in Tables 1.5 – 1.8 from the MIT Reciprocal Net site. `http://reciprocal.mit.edu/recipnet`.

[169] These data can be obtained free of charge from The Cambridge Crystallographic Data Centre via `http://www.ccdc.cam.ac.uk/data_request/cif`.

[170] Fonseca Guerra, C.; Snijders, J. G.; te Velde, G.; Baerends, E. J. *Theo. Chem. Acc.* **1998**, *99*, 391–403.

[171] Vosko, S. H.; Wilk, L.; Nusair, M. *Can. J. Phys.* **1980**, *58*, 1200–1211.

[172] Becke, A. D. *Phys. Rev. A* **1988**, *38*, 3098–3100.

[173] Perdew, J. P. *Phys. Rev. B* **1986**, *33*, 8822–8824; erratum: *Phys. Rev. B* **1986**, *34*, 7406.

[174] vanLenthe, E.; Snijders, J. G.; Baerends, E. J. *J. Chem. Phys.* **1996**, *105*, 6505–6516.

[175] van Lenthe, E.; Baerends, E. J.; Snijders, J. G. *J. Chem. Phys.* **1994**, *101*, 9783–9792.

[176] van Lenthe, E.; Ehlers, A.; Baerends, E. J. *J. Chem. Phys.* **1999**, *110*, 8943–8953.

[177] van Lenthe, E.; Baerends, E. J.; Snijders, J. G. *J. Chem. Phys.* **1993**, *99*, 4597–4610.

[178] Schreckenbach, G.; Ziegler, T. *Int. J. Quantum Chem.* **1997**, *61*, 899–918.

[179] Schreckenbach, G.; Ziegler, T. *J. Phys. Chem.* **1995**, *99*, 606–611.

[180] Wolff, S. K.; Ziegler, T. *J. Chem. Phys.* **1998**, *109*, 895–905.

[181] Wolff, S. K.; Ziegler, T.; van Lenthe, E.; Baerends, E. J. *J. Chem. Phys.* **1999**, *110*, 7689–7698.

[182] van Wüllen, C. *Phys. Chem. Chem. Phys.* **2000**, *2*, 2137–2144.

[183] Johnson, M. J. A.; Odom, A. L.; Cummins, C. C. *Chem. Commun.* **1997**, 1523–1524.

CHAPTER 2

Reactivity of *cyclo*-P_3 Complexes: A Route to Triphosphacyclobutadiene Reactive Intermediates

Contents

Reproduced in part with permission from:
Piro, N. A.; Cummins, C. C. *J. Am. Chem. Soc.* **2008**, *130*, 9524–9535, Copyright 2008 American Chemical Society;
Piro, N. A.; Cummins, C. C. *Angew. Chem., Int. Ed.* **2008**, *48*, 934–938, Copyright 2008 Wiley-VCH.

2.1 INTRODUCTION

The previous chapter focused on the development and study of a P_2-eliminating diphosphaazide complex. This complex served as a source of a neutral P_2 synthon for the synthesis of various molecules, including early transition metal *cyclo*-P_3 complexes. In this chapter the chemistry of the reactive niobium *cyclo*-P_3 anions is developed. In particular, a focus was placed on the study of reactions in which the complexes $[\{(OC)_5W\}_n(P_3)Nb(N[CH_2{}^tBu]Ar)_3]^-$ ($n = 0, 1, 2$; Ar = 3,5-dimethylphenyl) could serve as ${P_3}^{3-}$ synthons. Such reactions could be driven by salt elimination coupled with formation of strong NbX_2 bonds (X_2 = Cl_2, Br_2, O, NR). In this sense this chemistry complements the P_1 transfer chemistry of the niobium phosphide anion **3**, and the P_2 transfer chemistry of the diphosphaazide complex **1**, each driven by the formation of strong metal-ligand multiple bonds.[1,2]

Functionalizations of *cyclo*-P_3 complexes were first reported for the series $(P_3)M(triphos)$ (M = Co, Rh, Ir; triphos = $CH_3C(CH_2PPh_2)_3$) and required the highly electrophilic reagents

$[Me_3O][BF_4]$ or MeOTf to afford the methylated species.[3] The $[MeP_3Co(triphos)]^+$ complex was crystallographically characterized and it displays structural distortions similar to those in $(OC)_5W(P_3)W(N[^iPr]Ar)_3$, where rehybridization at the methylated phosphorus results in a shortening of bonds to this atom. An alternative bonding scenario exists wherein the third, functionalized phosphorous is more removed from the metal at a distance where any bonding interaction can be considered weak at best. In this case, the bonding is best described according to a coordinated diphosphene model, with coordinated diphosphenes being well known.[4–11] When the diphosphene is part of an all-phosphorus, three-membered ring, the ligand can then be regarded as a coordinated triphosphirene. The η^2-triphosphirene moiety has precedent in other P_4-derived complexes of Peruzzini and co-workers.[12,13]

While the neutral, late-metal *cyclo*-P_3 complexes built on triphos scaffolds were difficult to functionalize, the anionic nature of the *cyclo*-P_3 niobium complexes described herein imparts them with more nucleophilic character, allowing functionalization with more mild reagents. This nucleophilicity has been exploited to give products that contain various triphosphirenes as complexed ligands. In particular, acyltriphosphirenes have been explored for their ability to release reactive triphosphacyclobutadiene complexes into solution. The chemistry of these bis-$W(CO)_5$ adducts of triphosphacyclobutadiene has been explored with a focus on cycloaddition reactions, an approach also used to characterize the parent cyclobutadiene.[14–16] This comparison is appropriate because the the ability to replace "RC" units in organic motifs by the isolobal phosphorus atom, while retaining behavior in cycloaddition reactions, is well known.[8] In fact, the general similarities between phosphorus and its diagonal partner, carbon, have led to phosphorus being dubbed the "carbon copy."[8] One obvious difference between RC and P groups is the accessible phosphorus lone pair. This will sometimes lead to unwanted side reactions and it has been noted that *"blocking this lone pair by unreactive and tightly bound transition metal complexing groups such as $W(CO)_5$ allows the analogy to be much more clearly expressed."*[8] In the previous chapter the $W(CO)_5$ group was also used to stabilize unsaturated intermediates without shutting down reactivity of the π systems.

An intermediate triphosphacyclobutadiene complex has also given access to tetraphosphabenzenes complexed by protective $W(CO)_5$ units. These tetraphosphacyclobutadienes and tetraphosphabenzenes are among the most phosphorus-rich analogues of benzene and cyclobutadiene known. The all-phosphorus analogs of benzene and cyclobutadiene have been considered theoretically but remain synthetically elusive;[17–20] however, a few examples of reduced P_6 and P_4 ligands complexed to one or more metal centers are known.[21–24] Diphosphacyclobutadienes and valence isomers of triphosphabenzenes have been accessed through metal-mediated oligomerization of phosphaalkynes,[25–27] and two related reactions generate triphosphacyclobutadiene ligands π-complexed to reducing metal centers.[28,29] There is also one example of a highly distorted $P_4(C^tBu)_2$ ligand complexed between two Rh centers,[30] and a diradical valence isomer of a tetraphosphabenzene has been reported to contain multiple $1e^-$ bonds.[31]

2.2 REACTIONS OF *cyclo*-P_3 COMPLEXES WITH ELECTROPHILES

2.2.1 Stannylation with Ph_3SnCl

Initial studies in functionalization of *cyclo*-P_3 complexes focused on the formation of new main-group substituted triphosphirene ligands. Accordingly, in order to afford a stannylated triphosphirene complex, the *cyclo*-P_3 complex $[(12\text{-crown-4})_2Na][(OC)_5W(P_3)Nb(N[CH_2{}^tBu]Ar)_3]$ was treated with triphenyltin chloride in dimethoxyethane and the reaction mixture was heated to 75 °C for 14 h. This yielded the *P*-stannylated species $(OC)_5W(Ph_3SnP_3)Nb(N[CH_2{}^tBu]Ar)_3$, **19**, following separation from residual starting material and free aniline, Scheme 2.1. This compound can also be isolated in low yields by selective crystallization from the reaction between $[(Et_2O)Na][(OC)_5W(P_3)Nb(N[CH_2{}^tBu]Ar)_3]$ and Ph_3SnCl in a reaction where loss of $W(CO)_5$ occurs. The ^{31}P NMR data for **19** consist of a broad multiplet for the stannylated phosphorus at –196 ppm and a very broad resonance for the $(P_2)W(CO)_5$ unit at –235 ppm, Figure 2.1. The broadness of both resonances is indicative of dynamic processes, such as mobility of $W(CO)_5$ across the incompletely reduced P−P π bond. A similar exchange process was observed for $(OC)_5WP_2[Pt(PPh_3)_2]_2$, Section 1.6.4. In addition, a second process whereby the stannyl group migrates around the ring is likely operative. The latter hypothesis is supported by a ^1H NMR spectrum indicative of C_{3v} symmetry and a complex ^{119}Sn NMR spectrum with a doublet ($^1J_{SnP}$ = 1440 Hz) centered around a broad feature at –76 ppm. The dynamic nature of the bonding in small phosphorus rings with heavy atoms is not unprecedented.[32]

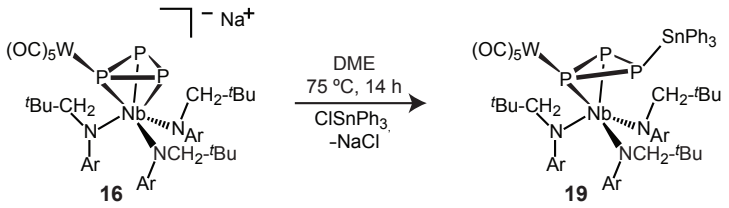

Scheme 2.1. Synthesis of $[(OC)_5W(Ph_3SnP_3)Nb(N[CH_2{}^tBu]Ar)_3$ (**19**).

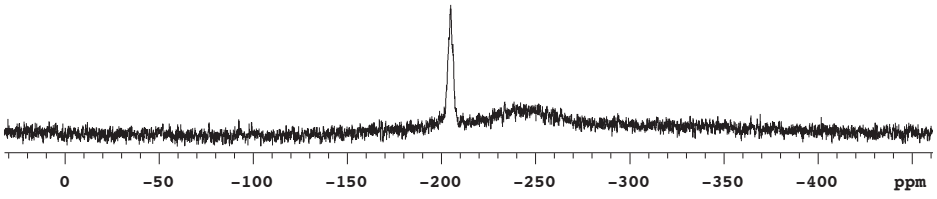

Figure 2.1. The ^{31}P NMR spectrum of **19** shows two broad resonances. The sharper resonance is attributed to the one P nucleus bearing the $SnPh_3$ substituent, and the broader resonance to the other two phosphorus atoms. The overall broadness is believed to be due to dynamic processes whereby the $W(CO)_5$ and $SnPh_3$ substituents circumambulate the *cyclo*-P_3 ring.

An X-ray crystallographic structure determination confirmed the assignment of the new ligand as an η^2-triphosphirene coordinated to the niobium trisanilide platform, Figure 2.2. The two short Nb–P distances, 2.5611(9) and 2.5676(9) Å, and one long interaction, 2.8379(9) Å, are characteristic of this description. The P1–P2 distance of 2.156(1) Å is intermediate between a P–P double (*ca.* 2.00 – 2.04 Å)[6] and P–P single bond (*cf.* 2.21 Å in P_4),[33] also consistent with the coordinated diphosphene model. The P1–P3 and P2–P3 bonds are each slightly longer at 2.188(1) and 2.213(1) Å, respectively. The P3–Sn1 distance is 2.5288(9) Å.

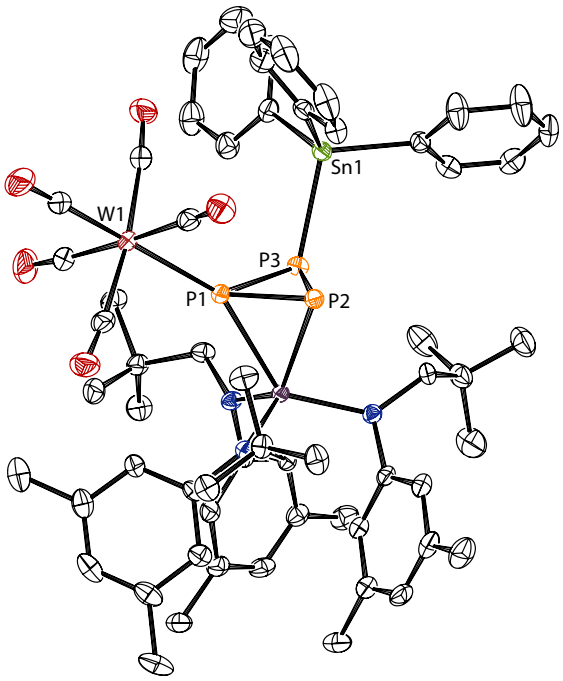

Figure 2.2. Thermal ellipsoid plot (50% probability) of **19** with hydrogen atoms omitted for clarity.

2.2.2 A Dynamic Mes*NP$_4$ Ligand

The reactions of other electrophiles with $[\{(OC)_5W\}_2(P_3)Nb(N[CH_2{}^tBu]Ar)_3]^-$, **17**, were also examined to explore the limits of functionalized triphosphirene complexes. In one example, the complex Na[**17**] was found to react readily with Mes*NPCl (Mes* = 2,4,6-tri-*tert*-butylphenyl). Analysis of the reaction mixture at early stages revealed a mixture of products by ^{31}P NMR spectroscopy. The major ^{31}P NMR resonances at early times (*ca.* 30 min) are at 364.5 (br *pseudo* d, $^1J_{PP}$ = 350 Hz, 1P), –110 to –118 (br m, 2P), and –132 (br *pseudo* t, $^1J_{PP}$ = 250 Hz, 1P) ppm. These are consistent with the expected Mes*NP–P(PW(CO)$_5$)$_2$ unit, where the downfield resonance can be attributed to the Mes*NP phosphorus, and the upfield resonances to the *cyclo*-P_3 ring. However, this intermediate decays over time and over 24 h the product distribution converges onto a single product, **20**. This final product exhibits a ^{31}P NMR spectrum with a downfield quartet (δ = 367 ppm, J_{PP} = 105 Hz) and an upfield doublet (δ = –137 ppm, J_{PP} = 105 Hz), Figure 2.3. The observed quartet

was particularly interesting because it suggested a Mes*NP$^+$ unit possessing equivalent interactions with all three P atoms of the *cyclo*-P_3 moiety.

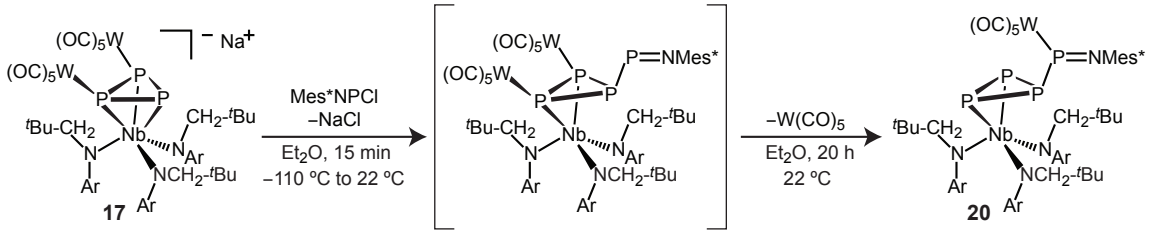

Scheme 2.2. Synthesis of Mes*NP[W(CO)$_5$]P$_3$Nb(N[CH$_2$^{t}Bu]Ar)$_3$ (**20**).

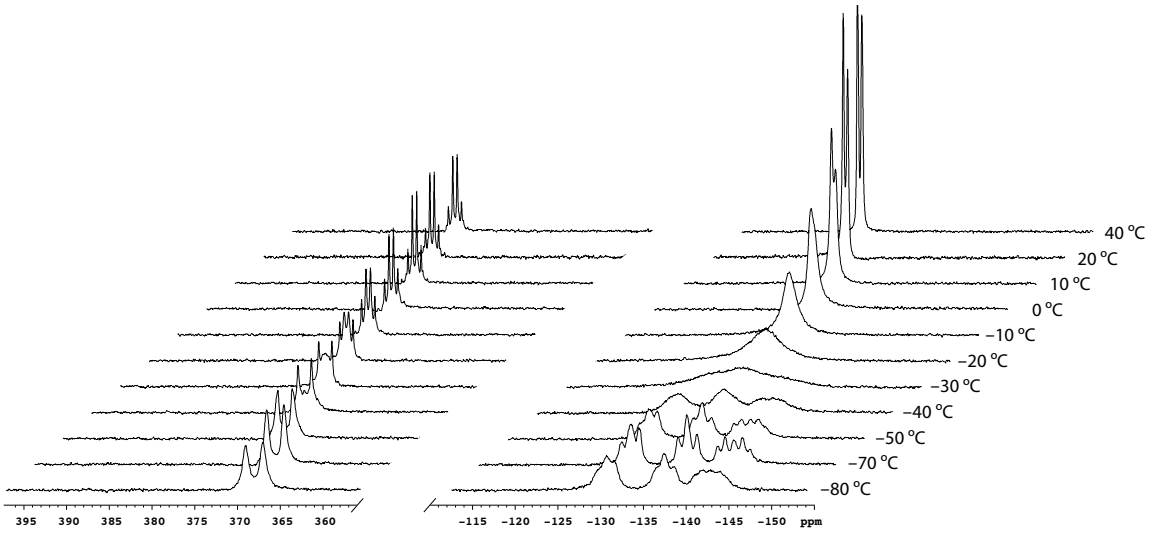

Figure 2.3. At 20 °C the ^{31}P NMR spectrum of **20** displays only two resonances, indicative of Mes*NP circumambulation. Upon cooling to –80 °C the two resonances split to four resonances that display couplings consistent with the solid state structure.

An X-ray crystallographic structure determination of **20** revealed an η^2-triphosphirene geometry, analogous to the stannyl derivative, Figure 2.4. In the structure of this new product, however, one W(CO)$_5$ unit has migrated to the iminophosphane moiety and the second W(CO)$_5$ of the starting material has been lost. The P−P distance between the Mes*NP unit and the *cyclo*-P$_3$ moiety is 2.2326(11) Å, the P−P distance of the coordinated diphosphene is 2.1650(11) Å and the other two P−P distances are *ca.* 2.20 Å. The three Nb−P distances were found to be 2.5655(9) and 2.5988(8) Å to the diphosphene unit and 3.0194(8) Å to the P atom bearing the Mes*NP$^+$ unit. All of these metrics are consistent with a coordinated diphosphene model. The Mes* group on N4 and the substituent at P4 are arranged *cis* in **20**, as has been observed previously for the chloroiminophosphane precursor as well as for certain iminophosphanes bearing metal carbonyls.[34,35] It is also noteworthy that the Mes*NP$^+$ group is seen here demonstrating its

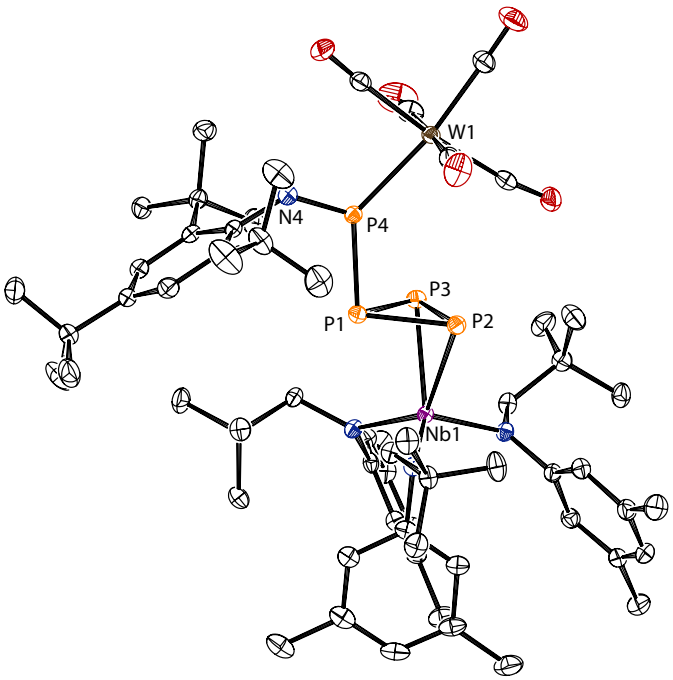

Figure 2.4. Thermal ellipsoid plot (50% probability) of **20** with hydrogen atoms omitted for clarity.

ambiphilic character, acting as both a Lewis acid to the *cyclo*-P_3 donor and a Lewis base to the $W(CO)_5$ unit.[36,37]

The ^{31}P NMR spectrum of this product can be explained by a dynamic process whereby at 20 °C the Mes^*NP^+ unit migrates around the *cyclo*-P_3 ring concomitant with formation and release of Nb−P interactions. Variable-temperature ^{31}P NMR spectra of **20** revealed that this process could be locked out at temperatures below –40 °C, Figure 2.3. At –70 °C the spectrum displays a downfield doublet and three upfield multiplets, consistent with the solid-state structure. Migration of $RN{\equiv}P^+$ (R = Mes^*, $^iPr_3Si$, ^tBu) units around unsaturated rings has been observed previously in the iminophosphanes $RNPCp^*$.[38] Interestingly, even the solid-state structure of $^iPr_3SiNPCp^*$ exhibits a slipped geometry wherein the C=C bond of the Cp^* ring binds in η^2 fashion to the P atom. It is noteworthy also that the $RN{\equiv}P^+$ unit is not unique in this behavior, and that the diphosphene $Cp^*P{=}PCp^*$ exhibits a single methyl environment at temperatures as low as –80 °C.[40]

2.2.3 Reaction with PCl_3: A Synthesis of P_4

The reactions with Ph_3SnCl and with Mes^*NPCl demonstrated the ability of the $W(CO)_5$-coordinated *cyclo*-P_3 complexes **16** and **17** to serve as nucleophiles. With the goal of using these complexes as P_3^{3-} synthons, potential electrophilic reaction partners that could serve as acceptors for a triply anionic phosphorus ring were investigated. The common electrophile PCl_3 was chosen for its potential to replace the niobium trisanilide fragment as the fourth vertex of the tetrahedron and generate P_4. The transfer of P_3^{3-} from a niobium *cyclo*-P_3 complex to PCl_3 would be driven by

the formation of NaCl and the replacement of Nb–P bonds with strong Nb–Cl bonds. Because P_4 serves as the initial entry point to this chemistry (see Scheme A.1) there is also a recognized irony in seeking to regenerate P_4 after so many synthetic steps.

The readily available Na[**17**], reacts cleanly with an excess of PCl_3 at 22 °C to generate $Cl_2Nb(N[CH_2{}^tBu]Ar)_3$ and P_4 (δ = –520 ppm), Scheme 2.3. In this reaction two equivalents of $W(CO)_5$ are lost to solution and likely decompose by various pathways.[41] The fact that $W(CO)_5$ is lost is unsurprising given that P_4 is known to be a poor ligand. In fact, no complexes of P_4 ligated only to $W(CO)_5$ are known: under photolytic conditions a combination of $W(CO)_6$ and P_4 will instead generate $P_4[W(CO)_5]_4W(CO)_4$.[23] Unfortunately, the reactions between $[\{(OC)_5W\}_nP_3Nb(N[CH_2{}^tBu]Ar)_3]^-$ and other ECl_3 molecules (E = As, Sb, PhSn) did not readily afford identifiable tetrahedra. However, the methodology of using *cyclo*-P_3 complexes of niobium as $P_3{}^{3-}$ transfer reagents has been successfully applied to a tris(alkoxy)niobium platform by Cossairt *et al*. to afford a synthesis of the simple tetratomic molecule AsP_3 in pure form.[42]

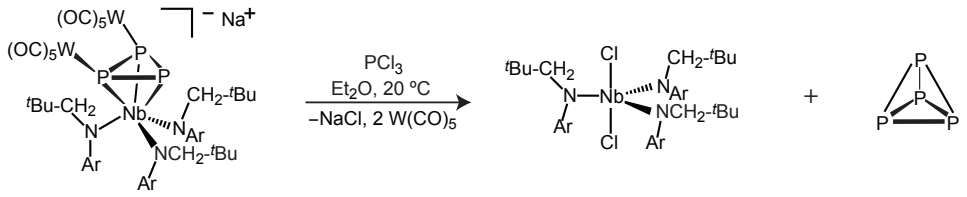

Scheme 2.3. Generation of P_4 from $[Na][\{(OC)_5W\}_2P_3Nb(N[CH_2{}^tBu]Ar)_3]$ and PCl_3.

2.3 Acyltriphosphirene Complexes and Ligand Deoxygenation

2.3.1 Synthesis and Structure

The above reaction chemistry of **17** with PCl_3 is driven by NaCl formation and the halophilicity of niobium, as Nb–Cl bonds replace weaker Nb–P bonds during the course of the reaction. Figueroa has similarly utilized the oxophilicity of niobium to drive the deoxygenation of an acylated phosphorus ligand for the formation of new phosphorus–element bonds concomitant with production of oxoniobium $ONb(N[CH_2{}^tBu]Ar)_3$, **21**.[1] Thus, as a potential avenue to using *cyclo*-P_3 complexes as $P_3{}^{3-}$ transfer reagents, a P-acylated triphosphirene complex was synthesized via the reaction between $[(THF)Na][(P_3)Nb(N[{}^tBu]Ar)_3]$ and 1-adamantanecarbonyl chloride in thawing Et_2O and warming to 20 °C, Scheme 2.4. The product acyltriphosphirene complex, $AdC(O)P_3Nb(N[CH_2{}^tBu]Ar)_3$, **22**, was isolated by crystallization from Et_2O in 74% yield as red orange crystals. The ^{31}P NMR spectrum of this compound consists of a doublet at –117 ppm and a triplet at –179 ppm, corresponding to the diphosphene and acylated centers, respectively. An X-ray crystallographic structure determination from a monoclinic crystal revealed two short Nb−P bonds,

2.5475(6) Å and 2.5915(6) Å, and one longer interaction at 2.9268(6) Å, Figure 2.5. The three P–P bonds are 2.1556(7) Å (P2–P3), 2.1724(8) Å (P1–P2) and 2.1956(8) Å (P1–P3). Thermolysis of **22** at 65 °C for 3 h affords oxoniobium **21**, but the several phosphorus-containing co-products were unable to be identified. Attention was thus turned to a variant upon **15** that contains two $W(CO)_5$ protecting groups.

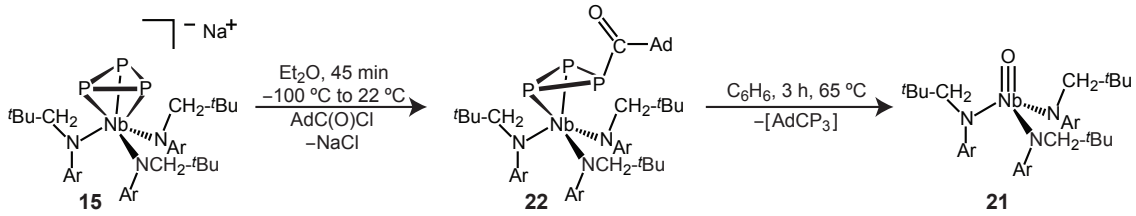

Scheme 2.4. Synthesis of the acyltriphosphirene complex $AdC(O)P_3Nb(N[CH_2{}^tBu]Ar)_3$ (**22**).

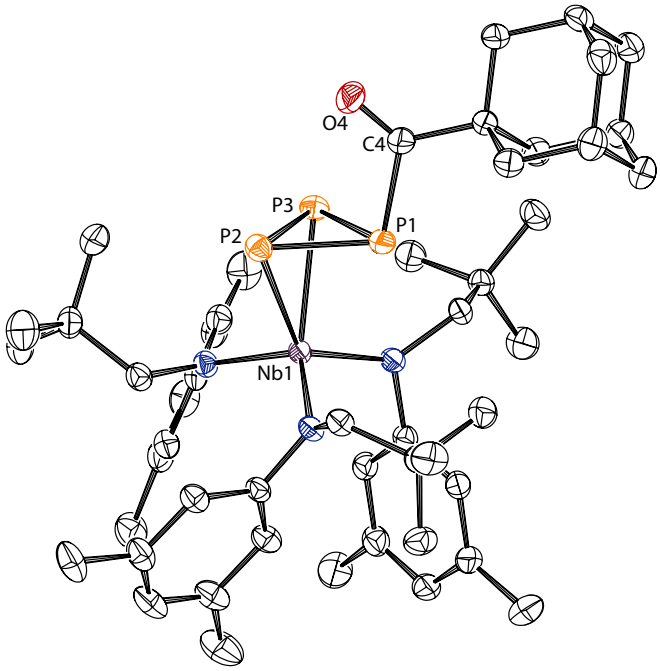

Figure 2.5. Thermal ellipsoid plot (50% probability) of **22** with hydrogen atoms omitted for clarity.

The bis-$W(CO)_5$ acyltriphosphirene complex was synthesized analogously by reaction of the sodium salt of **17** with $^1AdC(O)Cl$ in thawing Et_2O, followed by warming to room temperature briefly, and rapid work-up, Scheme 2.5. Analysis of the reaction mixture, following removal of NaCl, revealed the expected broad resonance attributed to the coordinated diphosphene (δ = –144 ppm) and a sharp triplet (δ = –204 ppm, J_{PP} = 180) for the acylated P center in the ^{31}P NMR spectrum; the ^1H NMR spectrum revealed one new, C_s-symmetric species. This red complex, $\{(OC)_5W\}_2AdC(O)P_3Nb(N[CH_2{}^tBu]Ar)_3$, **23**^{Ad}, was isolated in 60% yield by

precipitation from Et_2O at –35 °C. The *tert*-butyl variant, **23**^{tBu}, was synthesized similarly by replacing 1-adamantanecarbonyl chloride with pivaloyl chloride. This complex is also C_s-symmetric by ^{1}H NMR spectroscopy and displays ^{31}P resonances at –139 (d) and –203 (t) ppm.

A red crystal of **23**^{Ad} was grown at –35 °C from Et_2O solution and was subjected to an X-ray diffraction study that revealed the predicted η^2-bound triphosphirene, Figure 2.6. In **23**^{Ad}, the diphosphene P–P distance is 2.1453(9) Å and the other P–P distances are 2.2008(9) and 2.2320(9) Å. The Nb−P distances are 2.5770(7) and 2.6122(7) Å to the diphosphene unit and 3.0292(7) Å to the P atom bearing the acyl unit. These data compare well with the acyltriphosphirene **22**, which lacks the two pendant $W(CO)_5$ groups.

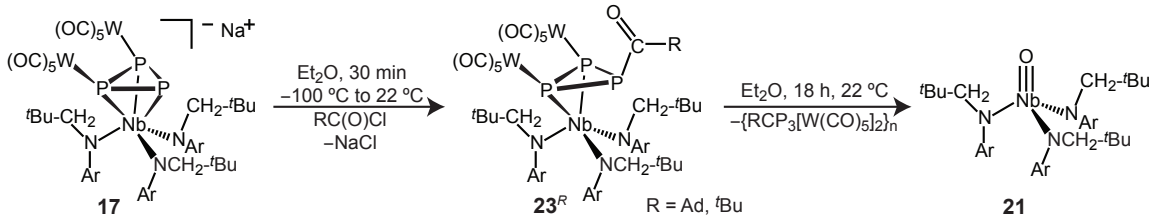

Scheme 2.5. Synthesis of the acyltriphosphirene complexes $[(OC)_5W]_2RC(O)P_3Nb(N[CH_2{}^tBu]Ar)_3$ (**23**^{R}).

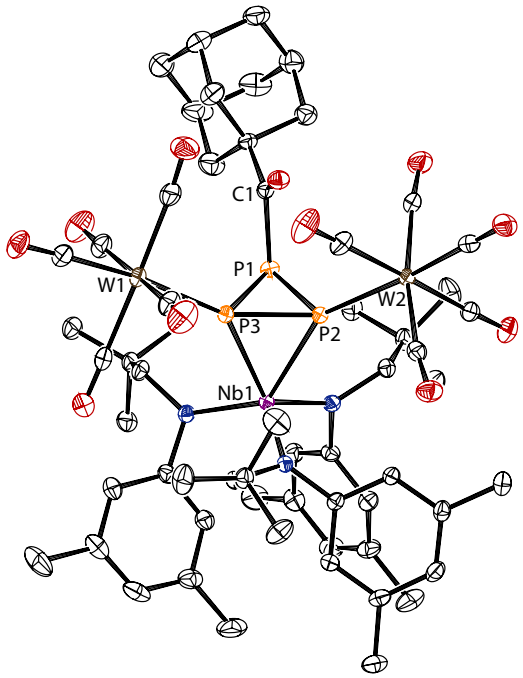

Figure 2.6. Thermal ellipsoid plot (50% probability) of **23**^{Ad} with hydrogen atoms omitted for clarity.

2.3.2 Degradation of Acyl Triphosphirenes and Characterization of $RCP_3[W(CO)_5]_2$ Dimers

Complexes $\mathbf{23}^{Ad}$ and $\mathbf{23}^{tBu}$ are thermally unstable and degrade at 20 °C to form ONb(N[$CH_2{}^t$Bu]Ar)$_3$, Scheme 2.5. For the adamantyl variant, the co-product is a red precipitate with very low solubility in a wide range of solvents (*e.g.*, *n*-pentane, THF, benzene, CH_2Cl_2, $C_2H_2Cl_4$, acetone, PhBr). By mass balance this red precipitate should be composed of compounds with an empirical formula $[\{(OC)_5W\}_2P_3CAd]_n$, and combustion analysis data support this formula. However, the exact identity of the product could not be definitively determined. The *tert*-butyl variant, $\mathbf{23}^{tBu}$, produces a co-product with slightly increased solubility in several solvents, allowing for a more thorough characterization by a variety of techniques including NMR spectroscopy, single crystal X-ray diffraction, and powder X-ray diffraction.

^{31}P NMR Spectra

Phosphorus-31 NMR data acquired on the crude reaction mixture formed by stirring $\mathbf{23}^{tBu}$ for several hours in CH_2Cl_2 at 22 °C revealed that a mixture of phosphorus-containing products had formed, though one major product was present, Figure 2.7. A fraction of the product that was insoluble in Et_2O and sparingly soluble in CH_2Cl_2 was isolated in *ca*. 30% yield. A ^{31}P NMR spectrum of this fraction confirmed that this was the major species identified in spectra of the crude reaction mixture, Figure 2.8. This species displays six inequivalent phosphorus resonances that are heavily coupled. The spectral pattern was simulated using *gNMR* and the parameters for the simulation are presented in Table 2.1.[43] The presence of six phosphorus nuclei suggests a dimer of the formula $[{}^t\text{BuCP}_3[\text{W(CO)}_5]_2]_2$.

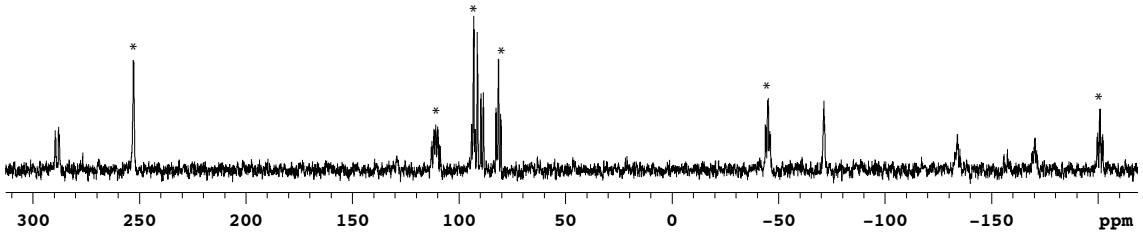

Figure 2.7. The ^{31}P NMR spectrum of the crude mixture following formation of oxoniobium **21** from $\mathbf{23}^{tBu}$ shows one major phosphorus-containing product, indicated with asterisks.

Single Crystal Studies

It was also possible to obtain several small, red-orange crystals from CH_2Cl_2 solutions of the product mixture originating from degradation of $\mathbf{23}^{tBu}$, and these crystals were subjected to X-diffraction analyses. These studies revealed three structurally distinct isomers, **24**, **25**, and **26**,

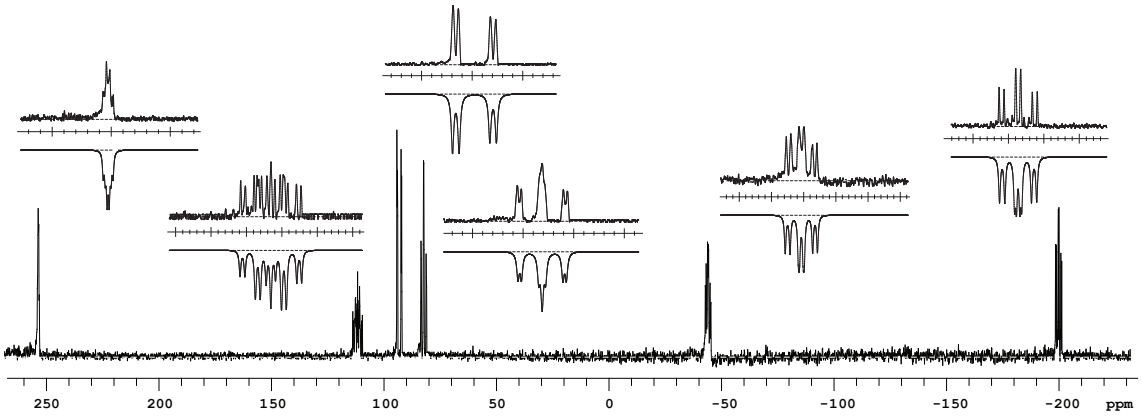

Figure 2.8. The experimental ^{31}P NMR spectrum of **24**. The insets show details of the experimental (upper) and simulated (reflected) patterns for the six multiplet resonances.

Table 2.1. ^{31}P NMR data for **24** from a best fit simulation.

		Chemical Shifts, δ^a	Coupling Constants, $\lvert J\rvert^b$				
			P^6	P^5	P^4	P^3	P^2
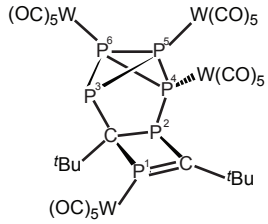	P^1	253	0	0	70	35	66
	P^2	93	0	0	373	0	–
	P^3	82	242	207	0	–	–
	P^4	111	215	224	–	–	–
	P^5	–44	76	–	–	–	–
	P^6	–200	–	–	–	–	–

[a] Chemical shifts in ppm. [b] Coupling constant magnitudes in Hz.

among the products formed, Figures 2.9 and 2.10 . The diffraction data from all the crystals allowed for the determination of unit cell parameters and connectivity, but on two of the three structures full structure refinement was not possible due to very high residual electron density (possibly resulting from a full-molecule disorder) or low-resolution data. The structure determinations revealed **24**, **25**, and **26** all to be dimers of the $^{t}BuCP_3[W(CO)_5]_2$ unit. The structures of these three can be compared to various structures known for *tert*-butylphosphaalkyne tetramers, Figure 2.11.[8,44–47] Conspicuously absent from the series **24**, **25** and **26** is the the cubane isomer that is analogous to a major product of phosphaalkyne tetramerization. Such an isomer could form by dimerization of the cofacial π bonds that result from an *endo* $[4+2]$ cycloaddition of triphosphacyclobutadiene monomers and should be favored by this mechanism (see Section 2.4). It is possible that such a cubane does form, but that is undergoes rearrangement, thermally or photochemically, to afford **24** and/or **25**.[44,48]

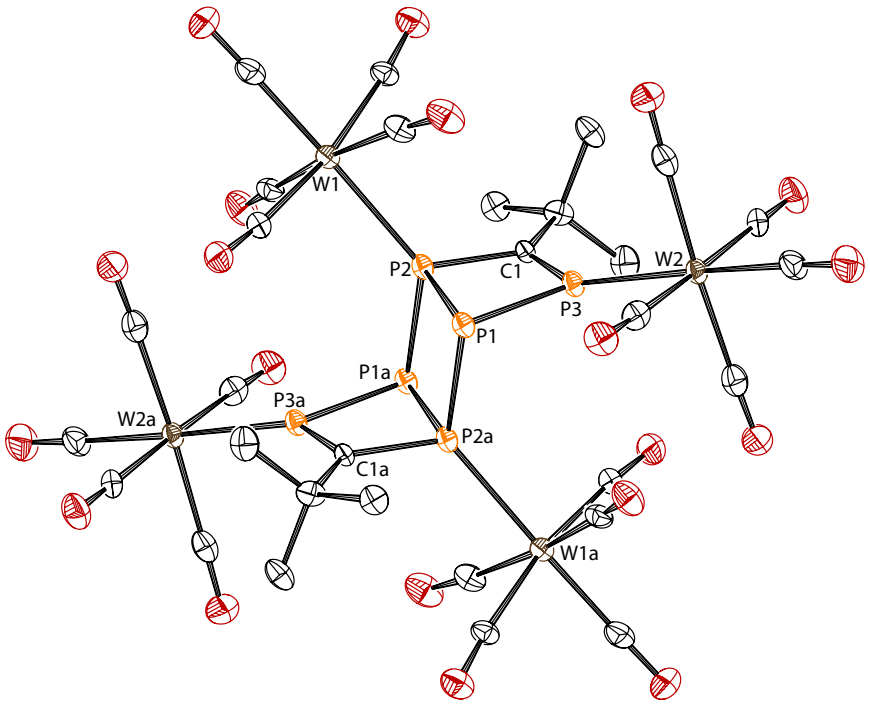

Figure 2.9. Thermal ellipsoid plot (50% probability) of **26** with hydrogen atoms omitted for clarity.

Powder Diffraction Studies

As a method of bulk characterization, the material isolated from the degradation of $\mathbf{23}^{tBu}$ was subjected to analysis by powder X-ray diffraction. Diffraction intensities of Cu Kα radiation from a sample of this powder deposited on a silicon crystal were measured as a function of angle over the range $3.5^\circ < 2\theta < 50^\circ$ at 20 °C. Powder diffraction patterns for **24**, **25**, and **26** were simulated based

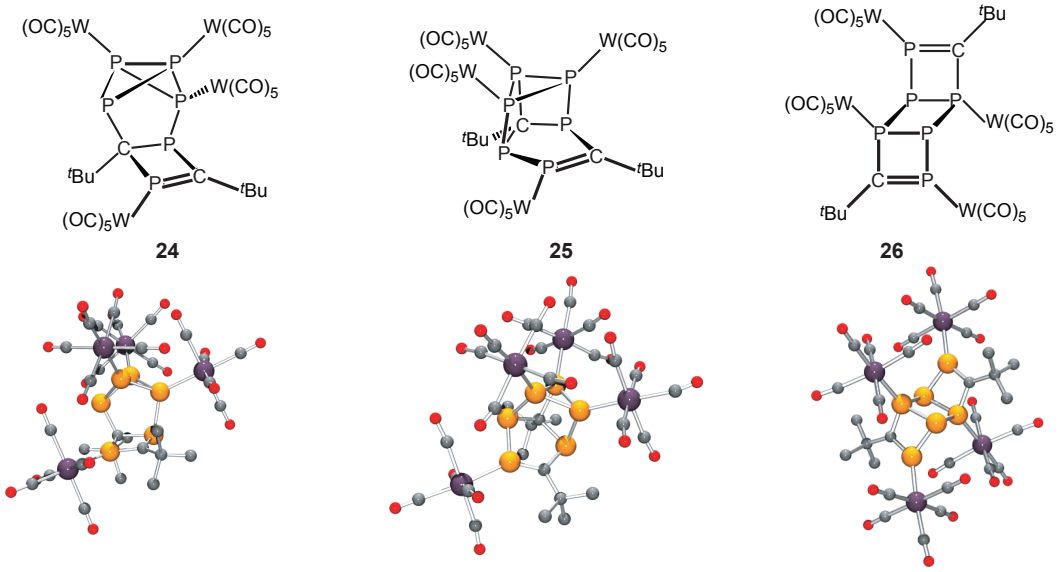

Figure 2.10. Three structures of $[^{t}\mathrm{BuCP}_3[\mathrm{W(CO)}_5]_2]_2$ identified by single-crystal X-ray diffraction.

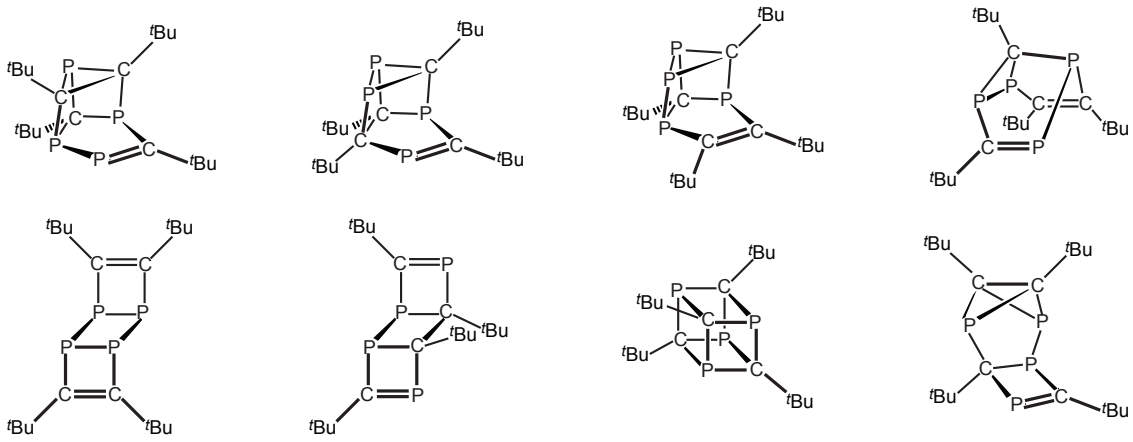

Figure 2.11. Eight structures of known ^{t}BuCP tetramers.

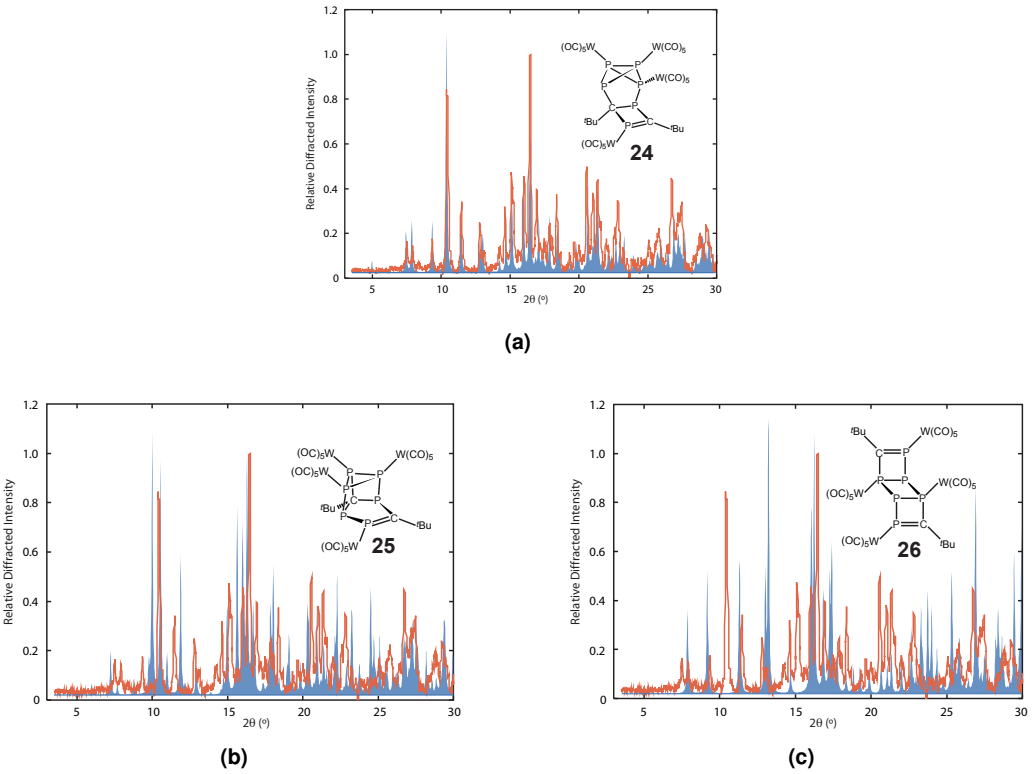

Figure 2.12. Simulated (solid blue) and experimental (red line) powder X-ray diffraction patterns for the three crystallized $[^{t}BuCP_3[W(CO)_5]_2]_2$ isomers, **24**-**26**.

on the single-crystal data and these patterns were compared to the experimental powder patterns for the isolated compound. The simulated pattern for **24** was in very good agreement with the diffraction pattern of the isolated powder, and this match is shown in Figure 2.12a. Simulations based on the crystal structures of the other two dimers gave poorer fits to the experimental powder pattern, Figure 2.12b-2.12c.[i] The NMR data shown in Figure 2.8 and Table 2.1 are also in agreement with the structure of **24**. While the structural identity of the product originating from the fragmentation of $\mathbf{23}^{Ad}$ could not be definitively confirmed, all available data assigns the products originating from fragmentation of $\mathbf{23}^{tBu}$ as various dimers of the formula $[^{t}BuCP_3[W(CO)_5]_2]_2$. Thus, the products resulting from fragmentation of $\mathbf{23}^{Ad}$ are assigned as isomers of $[AdCP_3[W(CO)_5]_2]_2$.

2.4 Trappings of a Triphosphacyclobutadiene Intermediate

As a monomer, the species $RCP_3[W(CO)_5]_2$, **27**, could possess an RCP_3 core with either a planar CP_3 core or a tetrahedrane structure: The former is analogous to the formally anti-aromatic, 4π-electron molecule cyclobutadiene, and would be one RC unit away from the elusive planar P_4. The latter is structurally similar to the stable isomer of P_4, and its generation from an acyltriphosphirene

[i]The single-crystal data were measured at 100 K and the powder data at 293 K. The temperature dependent variations were deemed to be small based on the alignment of the fits.

can be seen as similar to the formation of P_4 from the reaction of a *cyclo*-P_3 complex with PCl_3 described in Section 2.2.3. For C_4H_4, the tetrahedrane structure lies roughly 30 kcal/mol higher in energy than cyclobutadiene and while cyclobutadiene is an accessible intermediate, parent tetrahedrane remains elusive.[16,49] The difference in ring strain between phosphorus three-membered rings and all-carbon three-membered rings, and the general stability of phosphorus σ bonds over π bonds, suggest that for RCP_3 the opposite would be true: the tetrahedrane is expected to be more stable.[7,50,51] This was confirmed by DFT calculations that place planar $MeCP_3$ roughly 40 kcal/mol above the tetrahedrane. However, when two $W(CO)_5$ units complex the triphosphacyclobutadiene molecule it is significantly stabilized. Geometry optimization calculations on six linkage isomers of bis-$W(CO)_5$ complexes of the triphosphacyclobutadiene and the one tetrahedrane isomer reveal an energy span of only 9 kcal/mol, with a triphosphacyclobutadiene being lowest in energy, Figure 2.13.

The structures of **24**, **25**, and **26** further suggest the intermediacy of one of the triphosphacyclobutadiene isomers of $\mathbf{27}^R$. In particular, **26** can be seen as arising from such an intermediate via a $[4+2]$ cycloaddition between the $4e^-$ π system of one monomer and the reactive diphosphene π bond of a second monomer. In the analogous chemistry of phosphaalkyne dimers, diphosphacyclobutadiene molecules have been invoked as intermediates in the generation of several tetrameric products.[8,45,46] With the hypothesis that the deoxygenation of the acyltriphosphirene ligands of $\mathbf{23}^R$ affords the triphosphacyclobutadiene intermediates $\mathbf{27}^R$, experiments to trap this reactive species were investigated. This chemistry is described is terms of a triphosphacyclobutadiene molecule, given the relative inertness of the $W(CO)_5$ fragment. Nevertheless, the same effects that serve to stabilize the reactive intermediates are likely involved somewhat in directing the chemistry of $\mathbf{27}^R$. In fact, antimony Lewis acids have been implicated in directing the mechanistic pathways available to $(RC)_2P_2$ intermediates, and such Lewis acid effects are also possible for the two pendant $W(CO)_5$ units that appear here.[52]

2.4.1 Trapping with Low-Valent Platinum

The platinum complex $(C_2H_4)Pt(PPh_3)_2$ has been used successfully in several instances to trap units of P=P unsaturation with simple displacement of the ethylene molecule.[11,53–55] For this reason, $\mathbf{23}^{Ad}$ was allowed to fragment in the presence of this platinum reagent with the goal of binding the triphosphacyclobutadiene monomer $\mathbf{27}^{Ad}$ to the platinum center with concomitant displacement of the ethylene ligand. Analysis of the resultant product mixture by ^{31}P NMR spectroscopy revealed the formation of one major soluble, phosphorus-containing species and this product, **28**, was isolated in *ca.* 20% yield following successive extractions, Scheme 2.6. Characterization by NMR and IR spectroscopies and single-crystal X-ray diffraction revealed that this product had incorporated the ethylene unit of the starting platinum complex into the $AdCP_3$ framework to form $(Ph_3P)(OC)Pt(P_3C(C_2H_4)Ad)[W(CO)_5]_2$, Figures 2.14 and 2.15.

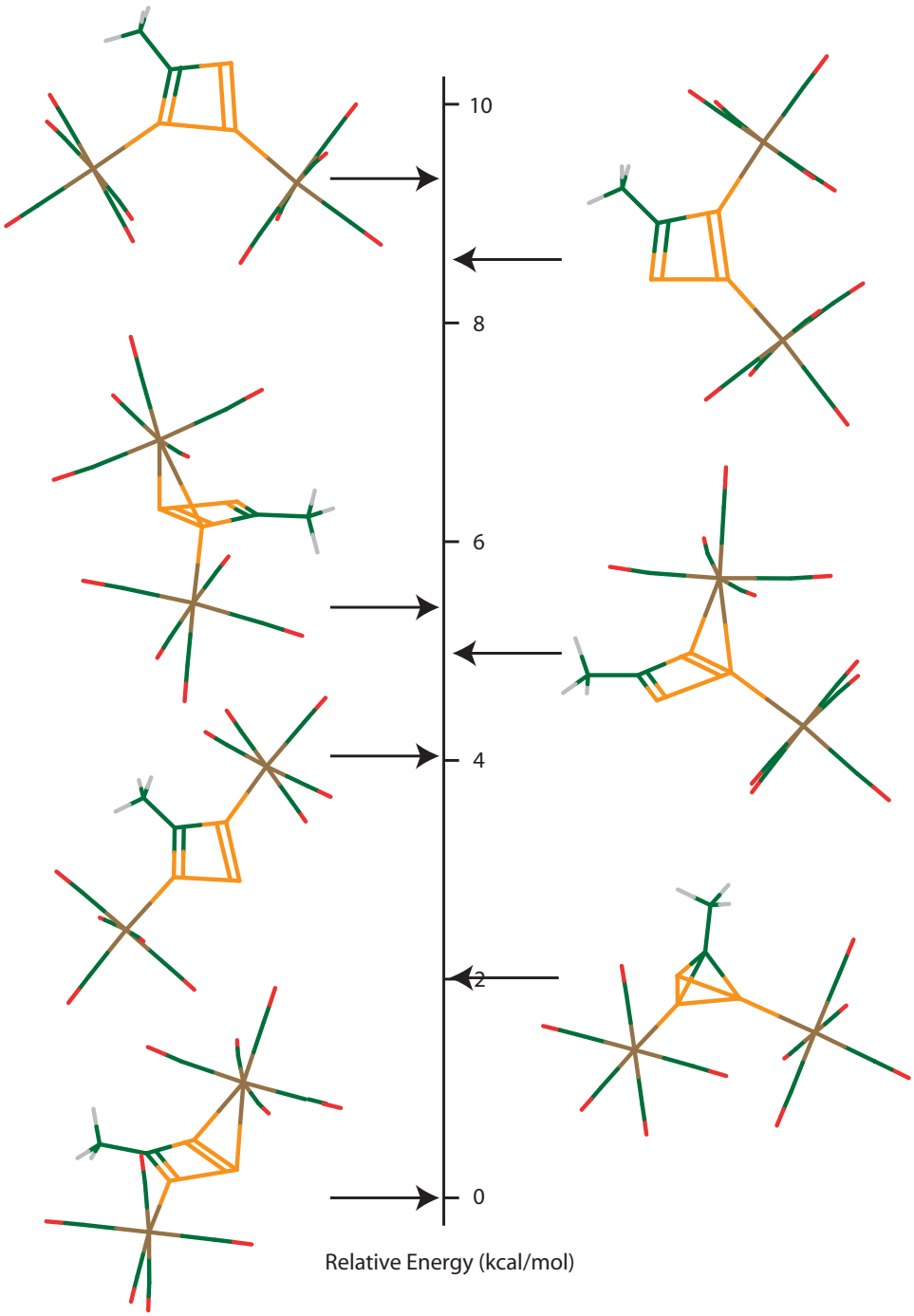

Figure 2.13. Relative electronic energies of seven linkage isomers of the model complex $MeCP_3[W(CO)_5]_2$. Phosphorus, orange; tungsten, brown; oxygen, red; carbon, green; hydrogen, gray.

The ^{31}P NMR spectrum of **28** consists of three resonances each with ^{195}Pt satellites: an upfield triplet at –153.7 ppm ($^{1}J_{PPt}$ = 580 Hz), a triphenylphosphine resonance corresponding to one Pt-bound PPh_3 per CP_3 unit ($^{1}J_{PPt}$ = 2130 Hz), and a doublet of twice the integral as the other resonances with weaker ^{195}Pt-^{31}P coupling ($^{2}J_{PPt}$ = 215 Hz). The platinum-bound carbonyl was located in the IR spectrum at 1922 cm^{-1} and likely originates from degradation of the $W(CO)_5$ unit. These spectroscopic data are consistent with the unexpected structure determined by X-ray diffraction. This unusual Pt complex contains a diphosphinoalkyl ligand with a Pt−C distance of 2.153(4) Å and a phosphido ligand bound at 2.3715(13) Å from platinum. The other two sites on the square planar center are a carbonyl *trans* to the phosphido at 1.927(5) Å from Pt, and a triphenylphosphine ligand *trans* to the alkyl donor at 2.3363(14) Å from Pt.

Despite the unexpected incorporation of the ethylene unit into the $AdCP_3$ framework, the presence of only one $AdCP_3$ unit is consistent with the hypothesis of monomeric $AdCP_3[W(CO)_5]_2$ being released from the acyltriphosphirene complex **23**^{Ad} and then being trapped by the bisphosphine platinum ethylene complex.

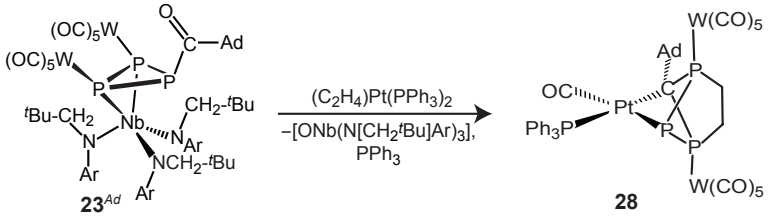

Scheme 2.6. Formation of the product $(Ph_3P)(OC)Pt(P_3C(C_2H_4)Ad)[W(CO)_5]_2$ (**28**).

2.4.2 Trapping with Organic Dienes

Seeking to trap the putative triphosphacyclobutadiene intermediate in a simple one-to-one reaction without disruption of the RCP_3 topology, organic dienes that are known to react via $[4+2]$ cycloadditions with diphosphenes were employed.[6,56] When **23**^{Ad} was allowed to fragment in the presence of either 1,3-cyclohexadiene or 2,3-dimethylbutadiene, mixtures of products were observed by ^{31}P NMR spectroscopy. Spiro[2.4]hepta-4,6-diene is known to be a particularly active Diels-Alder reagent,[57] and when **23**^{Ad} was allowed to fragment in the presence of this diene, one major product was observed by ^{31}P NMR spectroscopy, Scheme 2.7. This product, $C_7H_8(P_3CAd)[W(CO)_5]_2$, **29**, has resonances consistent with reaction at the diphosphene functional group while the phosphaalkene moiety (^{31}P NMR δ = 295 ppm) remains intact, Figure 2.17. Extracting away co-product oxoniobium **21** with *n*-pentane and recrystallization of the remaining fraction from toluene affords **29**, though complete removal of a minor product, believed to be an isomer of **29**, could not be achieved. A single-crystal X-ray diffraction study revealed the

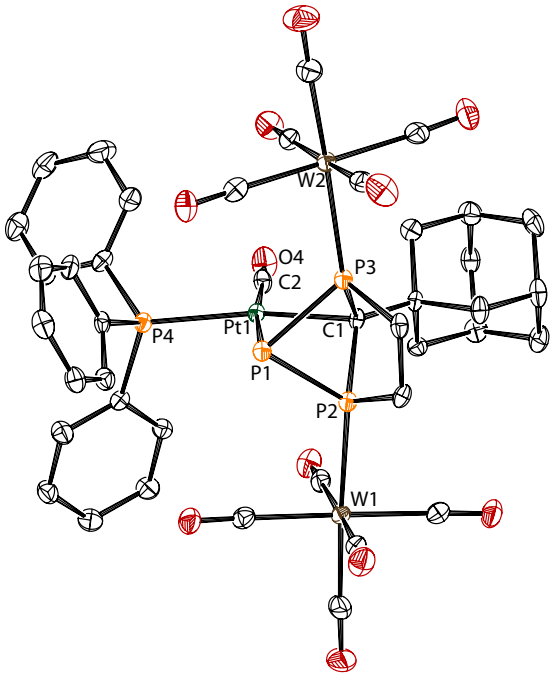

Figure 2.14. Thermal ellipsoid plot (50% probability) of **28** with hydrogen atoms omitted for clarity.

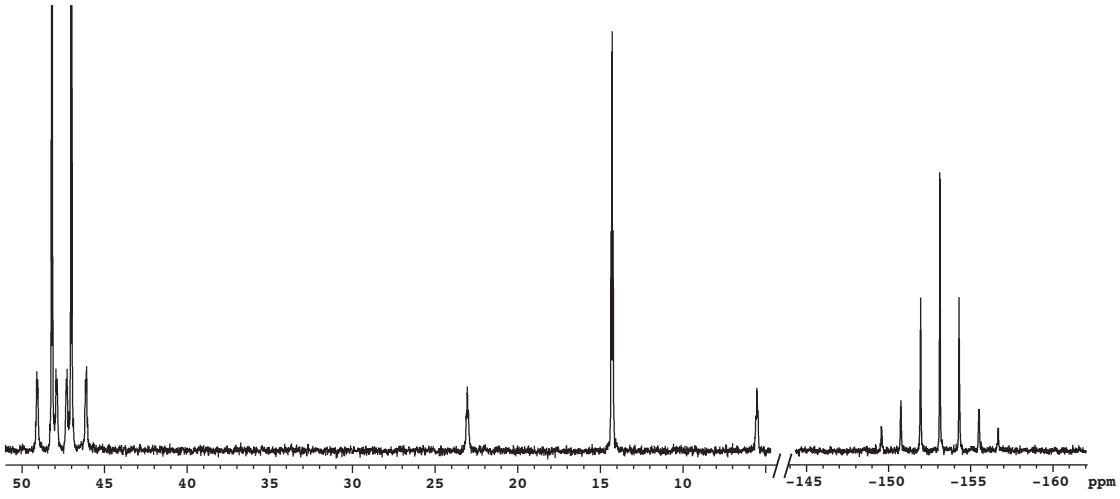

Figure 2.15. The ^{31}P NMR (C_6D_6, 202.5 MHz, 20 °C) spectrum of **28** reveals two inequivalent phosphorus environments from the RCP_3 unit (δ 47.6 ppm, $^{2}J_{PPt}$ = 215 Hz and δ –153.1 ppm, $^{1}J_{PPt}$ = 580 Hz), in addition to a Pt-coordinated PPh_3 (δ 14.3 ppm, $^{1}J_{PPt}$ = 2130 Hz).

stereochemistry of the product to be consistent with the prediction arrived at through consideration of steric and secondary orbital interactions: the π bonds of the diene/alkene interact with the 4-membered ring while the sterically protruding spiro group aligns opposite the ring, Figure 2.16. This product of a simple cycloaddition reaction demonstrates clean diphosphene-like reactivity for the proposed triphosphacyclobutadiene intermediate.

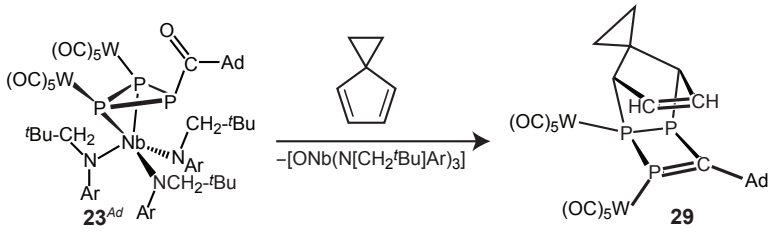

Scheme 2.7. Synthesis of the cycloaddition product $(C_7H_8)P_3CAd[W(CO)_5]_2$ (**29**).

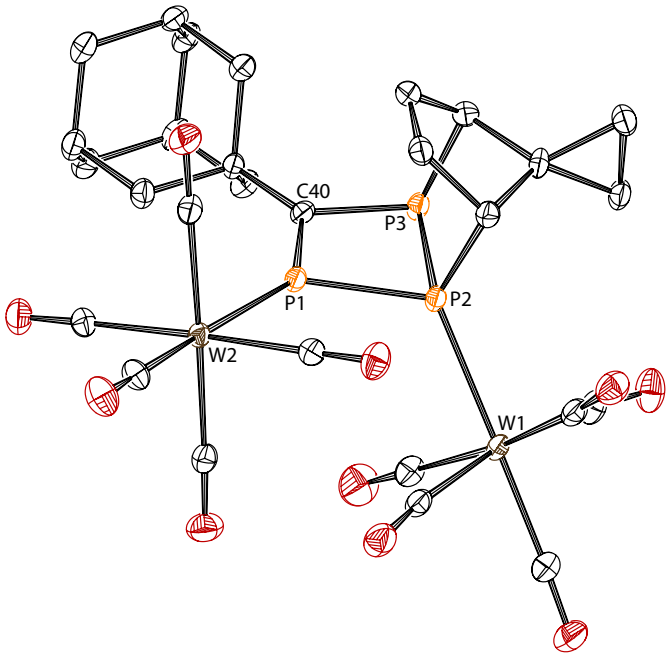

Figure 2.16. Thermal ellipsoid plot (50% probability) of **29** with hydrogen atoms omitted for clarity.

2.4.3 Synthesis of a Dewar Tetraphosphabenzene

The dimerization reactions of triphosphacyclobutadiene $\mathbf{27}^R$ that are observed when no trap is present in solution suggest that this intermediate can participate as both a dieneophile and as a diene-like partner in $[4+2]$-cycloaddition reactions. This dual reactivity is observed for many conjugated π systems, including cyclobutadiene itself. Early reactivity studies on C_4H_4 demonstrated its ability

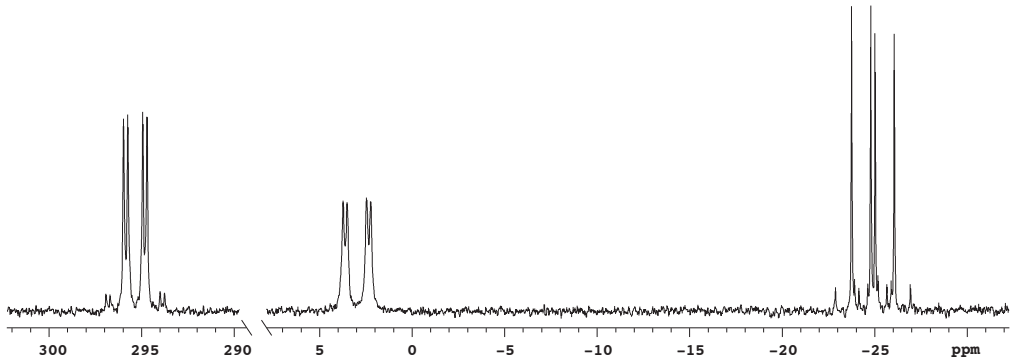

Figure 2.17. The ^{31}P NMR (C_6D_6, 202.5 MHz, 20 °C) spectrum of **29** reveals an intact phosphaalkene moiety (δ 295 ppm, $^{1}J_{PP}$ = 125 Hz, $^{2}J_{PP}$ = 26 Hz, $^{1}J_{PW}$ = 220 Hz) a central, $W(CO)_5$-bearing phosphorus (δ –26 ppm, $^{1}J_{PP}$ = 125 Hz, $^{1}J_{PP}$ = 155 Hz, $^{1}J_{PW}$ = 230 Hz), and a third, uncoordinated phosphorus of the CP_3 ring (δ 2 ppm, $^{1}J_{PP}$ = 155 Hz, $^{2}J_{PP}$ = 26 Hz).

to react with alkenes as a diene, and with cyclopentadiene as a dieneophile.[14,15] If this is the case for the triphosphorus system, then it should be possible to trap **27**^{R} with a molecule that can engage the 4e^- π system of **27** through reaction with a reactive π bond. 1-Adamantylphosphaalkyne was employed in this role because of its potential to yield the Dewar isomer of tetraphosphabenzene as a reaction product.[27,58] Gentle thermolysis of **23**^{Ad} and AdC≡P for 4 h at 35 °C in benzene afforded one major product as assayed by ^{31}P NMR spectroscopy, Scheme 2.8. This product exhibits two coupled resonances in the ^{31}P NMR spectrum at 248 ppm and –13 ppm. This AA′XX′ pattern was successfully simulated with two ^{31}P-^{31}P couplings, $^{1}J_{PP}$ = –247 Hz and $^{2}J_{PP}$ = 36 Hz, Figure 2.18. These data are consistent with the C_2-symmetric Dewar tetraphosphabenzene, $(AdCP)_2P_2[W(CO)_5]_2$, **30**.

This structure was confirmed by a single crystal X-ray diffraction study on an orange crystal of **30** grown from benzene solution and is depicted in Figure 2.19. Problems with twinning and disorder prevent a detailed discussion of all the metrical parameters, but the bond lengths are consistent with C=P double bonds to P1 and P4 (*ca.* 1.70 Å) and P−P single bonds of 2.19–2.23 Å for P1–P2, P2–P3, and P3–P4. The angle between the planes of the two 4-membered rings is *ca.* 103°.

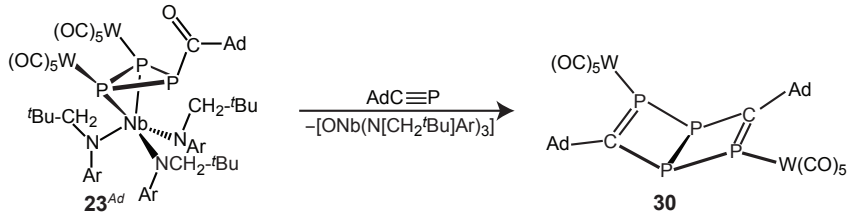

Scheme 2.8. Synthesis of the Dewar tetraphosphabenzene $(AdCP)_2P_2[W(CO)_5]_2$ (**30**).

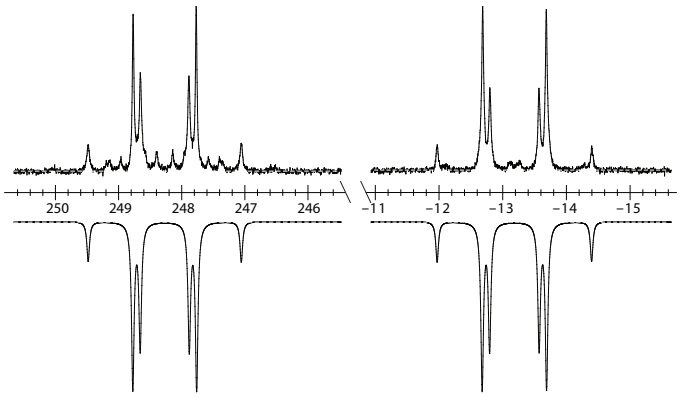

Figure 2.18. The experimental ^{31}P NMR spectrum of the Dewar isomer **30** is shown on top. Reflected is the simulated spectrum where the patterns attributed to ^{183}W satellites have been neglected.

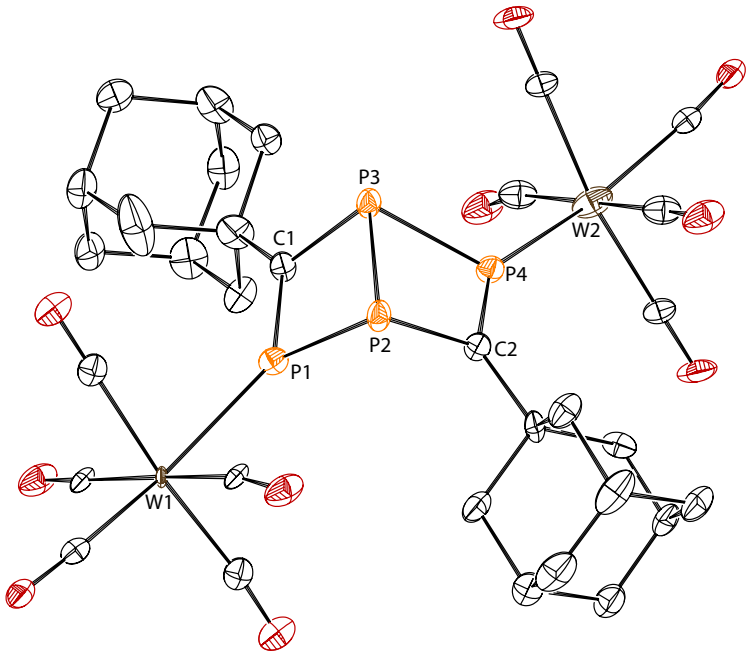

Figure 2.19. Thermal ellipsoid plot (30% probability) of **30** with hydrogen atoms omitted for clarity.

2.4.4 Photoisomerization: Synthesis of a Tetraphosphabenzvalene

Photoisomerizations of benzene valence isomers are well known.[59–61] Consequently, investigations of the Dewar tetraphosphabenzene **30** were undertaken with the goal of accessing other valence isomers of tetraphosphabenzene. As a prelude to such investigations, the UV-visible electronic absorption spectrum of orange **30** was collected, Figure 2.20. The spectrum shows one prominent absorption feature in the visible region at $\lambda_{max} = 413$ nm. The lowest energy absorption in phosphaalkenes is often assigned as an $n \rightarrow \pi^*$ transition, with the $\pi \rightarrow \pi^*$ transition close in energy.[62] Because the phosphorus lone pairs are tied up in bonding to $W(CO)_5$, absorption of **30** at 413 nm is assigned as a $\pi \rightarrow \pi^*$ transition of the C=P bonds. A second feature is present as a shoulder on the UV absorptions at 315 nm. The strong UV absorptions can be attributed to transitions of the two $W(CO)_5$ fragments.

Photolysis of **30** in THF with high intensity broadband light affords a new product in less than 20 min, Scheme 2.9. At 20 °C this product, **31**, displays two broad ^{31}P NMR resonances at +19 and –108 ppm and the resonances of the starting material are no longer observed. This transformation can also be monitored by UV-Vis spectroscopy. Figure 2.20 shows a spectrum of **30** immediately prior to and after photolysis of a dilute solution for several seconds. A bleach of the two prominent absorptions occurs, and the new product displays only a broad trailing band from the UV into the visible.

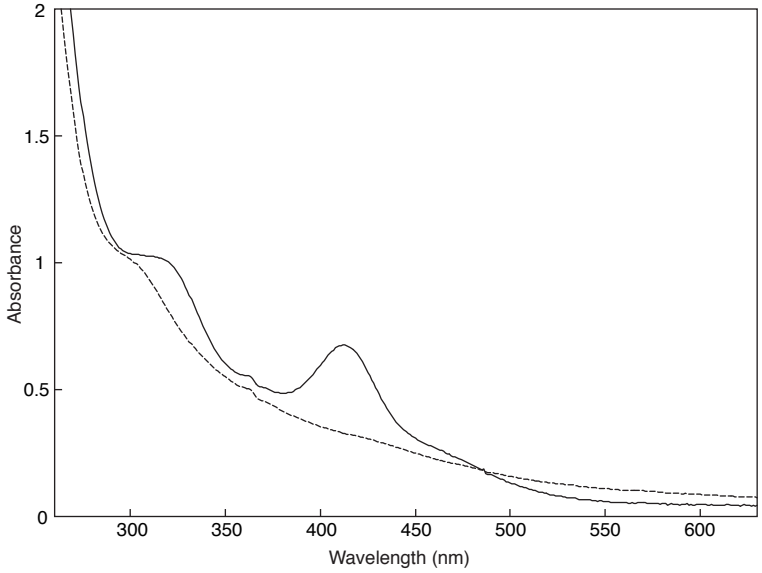

Figure 2.20. UV-visible absorption spectrum (20 °C, THF) of the Dewar tetraphosphabenzene **30** (solid), and the product following photolysis with UV light, **31** (dashed).

Upon prolonged exposure of solutions of **30** to ambient light this same isomerization takes place to provide **31**. An X-ray diffraction study performed on a crystals grown from mixtures of **30** that had been exposed to ambient light revealed a product with a benzvalene structure and a diphosphene

moiety η^2-coordinated to one $W(CO)_5$ unit and η^1-coordinated to the second $W(CO)_5$, Figure 2.21. This product can be seen as arising from intramolecular rearrangements. One possibility is a $[2+2]$ cycloaddition of the phosphaalkene moieties in **30** to generate a prismane that then undergoes radical rearrangements. The formation of **31**, which contains two 5-membered rings, is consistent with the photochemical "rule of five."[63] Such rearrangements have also been previously observed for isomers of monophosphabenzenes, including the Dewar isomer.[64] The *Z*-diphosphene of **31** displays a short P=P distance of 2.1047(15) Å and compressed angles at P of 96.93(14)° and 95.16(14)°. It is remarkable that such a species is stabilized by only one π complexation and one σ complexation from the relatively mild $W(CO)_5$ metal fragment.[65,66]

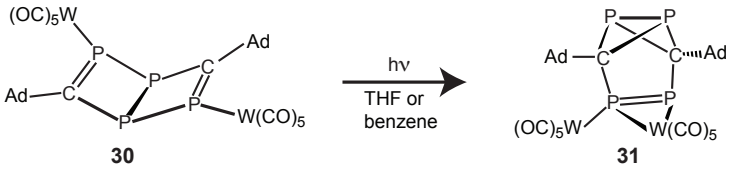

Scheme 2.9. Photoisomerization of the Dewar tetraphosphabenzene **30** to the tetraphosphabenzvalene **31**.

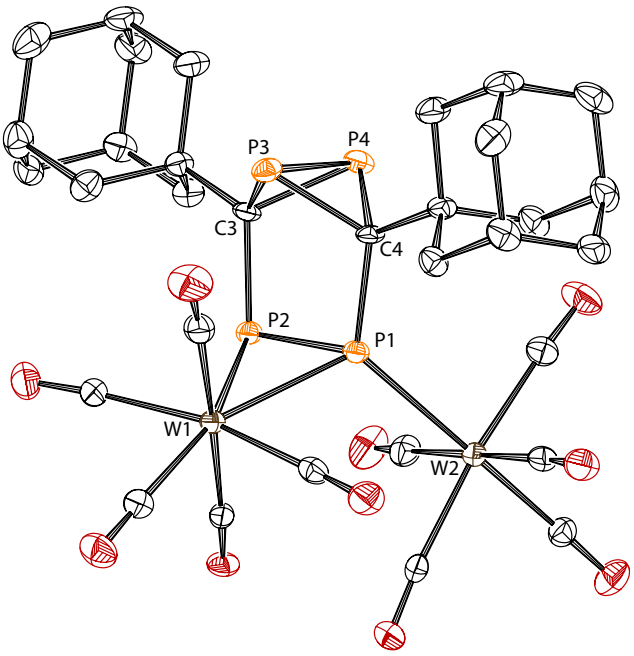

Figure 2.21. Thermal ellipsoid plot (50% probability) of **31** with hydrogen atoms omitted for clarity.

The presence of two broad signals in the ^{31}P NMR spectrum of **31** can be attributed to a dynamic process in which the exchange of $W(CO)_5$ units between faces and termini of the diphosphene can equate pairs of P atoms. Upon cooling to –100 °C, these two resonances resolve into four with a

doublet pair displaying 450 Hz coupling, Figure 2.22. This strong coupling is consistent with the P=P multiple bonding implied by the benzvalene structure.

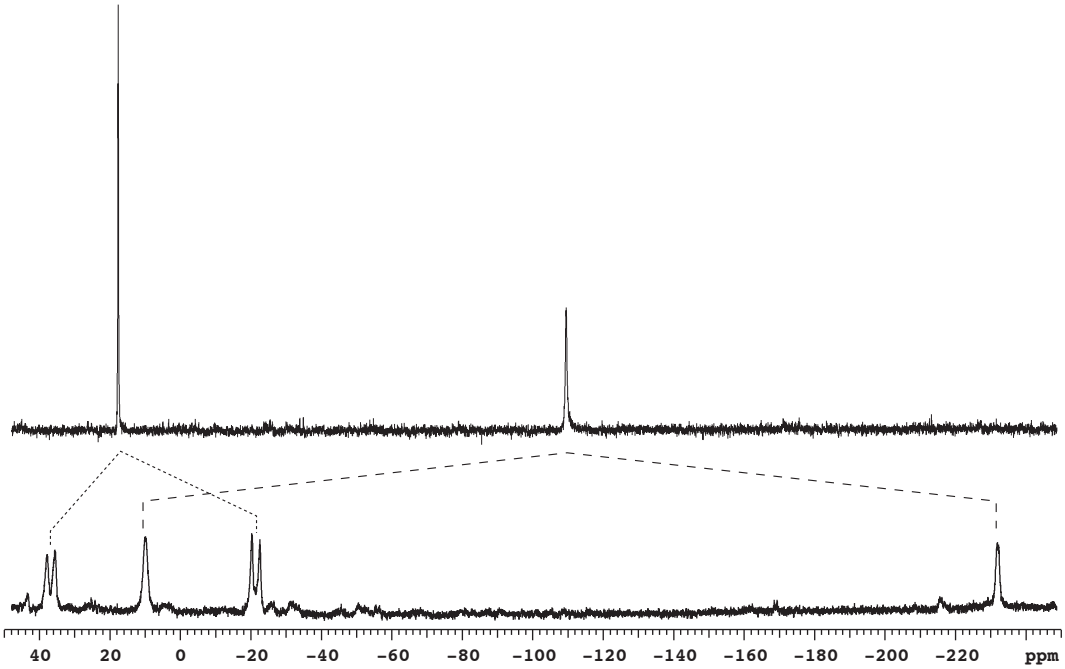

Figure 2.22. At 20 °C the ^{31}P NMR spectrum of the benzvalene isomer of $(AdC)_2P_4[W(CO)_5]_2$ displays only two broad resonances (above). Upon cooling to –100 °C the two resonances split to four resonances (below), consistent with the solid state structure of **31**.

2.5 Mechanism of Acyltriphosphirene Deoxygenation

2.5.1 An Observed Intermediate

To investigate the mechanism by which oxoniobium **21** and triphosphacyclobutadiene **27**^{Ad} are generated from **23**^{Ad}, this reaction was monitored by both ^{1}H and ^{31}P NMR spectroscopy. The decay of starting material **23**^{Ad} was found to follow clean first-order kinetics, but the appearance of an intermediate, **23′**, was found to accompany production of **21**. By NMR spectroscopy, this intermediate contains three magnetically inequivalent ^{31}P nuclei, and two distinct anilide ^{t}Bu groups are observed in a 2:1 ratio. The ^{31}P resonances are a triplet at –4 ppm (J_{PP} = 175 Hz) and two broad resonances at –28 and –37 ppm. By using labeled 1-adamantanecarbonyl chloride in the synthesis of **23**^{Ad}, a ^{13}C label was introduced at the acyl carbon, C1. This isotopic labeling gave rise to a doublet of triplets for the ^{31}P resonance at –4 ppm and a doublet for the ^{13}C resonance at 259 ppm (J_{CP} = 108 Hz). This ^{13}C chemical shift is downfield of the initial signal for the acyltriphosphirene complex **23**^{Ad} by 46 ppm, consistent with Lewis acid activation of the carbonyl group.[67] These data demonstrate that in **23′**, C1 is attached only to one phosphorus atom, and that the carbonyl oxygen is

likely coordinated to Nb. This leads to the proposed structure for **23′** that is shown in Scheme 2.10. This intermediate could arise from inversion at P1 and coordination of oxygen to the Lewis acidic metal center. While inversions at phosphorus are typically high energy processes, the pendant acyl group is expected to lower this barrier by stabilizing the planar transition state through π interactions with the C–O π^* orbital. This is analogous to the effect that makes carboxy amides planar and that reduces the barrier to inversion at acyl aziridines.[68]

From **23′** one can envision an attack by one of the niobium-bound phosphorus atoms on the Lewis acid-activated carbonyl to give **23″**, Scheme 2.10. This intermediate is then poised to eliminate the triphosphacyclobutadiene **27**^{Ad} upon formation of **21** via a 6e^- rearrangement with formation of the strong Nb≡O bond, Scheme 2.10. Importantly, the same intermediate **23′** was observed in the presence of either AdCP or spiro[2.4]hepta-4,6-diene, ruling out the possibility that this intermediate contains either species intended as a trap.

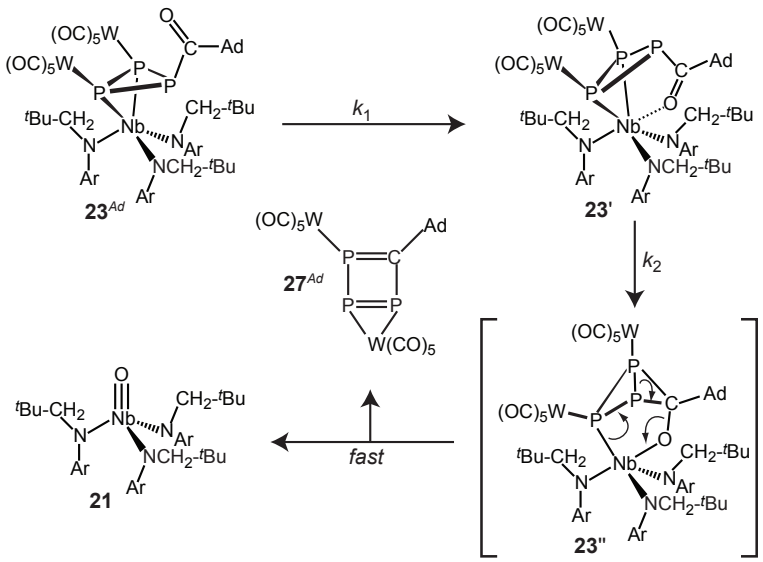

Scheme 2.10. Proposed mechanism for the deoxygenation of the acyltriphosphirene ligand of **23**^{Ad}.

2.5.2 Kinetics

The decay of starting material **23**^{Ad} follows first-order exponential behavior, but the ratios of species **23**^{Ad}, **23′**, and **21** did not fit the simple kinetic model described by two consecutive reactions. Rather, the data were better suited to a model where, in addition to the consecutive reaction pathway, there is a competitive process that proceeds with a rate constant k_1' and without an observable intermediate, Scheme 2.11.

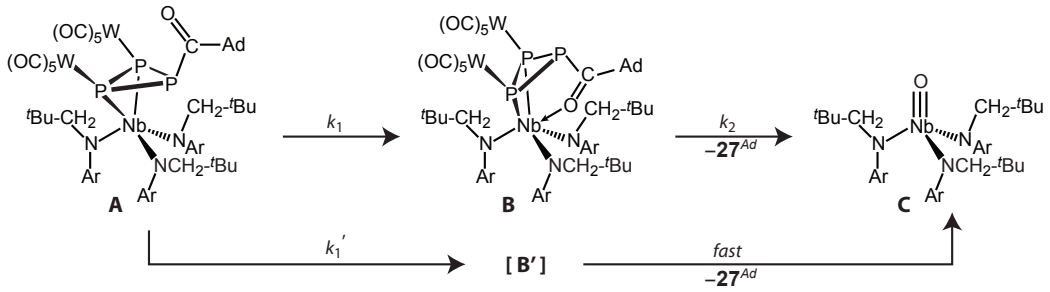

Scheme 2.11. Kinetic pathways for the deoxygenation of the acyltriphosphirene ligand of $\mathbf{23}^{Ad}$. **A** = $\mathbf{23}^{Ad}$; **B** = $\mathbf{23}'$; **C** = **21**; **B′** is an unobserved, postulated intermediate.

This more complex kinetic model is described by the following equations:

$$\frac{d[\mathbf{A}]}{dt} = -k_1[\mathbf{A}] - k_1'[\mathbf{A}] \tag{2.1}$$

$$\frac{d[\mathbf{B}]}{dt} = k_1[\mathbf{A}] - k_2[\mathbf{B}] \tag{2.2}$$

Solving this set of equations leads to the following expressions for the time-dependent concentrations, where $A_\circ$, $B_\circ$, and $C_\circ$ are the initial concentrations of their respective species:

$$[\mathbf{A}] = A_\circ e^{(k_1+k_1')t} \tag{2.3}$$

$$[\mathbf{B}] = \frac{A_\circ k_1 e^{k_2 t}}{k_2-k_1-k_1'}\left[e^{(k_2-k_1-k_1')t} + \frac{B_\circ(k_2-k_1-k_1')}{A_\circ k_1} - 1\right] \tag{2.4}$$

$$[\mathbf{C}] = A_\circ + B_\circ + C_\circ - [\mathbf{A}] - [\mathbf{B}] \tag{2.5}$$

The relative concentrations as a function of time at 30 °C, as measured by integration of the *tert*-butyl resonances in the ^{1}H NMR spectrum, were fit to these equations, Figure 2.23. These fits revealed that $k_1 \approx k_1'$ at 1.7×10^{-4} sec^{-1} and $k_2 = 3.4 \times 10^{-4}$ sec^{-1}, though the high correlation in the fits means large errors are possible. It is possible that the coordination sites of the two $W(CO)_5$ units couple to subtle conformational differences and lead to two rates of rearrangement from structures analogous to $\mathbf{23}'$. The observed behavior is explained if the rate of rearrangement to oxoniobium **21** from an alternate conformer of $\mathbf{23}'$ is fast relative to both k_1' and the interconversion of conformers. In any case, the kinetic profile is consistent with elimination of monomeric $\mathbf{27}^{Ad}$ into solution before it undergoes further chemistry.

2.6 Alternate Syntheses of Anionic Niobium *cyclo*-P_3 Complexes

In the previous chapter, *cyclo*-P_3 complexes were synthesized by the trapping of a postulated P_2 molecule with metal terminal phosphide complexes. This methodology afforded access to *cyclo*-P_3 complexes of Nb, Mo, and W, as well as provided evidence for P_2 and $(P_2)W(CO)_5$ as discrete intermediates. However, with the exception of the bis-$W(CO)_5$–coordinated *cyclo*-P_3 complex **17**,

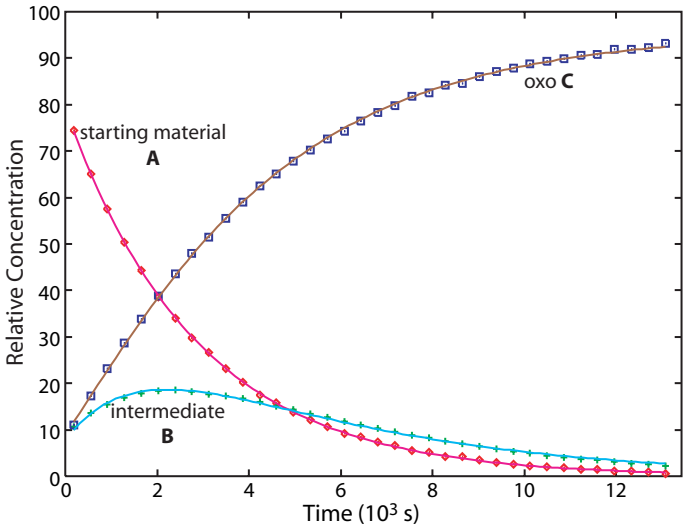

Figure 2.23. The kinetic profile for the concentrations of $\mathbf{23}^{Ad}$ (**A**), the intermediate, Lewis acid-activated complex $\mathbf{23}'$ (**B**) and the product oxoniobium complex **21** (**C**) fits the model described in Scheme 2.11, where $k_1 \approx k_1'$.

this method did not lend itself to large scale, preparative chemistry. As a result, an alternate synthesis of the anionic complex Na[(P_3)Nb(N[$CH_2{}^t$Bu]Ar)$_3$], Na[**15**], was sought. This would allow the chemistry of this complex to be explored in the future in ways analogous to those for the bis-$W(CO)_5$ complex **17** that has been studied thus far.

Recent work in the Cummins group by Cossairt and Diawara outlined a synthesis of [(*cyclo*-P_3)Nb(ODipp)$_3$]$^-$ (Dipp = 2,6-diisopropylphenyl) directly from Cl_2Nb(ODipp)$_3$ and P_4 by reduction with sodium amalgam.[42] This result has proven somewhat general and was expanded to the trisanilide system, Nb(N[$CH_2{}^t$Bu]Ar)$_3$. Addition of *ca.* 1% sodium amalgam to a mixture of $(TfO)_2$Nb(N[$CH_2{}^t$Bu]Ar)$_3$ and P_4 in THF serves to form a mixture of products, the two major components being the red, paramagnetic (μ-P)[Nb(N[$CH_2{}^t$Bu]Ar)$_3$]$_2$ and the desired *cyclo*-P_3 anion **15**. The two products can be separated by selective precipitation of **15** as its sodium salt at –35 °C in low yield. An alternate isolation procedure, wherein addition of 12-crown-4 causes the precipitation of [(12-crown-4)$_2$Na][(P_3)Nb(N[$CH_2{}^t$Bu]Ar)$_3$], yields the desired *cyclo*-P_3 complex in 54% yield.

A third procedure for the preparation of Na[**15**] was also developed in collaboration with Brandi Cossairt. In this procedure, the terminal phosphide complex [(Et_2O)Na][PNb(N[$CH_2{}^t$Bu]Ar)$_3$] is treated with 0.5 equiv of P_4 in benzene at 22 °C. This causes a color change to orange and analysis by ^{1}H and ^{31}P NMR reveals clean formation of [(P_3)Nb(N[$CH_2{}^t$Bu]Ar)$_3$]$^-$, which is isolated as its sodium salt in 84% yield by precipitation from *n*-pentane at –35 °C. The mechanism of this reaction has not yet been elucidated, but the nucleophilicity of the phosphide anion **3**, and/or its electron transfer ability, seem necessary to the reaction. The analogous neutral phosphide complex, PMo(N[^{i}Pr]Ar)$_3$, does not react with P_4, even at 75 °C over several hours.

2.7 Conclusions

The availability of *cyclo*-P_3 complexes derived from P_2 trapping reactions has provided access to triphosphirene complexes. These include a simple stannyl triphosphirene complex with a Sn−P bond and a complex with a dynamic Mes*NP_4 ligand. In addition, it was shown that *cyclo*-P_3 anions can serve as P_3^{3-} sources by demonstrating the synthesis of P_4 from one such anion and PCl_3. The preparation of acyltriphosphirene complexes led to accessible triphosphacyclobutadiene intermediates complexed to $W(CO)_5$. These species will dimerize in the absence of other reaction partners, but can be trapped when presented with suitable substrates. In such reactions the putative triphosphacyclobutadiene intermediate was found to behave as either a reactive *Z*-diphosphene or as a $4e^-$ cycloaddition partner. This reactivity has led to the synthesis of the most phosphorus-rich congeners of benzene isomers yet reported, the Dewar and benzvalene isomers of tetraphosphabenzene. This chemistry was accessed by exploiting the thermodynamic driving force of strong oxygen–niobium bond formation, together with NaCl elimination, to offset the energetic costs of generating high-energy, small molecule transients.[1,69]

2.8 Experimental Details

2.8.1 General Considerations

All manipulations were performed in a Vacuum Atmospheres model MO-40M glove box under an atmosphere of purified dinitrogen. Solvents were obtained anhydrous and oxygen-free from a Contour Glass Solvent Purification System, or by analogous methods.[70] Deuterated solvents for NMR spectroscopy were purchased from Cambridge Isotope Labs. Benzene-d_6 and toluene-d_8 were degassed and stored over molecular sieves for at least 2 days prior to use. $C_2D_2Cl_4$ was distilled off of CaH_2 and stored over molecular sieves. Celite 435 (EM Science), 4 Å molecular sieves (Aldrich), and alumina (EM Science) were dried by heating at 200 °C under dynamic vacuum for at least 24 hours prior to use. The complex $[(Et_2O)Na][PNb(N[CH_2{}^tBu]Ar)_3]$ was prepared according to the modified literature procedure presented in Appendix A.[1] The compounds $[(12\text{-crown-4})_2Na][(OC)_5WP_3Nb(N[CH_2{}^tBu]Ar)_3]$, $Na[\{(OC)_5W\}_2P_3Nb(N[CH_2{}^tBu]Ar)_3]$, $(C_2H_4)Pt(PPh_3)_2$,[71] Mes*NPCl,[35] and spiro[2.4]hepta-4,6-diene[72] were prepared according to methods in the previous chapter or literature procedures. 1-Adamantanecarbonyl chloride (Aldrich) and AdCP (Fluka) were purchased and used as received. All glassware was oven-dried at temperatures greater than 170 °C prior to use. NMR spectra were obtained on Varian Mercury 300 or Varian Inova 500 instruments equipped with Oxford Instruments superconducting magnets. ^{1}H NMR spectra were referenced to residual C_6D_5H (7.16 ppm), ^{13}C NMR spectra were referenced to C_6D_6 (128.39 ppm) or $CDCl_3$ (77.23 ppm). ^{31}P NMR spectra were referenced externally to 85% H_3PO_4 (0 ppm) and ^{195}Pt NMR spectra were referenced externally to

K_2PtCl_4 in D_2O (–1624 ppm). Elemental analyses were performed by Midwest Microlab, LLC (Indianapolis, Indiana).

2.8.2 Preparation of $(OC)_5W(Ph_3SnP_3)Nb(N[CH_2{}^tBu]Ar)_3$ (19)

A dimethoxyethane solution (5 mL) of $[(12\text{-crown-4})_2Na][(OC)_5W(P_3)Nb(N[CH_2{}^tBu]Ar)_3]$ (25 mg, 0.017 mmol) and Ph_3SnCl (7 mg, 0.018 mmol, 1.05 eq) was heated to 75 °C in a teflon-stoppered tube for 14 h. After this time the volatiles were removed under dynamic vacuum, the residue was extracted with Et_2O, and the extract was filtered through Celite, leaving behind off-white solids. The orange filtrate was concentrated to dryness and taken up in C_6D_6 for analysis by NMR spectroscopy, revealing a mixture containing *ca.* 40% of the desired product. This mixture was further purified by extraction with $O(SiMe_3)_2$, leaving behind most of the side products and giving a solution enriched in desired product but contaminated with free $HN[CH_2{}^tBu]Ar$. Pure compound was obtained in small quantities (*ca.* 10% yield) from the reaction of Ph_3SnCl with $Na[\{(CO)_5W\}_2P_3Nb(N[CH_2{}^tBu]Ar)_3]$ at 20 °C over several days and subsequent crystallization from toluene/$O(SiMe_3)_2$. ^{1}H NMR (C_6D_6, 500 MHz, 20 °C): δ 7.81 (d, 6H, J_{HSn} = 27 Hz, *o*-Ph), 7.24 (t, 6H, *m*-Ph), 7.13 (m, 3H, *p*-Ph), 6.77 (s, 6H, *o*-Ar), 6.57 (s, 3H, *p*-Ar), 3.82 (br s, 6H, NCH_2), 2.19 (s, 18H, $ArCH_3$), 0.72 (s, 27H, ^{t}Bu) ppm. $^{31}P\{^1H\}$ NMR (C_6D_6, 202.5 MHz, 20 °C): δ –196 (br m, $\Delta\nu_{\frac{1}{2}}$ = 650 Hz, $PSnPh_3$), –235 (br, $\Delta\nu_{\frac{1}{2}}$ = 6500 Hz, $NbP_2W(CO)_5$) ppm. $^{13}C\{^1H\}$ NMR (C_6D_6, 125.8 MHz, 20 °C): δ 198.0 (br, *ax*-CO), 197.9 ($^1J_{CW}$ = 130 Hz, *eq*-CO), 154.7 (br, *ipso*-Ar), 139.5, 138.6, 138.0 (J_{CSn} = 40 Hz), 136.9, 130.4, 129.6 (J_{CSn} = 56 Hz), 124.2 (br, *o*-Ar), 70.7 (br, NCH_2), 36.5($C(CH_3)_3$), 29.9 ($C(CH_3)_3$), 21.9 ($ArCH_3$) ppm. Elem. Anal. Calcd for $C_{62}H_{75}N_3O_5P_3NbWSn$: C, 52.05; H, 5.28; N, 2.94; Found: C, 51.86; H, 5.28; N, 2.90.

2.8.3 Preparation of $Mes^*NP[W(CO)_5]P_3Nb(N[CH_2{}^tBu]Ar)_3$ (20)

To a thawing Et_2O solution (7 mL) of red $Na[\{(OC)_5W\}_2P_3Nb(N[CH_2{}^tBu]Ar)_3$ (177 mg, 0.124 mmol) was added a thawing Et_2O solution (3 mL) of Mes^*NPCl (41 mg, 0.125 mmol, 1 eq). This mixture was allowed to stir at 22 °C for 24 h before the mixture was chilled to –35 °C for a further 24 h. The solution was then filtered through Celite that was subsequently washed with *n*-pentane and the combined filtrates were concentrated to dryness *in vacuo*. The dried residue was then dissolved in 1:1 benzene/*n*-pentane and filtered through Celite to remove insoluble material. Extraction with *n*-pentane once more and drying *in vacuo* gave a red-orange powder (158 mg, 0.115 mmol, 92% yield). ^{1}H NMR (C_6D_6, 500 MHz, 20 °C): δ 7.78 (s, 2H, Mes^*), 6.55 (s, 3H, *p*-Ar), 6.37 (s, 6H, *o*-Ar), 3.64 (s, 6H, NCH_2), 2.04 (s, 18H, $ArCH_3$), 1.77 (s, 18H, *o*-Mes^*), 1.45 (s, 9H, *p*-Mes^*), 0.77 (s, 27H, ^{t}Bu) ppm. $^{31}P\{^1H\}$ NMR (C_6D_6, 202.5 MHz, 20 °C): δ 367 (q, J_{PP} = 105 Hz, $PNMes^*$), –137 (d, J_{PP} = 105 Hz, P_3Nb) ppm. $^{13}C\{^1H\}$ NMR (C_6D_6, 125.8 MHz, 20 °C): δ 198.6 (d, J_{CP} = 40 Hz, *ax*-CO), 196.3 (d, J_{CP} = 8 Hz, J_{CW} = 130 Hz, *eq*-CO), 153.5 (d, J_{CP} = 25 Hz, *ipso*-Mes^*), 152.9 (*ipso*-Ar), 144.3 (d, J_{CP} = 5 Hz, *m*-Mes^*), 138.7 (*m*-Ar), 136.7 (d, J_{CP} = 15 Hz, *o*-Mes^*),

128.0 (*p*-Ar), 124.2 (*p*-Mes*), 122.4 (*o*-Ar), 73.6 (br, N*C*H_2), 37.0 ($CH_2C(CH_3)_3$), 35.4 (Mes* $C(CH_3)_3$), 35.1 (Mes* $C(CH_3)_3$), 32.8 (Mes* $C(CH_3)_3$), 32.5 (Mes* $C(CH_3)_3$), 30.1 ($CH_2C(CH_3)_3$), 21.8 (ArCH_3) ppm. Elem. Anal. Calcd for $C_{62}H_{89}N_4O_5P_4NbW$: C, 54.31; H, 6.54; N, 4.09; Found: C, 51.09; H, 6.24; N, 3.85.

2.8.4 Preparation of AdC(O)P_3Nb(N[$CH_2{}^t$Bu]Ar)$_3$ (22)

A thawing ether solution of AdC(O)Cl (71 mg, 0.36 mmol, 1.0 eq) was added dropwise to a thawing solution of [(THF)Na][(P_3)Nb(N[$CH_2{}^t$Bu]Ar)$_3$] (305 mg, 0.36 mmol). This orange mixture was stirred for 45 min, and then filtered through Celite and the filtrate was dried to an orange solid. This solid was extracted once with Et_2O/*n*-pentane mixture and filtered through Celite again. The filtrate was concentrated to 7 mL and stored at –35 °C to afford red-orange crystals. These crystals were collected (several crops), washed with cold *n*-pentane, and dried *in vacuo* (243 mg, 0.26 mmol, 74% yield). ^{1}H NMR (C_6D_6, 500 MHz, 20 °C): δ 6.65 (s, 6H, *o*-Ar), 6.58 (s, 3H, *p*-Ar), 3.90 (s, 6H, CH_2), 2.13 (s, 18H, ArCH_3), 2.10 (s, 6H, Ad), 1.92 (m, 3H, Ad), 1.57 (m, 6H, Ad), 0.86 (s, 27H, ^{t}Bu) ppm. ^{31}P{^{1}H} NMR (C_6D_6, 121.5 MHz, 20 °C): δ –117.4 (d, J_{PP} = 208 Hz, 2P, NbP_2), –179.0 (t, J_{PP} = 208 Hz, 1P, C(O)*P*) ppm. ^{13}C{^{1}H} NMR (C_6D_6, 125.8 MHz, 20 °C): δ 223.3 (J_{CP} = 115 Hz, C=O), 153.6 (*ipso*-Ar), 138.6 (*m*-Ar), 127.2 (*p*-Ar), 123.9 (*o*-Ar), 72.5 (NCH_2), 53.2 (J_{CP} = 27 Hz, Ad), 39.5 (J_{CP} = 5 Hz, Ad), 37.2 (Ad), 36.8 ($C(CH_3)_3$), 30.0 (C(CH_3)$_3$), 29.0 (Ad), 21.9 (ArCH_3) ppm.

2.8.5 Preparation of [(OC)$_5$W]$_2$AdC(O)P_3Nb(N[$CH_2{}^t$Bu]Ar)$_3$ (23^{Ad})

To a thawing Et_2O solution (15 mL) of red Na[{(OC)$_5$W}$_2$$P_3$Nb(N[$CH_2{}^t$Bu]Ar)$_3$] (475 mg, 0.333 mmol) was added a thawing Et_2O solution (5 mL) of AdC(O)Cl (66 mg, 0.333 mmol, 1.0 eq). This mixture was allowed to stir for 20 min, and then, working quickly and keeping the solution cold, the mixture was filtered through Celite and the volatiles were removed *in vacuo*. The solution dried to a foam that was quickly extracted once with Et_2O (5 mL). Upon concentration, the desired product began to precipitate from solution. The mixture was stored at –35 °C for 12 h and the bright red powder was isolated atop a frit. Two more crops were collected after concentration and crystallization from Et_2O to yield a bright red powder (300 mg, 0.19 mmol, 58% yield). ^{1}H NMR (C_6D_6, 500 MHz, 20 °C): δ 6.65 (br, 6H, *o*-Ar), 6.62 (s, 1H, *p*-Ar), 6.56 (s, 2H, *p*-Ar), 4.92 (d, $^2J_{HH}$ = 14 Hz, 2H, CH_2), 4.60 (d, $^2J_{HH}$ = 14 Hz, 2H, CH_2), 2.62 (br s, 2H, CH_2), 2.22 (s, 6H, ArCH_3), 2.16 (s, 6H, Ad), 2.09 (s, 12H, ArCH_3), 1.95 (m, 3H, Ad), 1.56 (m, 6H, Ad), 0.88 (s, 18H, ^{t}Bu), 0.60 (s, 9H, ^{t}Bu) ppm. ^{31}P{^{1}H} NMR (C_6D_6, 202.5 MHz, 20 °C): δ –144 (br, P_2Nb), –207 (t, $^1J_{PP}$ = 180 Hz, *P*C(O)Ad) ppm. ^{13}C{^{1}H} NMR (C_6D_6, 125.8 MHz, 20 °C): δ 213.5 (d, $^1J_{CP}$ = 125 Hz, (O)*C*P), 197.2 ($^2J_{CP}$ = 33 Hz, *ax*-CO), 195.5 ($^1J_{CW}$ = 128 Hz, *eq*-CO), 152.7 (*ipso*-Ar), 151.9 (*ipso*-Ar), 139.3 (Ar), 138.9 (Ar), 138.4 (Ar), 129.7(Ar), 128.2 (Ar), 127.0 (Ar), 123.8 (Ar), 121.3

(Ar), 76.3 (NCH_2), 60.0 (NCH_2), 38.9 (Ad), 36.9 (Ad), 36.6 ($C(CH_3)_3$), 35.5 ($C(CH_3)_3$), 29.8 (Ad), 29.1 (Ad), 28.7 ($C(CH_3)_3$), 21.8 ($ArCH_3$) ppm.

2.8.6 Generation and Fragmentation of $[(OC)_5W]_2{}^tBuC(O)P_3Nb(N[CH_2{}^tBu]Ar)_3$ (23^{tBu})

To a dark red-orange, thawing solution of $Na[\{(OC)_5W\}_2P_3Nb(N[CH_2{}^tBu]Ar)_3]$ (870 mg, 0.609 mmol, 1 eq) in Et_2O (75 mL) was added dropwise a thawing Et_2O solution (4 mL) of $^tBuC(O)Cl$ (75 mg, 0.621 mmol, 1.02 eq). This mixture rapidly turned dark red and was allowed to stir for 30 min. After this time, the reaction mixture was filtered through Celite to remove NaCl and a very small amount of some insoluble red solids, and the Celite bed was then washed with Et_2O (30 mL). The filtrate containing $[(OC)_5W]_2{}^tBuC(O)P_3Nb(N[CH_2{}^tBu]Ar)_3$ was transferred to a new flask and allowed to stir for 40 h at 22 °C. After this time, 30 mL of *n*-pentane was added and the mixture was stirred for 15 min. The red precipitate was then collected atop a sintered glass frit, washed with *n*-pentane, and dried (155 mg, 0.191 mmol of $^tBuCP_3[W(CO)_5]_2$, 31% yield). ^{31}P NMR data on the crude product mixture and isolated precipitate are presented in Figure 2.7, Figure 2.8, and Table 2.1. The spectral properties of the *in situ* formed $[(OC)_5W]_2{}^tBuC(O)P_3Nb(N[CH_2tBu]Ar)_3$ are as follows: ^1H NMR (C_6D_6, 300 MHz, 20 °C): δ 6.50-6.65 (br m, 9H, *o, p*-Ar), 4.86 (d, $^2J_{HH}$ = 14 Hz, 2H, CH_2), 4.60 (d, $^2J_{HH}$ = 14 Hz, 2H, CH_2), 2.61 (br s, 2H, CH_2), 2.21 (s, 6H, $ArCH_3$), 2.07 (s, 12H, $ArCH_3$), 1.23 (s, 9H, $C(O)^tBu$), 0.86 (s, 18H, ^tBu), 0.59 (s, 9H, ^tBu) ppm. ^{31}P NMR (C_6D_6, 121.5 MHz, 20 °C): δ –139 (br, P_2Nb), –203 (t, $^1J_{PP}$ = 182 Hz, $PC(O)^tBu$) ppm.

2.8.7 Powder X-Ray Diffraction of $[^tBuCP_3[W(CO)_5]_2]_2$ (24)

A sample of the precipitate isolated above was suspended in CH_2Cl_2 (4 mL) and stirred for 5 min. Drops of the stirring suspension were deposited onto a single-crystal Si sample holder, allowing the solvent to evaporate between drops, to afford a deposited layer of the compound. This sample was then sealed under a Kapton film and data were collected at 20 °C in the CMSE X-ray diffraction facility on a PANalytical Xpert Pro diffractometer using monochromated Cu Kα radiation over the range $3.5° < 2\theta < 50°$. A variable-width divergence slit was used to give a constant 8 mm illuminated length of sample in order to maximize signal to noise at high angles. This collection strategy necessitated an intensity correction of $\cos(2\theta)$ to the simulated patterns. Powder patterns were simulated using the program Mercury for each of the structures, **24**, **25** and **26** based on the unit cell and atom coordinates that were determined by single-crystal X-ray diffraction.[73] Data on which the simulations are based are provided in cif format at the end of this chapter.

2.8.8 Fragmentation of $[(OC)_5W]_2AdC(O)P_3Nb(N[CH_2{}^tBu]Ar)_3$

Red-orange $[(OC)_5W]_2AdC(O)P_3Nb(N[CH_2{}^tBu]Ar)_3$ (200 mg, 0.128 mmol) was dissolved in benzene (5 mL) and allowed to stand for 6 h. Over this time a red precipitate formed and the

solution faded to yellow-orange. The solution was frozen and upon thawing was filtered to remove the red precipitate, which was collected atop a frit and washed with *n*-pentane to yield a red powder (88 mg, 0.099 mmol, 77% yield as $[AdCP_3[W(CO)_5]_2]_2$). Elem. Anal. Calcd for $C_{21}H_{15}O_{10}P_3W_2$: C, 28.41; H, 1.70; P, 10.46. Found: C, 30.45; H, 1.99; P, 9.89.

The filtrate was concentrated to dryness and then extracted with *n*-pentane and filtered through Celite, leaving behind some red residue, and dried to a yellow powder of $ONb(N[CH_2{}^tBu]Ar)_3$ (84 mg, 0.124 mmol, 98% yield).

2.8.9 Formation of $(Ph_3P)(OC)Pt(P_3C(C_2H_4)Ad)[W(CO)_5]_2$ (28)

Solid red $[(OC)_5W]_2AdC(O)P_3Nb(N[CH_2{}^tBu]Ar)_3$ (305 mg, 0.195 mmol, 1 eq) and off-white $(C_2H_4)Pt(PPh_3)_2$ (142 mg, 0.190 mmol, 0.98 eq) were dissolved together in benzene (10 mL) and allowed to stir for 20 h. The solution changed in color from red to brown over this time, and the reaction mixture was then filtered through Celite. The filtrate was dried and the residue was extracted with Et_2O and concentrated to dryness *in vacuo*. The free PPh_3 was extracted away from the mixture with CH_3CN and the remaining solids were washed into a new flask with Et_2O and dried. This residue was then extracted with *n*-pentane to remove $ONb(N[CH_2{}^tBu]Ar)_3$ and leave behind a gray powder (125 mg). Crystallization from Et_2O or benzene affords **28** as a pale yellow solid in low yields (*ca.* 20%). ^{1}H NMR (C_6D_6, 500 MHz, 20 °C): δ 7.59 (dd, 6H, *o*-Ph), 7.10 (t, 6H, *m*-Ph), 7.00 (t, 3H, *p*-Ph), 2.06 (m, 3H, Ad), 1.99 (m, 2H, C_2H_4), 1.91(m, 6H, Ad), 1.73 (*pseudo* d, 3H, Ad), 1.59 (*pseudo* d, 3H, Ad), 1.35 (m, 2H, C_2H_4) ppm. ^{31}P NMR (C_6D_6, 202.5 MHz, 20 °C): δ 47.6 (dd, $^1J_{PP}$ = 143 Hz, $^3J_{PP}$ = 8 Hz, $^2J_{PtP}$ = 220 Hz, 2P, P_2CP), 14.3 (t, $^3J_{PP}$ = 8 Hz, $^1J_{PtP}$ = 2130 Hz, 1P, Pt*P*Ph$_3$), –153.1 (t, $^1J_{PP}$ = 143 Hz, $^1J_{PtP}$ = 575 Hz, 1P, Pt*P*CP$_2$) ppm. ^{13}C NMR (C_6D_6, 125.8 MHz, 20 °C): δ 200.0 (m, *ax*-CO), 198.3 (m, $^1J_{CW}$ = 125 Hz, *eq*-CO), 179.5 (m, Pt*C*O), 134.7 (d, J_{CP} = 12 Hz, *m*-Ph), 132.3 (*p*-Ph), 129.9 (d, J_{CP} = 53 Hz, *ipso*-Ph), 129.5 (d, J_{CP} = 11 Hz, *o*-Ph), 45.8 (J_{CPt} = 125 Hz, Ad), 43.4 (C_2H_4), 41.3 (Ad), 36.7 (Ad), 29.4 (Ad) ppm. The tertiary carbon bound to Pt could not be located, presumably because the pattern of high multiplicity results in very low intensity. ^{195}Pt NMR (C_6D_6, 107.0 MHz, 20 °C): δ –4170 (ddt, J_{PtP} = 2130 Hz, J_{PtP} = 575 Hz, J_{PtP} = 220 Hz) ppm. IR (thin film, KBr): $\tilde{\nu}$ 2907, 2852, 2062 (vs), 1977 (s), 1922 (br vs), 1436, 1291, 1099, 999, 741, 693 cm^{-1}.

2.8.10 Formation of $C_7H_8(P_3CAd)[W(CO)_5]_2$ (29)

Solid red $[(OC)_5W]_2AdC(O)P_3Nb(N[CH_2{}^tBu]Ar)_3$ (195 mg, 0.125 mmol, 1 eq) was dissolved in 2 g of a 14 wt% THF solution of spiro[2.4]hepta-4,6-diene (280 mg, 24 eq) and the solution was then diluted with THF to a total volume of 5 mL. The solution was stirred at 22 °C for 5 h, after which time the solution was bright yellow in color. The mixture was filtered through Celite and the filtrate was concentrated to dryness under dynamic vacuum. The resulting residue was suspended in *n*-pentane (4 mL) and cooled to –35 °C for 24 h to precipitate the product as a bright yellow powder,

which was collected atop a sintered glass frit, washed with cold *n*-pentane, and dried (65 mg, 0.066 mmol, 53% yield). ^{1}H NMR (C_6D_6, 500 MHz, 20 °C): δ 6.38 (m, 1H, olefinic C*H*), 5.25 (m, 1H, olefinic C*H*), 2.55 (dt, J_{HP} = 18 Hz, 1H, PC*H*), 2.28 (ddd, J_{HP} = 32 Hz, 1H, PC*H*), 1.84 (m, 3H, Ad), 1.45–1.65 (m, 12H, Ad) 0.67 (m, 1H, *spiro*), 0.39 (m, 1H, *spiro*), 0.12 (m, 1H, *spiro*), 0.00 (m, 1H, *spiro*) ppm. ^{31}P NMR (C_6D_6, 121.5 MHz, 20 °C): δ 295.4 (dd, $^{1}J_{PP}$ = 125 Hz, $^{2}J_{PP}$ = 28 Hz, $^{1}J_{PW}$ = 240 Hz, 1P, C=*P*), –3.0 (dd, $^{1}J_{PP}$ = 156 Hz, $^{2}J_{PP}$ = 28 Hz, 1P, C−*P*), –24.9 (dd, $^{1}J_{PP}$ = 156 Hz, $^{1}J_{PP}$ = 125 Hz, $^{1}J_{PW}$ = 210 Hz, 1P, C=P−*P*) ppm. ^{13}C NMR (C_6D_6, 125.8 MHz, 20 °C): δ 227.5 (m, $^{1}J_{CP}$ = 45 Hz, $^{2}J_{CP}$ = 8 Hz, *C*=P), 198.8 (d, $^{2}J_{CP}$ = 31 Hz, *ax*-CO), 197.8 (d, $^{2}J_{CP}$ = 26 Hz, *ax*-CO), 196.4 (d, $^{2}J_{CP}$ = 6 Hz, *eq*-CO), 195.8 (d, $^{2}J_{CP}$ = 6 Hz, *eq*-CO), 129.1 (m, *C*=C), 125.9 (m, C=*C*), 57.8 (dd, J_{CP} = 45, J_{CP} = 13 Hz, P*C*H), 56.0 (d, J_{CP} = 9 Hz, P*C*H), 45.4 (*pseudo* t, J_{CP} = 13 Hz, Ad), 42.7 (m, Ad), 36.4 (Ad), 28.9 (Ad), 11.1 (m, *spiro*), 9.50 (*spiro*), 7.25 (m, *spiro*) ppm. A minor product (*ca*. 10%) was also present with resonances at: ^{31}P NMR (C_6D_6, 121.5 MHz, 20 °C): δ 288.4 (d, J_{PP} = 195 Hz), –21.9 (d, J_{PP} = 150 Hz), –58.1 (dd, J_{PP} = 150 Hz , J_{PP} = 195 Hz) ppm. ^{1}H NMR (C_6D_6, 500 MHz, 20 °C): δ 6.00 (m), 5.50 (m), 2.47 (dt,), 2.26 (ddd), 1.95 (m, Ad), 1.5-1.7 (m, Ad) 1.26 (m, *spiro*), 0.36 (m, *spiro*), –0.10 (m, *spiro*) ppm. One spiro resonance may be obscured. This minor product may be an isomer of the major product with different coordination sites of the $W(CO)_5$ units.

2.8.11 Formation of $(AdCP)_2P_2[W(CO)_5]_2$ (30)

Solid red $[(OC)_5W]_2AdC(O)P_3Nb(N[CH_2{}^tBu]Ar)_3$ (360 mg, 0.230 mmol, 1 eq) and solid colorless AdCP (83 mg, 0.46 mmol, 2 eq) were mixed and then dissolved in benzene (10 mL) to give a deep red solution. The solution was heated to 35 °C for 3.5 h, after which time the orange mixture was filtered through Celite and evaporated to dryness. The orange residue was extracted with *ca.* 10 mL of *n*-pentane and the precipitate was collected on a frit and then washed with 3 mL of *n*-pentane and dried *in vacuo* to yield the desired product as an orange powder (130 mg, 0.122 mmol, 53% yield). ^{1}H NMR (C_6D_6, 500 MHz, , 20 °C): δ 1.90–2.05 (m, 9H, Ad), 1.60 (m, 6H, Ad) ppm. ^{31}P NMR (C_6D_6, 202.5 MHz, 20 °C): δ 248.3 (m, 2P, C=*P*), –13.3 (m, 2P) ppm. ^{13}C NMR ($CDCl_3$, 125.8 MHz, 20 °C): δ 223.9 (dm, $^{1}J_{CP}$ = 47 Hz, *C*=P), 195.9 (d, $^{2}J_{CP}$ = 19 Hz, *ax*-CO), 195.3 (*eq*-CO), 46.3 (d, $^{2}J_{CP}$ = 10 Hz, Ad), 42.4 (Ad), 36.2 (Ad), 28.6 (Ad) ppm. Elem. Anal. Calcd for $C_{32}H_{30}O_{10}P_4W_2$: C, 36.05; H, 2.84; P, 11.62. Found: C, 35.68; H, 3.11; P, 11.96.

2.8.12 Photochemical Isomerization of $(AdCP)_2P_2[W(CO)_5]_2$: Preparation of 31

A sealed NMR tube of orange **30** in THF was irradiated in a Rayonet photoreactor equipped with six RPR-4190 (emission maximum at 419 nm) and ten RPR-2540 (emission maximum at 254 nm) lamps for 20 min. The resulting lighter orange solution was analyzed by ^{31}P NMR to reveal complete conversion of **30** to **31**. Solutions of **30** exposed to ambient fluorescent lighting will also slowly isomerize to afford **31**. ^{31}P NMR (THF, 202.5 MHz, 20 °C): δ 19 (br s, 2P), –108 (br s, 2P)

Table 2.2. Rate constants[a] for deoxygenation of the acyl triphosphirene ligand in **23**^{Ad}.

	λ^b	k_1	k_1'	k_2
Run 1	3.66	1.98	1.68	4.08
Run 2	3.18	1.54	1.64	2.99
Run 3	3.51	1.68	1.83	3.18
Average	3.45	1.73	1.72	3.42
Std Dev	0.24	0.23	0.10	0.58

[a] Values are in units of 10^{-4} sec^{-1} [b] $\lambda = k_1 + k_1'$

ppm.^{31}P NMR (THF, 202.5 MHz, –100 °C): δ 37 (d, J_{PP} = 450 Hz, 1P, *P*=P), –21 (br s, 1P, *P*−P), –21 (d, J_{PP} = 450 Hz, 1P, P=*P*), –232 (br s, 1P, P−*P*) ppm.

2.8.13 Kinetics of $AdCP_3[W(CO)_5]_2$ Loss

Red $[(OC)_5W]_2AdC(O)P_3Nb(N[CH_2{}^tBu]Ar)_3$ (*ca.* 50 mg) and AdCP (*ca.* 7 mg, 1.5 eq) were dissolved in C_6D_6 (750 mg) containing $(Me_3Si)_2O$ as an internal standard and the solution was transferred to a sealable (J. Young) NMR tube. The tube was inserted into an NMR probe pre-heated to 30 °C and spectra were collected periodically over 2.5 h. The relative integrals of ^{t}Bu resonances for the starting material, intermediate, and product were measured and plotted as a function of time. (Note: There are two resonances for the C_s symmetric starting material and intermediate, and one for the C_{3v} product.) Relative concentrations were then plotted and fit to the integrated rate law equations derived from the kinetic scheme described in the text (Eq. 2.1–2.5), where for the reaction studied **A** = **23**^{Ad}, **B** = **23**′ and **C** = **21**. The measurements were repeated three times and the results of the fits are presented in Table 2.2.

Fits were obtained using the non-linear least squares refinement routine of *Gnuplot* in the following manner:[74] fit [**A**] via the variables A_0 and $\lambda = k_1 + k_1'$; then fit [**B**] via the variables B_0, k_1, and k_2; lastly, fit [**C**] via the variable C_0. This kinetic model supplied better fits of the data than the corresponding one when the constraint $k_1' = 0$ is applied.

2.8.14 Alternate Preparation of $[(12\text{-crown-4})_2Na][(P_3)Nb(N[CH_2{}^tBu]Ar)_3]$

A THF solution (10 mL) of $(TfO)_2Nb(N[CH_2{}^tBu]Ar)_3$ (500 mg, 0.52 mmol) and white phosphorus (75 mg, 0.60 mmol, 1.15 eq) was prepared. To this was added freshly prepared 0.9% sodium amalgam (90 mg Na, 3.9 mmol, 7.5 eq; 10 g Hg) affording a color change from yellow-orange to orange-red-brown. The mixture was stirred rapidly for 3 h, over which time the color darkened slightly. After this time the solution was decanted from the Hg and filtered through Celite.

An aliquot was removed for analysis by NMR spectroscopy, and the remaining solution was concentrated to dryness. (This aliquot revealed formation of the desired *cyclo*-P_3 complex.) The resulting residue was extracted once with *n*-hexane/Et_2O and dried again. Addition of 12-crown-4 (220 mg) to a stirring *n*-pentane/Et_2O solution resulted in precipitation of an orange powder. This powder was collected on a frit, and the filtrate was concentrated to afford a second crop. The combined pale orange solids were washed with *n*-pentane and dried to afford the desired product (315 mg, 0.28 mmol, 54% yield). The filtrate remained dark red in color and ^{1}H NMR spectroscopy suggested that the major component was the paramagnetic P[Nb(N[$CH_2{}^t$Bu]Ar)$_3$]$_2$, as even a large amount of dissolved compound gave relatively weak diamagnetic signals and broad resonances consistent with the known species.[75]

2.8.15 Alternate Preparation of [(THF)Na][(P_3)Nb(N[$CH_2{}^t$Bu]Ar)$_3$]

To a stirring solution of [(Et_2O)Na][PNb(N[$CH_2{}^t$Bu]Ar)$_3$] (200 mg, 0.252 mmol) in benzene (5 mL) was added a benzene solution (5 mL) of white phosphorus (16 mg, 0.55 eq). This solution was stirred for 10 min, after which time it was concentrated to dryness. The orange, solid residue was extracted with Et_2O/*n*-pentane and filtered through Celite. The filtrate was dried to an orange powder which was then suspended in *n*-pentane and chilled to –35 °C. The product was collected atop a sintered glass frit and dried (165 mg, 0.212 mmol, 84% yield).

2.8.16 X-Ray Structure Determinations

Diffraction quality crystals of **19** were grown from toluene/O($SiMe_3$)$_2$ at –35 °C, of **24** from CH_2Cl_2 at –35 °C. Crystals of **28** and **30** were grown from benzene at 22 °C, and crystals of **31** from toluene at –35 °C. Crystals of **20**, **22**, **23**^{Ad}, and **29** were each grown from Et_2O at –35 °C. Crystals were mounted in hydrocarbon oil on a nylon loop or a glass fiber. Low-temperature (100 K) data were collected on a Siemens Platform three-circle diffractometer coupled to a Bruker-AXS Smart Apex CCD detector with graphite-monochromated Mo Kα radiation ($\lambda = 0.71073$ Å) or monochromatic Cu Kα radiation ($\lambda = 1.54178$ Å) performing ϕ- and ω-scans. A semi-empirical absorption correction was applied to the diffraction data using SADABS.[76] All structures were solved by direct or Patterson methods using SHELXS[77,78] and refined against F^2 on all data by full-matrix least squares with SHELXL-97.[78,79] All non-hydrogen atoms were refined anisotropically. All hydrogen atoms were included in the model at geometrically calculated positions and refined using a riding model. The isotropic displacement parameters of all hydrogen atoms were fixed to 1.2 times the U_{eq} value of the atoms they are linked to (1.5 times for methyl groups). In structures where disorders were present, the disorders were refined within SHELXL with the help of rigid bond restraints as well as similarity restraints on the anisotropic displacement parameters for neighboring atoms and on 1,2- and 1,3-distances throughout the disordered components.[80] The relative occupancies of

disordered components were refined freely within SHELXL. Further details are provided in Tables 2.3 – 2.4, on Reciprocal Net,[81] or in the form of cif files available from the CCDC.[82]

2.8.17 Computational Studies

All calculations were carried out using ADF 2007.01 from Scientific Computing and Modeling (http://www.scm.com) on a thirty two-processor Quantum Cube workstation from Parallel Quantum Solutions (http://www.pqs-chem.com).[83–85] In all cases the LDA functional employed was that of Vosko, Wilk, and Nusair (VWN) while the GGA part was handled using the functionals of Becke and Perdew (BP86).[86–88] In addition, all calculations were carried out using the Zero Order Regular Approximation (ZORA) for relativistic effects.[89–92] The basis sets were triple-zeta with two polarization functions (TZ2P) as supplied with ADF, and frozen core approximations were made for tungsten (4d), carbon (1s) and oxygen (1s). Geometries were optimized to default convergence criteria and energies are uncorrected for zero-point energies.

Table 2.3. Crystal Data for Triphosphirene Complexes

	19	**20**	**22**
Reciprocal Net code	07136	07052	08242
Empirical formula	$C_{68}H_{93}N_3NbO_6P_3Si_2SnW$	$C_{65.11}H_{96.77}N_4NbO_{5.78}P_4W$	$C_{54}H_{85}N_3NbO_2P_3$
Formula weight	1592.99	1428.60	994.07
Temperature	100(2) K	90(2) K	150(2) K
Wavelength	0.71073 Å	0.71073 Å	0.71073 Å
Crystal system	Triclinic	Triclinic	Monoclinic
Space group	$P\bar{1}$	$P\bar{1}$	$P2_1/n$
Unit cell dimensions	$a = 12.1488(8)$ Å, $\alpha = 75.7190(10)^\circ$	$a = 12.553(2)$ Å, $\alpha = 67.754(3)^\circ$	$a = 12.3177(7)$ Å, $\alpha = 90^\circ$
	$b = 13.9473(9)$ Å, $\beta = 79.1700(10)^\circ$	$b = 16.226(3)$ Å, $\beta = 84.259(3)^\circ$	$b = 20.8376(13)$ Å, $\beta = 100.3270(10)^\circ$
	$c = 24.4655(15)$ Å, $\gamma = 66.6120(10)^\circ$	$c = 19.007(4)$ Å, $\gamma = 87.128(4)^\circ$	$c = 21.9361(13)$ Å, $\gamma = 90^\circ$
Volume	3668.4(4) Å^3	3564.9(12) Å^3	5539.2(6) Å^3
Z	2	2	4
Density (calculated)	1.442 Mg/m^3	1.331 Mg/m^3	1.192 Mg/m^3
Absorption coefficient	2.202 mm^{-1}	1.919 mm^{-1}	0.344 mm^{-1}
$F(000)$	1616	1473	2128
Crystal size	$0.19 \times 0.12 \times 0.09$ mm^3	$0.15 \times 0.15 \times 0.05$ mm^3	$0.29 \times 0.22 \times 0.05$ mm^3
Theta range for collection	1.62 to 28.70°	1.92 to 29.57°	1.36 to 29.13°
Index ranges	$-16 \le h \le 16$, $-18 \le k \le 18$,	$-17 \le h \le 17$, $-22 \le k \le 22$,	$-16 \le h \le 16$, $-28 \le k \le 28$,
	$-33 \le l \le 33$	$-26 \le l \le 26$	$-29 \le l \le 29$
Reflections collected	84933	80206	117373
Independent reflections	18922 [R(int) = 0.0613]	19964 [R(int) = 0.0613]	14909 [R(int) = 0.0509]
Completeness to θ_{max}	99.9%	99.7%	100.0%
Absorption correction	Semi-empirical from equivalents	Semi-empirical from equivalents	Semi-empirical from equivalents
Max. and min. transmission	0.8265 and 0.6798	0.9105 and 0.7626	0.9830 and 0.9069
Refinement method	Full-matrix least-squares on F^2	Full-matrix least-squares on F^2	Full-matrix least-squares on F^2
Data / restraints / parameters	18922 / 72 / 791	19964 / 129 / 809	14909 / 213 / 629
Goodness-of-fit[a]	1.043	1.030	1.015
Final R indices[b] [$I > 2\sigma(I)$]	$R_1 = 0.0359$, $wR_2 = 0.0662$	$R_1 = 0.0339$, $wR_2 = 0.0727$	$R_1 = 0.0388$, $wR_2 = 0.0842$
R indices[b] (all data)	$R_1 = 0.0591$, $wR_2 = 0.0746$	$R_1 = 0.0478$, $wR_2 = 0.0786$	$R_1 = 0.0626$, $wR_2 = 0.0960$
Largest diff. peak and hole	1.080 and -0.814 e Å^{-3}	1.140 and -0.725 e Å^{-3}	0.434 and -0.367 e Å^{-3}

[a] GooF = $\left[\frac{\Sigma[w(F_o^2-F_c^2)^2]}{(n-p)}\right]^{\frac{1}{2}}$ [b] $R_1 = \frac{\Sigma||F_o|-|F_c||}{\Sigma|F_o|}$; $wR_2 = \left[\frac{\Sigma[w(F_o^2-F_c^2)^2}{\Sigma[w(F_o^2)^2]}\right]^{\frac{1}{2}}$; $w = \frac{1}{\sigma^2(F_o^2)+(aP)^2+bP}$; $P = \frac{2F_c^2+\max(F_o^2,0)}{3}$

Table 2.4. Crystal Data for Complexes Related to Triphosphacyclobutadiene Elimination and Trapping

	23^{Ad}	**26**	**28**
Reciprocal Net code	06237	07105	08059
Empirical formula	$C_{62.50}H_{81}N_3NbO_{11}P_3W_2$	$C_{32}H_{22}Cl_4O_{20}P_6W_4$	$C_{60}H_{52}O_{11}P_4PtW_2$
Formula weight	1603.82	1789.52	1635.69
Temperature	100(2) K	100(2) K	100(2) K
Wavelength	0.71073 Å	0.71073 Å	0.71073 Å
Crystal system	Monoclinic	Triclinic	Triclinic
Space group	$P2_1/c$	$P\bar{1}$	$P\bar{1}$
Unit cell dimensions	$a = 13.9056(12)$ Å, $\alpha = 90°$	$a = 10.530(3)$ Å, $\alpha = 84.495(5)°$	$a = 13.430(6)$ Å, $\alpha = 65.975(7)°$
	$b = 21.2534(18)$ Å, $\beta = 106.2100(10)°$	$b = 11.069(3)$ Å, $\beta = 64.355(5)°$	$b = 14.603(6)$ Å, $\beta = 89.922(7)°$
	$c = 23.425(2)$ Å, $\gamma = 90°$	$c = 11.940(4)$ Å, $\gamma = 80.502(5)°$	$c = 16.493(7)$ Å, $\gamma = 81.239(7)°$
Volume	6647.7(10) Å^3	1237.0(7) Å^3	2913(2) Å^3
Z	4	1	2
Density (calculated)	1.602 Mg/m^3	2.402 Mg/m^3	1.865 Mg/m^3
Absorption coefficient	3.751 mm^{-1}	9.750 mm^{-1}	6.503 mm^{-1}
$F(000)$	3196	828	1572
Crystal size	$0.25 \times 0.25 \times 0.08$ mm^3	$0.08 \times 0.06 \times 0.01$ mm^3	$0.20 \times 0.14 \times 0.06$ mm^3
Theta range for collection	1.53 to 29.57°	1.87 to 29.57°	1.99 to 29.57°
Index ranges	$-19 \le h \le 19$, $-29 \le k \le 29$,	$-14 \le h \le 14$, $-15 \le k \le 15$,	$-18 \le h \le 18$, $-20 \le k \le 20$,
	$-32 \le l \le 32$	$-16 \le l \le 16$	$-22 \le l \le 22$
Reflections collected	144330	27941	75795
Independent reflections	18654 [R(int) = 0.0580]	6955 [R(int) = 0.0509]	16034 [R(int) = 0.0664]
Completeness to θ_{max}	100.0%	99.8%	99.7%
Absorption correction	Semi-empirical from equivalents	Semi-empirical from equivalents	Semi-empirical from equivalents
Max. and min. transmission	0.7534 and 0.4540	0.9529 and 0.5093	0.6963 and 0.3563
Refinement method	Full-matrix least-squares on F^2	Full-matrix least-squares on F^2	Full-matrix least-squares on F^2
Data / restraints / parameters	18654 / 219 / 827	6955 / 0 / 301	16304 / 186 / 734
Goodness-of-fit[a]	1.042	1.032	1.012
Final R indices[b] [$I > 2\sigma(I)$]	$R_1 = 0.0243$ $wR_2 = 0.0521$	$R_1 = 0.0333$, $wR_2 = 0.0624$	$R_1 = 0.0336$, $wR_2 = 0.0659$
R indices[b] (all data)	$R_1 = 0.0361$, $wR_2 = 0.0575$	$R_1 = 0.0503$, $wR_2 = 0.0696$	$R_1 = 0.0581$, $wR_2 = 0.0752$
Largest diff. peak and hole	1.171 and -0.829 e Å^{-3}	2.201 and -1.220 e Å^{-3}	2.724 and -1.979 e Å^{-3}

[a] GooF = $\left[\frac{\Sigma[w(F_o^2-F_c^2)^2]}{(n-p)}\right]^{\frac{1}{2}}$ [b] $R_1 = \frac{\Sigma||F_o|-|F_c||}{\Sigma|F_o|}$; $wR_2 = \left[\frac{\Sigma[w(F_o^2-F_c^2)^2}{\Sigma[w(F_o^2)^2]}\right]^{\frac{1}{2}}$; $w = \frac{1}{\sigma^2(F_o^2)+(aP)^2+bP}$; $P = \frac{2F_c^2+\max(F_o^2,0)}{3}$

Table 2.5. Crystal Data for Tetraphosphabenzenes and a Diene Adduct of a Tetraphosphacyclobutadiene

	29	**30**	**31**
Reciprocal Net code	D8_08026	08247	D8_08034
Empirical formula	$C_{28}H_{23}O_{10}P_3W_2$	$C_{32}H_{30}O_{10}P_4W_2$	$C_{35.50}H_{34}O_{10}P_4W_2$
Formula weight	980.07	1066.14	1112.21
Temperature	100(2) K	100(2) K	100(2) K
Wavelength	1.54178 Å	0.71073 Å	1.54178 Å
Crystal system	Monoclinic	Triclinic	Triclinic
Space group	$P2_1/n$	$P\bar{1}$	$P\bar{1}$
Unit cell dimensions	$a = 9.9020(2)$ Å, $\alpha = 90°$	$a = 6.8224(10)$ Å, $\alpha = 64.701(2)°$	$a = 10.12120(10)$ Å, $\alpha = 75.6130(10)°$
	$b = 14.1854(3)$ Å, $\beta = 98.1690(10)°$	$b = 12.2282(18)$ Å, $\beta = 77.653(2)°$	$b = 10.49990(10)$ Å, $\beta = 88.9930(10)°$
	$c = 22.1848(4)$ Å, $\gamma = 90°$	$c = 12.4215(19)$ Å, $\gamma = 76.026(2)°$	$c = 19.7853(2))$ Å, $\gamma = 67.2920(10)°$
Volume	3084.54(11) Å^3	901.9(2) Å^3	1871.57(3) Å^3
Z	4	1	2
Density (calculated)	2.110 Mg/m^3	1.963 Mg/m^3	1.974 Mg/m^3
Absorption coefficient	15.537mm^{-1}	6.603 mm^{-1}	13.291 mm^{-1}
$F(000)$	1856	510	1070
Crystal size	$0.12 \times 0.08 \times 0.02$ mm^3	$0.45 \times 0.35 \times 0.22$ mm^3	$0.10 \times 0.10 \times 0.02$ mm^3
Theta range for collection	3.71 to 67.56°	1.83 to 29.57°	4.63 to 66.59°
Index ranges	$-11 \le h \le 11$, $-16 \le k \le 15$,	$-9 \le h \le 9$, $-16 \le k \le 16$,	$-12 \le h \le 11$, $-12 \le k \le 12$,
	$-26 \le l \le 26$	$-17 \le l \le 17$	$-23 \le l \le 23$
Reflections collected	57405	22059	35261
Independent reflections	5560 [R(int) = 0.0314]	5054 [R(int) = 0.0506]	6395 [R(int) = 0.0460]
Completeness to θ_{max}	100.0%	99.6%	96.5%
Absorption correction	Semi-empirical from equivalents	Semi-empirical from equivalents	Semi-empirical from equivalents
Max. and min. transmission	0.7464 and 0.2572	0.2674 and 0.1179	0.7769 and 0.3499
Refinement method	Full-matrix least-squares on F^2	Full-matrix least-squares on F^2	Full-matrix least-squares on F^2
Data / restraints / parameters	5560 / 0 / 388	5054 / 247 / 373	6395 / 63 / 485
Goodness-of-fit[a]	1.096	1.200	1.031
Final R indices[b] [$I > 2\sigma(I)$]	$R_1 = 0.0216$ $wR_2 = 0.0508$	$R_1 = 0.0413$, $wR_2 = 0.0979$	$R_1 = 0.0259$, $wR_2 = 0.0619$
R indices[b] (all data)	$R_1 = 0.0236$, $wR_2 = 0.0517$	$R_1 = 0.0474$, $wR_2 = 0.1019$	$R_1 = 0.0323$, $wR_2 = 0.0650$
Largest diff. peak and hole	1.006 and -0.993 e Å^{-3}	2.651 and -1.873 e Å^{-3}	1.653 and -0.626 e Å^{-3}

[a] GooF = $\left[\frac{\Sigma[w(F_o^2-F_c^2)^2]}{(n-p)}\right]^{\frac{1}{2}}$ [b] $R_1 = \frac{\Sigma||F_o|-|F_c||}{\Sigma|F_o|}$; $wR_2 = \left[\frac{\Sigma[w(F_o^2-F_c^2)^2}{\Sigma[w(F_o^2)^2]}\right]^{\frac{1}{2}}$; $w = \frac{1}{\sigma^2(F_o^2)+(aP)^2+bP}$; $P = \frac{2F_c^2+\max(F_o^2,0)}{3}$

CIF Data Used for Powder Simulations

```
data_4a in P-1
_symmetry_cell_setting           triclinic
_symmetry_space_group_name_H-M   'P -1'
_symmetry_Int_Tables_number      2
loop_
_symmetry_equiv_pos_site_id
_symmetry_equiv_pos_as_xyz
1 x,y,z
2 -x,-y,-z
_cell_length_a                   10.985(4)
_cell_length_b                   12.309(5)
_cell_length_c                   18.043(7)
_cell_angle_alpha                70.483(6)
_cell_angle_beta                 88.500(6)
_cell_angle_gamma                84.026(7)
_cell_volume                     2286.83
loop_
_atom_site_label
_atom_site_type_symbol
_atom_site_fract_x
_atom_site_fract_y
_atom_site_fract_z
P1 P 0.676297 0.257696 0.834718
W1 W 0.748634 0.149515 0.969277
P2 P 0.594795 0.367873 0.689069
O11 O 0.779013 -0.079258 0.923726
C11 C 0.770776 -0.000816 0.939107
O12 O 0.492447 0.081022 1.04873
C12 C 0.580049 0.110381 1.0134
O13 O 0.705077 0.379695 1.0171
C13 C 0.720014 0.297806 1.00101
C14 C 0.930115 0.176992 0.942157
O14 O 1.03046 0.185932 0.929611
O15 O 0.845853 0.012171 1.1425
C15 C 0.813366 0.06125 1.07935
P3 P 0.614425 0.557353 0.655723
W3 W 0.679929 0.679267 0.524562
O31 O 0.715293 0.885498 0.591056
C31 C 0.703776 0.811947 0.567865
O32 O 0.410198 0.796937 0.468501
C32 C 0.504056 0.753818 0.490543
O33 O 0.630612 0.477552 0.457894
C33 C 0.648245 0.548408 0.483133
O34 O 0.961905 0.582589 0.548226
C34 C 0.859687 0.614297 0.542071
O35 O 0.764014 0.836435 0.358659
C35 C 0.734689 0.779781 0.416697
P4 P 0.461344 0.617092 0.719702
W4 W 0.293561 0.768999 0.702576
O41 O 0.179993 0.702393 0.563636
C41 C 0.222579 0.725117 0.613673
```

```
O42 O 0.164159 0.571704 0.832268
C42 C 0.207973 0.644194 0.78667
O43 O 0.413471 0.838892 0.834667
C43 C 0.372581 0.818405 0.790035
O44 O 0.054994 0.929644 0.704992
C44 C 0.140015 0.87686 0.701172
O45 O 0.425804 0.972541 0.578505
C45 C 0.379532 0.897254 0.621767
P5 P 0.651794 0.574611 0.771024
W5 W 0.79438 0.673143 0.823946
O51 O 0.945751 0.432992 0.917577
C51 C 0.888271 0.517544 0.883886
O52 O 0.959541 0.700228 0.673584
C52 C 0.900812 0.690021 0.729567
O53 O 0.663677 0.92902 0.747783
C53 C 0.710194 0.838587 0.772007
O54 O 0.996901 0.788879 0.887142
C54 C 0.919688 0.740976 0.867632
O55 O 0.617604 0.649933 0.967735
C55 C 0.674986 0.657155 0.920496
P6 P 0.505158 0.46758 0.825312
C60 C 0.528384 0.339775 0.790526
C61 C 0.406268 0.27442 0.801913
C62 C 0.31182 0.349235 0.738128
H62A H 0.346308 0.359468 0.685869
H62B H 0.292497 0.425144 0.744496
H62C H 0.236964 0.310377 0.743709
C63 C 0.439463 0.156492 0.789353
H63A H 0.476268 0.169358 0.737437
H63B H 0.365203 0.117429 0.79259
H63C H 0.497932 0.108036 0.830082
C64 C 0.347491 0.258519 0.881046
H64A H 0.404674 0.210764 0.922834
H64B H 0.272758 0.220125 0.884296
H64C H 0.326936 0.334359 0.887307
C70 C 0.73438 0.297231 0.743482
C71 C 0.860367 0.279055 0.709385
C72 C 0.846002 0.299081 0.622523
H72A H 0.926514 0.287958 0.599925
H72B H 0.809062 0.378324 0.596088
H72C H 0.793124 0.243935 0.615288
C73 C 0.94224 0.366937 0.721721
H73A H 0.950627 0.353578 0.778102
H73B H 0.904607 0.445959 0.695406
H73C H 1.02325 0.356838 0.699456
C74 C 0.914461 0.15224 0.749274
H74A H 0.924577 0.136967 0.805771
H74B H 0.994225 0.139429 0.726293
H74C H 0.8589 0.09987 0.741063
#END

data_4b in P-1
_symmetry_cell_setting           triclinic
_symmetry_space_group_name_H-M   'P -1'
```

```
_symmetry_Int_Tables_number      2
loop_
_symmetry_equiv_pos_site_id
_symmetry_equiv_pos_as_xyz
1 x,y,z
2 -x,-y,-z
_cell_length_a                   12.139(16)
_cell_length_b                   12.66(2)
_cell_length_c                   15.35(2)
_cell_angle_alpha                69.55(3)
_cell_angle_beta                 81.17(5)
_cell_angle_gamma                84.18(4)
_cell_volume                     2182.43
loop_
_atom_site_label
_atom_site_type_symbol
_atom_site_fract_x
_atom_site_fract_y
_atom_site_fract_z
P1 P 1.31057 -1.80663 1.87603
W1 W 1.27692 -1.85665 2.04815
O11 O 1.04968 -1.9849 2.08048
C11 C 1.13757 -1.928 2.05828
O12 O 1.50917 -1.7562 2.03514
C12 C 1.42028 -1.78309 2.04179
O13 O 1.40783 -2.09678 2.07479
C13 C 1.36057 -2.01108 2.06039
O14 O 1.26871 -1.91416 2.26661
C14 C 1.25904 -1.90688 2.19914
O15 O 1.13306 -1.62334 2.05058
C15 C 1.18286 -1.70404 2.04399
P2 P 1.40942 -1.669 1.77536
W2 W 1.50907 -1.51198 1.78745
O21 O 1.68742 -1.46844 1.60899
C21 C 1.61561 -1.49091 1.67276
O22 O 1.61251 -1.30624 1.80831
C22 C 1.56569 -1.38475 1.80859
O23 O 1.36415 -1.51595 1.97814
C23 C 1.41192 -1.52162 1.90963
O24 O 1.70365 -1.66544 1.88788
C24 C 1.62424 -1.62203 1.85463
O25 O 1.33481 -1.342 1.66395
C25 C 1.39042 -1.40332 1.71287
P3 P 1.23065 -1.66892 1.76395
W3 W 1.05641 -1.55187 1.76994
O31 O 1.15375 -1.38831 1.56635
C31 C 1.10791 -1.44301 1.64618
O32 O 0.951589 -1.71334 1.9688
C32 C 1.00002 -1.66144 1.89236
O33 O 1.14768 -1.39728 1.87034
C33 C 1.10784 -1.4537 1.83216
O34 O 0.935498 -1.69555 1.68304
C34 C 0.982453 -1.6627 1.71711
O35 O 0.82692 -1.40857 1.75947
```

```
C35 C 0.916559 -1.46806 1.76234
P4 P 1.23796 -1.85946 1.65038
W4 W 1.13997 -1.8525 1.51868
O41 O 1.37687 -1.79822 1.39799
C41 C 1.28291 -1.81757 1.4449
O42 O 0.915921 -1.92258 1.65715
C42 C 0.993912 -1.88552 1.59725
O43 O 1.08004 -1.58445 1.4826
C43 C 1.10151 -1.68328 1.50257
O44 O 1.02814 -1.81809 1.33674
C44 C 1.06967 -1.82869 1.39925
O45 O 1.19191 -2.10787 1.53275
C45 C 1.18113 -2.01811 1.53233
P5 P 1.30817 -1.70212 1.63388
P6 P 1.40123 -1.90352 1.78809
C50 C 1.29536 -1.94743 1.74083
C51 C 1.26396 -2.0754 1.79469
C52 C 1.24761 -2.11166 1.90559
H52A H 1.19367 -2.0586 1.92503
H52B H 1.31928 -2.11094 1.92726
H52C H 1.21978 -2.18783 1.93295
C53 C 1.35227 -2.15768 1.77052
H53A H 1.33013 -2.23507 1.80505
H53B H 1.42374 -2.14709 1.78783
H53C H 1.36009 -2.14412 1.70306
C54 C 1.14803 -2.10378 1.77645
H54A H 1.09008 -2.04911 1.78861
H54B H 1.12948 -2.17997 1.81825
H54C H 1.15243 -2.09993 1.71115
C60 C 1.42954 -1.75873 1.69778
C61 C 1.54233 -1.76034 1.6303
C62 C 1.54682 -1.85247 1.58651
H62A H 1.54296 -1.92649 1.63615
H62B H 1.61681 -1.84971 1.54455
H62C H 1.48356 -1.84024 1.55078
C63 C 1.54539 -1.64709 1.55278
H63A H 1.4795 -1.63547 1.52013
H63B H 1.61305 -1.64499 1.50836
H63C H 1.54559 -1.58729 1.57954
C64 C 1.64135 -1.78566 1.68603
H64A H 1.63359 -1.85906 1.73612
H64B H 1.6434 -1.7268 1.71349
H64C H 1.7107 -1.78739 1.64429
#END

data_4c in P-1
_symmetry_cell_setting           triclinic
_symmetry_space_group_name_H-M   'P -1'
_symmetry_Int_Tables_number      2
loop_
_symmetry_equiv_pos_site_id
_symmetry_equiv_pos_as_xyz
1 x,y,z
2 -x,-y,-z
```

```
_cell_length_a                    10.530(3)
_cell_length_b                    11.069(3)
_cell_length_c                    11.940(4)
_cell_angle_alpha                 84.495(5)
_cell_angle_beta                  64.355(5)
_cell_angle_gamma                 80.502(5)
_cell_volume                      1236.97
loop_
_atom_site_label
_atom_site_type_symbol
_atom_site_fract_x
_atom_site_fract_y
_atom_site_fract_z
P1 P -0.573 -0.461917 0.402525
P2 P -0.353987 -0.486721 0.393335
P3 P -0.479955 -0.644317 0.321592
C1 C -0.329542 -0.639994 0.337589
C2 C -0.197959 -0.737177 0.304456
C3 C -0.097104 -0.704941 0.356407
H3A H -0.066411 -0.625422 0.321375
H3B H -0.013787 -0.768122 0.33374
H3C H -0.147019 -0.700791 0.447125
C4 C -0.244479 -0.85926 0.362044
H4A H -0.28392 -0.855749 0.452752
H4B H -0.162446 -0.923694 0.3326
H4C H -0.317212 -0.87744 0.338093
C5 C -0.122468 -0.746463 0.163421
H5A H -0.189653 -0.762597 0.131825
H5B H -0.043129 -0.813507 0.14119
H5C H -0.086109 -0.669253 0.126616
W1 W -0.201196 -0.328563 0.270445
C11 C -0.094099 -0.192067 0.171478
O11 O -0.031577 -0.112285 0.116154
C12 C -0.360438 -0.191993 0.363096
O12 O -0.443341 -0.110291 0.405944
C13 C -0.289272 -0.344708 0.151624
O13 O -0.34099 -0.364168 0.088952
C14 C -0.028583 -0.439981 0.157716
O14 O 0.073147 -0.49476 0.0887
C15 C -0.112464 -0.340099 0.394309
O15 O -0.062333 -0.351186 0.462226
W2 W -0.574656 -0.749887 0.213576
C21 C -0.671482 -0.821064 0.126689
O21 O -0.72986 -0.861347 0.080976
C22 C -0.415913 -0.896016 0.162596
O22 O -0.329368 -0.978441 0.13216
C23 C -0.68882 -0.848558 0.370625
O23 O -0.750353 -0.905549 0.456041
C24 C -0.729981 -0.60181 0.256987
O24 O -0.81368 -0.517706 0.280043
C25 C -0.454394 -0.662187 0.052861
O25 O -0.383377 -0.61575 -0.036868
C1S C -0.220887 -0.837142 -0.23026
H1S1 H -0.206456 -0.860003 -0.153955
```

```
H1S2 H -0.212804 -0.74884 -0.248262
CL1S Cl -0.087344 -0.921071 -0.353539
CL2S Cl -0.391366 -0.861222 -0.203272
#END
```

2.9 REFERENCES

[1] Figueroa, J. S.; Cummins, C. C. *J. Am. Chem. Soc.* **2004**, *126*, 13916–13917.

[2] Piro, N. A.; Figueroa, J. S.; McKellar, J. T.; Cummins, C. C. *Science* **2006**, *313*, 1276–1279.

[3] Capozzi, G.; Chiti, L.; Di Vaira, M.; Peruzzini, M.; Stoppioni, P. *J. Chem. Soc., Chem. Commun.* **1986**, 1799–1800.

[4] Chatt, J.; Hitchcock, P. B.; Pidcock, A.; Warrens, C. P.; Dixon, D. A. *J. Chem. Soc., Chem. Commun.* **1982**, 932–933.

[5] Cossairt, B. M.; Cummins, C. C. *Inorg. Chem.* **2008**, *47*, 9363–9371.

[6] Weber, L. *Chem. Rev.* **1992**, *92*, 1839–1906.

[7] Regitz, M.; Scherer, O. J. *Multiple Bonds and Low Coordination in Phosphorus Chemistry*; Thieme: Stuttgart, 1990.

[8] Dillon, K. B.; Mathey, F.; Nixon, J. F. *Phosphorus: The Carbon Copy*; Wiley: Chichester, 1998.

[9] Schäfer, H.; Binder, D.; Fenske, D. *Angew. Chem., Int. Ed. Engl.* **1985**, *24*, 522–524.

[10] Schäfer, H.; Binder, D. *Z. Anorg. Allg. Chem.* **1988**, *560*, 65–79.

[11] Phillips, I. G.; Ball, R.; Cavell, R. G. *Inorg. Chem.* **1992**, *31*, 1633–1641.

[12] Barbaro, P.; Ienco, A.; Mealli, C.; Peruzzini, M.; Scherer, O. J.; Schmitt, G.; Vizza, F.; Wolmershäuser, G. *Chem. Eur. J.* **2003**, *9*, 5195–5210.

[13] Yakhvarov, D.; Babaro, P.; Gonsalvi, L.; Carpio, S. M.; Midollini, S.; Orlandini, A.; Peruzzini, M.; Sinyashin, O.; Zanobini, F. *Angew. Chem., Int. Ed.* **2006**, *45*, 4182–4185.

[14] Watts, L.; Fitzpatrick, J. D.; Pettit, R. *J. Am. Chem. Soc.* **1965**, *87*, 3253–3254.

[15] Watts, L.; Fitzpatrick, J. D.; Pettit, R. *J. Am. Chem. Soc.* **1966**, *88*, 623–624.

[16] Maier, G. *Angew. Chem., Int. Ed. Engl.* **1988**, *27*, 309–446.

[17] Hofmann, M.; Schleyer, P. v. R.; Regitz, M. *Eur. J. Org. Chem* **1999**, 3291–3303.

[18] Kobayashi, K.; Miura, H.; Nagase, S. *THEOCHEM* **1994**, *311*, 69–77.

[19] Ohanessian, G.; Hiberty, P. C.; Lefour, J. M.; Flament, J. P.; Shaik, S. S. *Inorg. Chem.* **1988**, *27*, 2219–2224.

[20] Nagase, S.; Ito, K. *Chem. Phys. Lett.* **1986**, *126*, 43–47.

[21] Scherer, O. J.; Vondung, J.; Wolmershäuser, G. *Angew. Chem., Int. Ed. Engl.* **1989**, *28*, 1355–1357.

[22] Scherer, O. J.; Winter, R.; Wolmershäuser, G. *Z. Anorg. Allg. Chem.* **1993**, *619*, 827–835.

[23] Barr, M. E.; Smith, S. K.; Spencer, B.; Dahl, L. F. *Organometallics* **1991**, *10*, 3983–3991.

[24] Scherer, O. J.; Sitzmann, H.; Wolmershäuser, G. *Angew. Chem., Int. Ed. Engl.* **1985**, *24*, 351–353.

[25] Binger, P.; Stannek, J.; Gabor, B.; Mynott, R.; Bruckmann, J.; Krüger, C.; Leininger, S. *Angew. Chem., Int. Ed. Engl.* **1995**, *34*, 2227–2230.

[26] Gleiter, R.; Lange, H.; Binger, P.; Stannek, J.; Krüger, C.; Bruckmann, J.; Zenneck, U.; Kummer, S. *Eur. J. Inorg. Chem.* **1998**, *1998*, 1619–1621.

[27] Mack, A.; Danner, S.; Bergsträßer, U.; Heydt, H.; Regitz, M. *J. Organomet. Chem.* **2002**, *643-644*, 409–415.

[28] Binger, P.; Leininger, S.; Günther, K.; Bergsträßer, U. *Chem. Ber.* **1997**, *130*, 1491–1494.

[29] Scheer, M.; Krug, J. *Z. Anorg. Allg. Chem.* **1998**, *624*, 399–405.

[30] Binger, P.; Biedenbach, B.; Mynott, R.; Benn, R.; Rufińska, A.; Betz, P.; Krüger, C. *J. Chem. Soc., Dalton Trans.* **1990**, 1771–1777.

[31] Canac, Y.; Bourissou, D.; Baceiredo, A.; Gornitzka, H.; Schoeller, W. W.; Bertrand, G. *Science* **1998**, *279*, 2080–2082.

[32] Fish, C.; Green, M.; Jeffery, J. C.; Kilby, R. J.; Lynam, J. M.; McGrady, J. E.; Pantazis, D. A.; Russell, C. A.; Willans, C. *Angew. Chem., Int. Ed.* **2006**, *45*, 6685–6689.

[33] Greenwood, N. N.; Earnshaw, A. *Chemistry of the Elements*, 2nd ed.; Butterworth-Heinemann: Oxford, 1997.

[34] Pohl, S. *J. Organomet. Chem.* **1977**, *142*, 185–194.

[35] Niecke, E.; Nieger, M.; Reichert, F. *Angew. Chem., Int. Ed. Engl.* **1988**, *27*, 1715.

[36] Gudat, D. *Coord. Chem. Rev.* **1997**, *163*, 71–106.

[37] Burford, N.; Cameron, T. S.; LeBlanc, D. J.; Losier, P.; Sereda, S.; Wu, G. *Organometallics* **1997**, *16*, 4712–4717.

[38] Gudat, D.; Schiffner, H. M.; Nieger, M.; Stalke, D.; Blake, A. J.; Grondey, H.; Niecke, E. *J. Am. Chem. Soc.* **1992**, *114*, 8857–8862.

[39] Gudat, D.; Niecke, E.; Krebs, B.; Dartmann, M. *Organometallics* **1986**, *5*, 2376–2377.

[40] Jutzi, P.; Meyer, U.; Krebs, B.; Dartmann, M. *Angew. Chem., Int. Ed. Engl.* **1986**, *25*, 919–921.

[41] Wrighton, M. *Chem. Rev.* **1974**, *74*, 401–430.

[42] Cossairt, B. M.; Diawara, M.-C.; Cummins, C. C. *Science* **2009**, *323*, 602.

[43] Budzelaar, P. H. *gNMR*; 5.1, 2005. `http://home.cc.umanitoba.ca/~budzelaa/gNMR/gNMR.html`.

[44] Mack, A.; Regitz, M. *Chem. Ber.* **1997**, *130*, 823–834.

[45] Wettling, T.; Schneider, J.; Wagner, O.; Kreiter, C. G.; Regitz, M. *Angew. Chem., Int. Ed. Engl.* **1989**, *28*, 1013–1014; *Angew. Chem.* **1989**, *101*, 1035–1036.

[46] Geissler, B.; Barth, S.; Bergsträßer, U.; Slany, M.; Durkin, J.; Hitchcock, P. B.; Hofmann, M.; Binger, P.; Nixon, J. F.; Schleyer, P. v. R.; Regitz, M. *Angew. Chem., Int. Ed. Engl.* **1995**, *34*, 484–487.

[47] Hitchcock, P. B.; Jones, C.; Nixon, J. F. *J. Chem. Soc., Chem. Commun.* **1995**, 2167–2168.

[48] Mack, A.; Breit, B.; Wettling, T.; Bergsträßer, U.; Leininger, S.; Regitz, M. *Angew. Chem., Int. Ed. Engl.* **1997**, *36*, 1337–1340.

[49] Nemirowski, A.; Reisenauer, H. P.; Schreiner, P. R. *Chem. Eur. J.* **2006**, 7411–7420.

[50] Schiffer, H.; Ahlrichs, R.; Häser, M. *Theor. Chim. Acta.* **1989**, *75*, 1–10.

[51] Schoeller, W. W.; Staemmler, V.; Rademacher, P.; Niecke, E. *Inorg. Chem.* **1986**, *25*, 4382–4385.

[52] Fish, C.; Green, M.; Kilby, R. J.; McGrady, J. E.; Pantazis, D. A.; Russell, C. A. *Dalton Trans.* **2008**, 3753–3758.

[53] Pietschnig, R.; Niecke, E. *Organometallics* **1996**, *15*, 891–893.

[54] Jutzi, P.; Meyer, U.; Opiela, S.; Neumann, B.; Stammler, H. G. *J. Organomet. Chem.* **1992**, *439*, 279–301.

[55] Burckett-St.Laurent, J. C. T. R.; Hitchcock, P. B.; Kroto, H. W.; Nixon, J. F. *J. Chem. Soc., Chem. Commun.* **1981**, 1141–1143.

[56] Masuda, J.; Schoeller, W. W.; Donnadieu, B.; Bertrand, G. *Angew. Chem., Int. Ed.* **2007**, *46*, 7052–7055.

[57] Menchikov, L. G.; Nefedov, O. M. *Russ. Chem. Rev.* **1994**, *63*, 449–469.

[58] Fink, J.; Rösch, W.; Vogelbacher, U. J.; Regitz, M. *Angew. Chem., Int. Ed. Engl.* **1986**, *25*, 280–282.

[59] Van Tamelen, E. E. *Acc. Chem. Res.* **1972**, *5*, 186–192.

[60] Kent, J. E.; Harman, P. J.; O'Dwyer, M. F. *J. Phys. Chem.* **1981**, *85*, 2726–2730.

[61] Harman, P. J.; Kent, J. E.; O'Dwyer, M. F.; Griffith, D. W. T. *J. Phys. Chem.* **1981**, *85*, 2731–2733.

[62] Kawasaki, S.; Nakamura, A.; Toyota, K.; Yoshifuji, M. *Bull. Chem. Soc. Jpn.* **2005**, *78*, 1110–1120.

[63] Turro, N. J. *Modern Molecular Photochemistry*; University Science Books: Sausalito, 1991; pp 429–432.

[64] Blatter, K.; Rösch, W.; Vogelbacher, U. J.; Fink, J.; Regitz, M. *Angew. Chem., Int. Ed. Engl.* **1987**, *26*, 85–86.

[65] Yoshifuji, M.; Shinohara, N.; Toyota, K. *Tetrahedron Lett.* **1996**, *37*, 7815–7818.

[66] Huttner, G.; Borm, J.; Zsolnai, L. *J. Organomet. Chem.* **1986**, *304*, 309–321.

[67] Barich, D. H.; Nicholas, J. B.; Xu, T.; Haw, J. F. *J. Am. Chem. Soc.* **1998**, *120*, 12342–12350.

[68] Forni, A.; Moretti, I.; Mucci, A.; Prati, I.; Schenetti, L. *Chem. Heterocycl. Comp.* **1995**, *31*, 1071–1078.

[69] Cossairt, B. M.; Cummins, C. C. *Angew. Chem., Int. Ed.* **2008**, *47*, 8863–8866.

[70] Pangborn, A. B.; Giardello, M. A.; Grubbs, R. H.; Rosen, R. K.; Timmers, F. J. *Organometallics* **1996**, *15*, 1518–1520.

[71] Hartley, F. R. *Organomet. Chem. Rev. A* **1970**, *6*, 119–137.

[72] Joly, K. M.; Kariuki, B. M.; Coe, D. M.; Cox, L. R. *Organometallics* **2005**, *24*, 358–366.

[73] *Mercury*; 1.3; Cambridge Crystallographic Data Centre, 2004.

[74] Williams, T.; Kelley, C. *Gnuplot*; 3.8j, 2002. `http://www.gnuplot.info`.

[75] Figueroa, J. S.; Ph.D. thesis; Massachusetts Institute of Technology; 2005.

[76] Sheldrick, G. M. *SHELXTL*; Bruker AXS, Inc.: Madison, WI (USA), 2005–2008.

[77] Sheldrick, G. M. *Acta Crystallogr., Sect. A: Fundam. Crystallogr.* **1990**, *46*, 467–473.

[78] Sheldrick, G. M. *Acta Crystallogr., Sect. A: Fundam. Crystallogr.* **2008**, *64*, 112–122.

[79] Sheldrick, G. M. *SHELXL-97: Program for crystal structure determination*; University of Göttingen, 1997.

[80] Müller, P.; Herbst-Irmer, R.; Spek, A. L.; Schneider, T. R.; Sawaya, M. R. *Crystal Structure Refinement: A Crystallographer's Guide to SHELXL*; Müller, P., Ed.; IUCr Texts on Crystallography; Oxford University Press: Oxford, 2006.

[81] The Reciprocal Net Site Network is a distributed database for crystallographic information, supported by the National Science Digital Library, and is run by participating crystallography labs across the world. Crystallographic data for complexes in this chapter are available under the identification codes listed in Tables 2.3 – 2.5 from the MIT Reciprocal Net site. `http://reciprocal.mit.edu/recipnet`.

[82] These data can be obtained free of charge from The Cambridge Crystallographic Data Centre via `http://www.ccdc.cam.ac.uk/data_request/cif`.

[83] te Velde, G.; Bickelhaupt, F. M.; Baerends, E. J.; Fonseca Guerra, C.; van Gisbergen, S. J. A.; Snijders, J. G.; Ziegler, T. *J. Comput. Chem.* **2001**, *22*, 931–967.

[84] Fonseca Guerra, C.; Snijders, J. G.; te Velde, G.; Baerends, E. J. *Theo. Chem. Acc.* **1998**, *99*, 391–403.

[85] *ADF*; 2007.01; Scientific Computing & Modeling: Theoretical Chemistry, Vrije Universiteit, Amsterdam, The Netherlands, 2007. `http://www.scm.com`.

[86] Vosko, S. H.; Wilk, L.; Nusair, M. *Can. J. Phys.* **1980**, *58*, 1200–1211.

[87] Becke, A. D. *Phys. Rev. A* **1988**, *38*, 3098–3100.

[88] Perdew, J. P. *Phys. Rev. B* **1986**, *33*, 8822–8824; erratum: *Phys. Rev. B* **1986**, *34*, 7406.

[89] vanLenthe, E.; Snijders, J. G.; Baerends, E. J. *J. Chem. Phys.* **1996**, *105*, 6505–6516.

[90] van Lenthe, E.; Baerends, E. J.; Snijders, J. G. *J. Chem. Phys.* **1994**, *101*, 9783–9792.

[91] van Lenthe, E.; Ehlers, A.; Baerends, E. J. *J. Chem. Phys.* **1999**, *110*, 8943–8953.

[92] van Lenthe, E.; Baerends, E. J.; Snijders, J. G. *J. Chem. Phys.* **1993**, *99*, 4597–4610.

CHAPTER 3

Silylphosphinidene and Silyldiphosphenido Complexes of Niobium and Molybdenum

Contents

3.1 INTRODUCTION

Twenty years ago, the first terminal phosphinidene complex had yet to be isolated, but over the past 15 years a variety of phosphinidene complexes have been synthesized.[1–3] Terminal phosphinidenes have come to be known in both early transition-metal, high oxidation state complexes[4–11], and in late transition-metal, low-oxidation state complexes.[12,13] In addition, a terminal phosphinidene complex of the actinide uranium and a bridging phosphinidene complex of the lanthanide lutetium are known.[14,15] Nevertheless, the chemistry of phosphinidenes remains underdeveloped relative to the rich chemistry that has emerged for other metal-ligand multiply bonded systems, particularly carbenes and imido ligands.[16]

The potential synthetic utility of terminal phosphinidene complexes was acknowledged even before their first synthesis.[1] Since then, late-metal phosphinidene complexes have demonstrated utility in oxidative phosphinidene transfer reactions,[13] while the early-metal complexes have served to transfer phosphinidenes metathetically in exchange for oxo, imido, or halide ligands.[4,6,9,15,17] Stephan and co-workers have explored the widest scope of substrates for such reactions, using a Zr(IV) complex to transfer the very bulky Mes*P group.[6] These reactions, and those reported by others, are driven by the high oxo-, aza- or halophilicity of early metal fragments. Through such reactions, phosphinidene complexes have served as precursors to a variety of unsaturated phosphorus compounds, especially phosphaalkenes.[4,6,17] Nevertheless, reactions that make use of early-metal phosphinidenes in further syntheses are relatively rare.

In this chapter, metathesis reactions of niobium silylphosphinidenes are explored. In particular, these complexes are shown to undergo O-for-P metathesis reactions with organic isocyanates, carbon dioxide, and a molybdenum terminal phosphorus monoxide complex. The first set of reactions provides syntheses for amino-substituted phosphaalkynes from isocyanates, chemistry that was not accessible from a niobium phosphide anion.[18,19] Metathesis reactions between an anionic niobium terminal phosphide complex, as well as related silylphosphinidenes, and CO_2 have allowed this generally inert molecule to serve as the carbon source for the OCP^- anion, as well as for a siloxy-substituted phosphaalkyne, under mild conditions. Also described are the syntheses and properties of three NbPPO metallacycles. Furthermore, the high oxophilicity of the niobium *tris*-anilide platform, $Nb(N[CH_2{}^tBu]Ar)_3$ (Ar = 3,5-dimethylphenyl), has allowed for the synthesis of a molybdenum diphosphenido complex from a silylphosphinidene and a molybdenum phosphorus monoxide complex. While diphosphenido complexes of mid and late transition metals have been established for some time, this is believed to be the first report of a diphosphenido complex where the ligand serves as a $3e^-$ donor. This unique bonding situation gives rise to chemistry that is very different from that of the $1e^-$ donor complexes.

3.2 Silylphosphinidenes of Niobium Trisanilide

3.2.1 Synthesis and Structure

Figueroa *et al*. first reported the synthesis of the niobium silylphosphinidene $Me_3SiPNb(N[CH_2{}^tBu]Ar)_3$, **32**, in conjunction with the report of the first stannylphosphinidene complex, Me_3Sn-$PNb(N[CH_2{}^tBu]Ar)_3$.[20] These compounds were synthesized by reaction of the corresponding chloro compounds with the nucleophilic terminal phosphide complex $[PNb(N[CH_2{}^tBu]Ar)_3]^-$, **3**. Subsequently, the structure of the silylphosphinidene **32** was determined and revealed a bent phosphinidene with a Nb−P−Si angle of 131.47(3)° and a Nb−P distance of 2.2382(7) Å, Figure 3.1a. Also observed in this structure was the rotation of one anilide ligand perpendicular to the Nb−P vector. This allows the steric bulk of the neopentyl anilide to move away from the trimethylsilyl group while also maximizing π donation by the anilide ligands to the metal. This ligand rotation is likely coupled to the bending at phosphorus, as the related phosphinidene complexes $RPTa[(N(SiMe_3)CH_2CH_2)_3N]$, bearing a chelate that does not allow for ligand rotation, show near linear phosphinidene moieties.[21] Without a rotated amide donor there remains one electrophilic, non-bonding d orbital (d_{xz} or d_{yz}) that the phosphinidene can satisfy through P(pπ)→M(dπ) donation by adopting a linear geometry. This extra donation then results in a very short phosphinidene bond of 2.145(7) Å (for R = Cy) and the strong bonding interaction results in an upfield shift in the ^{31}P NMR resonance relative to related bent phosphinidenes.[4,5,i]

[i]For comparison, the linear phosphinidene $CyPTa[(N(SiMe_3)CH_2CH_2)_3N]$ resonates at 210 ppm, while the bent phosphinidene **32** resonates at 530 ppm.

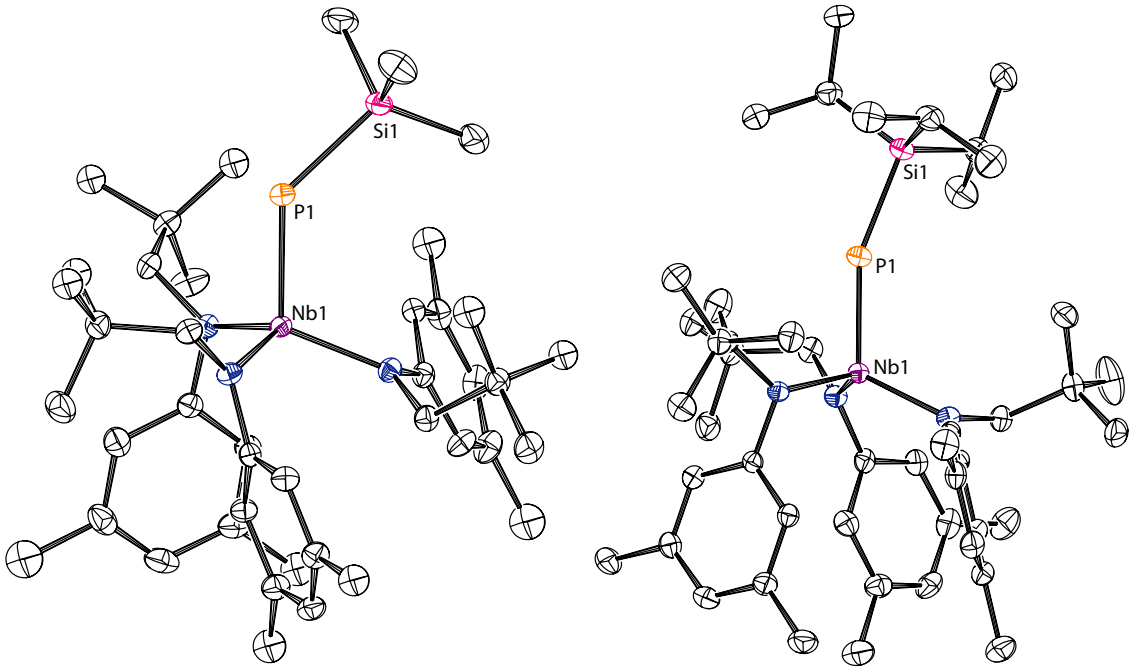

Figure 3.1. Thermal ellipsoid plots (50% probability) of (a) **32** and (b) **33** with hydrogen atoms omitted for clarity.

The tris(*iso*-propyl)silylphosphinidene complex, $^{i}Pr_3SiPNb(N[CH_2{}^{t}Bu]Ar)_3$, **33**, is synthesized from the reaction between $^{i}Pr_3SiOTf$ (OTf^{-} = trifluoromethylsulfonate) and the sodium salt of $[PNb(N[CH_2{}^{t}Bu]Ar)_3]^{-}$. Complex **33** is isolated as an orange solid in 61% yield by crystallization from Et_2O and displays a broad ^{31}P NMR resonance at 433 ppm. This chemical shift is 95 ppm upfield of that of the trimethylsilyl complex, suggestive of a more linear Nb−P−Si angle.[20] A single crystal X-ray diffraction study of this complex again revealed a short Nb−P distance of 2.2454(6) Å and, as expected, a more linear Nb−P−Si angle of 158.34(4)°, Figure 3.1b. The increase in angle is likely due to greater steric constraints and not any significant change in electronics imposed by the silyl group. Again, one rotated ligand is present to maximize π donation to the electrophilic metal center.

3.2.2 P-for-O Metathesis Reactions with Isocyanates and CO_2

The reactions of both terminal and bridging phosphinidene complexes with aldehydes and ketones have been shown in several cases to yield phosphaalkenes, oftentimes with very good E/Z-selectivity.[4,6,11] Less studied has been the the application of phosphinidenes to the synthesis of other low-coordinate phosphorus compounds. Stephan and co-workers report one example of a reaction with phenyl isothiocyanate to generate a phosphaazallene, but this methodology has not been further explored.[6] This is despite the fact that reactions between nucleophilic phosphinidenes

and such electrophilic, chalcogen sources of formula Z=C=E (Z = O, S; E = O, NR, CR_2) might be expected to be relatively facile given the ease with which the electrophilic, cylindrical C=Z bond could insert itself into the metal coordination sphere. When Z = O, a metathetical reaction could then be expected to afford a strong metal-oxo bond and a phosphacumulene of formula RP=C=E.

Stable phosphacumulenes first appeared in the early 1980s with reports of ^{t}BuP=C=N^{t}Bu, Mes*P=C=O, and Mes*P=C=CPh_2 being prepared through syntheses that took advantage of the low P−Si bond strength to drive P=C bond formation by the elimination of strong Si−Cl and Si−O bonds.[22–24] A similar strategy was employed to synthesize the first stable heteroatom-substituted phosphaalkyne.[25] In this reaction, Me_3SiP=C=N^{i}Pr is a proposed intermediate that undergoes a P-to-N silyl migration to afford the product aminophosphaalkyne. Thus the generation of intermediate silylphosphacumulenes from silylphosphinidenes might serve as a route to other heteroatom-substituted phosphaalkynes by taking advantage of the propensity of silyl groups to undergo migration from phosphorus to more electronegative elements.[26]

Generation of Phosphaazallenes and Aminophosphaalkynes

Figueroa showed that niobium phosphide anion **3** adds to mesityl isocyanate at the the isocyanate carbon to yield a metallacycle with the nitrogen uncoordinated to Nb and bearing the negative charge.[19] The nitrogen was then silylated to yield a metallacycle that appears to be a potential precursor to *N*-(trimethylsilyl)-*N*-(mesityl)aminophosphaalkyne. However, thermolysis of this compound yields an unidentified product, Scheme 3.1.[19] As an alternate route to an aminophosphaalkyne, an analogous reaction was investigated wherein niobium phosphide **3** is treated with trimethylsilylchloride and an isocyanate in the opposite order: treatment with trimethylsilylchloride first to afford the silylphosphinidene, followed by investigations of treatments with organic isocyanates.

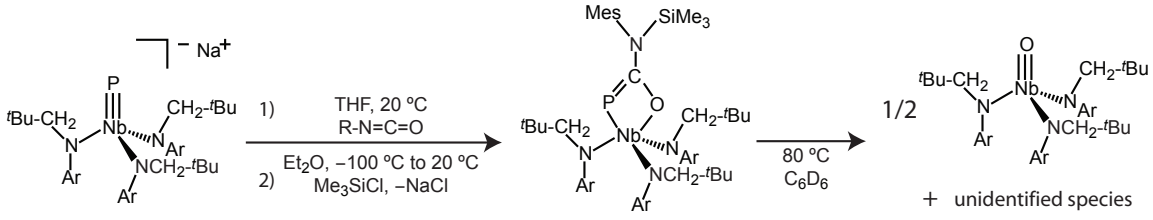

Scheme 3.1. Reaction of mesityl isocyanate with the anionic niobium phosphide **3**, and its subsequent reactivity, as reported by Figueroa.[19]

The niobium trimethylsilylphosphinidene, **32**, reacts slowly with mesityl isocyanate in a metathesis reaction to yield oxoniobium **21** and *P*-(trimethylsilyl)-*N*-(mesityl)phosphaazallene, which is identified by its upfield ^{31}P NMR chemical shift of –263 ppm and IR absorbance frequency of 1927 cm^{-1}. Similar chemical shifts and IR frequencies have been reported for other phosphaazallenes.[22,27,28] This phosphaazallene then diminishes over several hours at 22 °C

as a second product with a chemical shift of –163 ppm grows in. The change in ^{31}P NMR chemical shift and the loss of P-H coupling in the trimethylsilyl ^{1}H NMR resonances is consistent with a P-to-N silyl migration that yields the aminophosphaalkyne, Mes(Me_3Si)NC≡P, as the final product, Scheme 3.2. To support the identification of intermediates and products, a known aminophosphaalkyne was prepared by this method. The chemistry described above proceeds analogously for isopropyl isocyanate: a phosphaazallene with chemical shift of –242 ppm is formed and then this intermediate slowly isomerizes to the aminophosphaalkyne, ^{i}Pr(Me_3Si)NC≡P, the latter of which has been independently reported.[25,28]

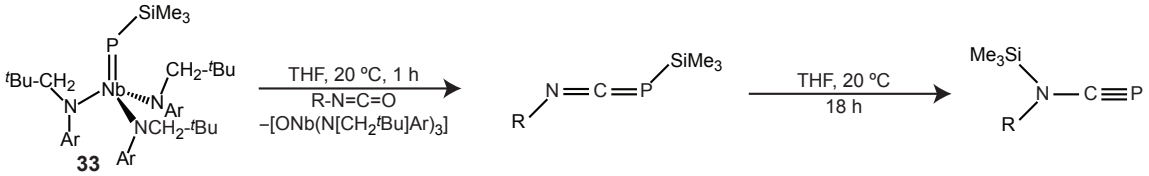

Scheme 3.2. Generation of R(Me_3Si)NCP (R = Mes, ^{i}Pr) from isocyanates and the niobium silylphosphinidene **32**.

Synthesis of NaOCP and $^{i}Pr_3SiOCP$

The reactivity that was observed for isocyanates prompted an investigation of reactions with the isoelectronic molecule CO_2, perhaps the most desirable of carbon feedstocks.[29] The reaction between niobium phosphide anion **3** and CO_2 would yield the OCP^- anion, while the reaction between CO_2 and a silylphosphinidene would make a siloxyphosphaketene, or following silyl migration, an oxyphosphaalkyne.[ii] Indeed, introduction of carbon dioxide to an orange solution of niobium phosphide **3** in benzene results in a rapid color change to yellow, concomitant with the formation of a precipitate. The soluble product was confirmed by NMR spectroscopy to be the oxoniobium complex **21**. If instead THF is used as a solvent, all products remain in solution and the phosphorus containing product could be located in the ^{31}P NMR spectrum as a sharp singlet at –393 ppm. This species has a strong absorbance in the IR at 1756 cm^{-1}, as well as a ^{13}C chemical shift (δ = 169 ppm, $^{1}J_{CP}$ = 52 Hz) that confirm it as the OCP^- anion.[30–32] The NaOCP salt was isolated by precipitation as a gray powder.

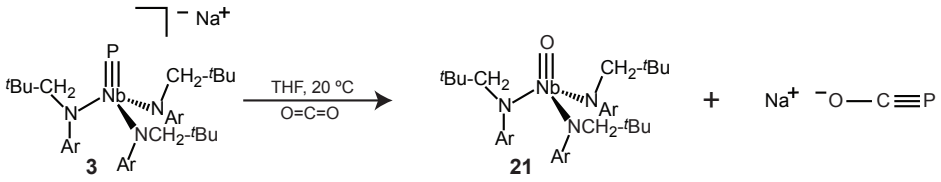

Scheme 3.3. Synthesis of NaOCP from CO_2 and the niobium phosphide anion **3**.

[ii] It is worth noting that certain phosphinidene complexes are themselves synthesized from a stable phosphaketene.[12]

If the trimethylsilylphosphinidene **32** is used in place of the phosphide anion **3**, the reaction proceeds more slowly and an intermediate can be observed before oxoniobium formation. Based on the relative sharpness of the ^{31}P NMR signal at –307 ppm, it is expected that phosphorus is not bound to niobium in this observed intermediate, and it is believed to be the κ^2-bound O_2CPR complex depicted in Scheme 3.4. The upfield chemical shift for this species is unusual for a traditional phosphaalkene, but not unreasonable given the relatively upfield shift (–10 ppm) reported for $Cp_2Zr(\kappa^2$-CyNC(=PR)NCy) and the potential effect of the electron-rich silyl group.[6] In any case, this intermediate could not be isolated, as it proceeds on to form oxoniobium **21** at a rate comparable to that at which it is produced. The co-product of this reaction, either silylphosphaketene or the siloxyphosphaalkyne, appears unstable with respect to oligomerization since no phosphorus-containing products can be located by NMR in the final product mixture. This is a common mode of degradation for low-coordinate phosphorus species that lack sufficient electronic or steric stabilization.[33–35] The bulkier $^{i}Pr_3SiOCP$ is less prone to degradation, even allowing for detailed NMR studies.[36] Accordingly, the reaction of the niobium phosphinidene **33** with CO_2 proceeds over several hours to afford oxoniobium **21** and the siloxyphosphaalkyne as the only products observed by NMR spectroscopy. The identity of the phosphaalkyne was confirmed by its diagnostic upfield ^{31}P NMR chemical shift of –396 ppm.[36] No intermediates are observed in this reaction, likely because the approach of CO_2 to the more hindered metal center is rate-limiting.

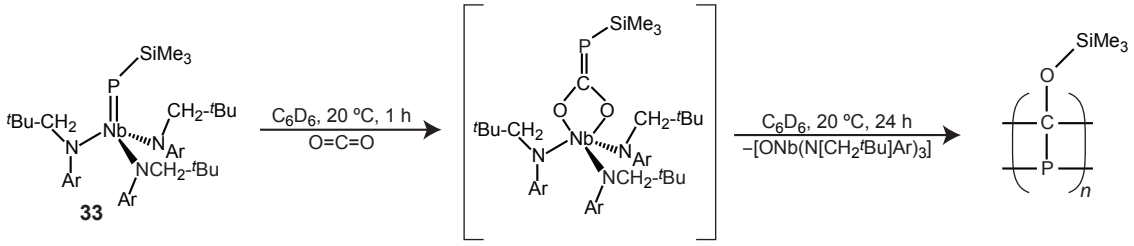

Scheme 3.4. The reaction of silylphosphinidene **32** with CO_2 proceeds through an intermediate, tentatively assigned as a metallacycle with an exocyclic phosphaalkene, and onto oxoniobium **21** and a phosphorus product believed to be polymeric Me_3SiOCP.

The breaking of a C=O bond of CO_2 demonstrated here is another manifestation of the high degree of oxophilicity possessed by the niobium trisanilide fragment, $Nb(N[CH_2{}^tBu]Ar)_3$, and how this fact can be exploited for the synthesis of multiple bonds to phosphorus.

3.3 METALLACYCLIC PHOSPHORYLPHOSPHINIDENE COMPLEXES

In the niobium-mediated syntheses of phosphaalkynes developed by Figueroa, isolable, meta-stable NbPCO metallacycles serve as intermediates.[18] Upon heating, these metallacycles fragment to afford oxoniobium **21** and a phosphaalkyne in a process that is driven by the high bond energy of the Nb≡O bond. In Chapter 1, a NbPPN metallacycle is proposed to precede P_2 elimination from

a diphosphaazide complex. This demonstrated ability of niobium to form metallacycles that can then release multiply-bonded small molecules prompted investigation of other such metallacycles. The generation of NbPPO metallacycles from phosphinic or phosphoryl chlorides and niobium phosphide was one such investigation.

3.3.1 Synthesis and Structure

The reaction of niobium phosphide **3** with diphenylphosphoryl chloride at low temperature proceeds smoothly to give a single product, **34**, which could be isolated as an orange powder by precipitation from hexamethyldisiloxane, Scheme 3.5. The ^{31}P NMR spectrum of **34** displays two sets of doublets—one broad (due to Nb, $I = \frac{9}{2}$) at 173 ppm, and one sharp at 73 ppm—with a large coupling constant, $^{1}J_{PP}$ = 595 Hz. This large coupling supports the structural assignment of a metallacycle that has significant P−P multiple bonding.

This methodology was expanded to synthesize a variety of such complexes, varying only in the substituents at the β phosphorus. Reactions of $Ph_2P(O)Cl$ and $(Me_2N)_2P(O)Cl$ with **3** proceeded as discussed for $(PhO)_2P(O)Cl$ to give the corresponding metallacycles, Scheme 3.5. The ^{31}P NMR spectra of these complexes are very similar to that of **34**, but with slightly smaller coupling constants: 480 Hz for both R = NMe_2 and R = Ph. The metallacycle complex with dimethylamino substituents, **35**, is particularly attractive because it is highly crystalline; correspondingly, an X-ray structure of this complex was obtained, Figure 3.2. This analysis revealed a *pseudo* trigonal bipyramidal structure with the phosphinidene-like phosphorus and two anilides in the equatorial plane. This positioning of the phosphinidene allows maximal π interactions with the metal center. The distances around the metallacycle ring are: Nb−P, 2.4509(5) Å; P−P, 2.0900(7) Å; P−O, 1.5481(14) Å; and Nb−O, 2.1597(13) Å. These distances reflect the bonding shown in the second resonance structure of Scheme 3.5, with a relatively long Nb−P and a short P−P bond. Single-crystals were also grown of the phenoxy substituted metallacycle **34** and one such crystal was subjected to an X-ray diffraction study, Figure 3.3. The structure is very similar to the dimethylamino relative and shows an even shorter P=P bond (2.054 Å, average of two independent molecules) that is consistent with the even larger ^{31}P-^{31}P coupling constant measured for **34**.

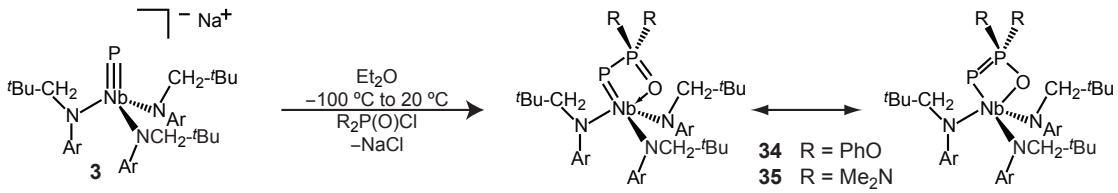

Scheme 3.5. Synthesis of the metallacyclic phosphinidene complexes $R_2P(O)PNb(N[CH_2{}^tBu]Ar)_3$ (R = PhO, Me_2N, Ph).

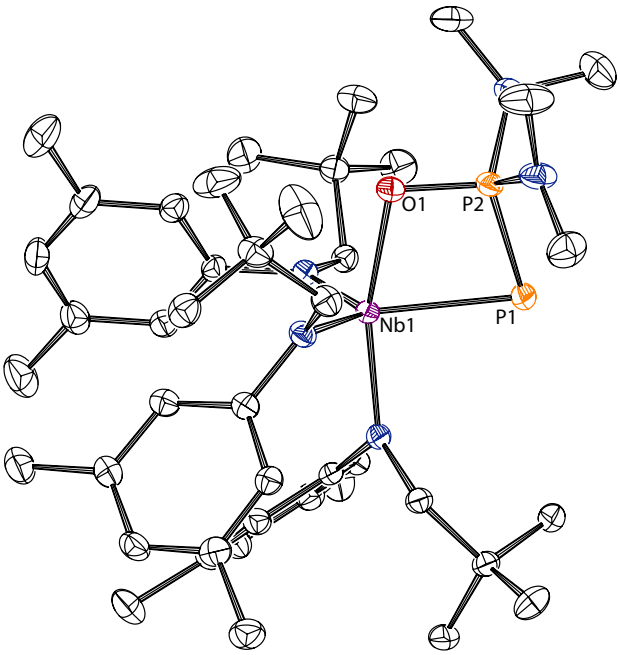

Figure 3.2. Thermal ellipsoid plot (50% probability) of **35** with hydrogen atoms omitted for clarity.

Thermolysis of these metallacycles at temperatures up to 90 °C proceeds only slowly over the course of days to afford oxoniobium **21**, and the fate of the phosphorus atoms could not be ascertained. It is believed that R-group migration is involved in the elimination reaction, but the high temperatures, slow reactions, and intractable products have prevented detailed studies.

3.3.2 Opening of a Metallacycle with $AlCl_3$

The reluctance of **34** and related species to eliminate phosphanylphosphinidenes or diphosphenes cleanly upon thermolysis prompted attempts to remove the substituents from the β phosphorus. It was expected that the resulting species, a metal complex of the molecule P_2O, would not only provide a direct analogue of the NbPCO metallacycles of Figueroa, but could also serve as an alternate method to that described in Chapter 1 for generating the P_2 molecule. As one potential route to such a complex, reactions to substitute the phenoxy and dimethylamino substituents of **34** and **35** with more easily removed chlorine atoms were attempted. Such an approach is necessary as reactions between the niobium phosphide **3** and $OPCl_3$ afford $Cl_2Nb(N[CH_2{}^tBu]Ar)_3$ as the major product, and no evidence for the desired $OP(Cl)_2PNb(N[CH_2{}^tBu]Ar)_3$ is observed.

Reactions between **34** and **35** and a variety of halogenating agents—such as PCl_3, PCl_5, $AlCl_3$, and Me_3SiCl—were screened, but no selective removal of the PhO or Me_2N groups was observed. Most reactions gave $Cl_2Nb(N[CH_2{}^tBu]Ar)_3$ as the major product. The reaction of **35** with 1 equivalent of the potent Lewis acid $AlCl_3$, however, was selective for one new major product, **36**, a bright red-orange powder that was isolated from *n*-hexane in 83% yield. This product displays

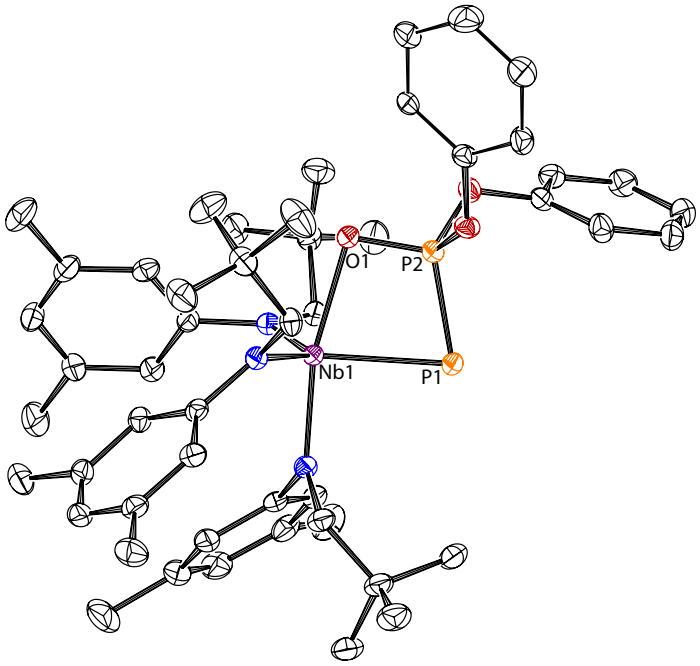

Figure 3.3. Thermal ellipsoid plot (50% probability) of **34** with hydrogen atoms omitted for clarity.

a downfield shift for the broadened phosphorus resonance at 421 ppm, suggesting a disruption of the metallacycle to give a more "phosphinidene-like" functional group, Scheme 3.6. Indeed, characterization of this product by single-crystal X-ray diffraction revealed an opened metallacycle where $AlCl_3$ replaces Nb as the Lewis acid bound to the phosphoryl oxygen atom, Figure 3.4. This change in structure results in stronger Nb–P π bonding that is reflected in a shortening of the Nb−P distance to 2.3580(8) Å and a lengthening of the P−P bond to 2.1346(11) Å.

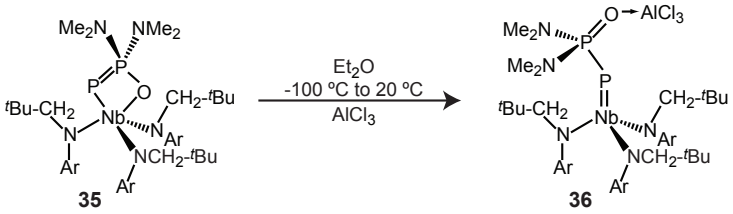

Scheme 3.6. Opening of the metallacyclic phosphinidene complex **35** with $AlCl_3$.

3.3.3 Bonding Analysis by DFT

The ability to open the metallacycle by addition of an external Lewis acid allows a direct measurement of the effect of the metallacycle geometry on electronic organization. The large difference in ^{31}P NMR chemical shifts of the open and closed metallacycles suggests significant differences in bonding through the Nb−P−P−O system between the two structures.

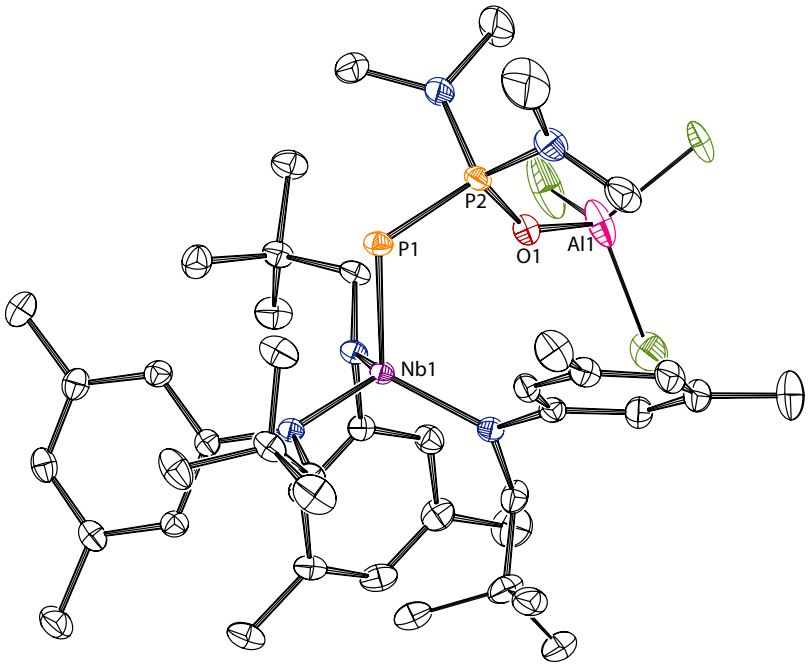

Figure 3.4. Thermal ellipsoid plot (50% probability) of **36** with hydrogen atoms omitted for clarity.

This prompted a computational study on model complexes $(H_2N)_2P(O)PNb(N[Me]Ph)_3$ and $(H_2N)_2P(OAlCl_3)PNb(N[Me]Ph)_3$. In addition to optimizing structures, bond multiplicities were calculated by the Nalewajski-Mrozek method using the ADF package.[37] This method for calculating bond multiplicity has recently been shown to correlate well with chemical intuition and measurable quantities, as well as to be relatively independent of the basis set used for the calculations.[38] Optimized internuclear distances for the open and closed structures, as well as the calculated values for relevant bond multiplicities are presented in Table 3.2.

These molecules were also considered through the Atoms in Molecules (AIM) approach developed by Bader.[39] Under this approach, it is the physical quantity of electron density, and the topology of this quantity, that are considered in analysis of bonding. Between each pair of bonded atoms there should lie a bond critical point, a saddle point in the electron density from which the density increases along the bond path and decreases in the perpendicular directions. The value of the electron density at this point correlates with the strength of the bonding interaction, while the ellipticity at the point (a measure of the difference between the rates of decrease in electron density in the directions perpendicular to the bond path) correlates with differences in π bonding in the two planes.

Bond critical points were located along each of the Nb−P, P−P, P−O, and O−M bond paths and the values of the electron density and the ellipticities at these points are included in Table 3.2. Together with the bond multiplicity values, these data provide a picture of the reorganization of electrons between the closed (κ^2) and open (κ^1) forms of the PPO ligand. In the open form, the Nb−P bonding interaction is increased by all measures and the P−P bonding interaction is

Table 3.1. Bonding Analysis of Open and Closed NbPPO Metallacycles **35** and **36**

	Nb−P			P−P		
	r^a	ρ_{cp} $(\varepsilon)^b$	B.M.^{c}	r^a	ρ_{cp} $(\varepsilon)^b$	B.M.^{c}
Closed	2.48 Å	0.0852 (0.23)	1.295	2.09 Å	0.1325 (0.08)	1.146
Open	2.39 Å	0.0969 (0.29)	1.538	2.12 Å	0.1274 (0.05)	1.011
	P−O			O−M		
	r^a	ρ_{cp} $(\varepsilon)^b$	B.M.^{c}	r^a	ρ_{cp} $(\varepsilon)^b$	B.M.^{c}
Closed	1.57 Å	0.2053 (0.01)	1.234	2.19 Å	0.0770 (0.06)	0.610
Open	1.59 Å	0.1931 (0.01)	1.134	1.83 Å	0.0787 (0.03)	0.706

[a] Internuclear distance. [b] Electron density at the bond critical point in e/a_0^3; ellipticities at the bond critical point are in parentheses. [c] Nalewajski-Mrozek bond multiplicities.[38]

decreased, as compared to the closed form. These changes originate from a reorganization of the π system and support the different bonding depictions drawn for **34** and **35** compared to **36** in Schemes 3.5 and 3.6.

3.4 A Molybdenum Diphosphenido Complex

First reported in 1997 by Johnson *et al.*, the complex OPMo(N[^{t}Bu]Ar)$_3$, **37**, remains the only example of an isolable terminal phosphorus monoxide complex.[40] As a result, the chemistry of this unique functional group has remained largely unexplored. Initial reactivity studies by Johnson showed that **37** reacts with Cp_2ZrMe_2 to afford $Cp_2MeZrOP(Me)Mo(N[^tBu]Ar)_3$.[40] This result indicates that **37** behaves as an electrophile at phosphorus and a nucleophile at oxygen, properties that would assist in the formation of a P−P multiple bond through reaction with a suitable phospha-Wittig reagent. The product of such a reaction would be a diphosphenido ligand complexed atop the molybdenum trisanilide platform.

Diphosphenido ligands are known principally on $Cp^*(CO)_nM$ platforms.[41–46] The synthetic approaches to these complexes include Me_3SiCl elimination from the combination of $Cp^*(CO)_2M-P(SiMe_3)_2$ and $ArPCl_2$, as well as the insertion of metal carbonyl fragments into the Cp^*-P bond of $Cp^*P{=}PAr$.[42,45] The resulting complexes are the equivalent of metallodiphosphenes—they are bent at each phosphorus and best described as having a single M−P bond and a double P−P bond. These ligands are analogous to $1e^-$ donating diazenido ligands that adopt a singly bent structure, in contrast to the more ubiquitous $3e^-$ donating diazenido ligand.[47] This latter class includes the complex $Me_3SiNNMo(N[^tBu]Ar)_3$.[48] Thus the synthesis of a diphosphenido complex atop this same metal platform might provide access to a unique, $3e^-$ donor diphosphenide ligand.

Moreover, the analogous complex $Me_3SiNNMo(N[^tBu]Ar)_3$ can be deprotected with NaOMe to yield $[(N_2)Mo(N[^tBu]Ar)_3]^-$.[49] If a similar deprotection strategy could be developed for the diphosphenido species, a rare example of a monometallic P_2 complex could be achieved. Such complexes were not accessible by the P_2 trapping chemistry described in previous chapters, and the closest such example in the literature is provided by Stephan and co-workers, who characterized by NMR spectroscopy a complex of an η^2-P_2^{2-} ligand that is supported by Cp^*_2Zr and two K^+ ions.[50]

3.4.1 Generation and Characterization of $^iPr_3SiPPMo(N[^tBu]Ar)_3$

Complex **33** reacts with the purple phosphorus monoxide complex **37** over the course of several minutes at 22 °C to afford the oxoniobium complex **21** and one new species, **38**, which was identified by ^{31}P, ^1H, and ^{13}C NMR spectroscopies, Scheme 3.7. The ^{31}P NMR signals for **38** are a very broad doublet at 543 ppm and a less broad doublet at 158 ppm with a large P−P coupling constant, $^1J_{PP}$ = 655 Hz. These data are consistent with the desired silyldiphosphenido product, $^iPr_3SiPPMo(N[^tBu]Ar)_3$, where the downfield resonance is attributed to the phosphorus atom bound directly to the Mo center. This NMR assignment was corroborated by DFT calculations on the relative chemical shieldings for the two ^{31}P nuclei (*vide infra*). Unfortunately, due to similar solubility properties of oxoniobium **21** and diphosphenido **38**, it has not been possible to isolate significant quantities of pure **38**.[iii]

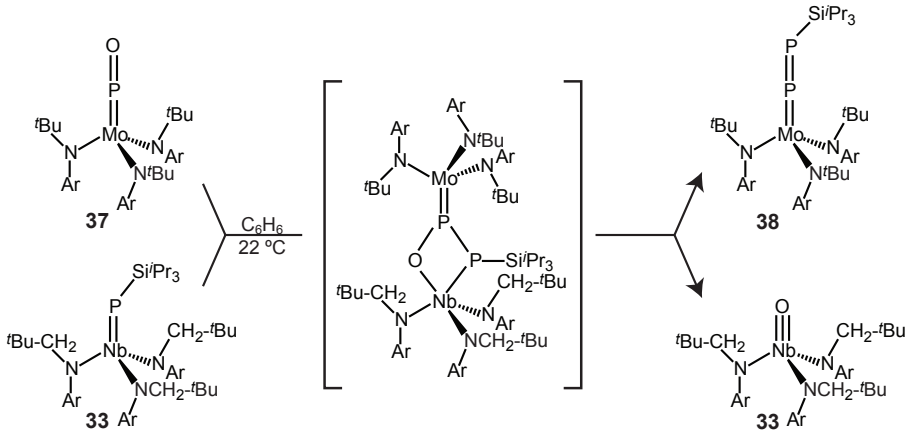

Scheme 3.7. Generation of ($^iPr_3SiPPMo(N[^tBu]Ar)_3$ (**38**) by an O-for-$PSiR_3$ metathesis reaction through a proposed (unobserved) intermediate.

A red-orange single-crystal grown from an Et_2O solution of the product mixture that contained **38** was subjected to an X-ray diffraction study to reveal the structure of the diphosphenido complex, Figure 3.5. The geometry is best described as "singly bent," with angles at P1 and P2 of

[iii] Prior work suggested that conversion of oxoniobium **21** to the less soluble bis(triflate) complex, $(TfO)_2Nb(N[CH_2{}^tBu]Ar)_3$, by treatment with Tf_2O could aid in separation.[51] However, the diphosphenido **38** reacts competitively with **21** to consume triflic anhydride and results in a mixture of products including $TfOMo(N[^tBu]Ar)_3$.

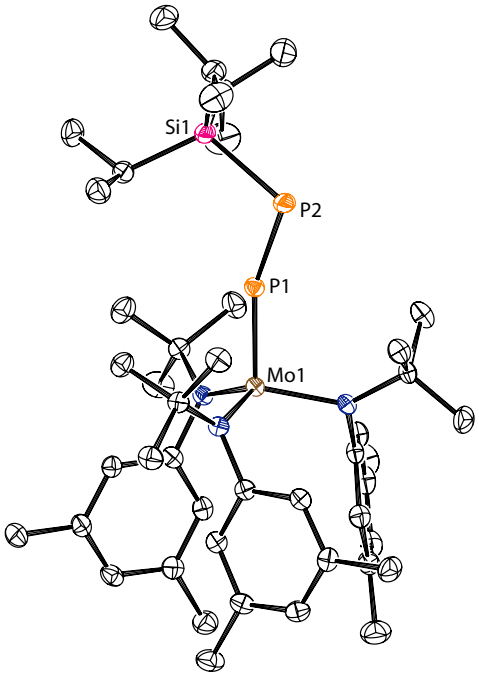

Figure 3.5. Thermal ellipsoid plot (50% probability) of **38** with hydrogen atoms omitted for clarity.

158.27(3)° and 104.46(3)°, respectively. The Mo−P and P−P distances, 2.1439(5) and 2.0398(7) Å, respectively, are both very short, and indicate multiple bonding across the Mo−P−P π system. These metric parameters are in contrast to the few known diphosphenido complexes,[44,45] which are best described as "doubly bent", with angles at both phosphorus being approximately 110° and their metal-phosphorus single bonds reflected in longer M−P distances.

3.4.2 DFT Studies on $Me_3SiPPMo(N[^tBu]Ar)_3$

To analyze the bonding in **38**, a DFT study was carried out on the slightly truncated complex $Me_3SiPPMo(N[^tBu]Ar)_3$, **38m**, using the ADF package.[37,52] The geometry optimization converged on a structure similar to that determined by X-ray crystallography, with a nearly linear Mo−P−P angle (163°) and a bent P−P−Si angle (106°), as well as short Mo−P and P−P distances of 2.145 Å and 2.059 Å, respectively. Moreover, the calculated chemical shift values of 497 and 195 ppm for the phosphorus atoms bound molybdenum and silicon, respectively, are in good agreement with the experimental values. An examination of the frontier orbitals, Figure 3.6, reveals that the HOMO and HOMO–1 of **38m** contain large contributions from the out-of-plane and in-plane p orbitals on the β phosphorus, respectively. The HOMO can be considered as a back-bond from a reducing, formally d^2 metal center to the strongly π-accepting diphosphenido ligand. Conversely, the HOMO–1 is formally the ligand-to-metal π donation. These orbitals are reminiscent of those observed for ketimide complexes of the same molybdenum fragment, which are nucleophilic at the β carbon.[53,54]

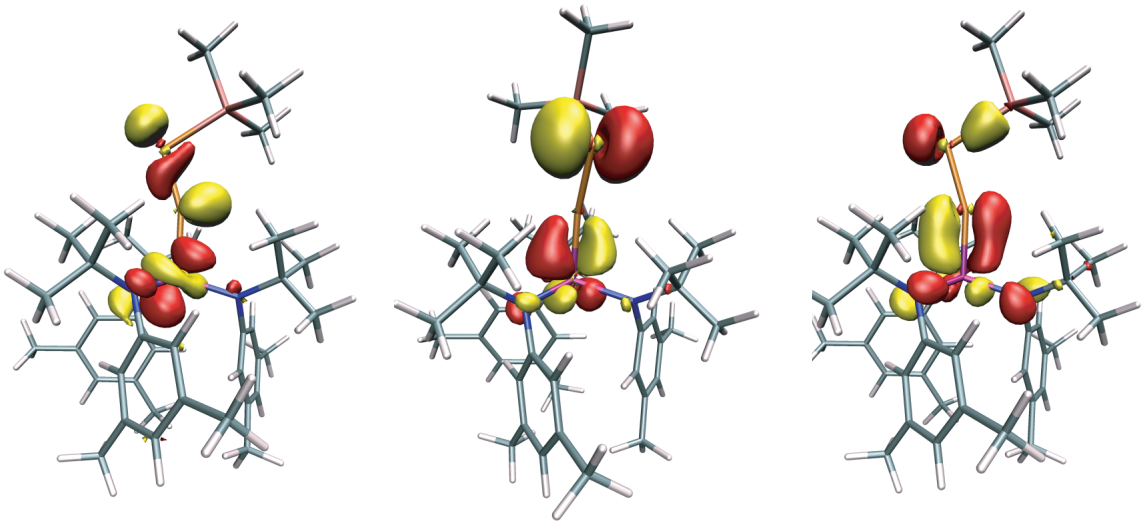

Figure 3.6. Frontier molecular orbitals of the molybdenum silyldiphosphenido complex **38m**.

The LUMO of **38m** is d_{z^2}-like at the metal, but also contains lobes on both the α and β phosphorus atoms, and appears partially P−P σ antibonding in character.

In light of the very short Mo−P and P−P bond distances in **38**, and the unique nature of this complex as containing a $3e^-$ diphosphenide ligand, the bonding was further analyzed through bond multiplicity calculations and an AIM analysis. The bonding in **38m** was compared to that in PMo(N[^{t}Bu]Ar)$_3$ and OPMo(N[^{t}Bu]Ar)$_3$, as well as to that in parent diphosphene (HP=PH) and a prototypical late-metal diphosphenido complex, Cp*(CO)$_2$FePPMe. These data indicate that the description of Cp*(CO)$_2$FePPMe as a metallodiphosphene is appropriate, as the P=P bond remains largely undisturbed relative to parent diphosphene, and the extent of Fe−P bonding is consistent with a single σ bond. The molybdenum diphosphenido complex, on the other hand, shows significantly different bonding. The extent of P−P bonding is decreased relative to diphosphene, while the M−P bonding is significantly increased. In fact, the value of ρ_{cp} along the Mo–P bond is similar to the value for the triply bonded terminal phosphide complex. The values of bond multiplicity also suggest that the best Lewis structure for **38** is one that includes both Mo=P and P=P double bonds, with contributions from a structure with Mo≡P triple bonding and P−P single bonding. These calculated data, Table 3.2, also confirm the unique nature of **38** as containing a $3e^-$ diphosphenido ligand.

3.4.3 Phosphinidene Transfer Pathways for ^{i}Pr$_3$SiPPMo(N[^{t}Bu]Ar)$_3$

Unlike nitrogen analogues of **38**, such as the silyldiazenido complex Me$_3$SiNNMo(N[^{t}Bu]Ar)$_3$ and the azaphosphenido complex MesNPMo(N[^{t}Bu]Ar)$_3$, the diphosphenido complex **38** is not stable in solution for extended periods of time.[48,56] Over the course of hours to days, or upon heating,

Table 3.2. Bonding Properties of Mo−P and P−P Containing Molecules[a]

			Bond Multiplicity			
	Bond	Length[b]	2-Center[c]	Total[d]	ρ_{cp}[e]	Ellipticity[f]
$PMoL_3$	Mo−P	2.1234	2.4759	2.5300	0.1459	0.01
$OPMoL_3$	Mo−P	2.1130	1.8551	1.6791	0.1157	0.03
	P−O	1.4934	1.5006	1.8646	0.2289	0.00
	Mo−O	3.6064	0.4019	0.5403	–	–
$Me_3SiPPMoL_3$	Mo−P	2.1490	1.8555	1.7629	0.1224	0.19
	P−P	2.0633	1.4139	1.5436	0.1280	0.23
	Mo−P_β	4.1634	0.4025	0.4476	–	–
$MePPFeCp^*(CO)_2$	Fe−P	2.2861	0.7249	0.8481	0.0852	0.06
	P−P	2.054	1.8585	2.0469	0.1431	0.31
HPPH	P−P	2.0396	2.0544	2.3177	0.1459	0.33

[a] L = N[^{t}Bu]Ar; Cp^* = Me_5C_5. [b] Internuclear distance in Å. [c] Bond multiplicity corresponding to the Gophinatan-Jug bond order.[38,55] [d] Nalewajski-Mrozek bond multiplicities based on Tr[**P**Δ**P**].[38] [e] Electron density at the bond critical point in e/a_0^3. [f] Ellipticity at the bond critical point.[39]

complex **38** reacts to form PMo(N[^{t}Bu]Ar)$_3$ (**39**), the cyclic phosphinidene trimer (^{i}Pr$_3$SiP)$_3$ (**40**), and the phosphinidene tetramer (^{i}Pr$_3$Si)$_2$P$_3$P(Si^{i}Pr$_3$)$_2$ (**41**); the latter two compounds were identified by their diagnostic ^{31}P NMR features and their second-order spectra were successfully simulated, Figures 3.7–3.8 and Table 3.3.[57,58] The spontaneous formation of three-membered phosphinidene rings is not unusual, as the ring strain for such species is significantly lower than in the corresponding hydrocarbons.[59,60]

Attempts to make analogues of **38** bearing smaller silyl groups (*e.g.*, Me$_3$Si, Ph$_3$Si) led to rapid formation of the corresponding phosphinidene trimers at 20 °C, such that the corresponding diphosphenido complexes were not observed. Also, the generation of **39** from **38** was observed to proceed more rapidly in concentrated solutions than in dilute solutions. Together, these observations suggest the following proposed mechanism: a bimolecular reaction between 2 equivalents of **38** generates 2 equivalents of the terminal phosphide complex **39** and 1 equivalent of ^{i}Pr$_3$SiP=PSi^{i}Pr$_3$ (**42**); this reactive diphosphene then consumes a third equivalent of **38** to yield the cyclic trimer **40**. The tetrameric product **41** can then arise from an insertion of the phosphinidene unit of **38** into a P−Si bond of trimer **40**, Scheme 3.8. This last step is supported by the qualitative observation that the ratio of **41** to **40** grows with time as the concentration of **40** increases. Unfortunately, attempts at quantitative kinetic measurements of this reaction were complicated by these many competitive PSi^{i}Pr$_3$ transfer pathways.

Inspection of the molecular orbitals described above and depicted in Figure 3.6 reveals contributions from the β phosphorus to both the HOMO and LUMO, a property suggestive of ambiphilic character that provides an explanation for the observed bimolecular reaction to form **42**. This behavior is in contrast to the doubly-bent diphosphenido complexes of late metals, where the chemistry is dominated by addition of various electrophilic reagents to the lone pair of the α phosphorus.[42,43,46]

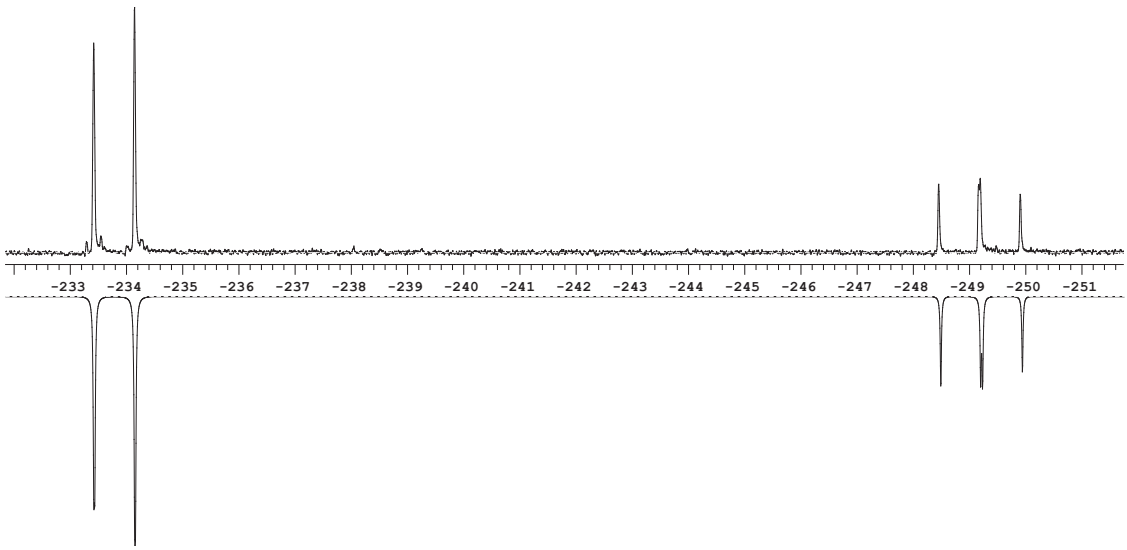

Figure 3.7. Experimental (C_6D_6, 202 MHz, 20 °C) and simulated (reflected) ^{31}P NMR spectra of $(^{i}Pr_3SiP)_3$. The AB_2 pattern was simulated with: δ_A = –249.2 ppm; δ_B = –233.8 ppm; J_{AB} = –147 Hz.

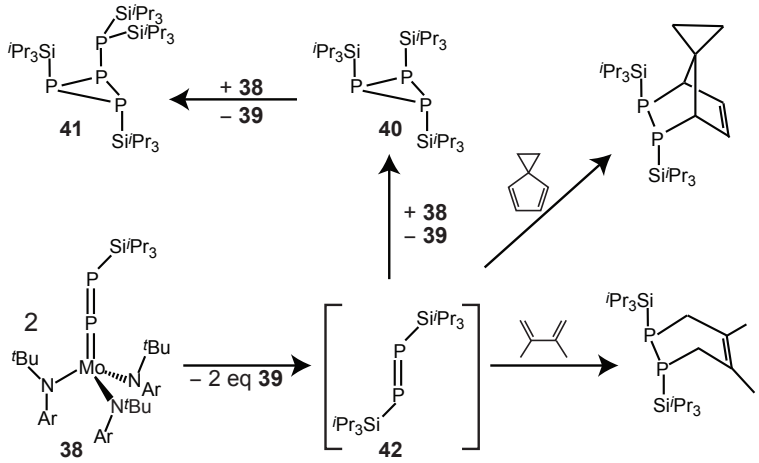

Scheme 3.8. Phosphinidene transfer pathways of **38** that account for the formation of the trimeric and tetrameric phosphinidene products, as well as the products of diphosphene capture by dienes.

3.4.4 Trapping Reactions of $^{i}Pr_3SiPPSi^{i}Pr_3$

Having invoked an intermediate diphosphene in the degradation pathway of **38**, trapping experiments to probe the intermediacy of such a species were carried out.[61] Accordingly, complex **38** was warmed to 60 °C in a THF solution of spiro[2.4]hepta-4,6-diene and the product mixture was assayed by ^{31}P NMR spectroscopy. The $[2+4]$ cycloaddition product of *E*-diphosphene capture by the organic diene was observed as a pair of doublets in the ^{31}P NMR spectrum at –112.5 and –117.5 ppm ($^{1}J_{PP}$ = 240 Hz). Such a pattern is expected, as upon cycloaddition an

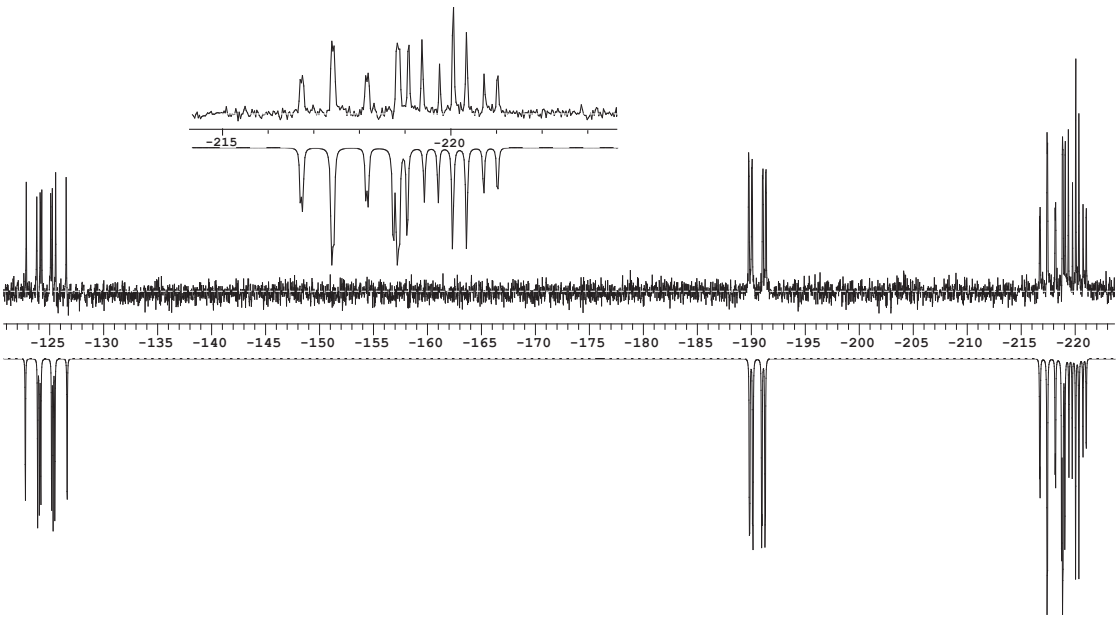

Figure 3.8. Experimental (C_6D_6, 202 MHz, 20 °C) and simulated (reflected) ^{31}P NMR spectra of $(^{i}Pr_3Si)_2P_3P(Si^{i}Pr)_2$, with the most upfield resonance also inset; parameters for the simulation are listed in Table 3.3.

Table 3.3. ^{31}P NMR Data for the Phosphinidene Tetramer **41**.

		Chemical Shifts, δ^a	Coupling Constants, $\lvert J\rvert^b$		
			P^4	P^3	P^2
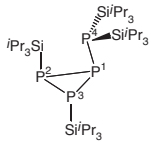	P^1	−124.7	230	262	292
	P^2	−217.9	8	137	–
	P^3	−219.8	63	–	–
	P^4	−190.6	–	–	–

[a] Chemical shifts in ppm. [b] Coupling constant magnitudes in Hz.

E-diphosphene would yield a *trans* disposition of silyl groups to give a C_1-symmetric product. When the experiment was repeated using 2,3-dimethylbutadiene, the now C_2-symmetric product displayed a single ^{31}P resonance at –138 ppm. This chemical shift compares well with those of the products obtained from the reaction of 2,3-dimethylbutadiene with the very bulky silyldiphosphenes $^{t}Bu_3SiPPSi^{t}Bu_3$ (–145 ppm) and $(Me_3Si)_3SiPPSi(SiMe_3)_3$ (–137 ppm).[62,63] The formation of these two species is consistent with the mechanism proposed above, Scheme 3.8. It is noteworthy that free phosphinidenes, as well as singlet phosphinidene complexes, are known to react with dienes via $[4+1]$ and $[4+2]$ cycloadditions to give phospholenes and phosphirenes, none of which are observed in the above reaction mixtures.[64–67] This suggests that phosphinidene ejection is not occurring and is consistent with bimolecular formation of diphosphene **42**.

3.4.5 Equilibrium Transfer of $^{i}Pr_3SiP$ Phosphinidene to PPh_3

The diphosphenido complex **38** was also found to engage in *reversible* phosphinidene transfer reactions with PPh_3 to form an equilibrium mixture of **38**, **39**, $^{i}Pr_3SiP{=}PPh_3$ and PPh_3. The phosphoranylidene phosphorane $^{i}Pr_3SiP{=}PPh_3$ was identified by its ^{31}P NMR spectrum, which exhibits two sharp doublets at 30.5 and –263.8 ppm ($^{1}J_{PP}$ = 590 Hz). The upfield shift of the phosphoranylidene phosphorus is comparable to other phosphoranylidene complexes, and the phosphine resonance is in line with phosphinidene adducts of PPh_3.[34,68] By varying the concentration of **39** and PPh_3, the equilibrium constant for this reaction was measured by ^{1}H NMR spectroscopy as K_{eq} = 0.67(3). This value near to unity was initially surprising, but a comparison of the relative energies of DFT optimized model complexes revealed a very small ΔE = 1.5 kcal/mol for the reaction $PPh_3 + Me_3SiP{=}PMo(N[^{t}Bu]Ar)_3 \rightleftharpoons Me_3SiP{=}PPh_3 + PMo(N[^{t}Bu]Ar)_3$. This equilibrium reaction demonstrates that **38** is susceptible to nucleophilic attack at its β phosphorus, resulting in transfer of the phosphinidene with the triply-bonded molybdenum terminal phosphide serving as a leaving group. In this sense, the reaction between **38** and PPh_3 serves as a model for the bimolecular reaction that forms diphosphene **42**.

3.5 Conclusions

Herein O-for-$PSiR_3$ metathesis reactions of niobium silylphosphinidenes with isocyanates, carbon dioxide, and a terminal phosphorus monoxide ligand have been described. This chemistry has led to the generation of heteroatom-substituted phosphaalkynes, including the OCP^{-} anion. Also, the synthesis of NbPPO metallacycles and their electronic properties have been studied. Moreover, a molybdenum diphosphenido complex, **38**, was arrived at via a metathesis reaction on a terminal PO complex, $OPMo(N[^{t}Bu]Ar)_3$. This diphosphenido ligand serves as a $3e^{-}$ donor, and its reactivity is distinct from previous examples of diphosphenido complexes that are $1e^{-}$ donors and nucleophilic at the α phosphorus. The very reducing nature of the molybdenum trisanilide platform, with its strong $2e^{-}$ backbond, encourages phosphinidene transfer reactions to cleave the P−P bond with terminal phosphide complex **39** serving as a stable leaving group. These facile phosphinidene transfer reactions have prevented a silyl deprotection of **38** to afford a monometallic P_2 complex, but are themselves interesting and may yet provide a useful source of silylphosphinidenes.

3.6 Experimental Details

3.6.1 General Considerations

All manipulations were performed in a Vacuum Atmospheres model MO-40M glove box under an atmosphere of purified dinitrogen. Solvents were obtained anhydrous and oxygen-free

from a Contour Glass Solvent Purification System, or by analogous methods.[69] Deuterated solvents for NMR spectroscopy were purchased from Cambridge Isotope Labs. Benzene-d_6 was degassed and stored over molecular sieves for at least 2 days prior to use. Celite 435 (EM Science), 4 Å molecular sieves (Aldrich), and alumina (EM Science) were dried by heating at 200 °C under dynamic vacuum for at least 24 hours prior to use. The complex $[(Et_2O)Na][PNb(N[CH_2{}^tBu]Ar)_3]$ was prepared by a modified literature procedure presented in Appendix A.[18] The compounds $Me_3SiPNb(N[CH_2{}^tBu]Ar)_3$,[20] $OPMo(N[{}^tBu]Ar)_3$,[40] and spiro[2.4]hepta-4,6-diene[70] were prepared according to literature methods. Isocyanates (Aldrich) and tris(*iso*-propyl)silyl triflate (Oakwood Chemicals) were purchased and used as received. Diphenylphosphoryl chloride (Aldrich) was distilled prior to use. Carbon dioxide was purchased from AirGas, and $^{13}CO_2$ was purchased from Cambridge Isotope Labs. All glassware was oven-dried at temperatures greater than 170 °C prior to use. NMR spectra were obtained on Varian Mercury 300 or Varian Inova 500 instruments equipped with Oxford Instruments superconducting magnets. ^{1}H NMR spectra were referenced to residual C_6D_5H (7.16 ppm), ^{13}C NMR spectra were referenced to C_6D_6 (128.39 ppm), and ^{31}P NMR spectra were referenced externally to 85% H_3PO_4 (0 ppm). Elemental analyses were performed by Midwest Microlab, LLC (Indianapolis, Indiana).

3.6.2 Preparation of ^{i}Pr$_3$SiPNb(N[CH$_2{}^t$Bu]Ar)$_3$ (33)

To a thawing Et_2O/THF solution (15 mL/2 mL) of $[(Et_2O)_{2.5}Na][PNb(N[CH_2{}^tBu]Ar)_3]$ (1.2 g, 1.33 mmol) was added a thawing Et_2O solution (2 mL) of $^iPr_3SiOTf$ (425 mg, 1.39 mmol, 1.04 eq). The orange mixture was allowed to stir while warming to 22 °C for 45 min. After this time the mixture was concentrated to dryness under dynamic vacuum. *n*-Hexane was added to the orange-brown residue and then removed under dynamic vacuum. The resulting solids were extracted with *n*-pentane and filtered through Celite to remove NaOTf. The filtrate was concentrated to dryness and the product was crystallized from Et_2O at –35 °C to afford red-orange crystals (715 mg, 0.839 mmol, 63% yield). ^{1}H NMR (C_6D_6, 500 MHz, 20 °C): δ 6.62 (s, 6H, *o*-Ar), 6.53 (s, 3H, *p*-Ar), 4.48 (s, 6H, NCH_2), 2.12 (s, 18H, ArCH_3), 1.40 (m, 3H, CH(CH$_3$)$_2$), 1.34 (d, 18H, CH(CH_3)$_2$), 1.08 (s, 27H, ^{t}Bu) ppm. ^{31}P{^{1}H} NMR (C_6D_6, 202 MHz, 20 °C): δ 433 (br, $\Delta\nu_{\frac{1}{2}}$ = 1000 Hz) ppm. ^{13}C{^{1}H} NMR (C_6D_6, 125.8 MHz, 20 °C): δ 153.7 (*ipso*-Ar), 138.7 (*m*-Ar), 125.7 (*p*-Ar), 121.9 (*o*-Ar), 79.0 (NCH_2), 36.2 (C(CH$_3$)$_3$), 30.0 (C(CH$_3$)$_3$), 21.9 (ArCH$_3$), 20.3 (SiCH(CH$_3$)$_2$), 16.1 (SiCH(CH$_3$)$_2$) ppm. Elem. Anal. Calcd for $C_{48}H_{81}N_3NbPSi$: C, 67.66; H, 9.58; N, 4.93. Found: C, 66.96; H, 9.37; N, 4.69.

3.6.3 Reaction of Me$_3$SiPNb(N[CH$_2{}^t$Bu]Ar)$_3$ and MesNCO: Generation of Mes(Me$_3$Si)NCP

A solution of $Me_3SiPNb(N[CH_2{}^tBu]Ar)_3$ (20 mg, 0.026 mmol) and MesNCO (4.2 mg, 1 eq) was prepared in C_6D_6 and the reaction progress monitored periodically by ^{1}H and ^{31}P NMR. After 1 h the anilide distribution was approximately 50% oxoniobium **21** and 50% starting material. A single

new ^{31}P resonance was located at –263 ppm and a trimethylsilyl doublet was observed in the ^{1}H NMR spectrum at 0.37 (d, $^{3}J_{HP}$ = 4.4 Hz). After 3 h, the reaction was 2:1 **21** to **32** with still the single new ^{31}P resonance and the trimethylsilyl doublet. After 27 h, the major ^{31}P signal is at –163 ppm and the trimethylsilyl resonance has shifted to a singlet at 0.12 ppm. Infrared spectral analysis performed by repeating this reaction in C_6H_6 and taking an IR after 5 h and after 30 h put the band for the intermediate MesNCPSiMe$_3$ species at 1927 cm^{-1}.

3.6.4 Reaction of $Me_3SiPNb(N[CH_2{}^tBu]Ar)_3$ and ^{i}PrNCO: Generation of ^{i}Pr(Me$_3$Si)NCP

A solution of $Me_3SiPNb(N[CH_2{}^tBu]Ar)_3$ (15 mg, 0.02 mmol) and ^{i}PrNCO (2 μL,1 eq) was prepared in C_6D_6, heated to 50 °C, and the reaction progress monitored periodically by ^{1}H and ^{31}P NMR. After 10 min the predominant anilide product was **21**, a trimethylsilyl doublet was observed in the ^{1}H NMR spectrum at 0.33 ppm (d, $^{3}J_{HP}$ = 5.4 Hz) and a ^{31}P signal at –242 ppm. Continued heating for 24 h gave a new trimethylsilyl product with a ^{1}H NMR resonance at 0.04 (s) ppm and a new ^{31}P NMR signal at –137 ppm. These NMR data are consistent with the literature values for the compound ^{i}Pr(Me$_3$Si)NCP.[25]

3.6.5 Preparation of $(Et_2O)_2NaOCP$

A 50 mL thick-walled glass vessel was loaded with $[(Et_2O)Na][PNb(N[CH_2{}^tBu]Ar)_3]$ (600 mg, 0.76 mmol) in THF/Et_2O (15 mL). This solution was gently degassed and an atmosphere of CO_2 was introduced. The vessel was shaken and then CO_2 was allowed to enter once more. The reaction mixture quickly turned from orange to yellow and was pumped to dryness. The oxoniobium complex **21** was extracted with Et_2O and the gray powder left behind was isolated and dried (120 mg, assuming formula of $(Et_2O)_2NaOCP$: 0.52 mmol, 69% yield). $^{13}C\{^{1}H\}$ NMR (THF, 75.5 MHz, 20 °C): δ 168.5 (d, J_{CP} = 52 Hz). $^{31}P\{^{1}H\}$ NMR (THF, 121.5 MHz, 20 °C): δ –393 ppm. IR (THF solution, KBr): $\tilde{\nu}$ 1756 cm^{-1}.

3.6.6 Reaction of $Me_3SiPNb(N[CH_2{}^tBu]Ar)_3$ and CO_2

A sealable (J. Young) NMR tube was loaded with $Me_3SiPNb(N[CH_2{}^tBu]Ar)_3$ (20 mg, 0.026 mmol) in C_6D_6 (0.7 mL), was degassed, and then an atmosphere of CO_2 was introduced. After 1 h, the ^{1}H NMR spectrum revealed a 1:1 mixture of oxoniobium **21** and intermediate **A**, with the following spectroscopic properties: ^{1}H NMR (C_6D_6, 300 MHz, 20 °C): δ 7.22 (s, 6H, *o*-Ar), 6.63 (s, 3H, *p*-Ar), 3.83 (s, 6H, NCH_2), 2.25 (s, 18H, ArCH_3), 0.81 (s, 27H, ^{t}Bu), 0.09 (s, 9H, SiMe$_3$) ppm. ^{31}P NMR (C_6D_6, 121.5 MHz, 20 °C): δ –307 (s) ppm. $^{13}C\{^{1}H\}$ NMR (C_6D_6, 75.5 MHz, 20 °C): δ 156.3 (d, J_{CP} = 16 Hz) ppm . After 24 h intermediate **A** is nearly consumed and the major product is oxoniobium **21**.

3.6.7 Reaction of $^{i}Pr_3SiPNb(N[CH_2{}^{t}Bu]Ar)_3$ and CO_2: Generation of $^{i}Pr_3SiOCP$

A sealable (J. Young) NMR tube was loaded with $^{i}Pr_3SiPNb(N[CH_2{}^{t}Bu]Ar)_3$ (24 mg, 0.028 mmol) in C_6D_6 (0.7 mL), was degassed, and to it was introduced an atmosphere of CO_2. After 1 h a ^{1}H NMR spectrum shows a 1:2 mixture of oxoniobium **21** and starting material, and after 20 h the reaction is complete, with **21** as the Nb-containing product and $^{i}Pr_3SiOCP$ as the P-containing product. ^{1}H NMR (C_6D_6, 500 MHz, 20 °C): δ 1.11 (m, 3H, C*H*$(CH_3)_2$), 0.99 (d, 18H, CH(C*H*$_3)_2$) ^{31}P NMR (C_6D_6, 121.5 MHz, 20 °C): δ –369 (s) ppm.

3.6.8 Preparation of $(PhO)_2P(O)PNb(N[CH_2{}^{t}Bu]Ar)_3$ (34)

To a thawing Et_2O/THF solution (20 mL/3 mL) of $[(Et_2O)Na][PNb(N[CH_2{}^{t}Bu]Ar)_3]$ (1.88 g, 2.37 mmol) was added a thawing Et_2O solution (5 mL) of $(PhO)_2P(O)Cl$ (638 mg, 2.37 mmol, 1 eq). This mixture took on a dark red color and was allowed to stir at 22 °C for 30 min before the mixture was filtered through Celite and the volatiles were removed *in vacuo*. The residue was treated with $(Me_3Si)_2O$ and stored at –35 °C to precipitate a bright orange powder (1.50 g, 1.62 mmol, 68% yield). ^{1}H NMR (C_6D_6, 500 MHz, 20 °C): δ 7.55 (d, 4H, *o*-Ph), 7.00 (t, 4H, *m*-Ph), 6.78 (t, 2H, *p*-Ph), 6.58 (s, 3H, *p*-Ar), 6.52 (br s, 6H, *o*-Ar), 4.26 (br s, 6H, NC*H*$_2$), 2.13 (s, 18H, ArC*H*$_3$), 0.96 (s, 27H, ^{t}Bu) ppm. ^{31}P{^{1}H} NMR (C_6D_6, 202 MHz, 20 °C): δ 172 (br, $^1J_{PP}$ = 595 Hz), 73 (d, $^1J_{PP}$ = 595 Hz) ppm. ^{13}C{^{1}H} NMR (C_6D_6, 125.8 MHz, 20 °C): δ 153.1 (d, J_{CP} = 10 Hz, *ipso*-Ph), 152.6 (br, *ipso*-Ar), 137.8 (*m*-Ar), 130.1 (*m*-Ph), 126.9 (*p*-Ar), 124.6 (*p*-Ph), 123.1 (br, *o*-Ar), 121.1 (d, J_{CP} = 6 Hz, *o*-Ph), 69.7 (br, NC*H*$_2$), 36.7 (*C*$(CH_3)_3$), 30.4 (C(*C*H$_3)_3$), 21.9 (Ar*C*H$_3$) ppm. Elem. Anal. Calcd for $C_{51}H_{70}N_3O_3P_2Nb$: C, 66.01; H, 7.60; N, 4.53. Found: C, 65.89; H, 7.52; N, 4.60.

3.6.9 Preparation of $(Ph)_2P(O)PNb(N[CH_2{}^{t}Bu]Ar)_3$

To a thawing Et_2O/THF solution (3 mL/3 drops) of $[(Et_2O)Na][PNb(N[CH_2{}^{t}Bu]Ar)_3]$ (36 mg, 0.045 mmol) was added a thawing Et_2O solution (3 mL) of $Ph_2P(O)Cl$ (10 mg, 0.043 mmol, 0.95 mmol). The initially orange solution reddened slightly and was allowed to stir at 22 °C for 20 min before the volatiles were removed *in vacuo*. The residue was extracted with C_6D_6 and filtered through Celite to afford the product. ^{1}H NMR (C_6D_6, 300 MHz, 20 °C): δ 8.24 (m, 4H, *o*-Ph), 7.00–7.11 (m, 6H, *m,p*-Ph), 6.67 (br s, 6H, *o*-Ar), 6.53 (s, 3H, *p*-Ar), 4.10 (br s, 6H, NC*H*$_2$), 2.12 (s, 18H, ArC*H*$_3$), 0.81 (s, 27H, ^{t}Bu) ppm. ^{31}P{^{1}H} NMR (C_6D_6, 202 MHz, 20 °C): δ 196 (br, $^1J_{PP}$ = 480 Hz), 76 (d, $^1J_{PP}$ = 480 Hz) ppm.

3.6.10 Preparation of $(Me_2N)_2P(O)PNb(N[CH_2{}^{t}Bu]Ar)_3$ (35)

To a thawing Et_2O/THF solution (15/1 mL) of $[(Et_2O)Na][PNb(N[CH_2{}^{t}Bu]Ar)_3$ (475 mg, 0.60 mmol) was added a thawing Et_2O/THF solution (2/2 mL) of $(Me_2N)_2P(O)Cl$ (100 mg, 0.59 mmol).

This mixture took on an orange color and was allowed to stir at 22 °C for 1 h before the mixture was filtered through Celite and the volatiles were removed *in vacuo*. The residue was extracted with *n*-pentane and then dried *in vacuo* once more. Crystallization from Et_2O at –35 °C yielded large red crystals. A second crop was collected following concentration and precipitation at –35 °C for a total of 270 mg (0.33 mmol, 56% yield). ^{1}H NMR (C_6D_6, 500 MHz, 20 °C): δ 6.73 (br, 6H, *o*-Ar), 6.55 (3H, *p*-Ar), 4.15 (6H, NCH_2), 2.76 (d, $^3J_{PH}$ = 10 Hz, NMe_2), 2.18 (18H, ArCH_3), 0.94 (27H, ^{t}Bu) ppm. ^{31}P{^{1}H} NMR (C_6D_6, 202 MHz, 20 °C): δ 250 (br d), 80 (d, $^1J_{PP}$ = 480 Hz) ppm. ^{13}C{^{1}H} NMR (C_6D_6, 125.8 MHz, 20 °C): δ 153.8 (*ipso*-Ar), 137.5 (*m*-Ar), 125.9 (*p*-Ar), 123.2 (*o*-Ar), 69.1 (NCH_2), 37.5 (d, $^2J_{CP}$ = 4 Hz, NMe_2), 36.5 (*C*$(CH_3)_3$), 30.5 (C(*C*$H_3)_3$), 21.9 (Ar*C*H_3) ppm.

3.6.11 Preparation of $(Me_2N)_2P(OAlCl_3)PNb(N[CH_2{}^tBu]Ar)_3$ (36)

To an Et_2O solution (5 mL) of $OP(NMe_2)_2PNb(N[CH_2{}^tBu]Ar)_3$ (105 mg, 0.126 mmol) at –35 °C was added a solution of $AlCl_3$ (17 mg, 0.126 mmol, 1 eq) in Et_2O (3 mL). The mixture was stirred for 20 min at 22 °C before the solvent was removed under dynamic vacuum. *n*-Hexane (2 mL) was added to precipitate a bright red-orange powder, and the solvent was removed once more under vacuum. Another 2 mL portion of *n*-hexane was added to form a bright red suspension. This mixture was frozen, and upon thawing the bright red-orange solids were collected on a frit and dried to constant mass (101 mg, 0.105 mmol, 83% yield). ^{1}H NMR (C_6D_6, 500 MHz, 20 °C): δ 6.85 (s, 6H, *o*-Ar), 6.49 (s, 3H, *p*-Ar), 4.54 (s, 6H, NCH_2), 2.59 (d, $^3J_{PH}$ = 10 Hz, NMe_2), 2.09 (s, 18H, ArCH_3), 0.88 (s, 27H, ^{t}Bu) ppm. ^{31}P{^{1}H} NMR (C_6D_6, 202 MHz, 20 °C): δ 421 (d, J_{PP} = 540 Hz), 72 (d, J_{PP} = 540 Hz) ppm. ^{13}C{^{1}H} NMR (C_6D_6, 125.8 MHz, 20 °C): δ 149.1 (*ipso*-Ar), 139.3 (*m*-Ar), 125.7 (*p*-Ar), 123.2 (*o*-Ar), 72.8 (NCH_2), 38.2 (d, $^2J_{CP}$ = 4 Hz, NMe_2), 37.1 (*C*$(CH_3)_3$), 30.1 (C(*C*$H_3)_3$), 21.6 (Ar*C*H_3) ppm. Elem. Anal. Calcd for $C_{43}H_{72}N_5AlCl_3OP_2Nb$: C, 53.62; H, 7.53; N, 7.27; Cl, 11.04. Found: C, 53.56; H, 7.61; N, 7.26; Cl, 10.75.

3.6.12 Generation of ^{i}Pr$_3$SiPPMo(N[^{t}Bu]Ar)$_3$ (38)

Solid purple $OPMo(N[^tBu]Ar)_3$ (40 mg, 0.060 mmol, 1.02 eq) and orange $^iPr_3SiPNb(N[CH_2{}^tBu]Ar)_3$ (50 mg, 0.059 mmol) were mixed and dissolved together in C_6D_6 (1 mL). The purple color of $OPMo(N[^tBu]Ar)_3$ dissipated, giving way to a red solution of oxoniobium **21** and $^iPr_3SiPPMo(N[^tBu]Ar)_3$. ^{1}H and ^{31}P NMR spectra collected after 30 min revealed the complete consumption of $^iPr_3SiPNb(N[CH_2{}^tBu]Ar)_3$, with a small residual amount of $OPMo(N[^tBu]Ar)_3$. The data corresponding to $^iPr_3SiPPMo(N[^tBu]Ar)_3$ are: ^{1}H NMR (C_6D_6, 500 MHz, 20 °C): δ 6.65 (s, 3H, *p*-Ar), 5.99 (br, 6H, *o*-Ar), 2.06 (s, 18H, ArCH_3), 1.54 (m, 3H, C$H(CH_3)_2$), 1.53 (s, 27H, ^{t}Bu), 1.41 (d, 18H, CH(C$H_3)_2$) ppm. ^{31}P{^{1}H} NMR (C_6D_6, 202 MHz, 20 °C): δ 543 (v br, $\Delta\nu_{\frac{1}{2}}$ = 1900 Hz), 158 (br d, $^1J_{PP}$ = 655 Hz, $\Delta\nu_{\frac{1}{2}}$ = 170 Hz) ppm. ^{13}C{^{1}H} NMR (C_6D_6, 125.8 MHz, 20 °C): δ 150.9 (*ipso*-Ar), 137.4 (*m*-Ar), 131.2 (*p*-Ar), 128.5 (*o*-Ar), 64.1 (*C*$(CH_3)_3$), 34.3 (C(*C*$H_3)_3$), 21.9 (Ar*C*H_3), 20.5 (SiCH(*C*$H_3)_2$), 16.3 (Si*C*$H(CH_3)_2$) ppm.

3.6.13 Formation of ($^{i}Pr_3Si)_3$ (40) and ($^{i}Pr_3Si)_2P_3P(Si^{i}Pr_3)_2$ (41)

An NMR tube containing a solution of crude $^{i}Pr_3SiPPMo(N[tBu]Ar)_3$ and $ONb(N[CH_2{}^{t}Bu]Ar)_3$ was allowed to stand at 22 °C for 10 d. Over this time the diphosphenido complex converted to the terminal phosphide complex **39** with generation of two phosphinidene oligomers, $(^{i}Pr_3SiP)_3$ and $(^{i}Pr_3Si)_2P_3P(Si^{i}Pr_3)_2$, in an approximate 1.5:1 ratio, that were identified by their ^{31}P NMR spectra. These spectra were simulated with *gNMR* to extract the NMR parameters, see Figures 3.7 and 3.8 and Table 3.3. The trimer and the tetramer were also identified in the reaction mixture by EI-MS at m/z 564.34 and 752.45 amu/e, respectively.

3.6.14 Formation of $(R_3SiP)_3$ (R = Me, Ph)

The complexes $R_3SiPNb(N[CH_2tBu]Ar)_3$ were prepared by the reaction between $[(Et_2O)Na]$-$[PNb(N[CH_2{}^{t}Bu]Ar)_3]$ and the appropriate chlorosilane using a procedure analogous to that for **33**. The complex **32** was isolated as red crystal as reported previously.[20] The complex $Ph_3SiPNb(N[CH_2{}^{t}Bu]Ar)_3$ (^{31}P NMR δ = 464 ppm) was used as generated, following removal of NaCl, without recrystallization.

Equimolar amounts (*ca.* 0.1 mmol) of $OPMo(N[^{t}Bu]Ar)_3$ and the silylphosphinidene complex $R_3SiPNb(N[CH_2{}^{t}Bu]Ar)_3$ were dissolved in Et_2O (*ca.* 5 mL) at 23 °C. Upon mixing, the purple color of $OPMo(N[^{t}Bu]Ar)_3$ rapidly dissipated. Analysis by ^{31}P NMR spectroscopy after 10 min revealed clean formation of the cyclic phosphinidene trimers by their characteristic AB_2 patterns. ^{31}P NMR (Et_2O, 121 MHz, 20 °C): R = Ph, δ –218 (B_2), –244 (A); R = Me, δ –235 (B_2), –247 (A) ppm. Production of oxoniobium **21** and terminal phosphide **39** were confirmed by ^{1}H NMR spectroscopy.

3.6.15 Trapping of $^{i}Pr_3SiP{=}PSi^{i}Pr_3$ with C_7H_8: Generation of $(^{i}Pr_3SiP)_2C_7H_8$

A mixture of $OPMo(N[^{t}Bu]Ar)_3$ (20 mg, 0.030 mmol) and $^{i}Pr_3SiPNb(N[CH_2{}^{t}Bu]Ar)_3$ (25 mg, 0.030 mmol, 1 eq) was dissolved in a THF solution of spiro[2.4]hepta-4,7-diene (1 g, 14 wt%, 40+ eq). The reaction mixture was heated to 60 °C for *ca.* 10 h and then analyzed by ^{31}P NMR spectroscopy. The product $(^{i}Pr_3SiP)_2C_7H_8$ was observed as a pair of doublets ($^{1}J_{PP}$ = 240 Hz) at δ –112.5 and –117.5 ppm.

3.6.16 Trapping of $^{i}Pr_3SiP{=}PSi^{i}Pr_3$ with C_6H_{10}: Generation of $(^{i}Pr_3SiP)_2C_6H_{10}$

A mixture of $OPMo(N[^{t}Bu]Ar)_3$ (40 mg, 0.060 mmol) and $^{i}Pr_3SiPNb(N[CH_2{}^{t}Bu]Ar)_3$ (50 mg, 0.059 mmol, 1 eq) was dissolved in THF (2.5 g). To this mixture was added 2,3-dimethylbutadiene (400 mg, 4.8 mmol, 80 eq) and the solution was allowed to stir for 20 min, at which time formation of **38** was confirmed by ^{31}P NMR spectroscopy. The mixture was then heated to 60 °C for 18 h,

after which time analysis by ^{31}P NMR spectroscopy revealed formation of $(^{i}Pr_3SiP)_2C_6H_{10}$ as a singlet at –138.4 ppm. The identity of this product was supported by high-resolution EI-MS with a parent ion at m/z 458.308 amu/e. This procedure gave spectroscopic yields in the range 40–50%, as determined by integration versus PPh_3 (16 mg, 0.061 mmol) that was added at the end of the reaction.

3.6.17 Equilibrium Generation of $^{i}Pr_3SiP{=}PPh_3$

Solid $OPMo(N[^{t}Bu]Ar)_3$ (20 mg, 0.030 mmol), $^{i}Pr_3SiPNb(N[CH_2{}^{t}Bu]Ar)_3$ (25 mg, 0.030 mmol) and PPh_3 (20 mg, 0.08 mmol) were mixed as solids and then dissolved together in *ca.* 0.7 mL of C_6D_6. ^{31}P and ^{1}H NMR spectra collected after several minutes revealed the presence of $ONb(N[CH_2{}^{t}Bu]Ar)_3$, $^{i}Pr_3SiPPMo(N[^{t}Bu]Ar)_3$, $PMo(N[^{t}Bu]Ar)_3$, PPh_3, and $^{i}Pr_3SiP{=}PPh_3$. Relative concentrations of these species were measured by integration in the ^{1}H NMR spectrum, and then the tube was returned to the glove box. In a procedure repeated twice, portions of $PMo(N[^{t}Bu]Ar)_3$ were added to the tube and the integrals were remeasured. The ratio $K = \frac{[\mathbf{39}][^{i}Pr_3SiP{=}PPh_3]}{[\mathbf{38}][PPh_3]}$ varied from 0.63 to 0.71 over three measurements, giving an average K_{eq} = 0.67. The spectral data for $^{i}Pr_3SiP{=}PPh_3$ are as follows: ^{1}H NMR (C_6D_6, 500 MHz, 20 °C): δ 7.99 (m, 6H, *o*-Ph), 6.98 (m, 9H, *m,p*-Ph), 1.26 (m, 3H, C*H*$(CH_3)_2$), 1.21 (d, 18H, CH(C*H*$_3)_2$) ppm. ^{31}P NMR (C_6D_6, 202 MHz, 20 °C): δ 30.5 (d, $^{1}J_{PP}$ = 590 Hz), –263.8 (d, $^{1}J_{PP}$ = 590 Hz) ppm.

3.6.18 X-Ray Structure Determinations

Diffraction quality crystals of **32**, **34**, **35** and **36** were grown from Et_2O at –35 °C. Crystals of **33** were grown from $(SiMe_3)_2O$ at –35 °C, and of **38** from its reaction mixture in *n*-pentane at –35 °C. Crystals were mounted in hydrocarbon oil on a nylon loop or a glass fiber. Low-temperature (100 K) data were collected on a Siemens Platform three-circle diffractometer coupled to a Bruker-AXS Smart Apex CCD detector with graphite-monochromated Mo Kα radiation (λ = 0.71073 Å) performing ϕ- and ω-scans. A semi-empirical absorption correction was applied to the diffraction data using SADABS.[71] All structures were solved by direct or Patterson methods using SHELXS[72,73] and refined against F^2 on all data by full-matrix least squares with SHELXL-97.[73,74] All non-hydrogen atoms were refined anisotropically. All hydrogen atoms were included in the model at geometrically calculated positions and refined using a riding model. The isotropic displacement parameters of all hydrogen atoms were fixed to 1.2 times the U_{eq} value of the atoms they are linked to (1.5 times for methyl groups). In structures where disorders were present, the disorders were refined within SHELXL with the help of rigid bond restraints as well as similarity restraints on the anisotropic displacement parameters for neighboring atoms and on 1,2- and 1,3-distances throughout the disordered components.[75] The relative occupancies of disordered components were refined freely within SHELXL. Further details are provided in Tables 3.4 and 3.5, on Reciprocal Net,[76] or in the form of cif files available from the CCDC.[77]

3.6.19 Computational Studies

All calculations were carried out using ADF 2007.01 from Scientific Computing and Modeling (http://www.scm.com) on a thirty two-processor Quantum Cube workstation from Parallel Quantum Solutions (http://www.pqs-chem.com).[37,52,78] In all cases the LDA functional employed was that of Vosko, Wilk, and Nusair (VWN) while the GGA part was handled using the functionals of Becke and Perdew (BP86).[79–81] In addition, all calculations were carried out using the Zero Order Regular Approximation (ZORA) for relativistic effects.[82–85] The basis sets were triple-zeta with two polarization functions (TZ2P) as supplied with ADF, and frozen core approximations were made for carbons on the anilide ligands (1s). Geometries were optimized to default convergence criteria and energies are uncorrected for zero-point energies. Bond multiplicities were calculated using the method of Nalewajski and Mrozek within ADF.[38] Electron density topologies and orbital contours were analyzed using the packages DGrid and Basin by Kohout.[86]

Chemical shielding tensors were calculated for the ^{31}P nuclei in the optimized structures by the GIAO method using the ADF package.[87–90] The functionals, basis sets and relativistic approximations used were the same as described above, with the exception that for no frozen core approximations were made. Diamagnetic and paramagnetic contributions were included in the absolute chemical shielding calculations. The total isotropic shielding value was converted to a chemical shift (downfield of 85% phosphoric acid) by comparison to calculated shieldings and experimental chemical shifts for PH_3 or $OPMo(N[^tBu]Ar)_3$.[40,91]

Table 3.4. Crystal Data for Niobium Phosphinidene Complexes

	32	**33**	**35**
Reciprocal Net code	05032	08307	07207
Empirical formula	$C_{42}H_{69}N_3NbPSi$	$C_{48}H_{81}N_3NbPSi$	$C_{43}H_{72}N_5NbOP_2$
Formula weight	767.97	852.13	829.91
Temperature	100(2) K	100(2) K	100(2) K
Wavelength	0.71073 Å	0.71073 Å	0.71073 Å
Crystal system	Triclinic	Triclinic	Monoclinic
Space group	$P\bar{1}$	$P\bar{1}$	$P2_1/n$
Unit cell dimensions	$a = 10.7601(5)$ Å, $\alpha = 81.2700(10)^\circ$	$a = 11.9212(14)$ Å, $\alpha = 86.970(2)^\circ$	$a = 17.4705(8)$ Å, $\alpha = 90^\circ$
	$b = 11.5434(5)$ Å, $\beta = 88.4410(10)^\circ$	$b = 13.8989(16)$ Å, $\beta = 84.260(2)^\circ$	$b = 13.9994(6)$ Å, $\beta = 90.1290(10)^\circ$
	$c = 18.0478(7)$ Å, $\gamma = 78.7850(10)^\circ$	$c = 15.3715(18)$ Å, $\gamma = 84.825(2)^\circ$	$c = 19.1376(9)$ Å, $\gamma = 90^\circ$
Volume	2173.40(16) Å^3	2521.4(5) Å^3	4680.6(4) Å^3
Z	2	2	4
Density (calculated)	1.174 Mg/m^3	1.122 Mg/m^3	1.178 Mg/m^3
Absorption coefficient	0.371 mm^{-1}	0.326 mm^{-1}	0.361 mm^{-1}
$F(000)$	824	920	1776
Crystal size	$0.25 \times 0.17 \times 0.16$ mm^3	$0.35 \times 0.20 \times 0.08$ mm^3	$0.25 \times 0.18 \times 0.15$ mm^3
Theta range for collection	1.14 to 28.43°	1.33 to 28.70°	1.58 to 29.80°
Index ranges	$-14 \le h \le 14$, $-15 \le k \le 15$,	$-16 \le h \le 16$, $-18 \le k \le 18$,	$-24 \le h \le 24$, $-19 \le k \le 19$,
	$0 \le l \le 24$	$-20 \le l \le 20$	$-26 \le l \le 26$
Reflections collected	45310	49198	122364
Independent reflections	10903 [R(int) = 0.0288]	12981 [R(int) = 0.0697]	13405 [R(int) = 0.0725]
Completeness to θ_{max}	99.6%	99.7%	100.0%
Absorption correction	Semi-empirical from equivalents	Semi-empirical from equivalents	Semi-empirical from equivalents
Max. and min. transmission	0.9430 and 0.9129	0.9744 and 0.8944	0.9479 and 0.9152
Refinement method	Full-matrix least-squares on F^2	Full-matrix least-squares on F^2	Full-matrix least-squares on F^2
Data / restraints / parameters	10903 / 0 / 391	12981 / 0 / 508	13405/ 0 / 488
Goodness-of-fit[a]	1.059	1.027	1.042
Final R indices[b] [$I > 2\sigma(I)$]	$R_1 = 0.0373$, $wR_2 = 0.0913$	$R_1 = 0.0428$, $wR_2 = 0.0930$	$R_1 = 0.0387$, $wR_2 = 0.0817$
R indices[b] (all data)	$R_1 = 0.0414$, $wR_2 = 0.0940$	$R_1 = 0.0700$, $wR_2 = 0.1046$	$R_1 = 0.0597$, $wR_2 = 0.0918$
Largest diff. peak and hole	1.132 and -0.707 e Å^{-3}	0.753 and -0.720 e Å^{-3}	0.574 and -0.672 e Å^{-3}

[a] GooF = $\left[\frac{\Sigma[w(F_o^2-F_c^2)^2]}{(n-p)}\right]^{\frac{1}{2}}$ [b] $R_1 = \frac{\Sigma||F_o|-|F_c||}{\Sigma|F_o|}$; $wR_2 = \left[\frac{\Sigma[w(F_o^2-F_c^2)^2}{\Sigma[w(F_o^2)^2]}\right]^{\frac{1}{2}}$; $w = \frac{1}{\sigma^2(F_o^2)+(aP)^2+bP}$; $P = \frac{2F_c^2+\max(F_o^2,0)}{3}$

Table 3.5. Crystal Data for More Niobium Phosphinidene Complexes and a Molybdenum Diphosphenido Complex

	36	**34**	**38**
Reciprocal Net code	07224	05164	08299
Empirical formula	$C_{43}H_{72}AlCl_3N_5NbOP_2$	$C_{51}H_{70}N_3NbO_3P_2$	$C_{48}H_{82}MoN_3P_2Si$
Formula weight	963.24	927.95	887.14
Temperature	100(2) K	100(2) K	100(2) K
Wavelength	0.71073 Å	0.71073 Å	0.71073 Å
Crystal system	Monoclinic	Triclinic	Triclinic
Space group	$P2_1/c$	$P\bar{1}$	$P\bar{1}$
Unit cell dimensions	$a = 10.533(3)$ Å, $\alpha = 90°$	$a = 13.8932(5)$ Å, $\alpha = 93.1790(10)°$	$a = 11.4081(10)$ Å, $\alpha = 65.2370(10)°$
	$b = 22.218(6)$ Å, $\beta = 102.897(5)°$	$b = 16.9039(5)$ Å, $\beta = 91.7190(10)°$	$b = 15.4385(14)$ Å, $\beta = 72.983(2)°$
	$c = 22.231(6)$ Å, $\gamma = 90°$	$c = 21.4350(7)$ Å, $\gamma = 95.5160(10)°$	$c = 16.7680(15)$ Å, $\gamma = 75.312(2)°$
Volume	5071(2) Å^3	4999.8(3) Å^3	2534.9(4) Å^3
Z	4	4	2
Density (calculated)	1.262 Mg/m^3	1.233 Mg/m^3	1.162 Mg/m^3
Absorption coefficient	0.511 mm^{-1}	0.347 mm^{-1}	0.378 mm^{-1}
$F(000)$	2032	1968	954
Crystal size	$0.24 \times 0.19 \times 0.07$ mm^3	$0.21 \times 0.19 \times 0.11$ mm^3	$0.45 \times 0.30 \times 0.05$ mm^3
Theta range for collection	1.31 to 28.70°	1.47 to 29.58°	1.37 to 29.13°
Index ranges	$-14 \le h \le 14$, $-30 \le k \le 30$,	$-19 \le h \le 19$, $-23 \le k \le 23$,	$-15 \le h \le 15$, $-21 \le k \le 21$,
	$-30 \le l \le 30$	$-29 \le l \le 29$	$-22 \le l \le 22$
Reflections collected	122032	111887	62760
Independent reflections	13101 [R(int) = 0.0869]	27938 [R(int) = 0.0437]	13603 [R(int) = 0.0567]
Completeness to θ_{max}	100.0%	99.6%	99.8%
Absorption correction	Semi-empirical from equivalents	Semi-empirical from equivalents	Semi-empirical from equivalents
Max. and min. transmission	0.9651 and 0.8871	0.9628 and 0.9307	0.9813 and 0.8483
Refinement method	Full-matrix least-squares on F^2	Full-matrix least-squares on F^2	Full-matrix least-squares on F^2
Data / restraints / parameters	13101 / 132 /544	27938/ 602 /1203	13603/ 220 / 599
Goodness-of-fit[a]	1.041	1.100	1.013
Final R indices[b] [$I > 2\sigma(I)$]	$R_1 = 0.0453$, $wR_2 = 0.0898$	$R_1 = 0.0459$, $wR_2 = 0.1113$	$R_1 = 0.0342$, $wR_2 = 0.0734$
R indices[b] (all data)	$R_1 = 0.0728$, $wR_2 = 0.1003$	$R_1 = 0.0629$, $wR_2 = 0.1224$	$R_1 = 0.0528$, $wR_2 = 0.0816$
Largest diff. peak and hole	0.855 and -0.792 e Å^{-3}	1.806 and -0.535 e Å^{-3}	0.605 and -0.559 e Å^{-3}

[a] GooF = $\left[\frac{\Sigma[w(F_o^2-F_c^2)^2]}{(n-p)}\right]^{\frac{1}{2}}$ [b] $R_1 = \frac{\Sigma||F_o|-|F_c||}{\Sigma|F_o|}$; $wR_2 = \left[\frac{\Sigma[w(F_o^2-F_c^2)^2}{\Sigma[w(F_o^2)^2]}\right]^{\frac{1}{2}}$; $w = \frac{1}{\sigma^2(F_o^2)+(aP)^2+bP}$; $P = \frac{2F_c^2+\max(F_o^2,0)}{3}$

3.7 REFERENCES

[1] Cowley, A. H.; Barron, A. R. *Acc. Chem. Res.* **1988**, *21*, 81–87.

[2] Lammertsma, K. *New Aspects In Phosphorus Chemistry III*; Topics In Current Chemistry:, Vol. 229; Springer, 2003; pp 407–422.

[3] Cowley, A. H. *Acc. Chem. Res.* **1997**, *30*, 445–451.

[4] Cummins, C. C.; Schrock, R. R.; Davis, W. M. *Angew. Chem., Int. Ed. Engl.* **1993**, *32*, 756–759.

[5] Bonanno, J. B.; Wolczanski, P. T.; Lobkovsky, E. B. *J. Am. Chem. Soc.* **1994**, *116*, 11159–11160.

[6] Breen, T. L.; Stephan, D. W. *J. Am. Chem. Soc.* **1995**, *117*, 11914–11921.

[7] Freundlich, J. S.; Schrock, R. R.; Davis, W. M. *J. Am. Chem. Soc.* **1996**, *118*, 3643–3655.

[8] Mösch-Zanetti, N. C.; Schrock, R. R.; Davis, W. M.; Wanninger, K.; Seidel, S. W.; O'Donoghue, M. B. *J. Am. Chem. Soc.* **1997**, *119*, 11037–11048.

[9] Basuli, F.; Tomaszewski, J.; Huffman, J. C.; Mindiola, D. J. *J. Am. Chem. Soc.* **2003**, *125*, 10170–10171.

[10] Basuli, F.; Bailey, B. C.; Huffman, J. C.; Baik, M. H.; Mindiola, D. J. *J. Am. Chem. Soc.* **2004**, *126*, 1924–1925.

[11] Cossairt, B. M.; Cummins, C. C. *Angew. Chem., Int. Ed.* **2008**, *46*, 169–172.

[12] Cowley, A. H.; Pellerin, B.; Atwood, J. L.; Bott, S. G. *J. Am. Chem. Soc.* **1990**, *112*, 6734–6735.

[13] Melenkivitz, R.; Mindiola, D. J.; Hillhouse, G. L. *J. Am. Chem. Soc.* **2002**, *124*, 3846–3847.

[14] Arney, D. S. J.; Schnabel, R. C.; Scott, B. C.; Burns, C. J. *J. Am. Chem. Soc.* **1996**, *118*, 6780–6781.

[15] Masuda, J. D.; Jantunen, K. C.; Ozerov, O. V.; Noonan, K. J. T.; Gates, D. P.; Scott, B. L.; Kiplinger, J. L. *J. Am. Chem. Soc.* **2008**, *130*, 2408–2409.

[16] Nugent, W. A.; Mayer, J. M. *Metal-Ligand Multiple Bonds: The Chemistry of Transition Metal Complexes Containing Oxo, Nitrido, Imido, Alkylidene, or Alkylidyne Ligands*; John Wiley & Sons, Inc.: New York, 1988.

[17] Cossairt, B. M.; Cummins, C. C. *Angew. Chem., Int. Ed.* **2008**, *47*, 8863–8866.

[18] Figueroa, J. S.; Cummins, C. C. *J. Am. Chem. Soc.* **2004**, *126*, 13916–13917.

[19] Figueroa, J. S.; Ph.D. thesis; Massachusetts Institute of Technology; 2005.

[20] Figueroa, J. S.; Cummins, C. C. *Angew. Chem., Int. Ed.* **2004**, *43*, 984–988.

[21] This angle was measure by X-ray crystallography for R = Cy, and inferred from the upfield chemical shifts ($\delta = 157 - 227$) for a series of seven compounds[4,7].

[22] Kolodiazhnyi, O. I. *Tetrahedron Lett.* **1982**, *23*, 4933 – 4936.

[23] Appel, R.; Paulen, W. *Angew. Chem., Int. Ed. Engl.* **1983**, *22*, 785–786; *Angew. Chem.* **1983**, *95*, 807.

[24] Yoshifuji, M.; Toyota, K.; Shibayama, K.; Inamoto, N. *Tetrahedron Lett.* **1984**, *25*, 1809 – 1812.

[25] Appel, R.; Poppe, M. *Angew. Chem., Int. Ed. Engl.* **1989**, *28*, 53–54.

[26] Appel, R.; Knoll, F.; I., R. *Angew. Chem., Int. Ed. Engl.* **1981**, *20*, 731–744.

[27] Wentrup, C.; Briehl, H.; Becker, G.; Uhl, G.; Wessely, H. J.; Maquestiau, A.; Flammang, R. *J. Am. Chem. Soc.* **1983**, *105*, 7194–7195.

[28] Becker, G.; Brombach, H.; Horner, S. T.; Niecke, E.; Schwarz, W.; Streubel, R.; Wurthwein, E. U. *Inorg. Chem.* **2005**, *44*, 3080–3086.

[29] Arakawa, H.; et al. *Chem. Rev.* **2001**, *101*, 953–996.

[30] Hübler, K.; Schwerdtfeger, P. *Inorg. Chem.* **1999**, *38*, 157–164.

[31] Westerhausen, M.; Schneiderbauer, S.; Piotrowski, H.; Suter, M.; Noth, H. *J. Organomet. Chem.* **2002**, *643*, 189–193.

[32] Becker, G.; Schwarz, W.; Seidler, N.; Westerhausen, M. *Z. Anorg. Allg. Chem.* **1992**, *612*, 72–82.

[33] Gier, T. E. *J. Am. Chem. Soc.* **1961**, *83*, 1769–1770.

[34] Regitz, M.; Scherer, O. J. *Multiple Bonds and Low Coordination in Phosphorus Chemistry*; Thieme: Stuttgart, 1990.

[35] Dillon, K. B.; Mathey, F.; Nixon, J. F. *Phosphorus: The Carbon Copy*; Wiley: Chichester, 1998.

[36] Heckmann, G.; Becker, G.; Kraft, H. *Magn. Reson. Chem.* **1999**, *37*, 667–671.

[37] *ADF*; 2007.01; Scientific Computing & Modeling: Theoretical Chemistry, Vrije Universiteit, Amsterdam, The Netherlands, 2007. `http://www.scm.com`.

[38] Michalak, A.; DeKock, R. L.; Ziegler, T. *J. Phys. Chem. A* **2008**, *112*, 7256–7263.

[39] Bader, R. F. W. *Atoms in Molecules: A Quantum Theory*; International Series of Monographs on Chemistry, Vol. 22; Oxford University Press: Oxford, 1990.

[40] Johnson, M. J. A.; Odom, A. L.; Cummins, C. C. *Chem. Commun.* **1997**, 1523–1524.

[41] Weber, L.; Reizig, K. *Angew. Chem., Int. Ed. Engl.* **1985**, *24*, 865–866; *Angew. Chem.* **1985**, *97*, 868–869.

[42] Weber, L.; Frebel, M.; Boese, R. *Angew. Chem., Int. Ed. Engl.* **1987**, *26*, 1010–1011.

[43] Weber, L.; Meine, G.; Niederprüm, N.; Boese, R. *Organometallics* **1987**, *6*, 1989–1991.

[44] Weber, L.; Reizig, K.; Bungardt, D.; Boese, R. *Organometallics* **1987**, *6*, 110–114.

[45] Jutzi, P.; Meyer, U. *Chem. Ber.* **1988**, *121*, 559–560.

[46] Weber, L.; Kirchhoff, R.; Boese, R.; Stammler, H. G.; Neumann, B. *Organometallics* **1993**, *12*, 731–737.

[47] DuBois, D. L.; Hoffmann, R. *Nov. J. Chim.* **1977**, *1*, 479.

[48] Peters, J. C.; Cherry, J.-P. F.; Thomas, J. C.; Baraldo, L.; Mindiola, D. J.; Davis, W. M.; Cummins, C. C. *J. Am. Chem. Soc.* **1999**, *121*, 10053–10067.

[49] Figueroa, J. S.; Piro, N. A.; Clough, C. R.; Cummins, C. C. *J. Am. Chem. Soc.* **2006**, *128*, 940–950.

[50] Fermin, M. C.; Ho, J. W.; Stephan, D. W. *Organometallics* **1995**, *14*, 4247–4256.

[51] Fox, A. R.; Clough, C. R.; Piro, N. A.; Cummins, C. C. *Angew. Chem., Int. Ed.* **2007**, *46*, 973–976.

[52] te Velde, G.; Bickelhaupt, F. M.; Baerends, E. J.; Fonseca Guerra, C.; van Gisbergen, S. J. A.; Snijders, J. G.; Ziegler, T. *J. Comput. Chem.* **2001**, *22*, 931–967.

[53] Curley, J. J.; Sceats, E. L.; Cummins, C. C. *J. Am. Chem. Soc.* **2006**, *128*, 14036–14037.

[54] Sceats, E. L.; Figueroa, J. S.; Cummins, C. C.; Loening, N. M.; Van der Wel, P.; Griffin, R. G. *Polyhedron* **2004**, *23*, 2751–2768.

[55] Gopinathan, M.; Jug, K. *Theor. Chim. Acta* **1983**, *63*, 497.

[56] Laplaza, C. E.; Davis, W. M.; Cummins, C. C. *Angew. Chem., Int. Ed. Engl.* **1995**, *34*, 2042–2044.

[57] Baudler, M.; Makowka, B. *Z. Anorg. Allg. Chem.* **1985**, *528*, 7–21.

[58] Goerlich, J. R.; Schmutzler, R. *Z. Anorg. Allg. Chem.* **1994**, *620*, 173–176.

[59] Schoeller, W. W.; Staemmler, V.; Rademacher, P.; Niecke, E. *Inorg. Chem.* **1986**, *25*, 4382–4385.

[60] Schiffer, H.; Ahlrichs, R.; Häser, M. *Theor. Chim. Acta.* **1989**, *75*, 1–10.

[61] Weber, L. *Chem. Rev.* **1992**, *92*, 1839–1906.

[62] Wiberg, N.; Wörner, A.; Lerner, H.-W.; Karaghiosoff, K. *Z. Naturforsch., B: Chem. Sci.* **2002**, *57*, 1027–1035.

[63] Cappello, V.; Baumgartner, J.; Dransfeld, A.; Flock, M.; Hassler, K. *Eur. J. Inorg. Chem.* **2006**, 2393–2405.

[64] Li, X.; Lei, D.; Chiang, M. Y.; Gaspar, P. P. *J. Am. Chem. Soc.* **1992**, *114*, 8526–8531.

[65] van Eis, M. J.; de Kanter, F. J. J.; de Wolf, W. H.; Lammertsma, K.; Bickelhaupt, F.; Lutz, M.; Spek, A. L. *Tetrahedron* **2000**, *56*, 129 – 136.

[66] Lammertsma, K.; Vlaar, M. J. *Eur. J. Org. Chem* **2002**, 1127–1138.

[67] Quin, L. D. *A Guide to Organophosphorus Chemistry*; John Wiley & Sons, Inc.: New York, 2000; pp 314–317.

[68] Smith, R. C.; Shah, S.; Protasiewicz, J. D. *J. Organomet. Chem.* **2002**, *646*, 255 – 261.

[69] Pangborn, A. B.; Giardello, M. A.; Grubbs, R. H.; Rosen, R. K.; Timmers, F. J. *Organometallics* **1996**, *15*, 1518–1520.

[70] Joly, K. M.; Kariuki, B. M.; Coe, D. M.; Cox, L. R. *Organometallics* **2005**, *24*, 358–366.

[71] Sheldrick, G. M. *SHELXTL*; Bruker AXS, Inc.: Madison, WI (USA), 2005–2008.

[72] Sheldrick, G. M. *Acta Crystallogr., Sect. A: Fundam. Crystallogr.* **1990**, *46*, 467–473.

[73] Sheldrick, G. M. *Acta Crystallogr., Sect. A: Fundam. Crystallogr.* **2008**, *64*, 112–122.

[74] Sheldrick, G. M. *SHELXL-97: Program for crystal structure determination*; University of Göttingen, 1997.

[75] Müller, P.; Herbst-Irmer, R.; Spek, A. L.; Schneider, T. R.; Sawaya, M. R. *Crystal Structure Refinement: A Crystallographer's Guide to SHELXL*; Müller, P., Ed.; IUCr Texts on Crystallography; Oxford University Press: Oxford, 2006.

[76] The Reciprocal Net Site Network is a distributed database for crystallographic information, supported by the National Science Digital Library, and is run by participating crystallography labs across the world. Crystallographic data for complexes in this chapter are available under the identification codes listed in Tables 3.4 and 3.5 from the MIT Reciprocal Net site. `http://reciprocal.mit.edu/recipnet`.

[77] These data can be obtained free of charge from The Cambridge Crystallographic Data Centre via `http://www.ccdc.cam.ac.uk/data_request/cif`.

[78] Fonseca Guerra, C.; Snijders, J. G.; te Velde, G.; Baerends, E. J. *Theo. Chem. Acc.* **1998**, *99*, 391–403.

[79] Vosko, S. H.; Wilk, L.; Nusair, M. *Can. J. Phys.* **1980**, *58*, 1200–1211.

[80] Becke, A. D. *Phys. Rev. A* **1988**, *38*, 3098–3100.

[81] Perdew, J. P. *Phys. Rev. B* **1986**, *33*, 8822–8824; erratum: *Phys. Rev. B* **1986**, *34*, 7406.

[82] vanLenthe, E.; Snijders, J. G.; Baerends, E. J. *J. Chem. Phys.* **1996**, *105*, 6505–6516.

[83] van Lenthe, E.; Baerends, E. J.; Snijders, J. G. *J. Chem. Phys.* **1994**, *101*, 9783–9792.

[84] van Lenthe, E.; Ehlers, A.; Baerends, E. J. *J. Chem. Phys.* **1999**, *110*, 8943–8953.

[85] van Lenthe, E.; Baerends, E. J.; Snijders, J. G. *J. Chem. Phys.* **1993**, *99*, 4597–4610.

[86] Kohout, M. *Dgrid*; 4.3, 2008.

[87] Schreckenbach, G.; Ziegler, T. *Int. J. Quantum Chem.* **1997**, *61*, 899–918.

[88] Schreckenbach, G.; Ziegler, T. *J. Phys. Chem.* **1995**, *99*, 606–611.

[89] Wolff, S. K.; Ziegler, T. *J. Chem. Phys.* **1998**, *109*, 895–905.

[90] Wolff, S. K.; Ziegler, T.; van Lenthe, E.; Baerends, E. J. *J. Chem. Phys.* **1999**, *110*, 7689–7698.

[91] van Wüllen, C. *Phys. Chem. Chem. Phys.* **2000**, *2*, 2137–2144.

CHAPTER 4

Forays into Nitrogen and Arsenic Chemistry of Niobium Trisamides

Contents

4.1 Investigations of the Potential N_2 Chemistry of Niobium Trisamide and Trisanilide Systems

The previous three chapters have focused on chemistry derived from P_4 activation by the niobium platform Nb(N[$CH_2{}^tBu$]Ar)$_3$ (Ar = 3,5-dimethylphenyl). However, within the Cummins group, and the inorganic community at large, there has also been a long-standing interest in dinitrogen activation for efficient incorporation of the nitrogen atoms of N_2 into organic molecules.[1–8] Recent work by Curley *et al*. has made use of NMo(N[^{t}Bu]Ar)$_3$, **43**, to afford nitriles in good yields through a synthetic cycle that stems from the spontaneous, homobimetallic N_2-cleavage reaction of Mo(N[^{t}Bu]Ar)$_3$.[8] Figueroa *et al*. have shown that the Mo/Nb, heterobimetallic complex (Ar[^{t}BuCH$_2$]N)$_3$NbN$_2$Mo(N[^{t}Bu]Ar)$_3$ will, upon $1e^-$ reduction, also cleave N_2. This reaction affords the anionic, terminal nitride complex [NNb(N[$CH_2{}^tBuAr$)$_3$]$^-$, **44**, along with the neutral molybdenum nitride **43**.[7] The anionic nitride complex **44** was shown to react readily with acid chlorides to yield nitriles accompanying the formation of the strong Nb≡O bond in oxoniobium **21**. The oxoniobium complex can then be recycled back to the niobium nitride **44** in a closed synthetic cycle. In this scheme, however, molybdenum is necessary to accomplish the N_2-binding step, and one half of the N_2 molecule gets funneled to the less reactive **43** and goes unused.

A proposed niobium-based synthetic cycle for conversion of N_2 to organic nitriles is depicted in Scheme 4.1. Such a scheme is attractive because both atoms of N_2 are converted to the versatile, reactive nitride anion **44**. The two steps comprising the left side of this cycle have already been developed as part of the heterobimetallic system described above.[7] Depicted on the right side of the scheme are the remaining hurdles to a closed, versatile dinitrogen incorporation cycle. These are:

(1) Binding of dinitrogen by the niobium trisamide platform to form (μ-N_2)[Nb(N[$CH_2{}^tBu$]Ar)$_3$]$_2$, and

(2) Reductive cleavage of this species to two molecules of a terminal nitride.

With regard to the first goal, there are several low-coordinate, d^2, group 5 systems that are reported to bind dinitrogen, including V(Mes)$_3$, V($CH_2{}^tBu$)$_3$, V(NCy$_2$)$_3$, and Nb(NCy$_2$)$_3$.[9–12] For the amide donor systems, these molecules possess strong metal-nitrogen bonds and display metrical parameters that are consistent with a high degree of dinitrogen reduction. These properties should aid in carrying out the second step, which is reminiscent of the reduction of the analogous μ-P_2 complex to two equivalents of a terminal phosphide anion.

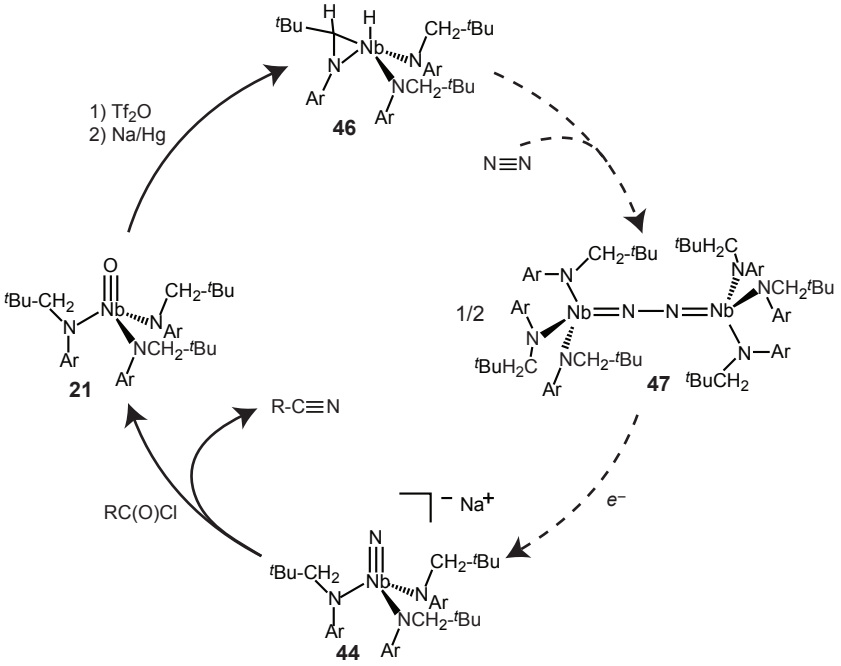

Scheme 4.1. A hypothetical cycle for niobium-mediated N_2 functionalization. The two steps on the left are known, while the two on the right are desired.

4.1.1 Investigations of the Niobium Tris(dicyclohexylamide) System

To gain insight into the N_2 binding step, it was decided to study a system where such a reaction was reported to occur. Of particular interest was Gambarotta's report of the N_2-derived complex, $N_2[Nb(NCy_2)_3]_2$, because this particular niobium fragment is similar to the $Nb(N[CH_2{}^tBu]Ar)_3$ platform. Not only is the metal supported by three amide ligands, but both cyclohexyl amides and neopentyl anilides have displayed a propensity to form niobaziridine rings.[12,13] The bridging N_2 complex $N_2[Nb(NCy_2)_3]_2$ is reportedly formed via a reduction of the niobaziridine chloride complex $ClNb(\eta^2\text{-}C_6H_{10}{=}NCy)(NCy_2)_2$ with $NaHBEt_3$ in toluene under an N_2 atmosphere.[12] It was thus tempting to suggest a pathway for this reaction wherein a hydride substitutes for the niobium-bound chloride to yield an intermediate niobaziridine hydride complex, $HNb(\eta^2\text{-}C_6H_{10}{=}NCy)(NCy_2)_2$, **45**. A retrocyclometallation upon dinitrogen binding to the metal, followed by capping with a second equivalent of **45** could then afford the observed $N_2[Nb(NCy_2)_3]_2$ product. To test this hypothesis, an independent synthesis of the niobaziridine hydride **45** was sought so that its reaction with N_2 could be studied.

The synthetic route developed for $HNb(\eta^2\text{-}{}^t\text{BuCH}{=}\text{NAr})(N[CH_2{}^t\text{Bu}]\text{Ar})_2$, **46**, in Section A.1 was readily amenable to a synthesis of **45**. Three dicyclohexylamide ligands were introduced onto $ONbCl_3(THF)_2$ to yield $ONb(NCy_2)_3$. The Nb–O bond was then activated with Tf_2O to afford the tris(amide)bis(triflate)niobium complex. Removal of the triflate groups by reduction with magnesium anthracene afforded the niobaziridine hydride complex **45**, Scheme 4.2. This compound was characterized by NMR, as well crystallographically in the triclinic space group $P\bar{1}$, Figure 4.1.

The hydride ligand was found in the ^{1}H NMR spectrum as a broad resonance at 9.0 ppm, and also located crystallographically in the Fourier difference map at a distance 1.8 Å from Nb. This niobium hydride complex was further characterized through its reaction with benzaldehyde, which readily inserts into the Nb–H bond to afford a C_s-symmetric benzyloxy complex, Scheme 4.3. This reaction is analogous to the insertion of benzaldehyde into HNb(η^2-^{t}BuCH=NAr)(N[CH$_2$^{t}Bu]Ar)$_2$ and is characteristic of the niobaziridine hydride functional group.[13,14]

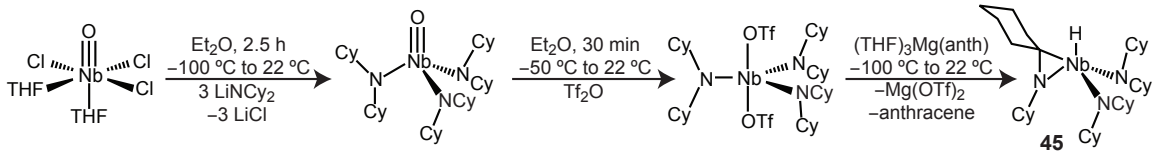

Scheme 4.2. Synthesis of HNb(η^2-C$_6$H$_{10}$=NCy)(NCy$_2$)$_2$ (**45**).

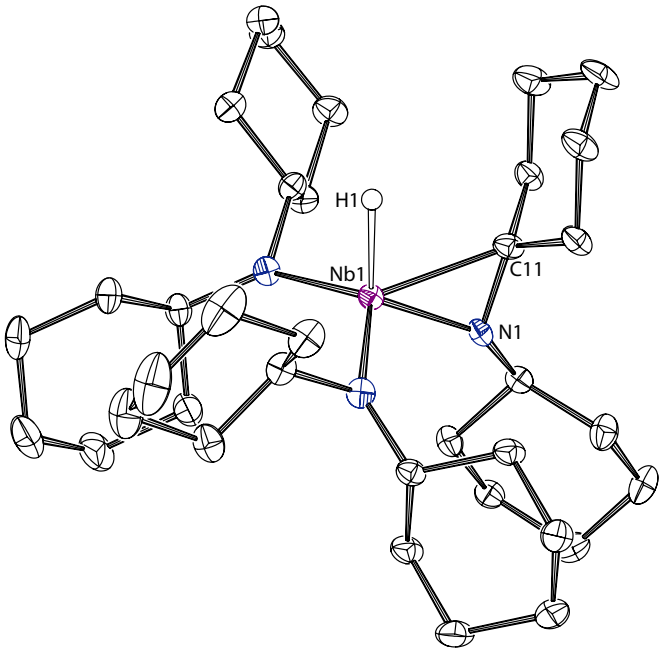

Figure 4.1. Thermal ellipsoid plot (50% probability) of **45** with hydrogen atoms at calculated positions omitted for clarity.

In light of Gambarotta's synthesis of N$_2$[Nb(NCy$_2$)$_3$]$_2$, it was surprising that **45** does not bind N$_2$ over days at atmospheric pressure in toluene, even in the presence of NaHBEt$_3$ or BEt$_3$, Scheme 4.3.[12] These results suggest that **45** is either not an intermediate in the reaction that affords N$_2$[Nb(NCy$_2$)$_3$]$_2$, or that its reaction with N$_2$ is promoted by impurities in certain reaction mixtures. Moreover, the niobaziridine chloride complex ClNb(η^2-C$_6$H$_{10}$=NCy)(NCy$_2$)$_2$—synthesized by reaction of **45** with CH$_2$Cl$_2$—has neither yielded N$_2$[Nb(NCy$_2$)$_3$]$_2$ nor **45** when

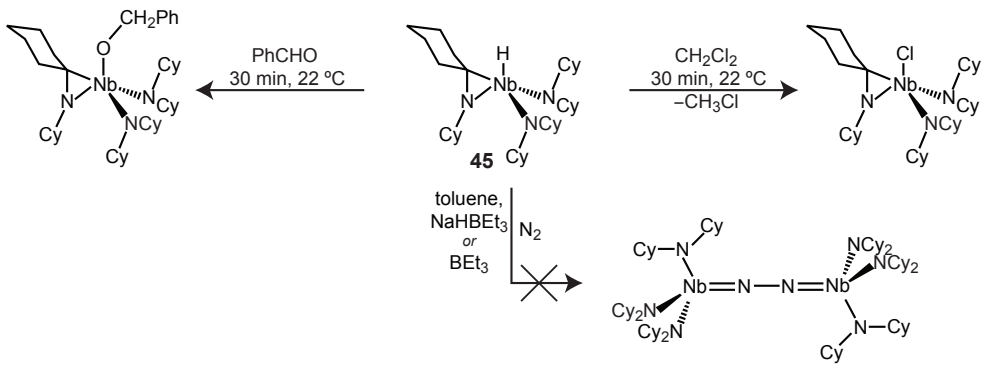

Scheme 4.3. Niobaziridine hydride **45** inserts benzaldehyde and reacts with CH_2Cl_2. It does not, however, bind N_2.

treated with $NaHBEt_3$ in our hands; in fact, no reaction between the niobaziridine chloride and $NaHBEt_3$ was observed in toluene over 24 h. This is in direct contrast to the literature report and suggests a complicated reaction mechanism for the formation of $N_2[Nb(NCy_2)_3]_2$ that is very sensitive to the exact nature of the reaction mixture. In any case, it is apparent that much remains to be understood about the factors that affect N_2-binding by niobium trisamide systems.

4.1.2 Synthesis of the Homobimetallic Complex (μ-N_2)[Nb(N[$CH_2{}^tBu$]Ar)$_3$]$_2$

Though conditions under which the Nb(N[$CH_2{}^tBu$]Ar)$_3$ platform can pick up and bind N_2 have remained elusive, the potential viability of (μ-N_2)[Nb(N[$CH_2{}^tBuAr$)$_3$]$_2$, **47**, as a precursor to the niobium nitride anion **44** was of interest. Accordingly, an independent synthesis of **47**, and conditions for its reduction to the terminal nitride anion **44**, were investigated.

Schrock and co-workers first reported the μ-N_2 complex $(N_2)[NbCl_3(THF)_2]_2$, which seemed a suitable starting material for synthesis of **47**.[15] An alternate preparation of this compound was reported by Dilworth *et al.*, making it available in one step from $NbCl_5$ and tetrakis(trimethylsilyl)hydrazine;[16] the latter is available in one step from commercially available hydrazine and tetramethyldisilane.[17] The synthesis of **47** was achieved by introduction of 6 equivalents of $(Et_2O)LiN[CH_2{}^tBu]Ar$ to purple $(N_2)[NbCl_3(THF)_2]_2$ in thawing Et_2O, warming to 22 °C, and stirring for several hours, Scheme 4.4. Extraction of the yellow product with benzene, trituration with *n*-hexane, and precipitation from cold *n*-pentane afforded **47** in 91% yield as a canary yellow powder. The structure of **47** was confirmed by a single-crystal X-ray diffraction study. This molecule, shown in Figure 4.2, crystallizes in the monoclinic space group $C2/c$ with half a molecule per asu: the C_2 axis skewers the molecule through the N–N bond. The Nb–N distance of 1.795(2) Å and N–N distance of 1.291(4) Å are consistent with a heavily back-bonded system and a strongly reduced dinitrogen unit. The N–N distance in **47** is 0.19 Å longer than in

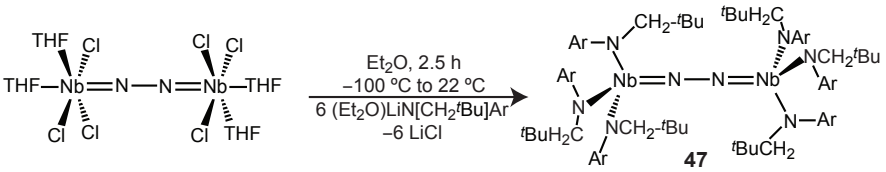

Scheme 4.4. Synthesis of $(\mu\text{-}N_2)[Nb(N[CH_2{}^tBu]Ar)_3]_2$ (**47**).

free dinitrogen.[18] Moreover, a strong Raman stretch attributed to the N–N bond of **47** was located at 1337 cm^{-1} in benzene, also indicative of a very reduced dinitrogen unit.

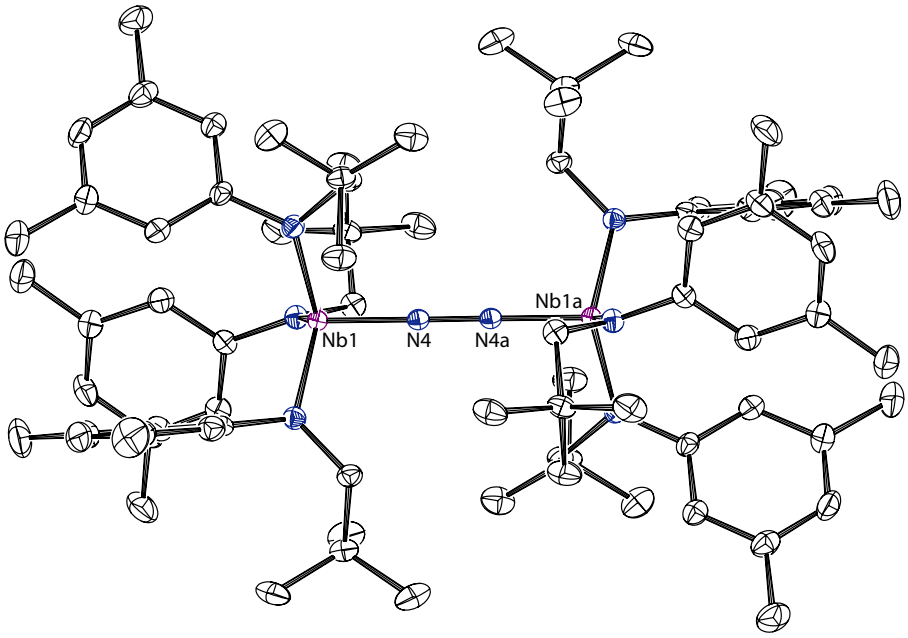

Figure 4.2. Thermal ellipsoid plot (50% probability) of **47** with hydrogen atoms omitted for clarity.

Having secured a synthesis of **47**, albeit not from dinitrogen, the reduction chemistry of this species was investigated. A cyclic voltammogram of **47** revealed one reversible reduction event at –2650 mV (vs. Fc/Fc^+). This is the only electrochemical event within the THF solvent window and likely corresponds to the $1e^-$ [**47**]/[**47**]$^-$ couple. The assignment as a $1e^-$ reduction event is supported by analogy to the electrochemistry of related molybdenum species that can be isolated in three states of charge.[5] This reduction event would form a molecule that is isoelectronic to the neutral $(Ar[^tBuCH_2]N)_3NbN_2Mo(N[^tBu]Ar)_3$, which is $1e^-$ shy of cleaving the N–N bond.

The very negative potential for the first reduction of **47** suggested that a *very* potent reductant would be needed to afford the $2e^-$ reductive cleavage to **44**. Indeed, neither Mg metal, nor $(THF)_3Mg(C_{14}H_{10})$, nor $K_2(C_8H_8)$ reduced the μ-N_2 complex. In one experiment, reduction of **47** to $Na[NNb(N[CH_2{}^tBu]Ar)_3]$ was afforded by treatment with sodium metal in THF over 18 h

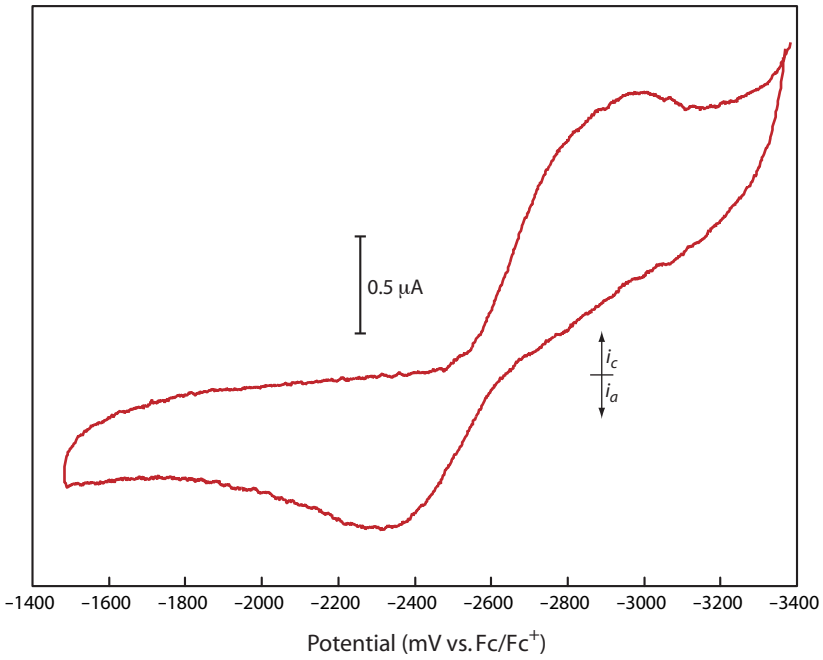

Figure 4.3. Cyclic voltammogram of (μ-N_2)[Nb(N[$CH_2{}^t$Bu]Ar)$_3$]$_2$ in THF with 0.2 M [Bu_4N][PF_6] electrolyte and a sweep rate of 300 mV/s.

in 16% yield. However, attempts to reproduce this result yielded only Na(N[$CH_2{}^t$Bu]Ar) as the isolated product. As a result, a very strong but soluble reductant was sought. These criteria are met by sodium naphthalenide, which has a reduction potential in THF of –3.10 V.[19] When a green THF solution of freshly prepared sodium naphthalenide was added to an orange solution of **47** the green color rapidly dissipated giving way to a yellow-brown solution. From the product mixture the desired anionic nitride complex , **44**, was isolated in 52% yield by precipitation from *n*-pentane and recrystallization from THF/Et_2O. This reduction is reproducible and demonstrates that the μ-N_2 complex **47** is susceptible to reductive cleavage. This cleavage reaction could serve as one step in a potential niobium-based N_2 fixation cycle.[i]

4.2 Activation Chemistry of As_4 by Niobium and Molybdenum Trisanilides

Relative to the chemistry of terminal phosphides, the chemistry of terminal arsenide complexes is even more scarce.[20,21] A few examples were prepared independently by Schrock and Scheer on molybdenum and tungsten trisamido amine scaffolds.[22,23] Niobium indium arsenide Zintl phase ions that bear terminal niobium arsenide “handles” on cubane structures have also been reported.[24,25] Reaction chemistry of these species, however, is largely unexplored. Given the

[i]Initial experiments showed that reductive cleavage of **47**, quenching with ^{t}BuC(O)Cl, and vacuum transfer of the volatiles onto an internal standard afforded ^{t}BuCN in 30% yield, prior to optimization.

rich chemistry that has developed for terminal phosphide complexes, there was interest in investigating some related arsenic compounds. However, molecular, yellow arsenic, As_4, unlike white phosphorus, is photochemically and thermally unstable in the solid state, which precludes the use and handling of solid As_4 as a starting material.[18,26] Solutions of yellow arsenic are considerably more stable than the solid and can be prepared by sublimation of gray arsenic at elevated temperatures (>550 °C) under a stream of inert gas and collection of the As_4 vapors by bubbling through a chilled solvent.[27] This method has been applied in a handful of cases when As_4 was desired for reactions with organometallic fragments.[28–32]

The first samples of As_4 in our lab were made in small quantities using glass reaction vessels developed for this purpose. In these setups, solid grey arsenic was heated in a side arm using heating tape or a propane gas flame while a stream of argon carried the vapors down a tube into a dry-ice–cooled toluene solution. The exiting gas stream was then funneled through a bleach bubbler before being passed into the fume hood. Keeping the solution in the dark, it was quickly transferred into an inert-atmosphere glove box, and was then treated with small quantities of a metal complex. Unfortunately, these toluene solutions were of relatively low and unknown arsenic concentrations and so initial scales were limited to *ca.* 100 mg of metal complex. A procedure for larger scale preparations of As_4 that utilizes a custom built tube furnace setup has since been developed in our group, allowing for multi-gram syntheses. This apparatus is based on one described in early reports of As_4 generation by Erdmann and the modern version has recently been described by Spinney *et al.*[27,33]

4.2.1 A Molybdenum Terminal Arsenide Complex

In analogy to its P_4 activation chemistry, $Mo(N[^tBu]Ar)_3$ reacts with solutions of As_4 to generate the terminal arsenide complex $AsMo(N[^tBu]Ar)_3$, **48**. This compound represents the first terminal arsenide complex generated directly from molecular arsenic. An X-ray crystal structure determination revealed the Mo–As distance in **48** to be 2.2248(5) Å, the shortest such distance reported to date, Figure 4.4.[34] In collaboration with John Curley, the Mo–As stretching mode was located in the IR and Raman spectra of **48** by comparison to independent samples of the related phosphide complex, $PMo(N[^tBu]Ar)_3$. The Mo–As stretch is at 394 cm^{-1}, while the related Mo–P stretch resonates at 538 cm^{-1}. Under the harmonic oscillator approximation, these values correspond to force constants of 3.9 and 4.0 mdyne $Å^{-1}$, respectively, indicating that the bonding in the terminal arsenide and phosphide ligands is quite similar. For comparison, the Mo–N bond of the terminal nitride has a force constant roughly twice as large, at 7.8 mdyne $Å^{-1}$.[35]

Initial reactivity screening of **48** revealed it to be even more inert than its phosphorus analog. For example, **48** shows no reaction with dimethyl dioxirane, S_8, or $SSbPh_3$, all reagents that serve to install a terminal chalcogen onto the related phosphide ligand.[36–38] The observed lack of reactivity

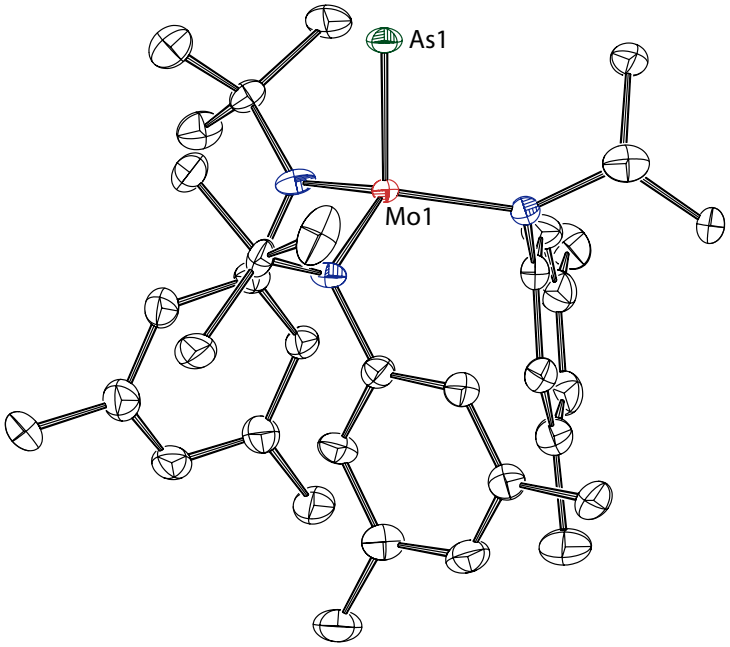

Figure 4.4. Thermal ellipsoid plot (50% probability) of **48** with hydrogen atoms omitted for clarity.

in these cases is consistent with a heavily depressed lone pair and can be regarded as a manifestation of the inert pair effect.[39,40]

4.2.2 A Niobium Terminal Arsenide Complex

The synthesis of **48** serves as an example of an As_4-derived terminal arsenide complex, but initial studies suggested that the reaction chemistry of this neutral compound would prove very limited. In contrast, an anionic terminal arsenide complex might exhibit rich reactivity, similar to the phosphide anion **3**. In particular, the arsenide anion might serve as a precursor to an arsaphosphaazide complex that is analogous to the diphosphaazide complex **1** and is a potential source of the heterodiatomic molecule AsP.

The diniobium μ-P_2 complex, (μ-P_2)[Nb(N[$CH_2{}^t$Bu]Ar)$_3$]$_2$, is formed from P_4 and the niobaziridine hydride complex HNb(η^2-^{t}BuCH=NAr)(N[$CH_2{}^t$Bu]Ar)$_2$, **46**, in high yield.[13] It was believed that treatment of **46** with As_4 would similarly yield the μ-As_2 complex.[41] Indeed, addition of **46** to toluene solutions of As_4 afforded the desired bridging As_2 complex, (μ-As_2)[Nb(N[$CH_2{}^t$Bu]Ar)$_3$]$_2$, **49**, as a green powder following removal of grey arsenic and precipitation from *n*-hexane, Scheme 4.5. By ^{1}H NMR spectroscopy, **49** is nearly identical to the phosphorus analogue. An X-ray diffraction study similarly revealed that **49** is both isomorphous and isostructural to its phosphorous analogue. While the X-ray structure solution suffered from crystallographic maladies, the butterfly core was resolved with an As–As distance of 2.38 Å and an average Nb–As distance of 2.6 Å. This As–As bond is only slightly shorter than the single bonds in

As_4 (2.435 Å), and longer than As–As double bonds such as in the terphenyl diarsenes reported by Power (2.28 Å).[42] These data indicate a high degree of backbonding into the As_2 unit of **49**, such that a description which contains an As–As single bond is most appropriate.

Reduction of **49** by 1% sodium amalgam in THF afforded the terminal arsenide complex, $[AsNbN(CH_2tBu]Ar)_3]^-$, **50**, again spectroscopically similar to the phosphorus analogue, Scheme 4.5. This complex was characterized crystallographically as a sodium bridged dimer with one niobium arsenide per asu, Figure 4.5. The Nb–As distance was found to be 2.3106(3) Å. The fact that this bond is nearly 0.1 Å longer than the Mo–As bond in **48** can be attributed to the anionic charge of **50**. It is this negative charge that opens this arsenide complex to a wealth of potential chemistry.

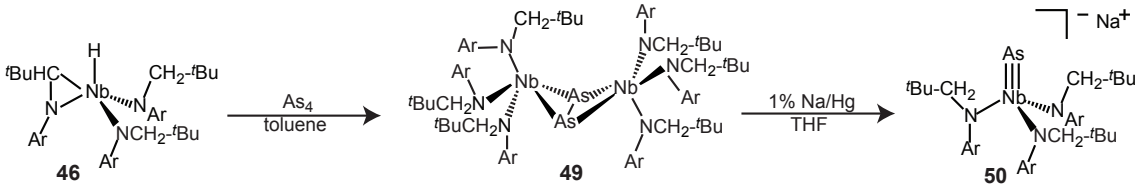

Scheme 4.5. Synthesis of $(\mu\text{-}As_2)[Nb(N[CH_2{}^tBu]Ar)_3]_2$ (**49**) and $[AsNb(N[CH_2{}^tBu]Ar)_3]^-$ (**50**).

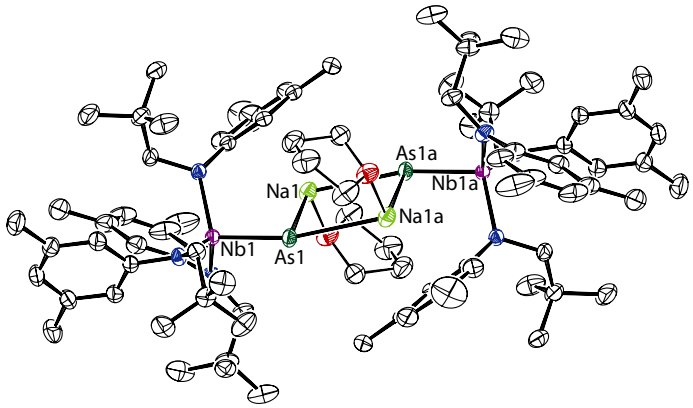

Figure 4.5. Thermal ellipsoid plot (50% probability) of dimeric [(THF)Na][**50**] with hydrogen atoms omitted for clarity.

4.3 Complexes for the Potential Elimination of AsP and PN

In Chapter 1, the P_2-elimination chemistry of a diphosphaazide complex was described. The synthesis of this diphosphaazide complex was afforded by the nucleophilicity of the niobium phosphide anion **3**. The N_2 cleavage reactions of $(Ar[{}^tBuCH_2]N)_3Nb(\mu\text{-}N_2)Mo(N[{}^tBu]Ar)_3$ and **47** provide syntheses of the nitride anion $[NNb(N[CH_2{}^tBu]Ar)_3]^-$, **44**, and a preparation of the arsenide anion **50** is described above.[7] Having these reagents in hand, an expansion of the diphosphaazide

chemistry to a monophosphaazide complex and an arsaphosphaazide complex was sought, as these complexes are potential precursors to the heterodiatomic molecules PN and AsP, respectively.

4.3.1 A Monophosphaazide Complex

The monophosphaazide complex (Mes*NPN)Nb(N[$CH_2{}^t$Bu]Ar)$_3$, **51**, was prepared by addition of Mes*NPCl to a thawing suspension of Na[**44**] in Et_2O and stirring for 1 h, Scheme 4.6. The product was isolated as an orange powder in 78% yield following removal of NaCl and precipitation from *n*-pentane. This monophosphaazide complex has its phosphorus in the β position, and this nucleus has a ^{31}P NMR chemical shift of 243 ppm. Characterization by single-crystal X-ray diffraction revealed a short Nb imido bond, 1.8222(11) Å, a nearly linear Nb–N–P linkage of 157.81(7)°, and alternating long and short P–N distances, 1.6630(11) Å to the imido nitrogen N4 and 1.5518(12) Å to N5, Figure 4.6. These data are all consistent with the representation of this product as an iminophosphane-substituted niobium imido complex. As such, it is not surprising that thermolysis of this compound at temperatures of up to 90 °C did not afford extrusion of the PN molecule to form the Mes* imido **2**. Not only has the driving force for formation of **2** been removed by starting with a strong niobium imido bond, but the preference for a linear imido bond also adds a barrier to any intramolecular rearrangement that puts the γ nitrogen (N5) on the niobium center. The related ^{t}BuNPN ligand has been previously synthesized atop V(N[^{t}Bu]Ar)$_3$ and Nb(N[^{t}Bu]Ar)$_3$ platforms using a dehydrohalogenation strategy.[43] While the latter niobium species was observed to dimerize at the P=N bond upon concentration, neither the Vn or Nb species were observed to eliminate the PN fragment.[43]

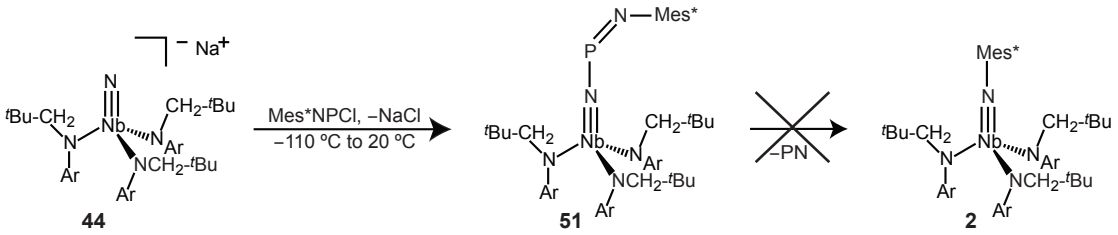

Scheme 4.6. Synthesis of (Mes*NPN)Nb(N[$CH_2{}^t$Bu]Ar)$_3$ (**51**), which does not form imido **2** under thermolysis, photolysis, or treatment with (THF)W(CO)$_5$.

It was seen that introduction of a W(CO)$_5$ unit to the diphosphaazide complex **1** lowered the barrier to formation of **2** and extrusion of the P_2 fragment, so this strategy was also examined in the context of the monophosphaazide system. Treatment of **51** with (THF)W(CO)$_5$ afforded a new product—believed to be a simple σ complex formed by using the P lone pair of **51** as a ligand for W(CO)$_5$—but this product does not go on to form **2** with extrusion of the PN unit. Irradiation of **51** with UV light for several days in C_6D_6 also did not afford **2**. It seems that if a monophosphaazide complex of Nb(N[$CH_2{}^t$Bu]Ar)$_3$ is going to serve a precursor to the PN molecule, the driving force for formation of this high energy species needs to be restored. This can likely be accomplished

through a synthesis of the isomeric monophosphaazide complex (Mes*NNP)Nb(N[$CH_2{}^tBu$]Ar)$_3$. The synthetic challenges involved in the synthesis of such a complex make it a thus far elusive target, but an attractive one for future work.

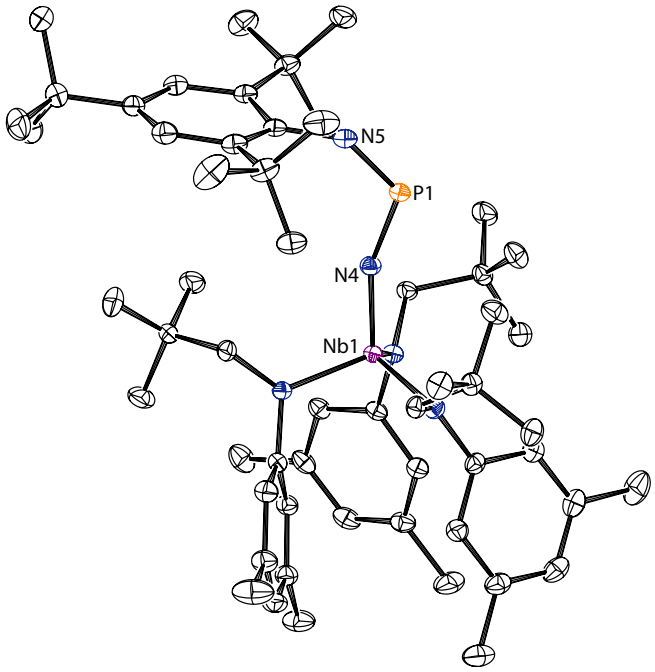

Figure 4.6. Thermal ellipsoid plot (50% probability) of **51** with hydrogen atoms omitted for clarity.

4.3.2 An Arsaphosphaazide Complex

The similarities between arsenic and phosphorus are much greater than those between phosphorus and nitrogen. It thus seemed likely that even though **51** was, in fact, not a PN-eliminating complex, the arsaphosphaazide complex (Mes*NPAs)Nb(N[$CH_2{}^tBu$]Ar)$_3$, **52**, would show reactivity more akin to that of **1**. Accordingly, **52** was synthesized analogously to **1** by substituting the terminal arsenide **50** for the terminal phosphide **3**, Scheme 4.7. The arsaphosphaazide complex **52** is spectroscopically similar to **1** by ^{1}H NMR spectroscopy, and displays a single ^{31}P NMR resonance at 348 ppm, 33 ppm downfield of the analogous signal in the diphosphaazide complex. The solid-state structure of **52** is also both isomorphous and isostructural to the diphosphorus analogue, **1**. The structure of **52** displays an η^2-AsP complexation of the arsaphosphaazide ligand with a long Nb–As distance of 2.6704(3) Å that is considerably longer than the sum of covalent radii, r_{As}(1.19 Å) + r_{Nb}(1.37 Å) = 2.56 Å. The As–P distance is meanwhile very short at 2.1296(6) Å (*cf.* 2.00 Å in AsP) and the P–N distance of 1.564(2) Å is about that in doubly-bonded iminophosphanes.[44,45] These data are all consistent with the delocalized, multiple bonding descriptions provided for **1**.

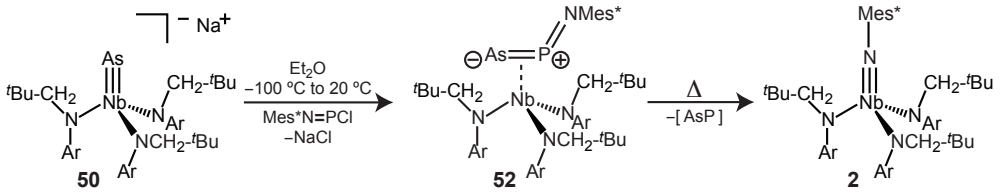

Scheme 4.7. Synthesis of (Mes*NPAs)Nb(N[$CH_2{}^tBu$]Ar)$_3$ (**52**).

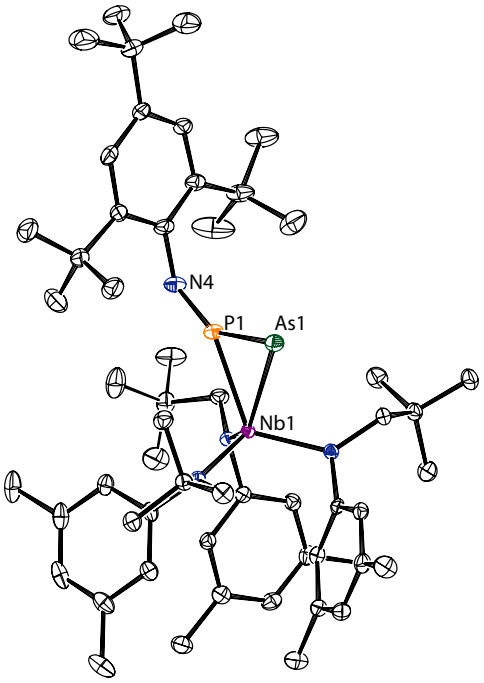

Figure 4.7. Thermal ellipsoid plot (50% probability) of **52** with hydrogen atoms omitted for clarity.

This arsaphosphaazide complex is also noteworthy as it contains a chain of three different group 15 elements.

The arsaphosphaazide complex **52** was found to be thermally sensitive with respect to formal AsP loss to give niobium imido **2**. This observation was promising for potential solution phase chemistry of the heterodiatomic AsP, but this proposed intermediate seemed to be even more difficult to engage in clean reactivity than the putative P_2 intermediate of Chapter 1. For example, heating a solution of **52** in neat cyclohexadiene for several hours did not give any major product in appreciable yields. While a ^{31}P NMR resonance consistent with the diene trapping product AsP(C_6H_8)$_2$ could be located at –79 ppm (*cf.* –80 ppm for the P_2 analogue), the intensity of the signal indicated that the concentration of this species was very low.

Introduction of the W(CO)$_5$ group to the arsenic center in **52** was found to accelerate the formation of niobium imido **2**, and aid in increasing the efficiency at which the AsP unit could be incorporated into substrate molecules. As for P_2, these effects likely arise from stabilization of the AsP molecule by complexation to the W center. The product (OC)$_5$W(AsP)(C_6H_8)$_2$ was

identified in the product mixture resulting from a reaction in which cyclohexadiene was introduced to a solution of *in situ* generated **52**-$W(CO)_5$ and the mixture was stirred for several hours. In this trapping product the $W(CO)_5$ group was found coordinated to phosphorus, as judged by ^{183}W satellites in the ^{31}P NMR spectrum ($^1J_{WP}$ = 220 Hz). This suggests that an intermediate bearing As–P multiple bonding, which could mediate the migration process, was present at some point during the course of the reaction (see Section 1.6.4). This is, of course, consistent with the working hypothesis that (AsP)$W(CO)_5$ exists as a discrete molecule in the course of these trapping experiments.

The synthesis and chemistry of this arsaphosphaazide complex, including optimized procedures for As_4 generation, trapping reactions of AsP with terminal phosphide complexes, and various trappings of (AsP)$W(CO)_5$ have since been worked out beautifully by Dr. Heather Spinney and are the subject of an upcoming publication.[33]

4.4 Experimental Details

4.4.1 General Considerations

All manipulations were performed in a Vacuum Atmospheres model MO-40M glove box under an atmosphere of purified dinitrogen. Solvents were obtained anhydrous and oxygen-free from a Contour Glass Solvent Purification System, or by analogous methods.[46] Celite 435 (EM Science), 4 Å molecular sieves (Aldrich), and alumina (EM Science) were dried by heating at 200 °C under dynamic vacuum for at least 24 hours prior to use. All glassware was oven-dried at temperatures greater than 170 °C prior to use. Deuterated solvents for NMR spectroscopy were purchased from Cambridge Isotope Labs. Benzene-d_6 was degassed and stored over molecular sieves for at least 2 days prior to use. $CDCl_3$ was distilled off of CaH_2 and stored over molecular sieves. The compounds $ONbCl_3(THF)_2$,[47] (μ-N_2)[$NbCl_3(THF)_2$]$_2$,[16] Na[NNb(N[$CH_2{}^t$Bu]Ar)$_3$],[7] Mo(N[^{t}Bu]Ar)$_3$,[6] and Mes*NPCl,[48] were prepared according to literature procedures. Dienes were purchased from Aldrich, distilled from $NaBH_4$, and stored over molecular sieves prior to use. $LiNCy_2$ (Aldrich) and $W(CO)_6$ (Strem) were purchased and used as received. NMR spectra were obtained on Varian Mercury 300 or Varian Inova 500 instruments equipped with Oxford Instruments superconducting magnets. ^1H NMR spectra were referenced to residual C_6D_5H (7.16 ppm) or $CHCl_3$ (7.27 ppm). ^{13}C NMR spectra were referenced to C_6D_6 (128.39 ppm) or $CDCl_3$ (77.23 ppm). ^{31}P NMR spectra were referenced externally to 85% H_3PO_4 (0 ppm). Elemental analyses were performed by Midwest Microlab, LLC (Indianapolis, Indiana).

4.4.2 Preparation of $ONb(NCy_2)_3$

Solid $LiNCy_2$ (7.0 g, 59.3 mmol, 3.04 eq) was added to a thawing Et_2O slurry (100 mL) of $ONbCl_3(THF)_2$ (7.0 g, 19.5 mmol, 1 eq). The color of the mixture changed from white to purple and then brown over the course of the addition and the following 2.5 h, over which time it was stirred while warming to 23 °C. After this time, the mixture was filtered through Celite and then dried *in vacuo*. The residue was extracted with a *n*-pentane/toluene mixture and filtered once more. Precipitation from 30 mL of *n*-pentane at –35 °C afforded the desired product as an off-white powder (4.95 g, 40% yield). Bright white powders were obtained by crystallization from toluene/Et_2O. ^{1}H NMR (C_6D_6, 500 MHz, 20 °C): δ 3.01 (m, 6H, NC*H*), 1.89 (m, 12H, Cy), 1.79 (dd, 24H, Cy) 1.57 (d, 6H, Cy), 1.32 (q, 12H, Cy), 1,18 (t, 6H, Cy) ppm. ^{13}C NMR (C_6D_6, 125.8 MHz, 20 °C): δ 60.1 (N*C*), 37.2 (Cy), 27.7 (Cy), 26.4 (Cy) ppm. Elem. Anal. Calcd for $C_{36}H_{66}N_3ONb$: C, 66.54; H, 10.24; N, 6.47. Found: C, 66.74; H, 10.02; N, 6.48.

4.4.3 Preparation of $(TfO)_2Nb(NCy_2)_3$

To a *ca*. –50 °C, yellow-brown solution of $ONb(NCy_2)_3$ (2.9 g, 4.46 mmol) in Et_2O (80 mL) was added a –35 °C solution of Tf_2O (1.25 g, 4.43 mmol, 0.98 mmol) in Et_2O (10 mL). Upon addition, the solution turned bright yellow concomitant with the formation of a yellow precipitate. After stirring for 30 min, the solids were filtered off and washed with *n*-pentane to afford the desired product (3.6 g, 3.86 mmol, 87% yield). ^{1}H NMR (C_6D_6, 500 MHz, 20 °C): δ 4.86 (m, 6H, NC*H*), 2.24 (m, 12H, Cy), 1.79 (m, 12H, Cy), 1.58 (m, 30H, Cy), 0.97 (m, 6H, Cy) ppm. ^{13}C NMR (C_6D_6, 125.8 MHz, 20 °C): δ 65.6 (N*C*H), 36.2 (Cy), 27.7(Cy), 26.2 (Cy) ppm. Elem. Anal. Calcd for $C_{38}H_{66}N_3O_6F_6S_2Nb$: C, 48.97; H, 7.14; N, 4.51. Found: C, 48.66; H, 6.87; N, 4.30.

4.4.4 Preparation of $(H)Nb(\eta^2\text{-}C_6H_{10}{=}NCy)(NCy_2)_3$ (45)

To a thawing THF solution of $(TfO)_2Nb(NCy_2)_3$ (250 mg, 0.27 mmol) was added $(THF)_3Mg(C_{14}H_{10})$ (125 mg, 0.30 mmol, 1.1 eq) as a solid in small portions. After the addition, the mixture was allowed to stir for 45 min, and then the solvent was removed under dynamic vacuum. The residue was extracted with thawing *n*-pentane and filtered through pre-chilled Celite to remove anthracene and salts. The filtrate was dried *in vacuo* to give an orange powder which was recrystallized from $Et_2O/O(SiMe_3)_2$ in good yield (*ca*. 70%). ^{1}H NMR (C_6D_6, 500 MHz, 20 °C): δ 9.0 (br s, 1H, Nb*H*), 2.88 (m, 2H), 2.69 (*pseudo*-t, 1H), 2.46 (m, 2H), 1.0-2.1 (m, 60H) ppm. ^{13}C NMR (C_6D_6, 125.8 MHz, 20 °C): 73.4 (N=C), 63.8 (N*C*H), 53.7 (N*C*H), 40.5, 38.9, 38.3, 37.3, 28.6, 27.45, 27.35, 27.3, 27.2, 26.5, 26.4 ppm.

4.4.5 Preparation of (PhCH$_2$O)Nb(η^2-C$_6$H$_{10}$=NCy)(NCy$_2$)$_2$

At –35 °C, an Et_2O solution (2 mL) of benzaldehyde (22 mg, 0.21 mmol, 1.0 equiv) was added to an Et_2O solution (4 mL) of orange HNb(η^2-(C_6H_{11})N=C_6H_{10})(NCy_2)$_3$ (130 mg, 0.21 mmol). The solution immediately lightened slightly to yellow. After 30 min the solvent was removed *in vacuo* to afford the product as a yellow powder. ^{1}H NMR (C_6D_6, 300 MHz, 20 °C): δ 7.78 (d, 2H, *o*-Ph), 7.27 (t, 2H, *m*-Ph), 7.13 (t, 1H, *p*-Ph), 5.73 (s, 2H, PhCH_2), 3.71 (m, 1H), 3.2 (m, 4H), 2.69 (m, 2H), 2.45 (m, 2H), 2.15 (m, 2H), 1.0–2.0 (m, 54H) ppm.

4.4.6 Preparation of (μ-N$_2$)[Nb(N[CH$_2$^{t}Bu]Ar)$_3$]$_2$ (47)

To a thawing suspension of (μ-N_2)[$NbCl_3$(THF)$_2$]$_2$ (2.20 g, 3.08 mmol) in Et_2O (50 mL) was added solid (Et_2O)LiN[CH_2^{t}Bu]Ar (5.10 g, 6.1 eq) in small portions. No immediate color change was observed upon addition, and the purple/white suspension was allowed to warm to room temperature. After 20 min the reaction mixture had begun to turn yellow and was allowed to stir for another 2 h. After this time, the yellow-orange mixture was evaporated to dryness. The product was extracted with 150 mL of benzene and filtered through Celite to remove LiCl. The filtrate was evaporated to dryness, *n*-hexane was added to give a suspension, and the mixture was evaporated to dryness once more. The resulting yellow solids were suspended in *n*-pentane, and this suspension was chilled to –35 °C. The resulting canary yellow precipitate was collected on a sintered glass frit and dried to constant mass (3.81 g, 2.81 mmol, 91% yield). ^{1}H NMR (C_6D_6, 500 MHz, 20 °C): δ 6.59 (s, 3H, *p*-Ar), 6.52 (s, 6H, *o*-Ar), 4.42 (s, 6H, NCH_2), 2.16 (s, 18H, ArCH_3), 1.16 (s, 27H, ^{t}Bu) ppm. ^{13}C NMR (125.8 MHz, C_6D_6, 20 °C): δ 154.0 (*ipso*-Ar), 138.9 (*m*-Ar), 126.0 (*p*-Ar), 123.5 (*o*-Ar), 74.1 (N*C*H_2), 36.3 (*C*(CH_3)$_3$), 29.8 (C(*C*H_3)$_3$), 22.1 (Ar*C*H_3) ppm. Raman (λ_{ex} = 785 nm, C_6H_6 solution): $\Delta\tilde{\nu}_{NN}$ 1377 cm^{-1}. Elem. Anal. Calcd for $C_{78}H_{120}N_8$: C, 69.10; H, 8.92; N, 8.27. Found: C, 69.70; H, 9.01; N, 7.89.

4.4.7 Reduction of (μ-N$_2$)[Nb(N[CH$_2$^{t}Bu]Ar)$_3$]$_2$ to Na[NNb(N[CH$_2$^{t}Bu]Ar)$_3$]

The bottom of a 20 mL vial was smeared with a layer of sodium metal (*ca.* 200 mg) and to it was added a THF solution of naphthalene (100 mg, 0.78 mmol, 2.6 eq) in THF (7 mL), which immediately turned dark green. This mixture was allowed to stir for 2 h before it was added to a solution of (μ-N_2)[Nb(N[CH_2^{t}Bu]Ar)$_3$]$_2$ (400 mg, 0.29 mmol) in THF (10 mL). The green color rapidly dissipated and the mixture was allowed to stir for 20 min before being evaporated to dryness. The residue was triturated once with *n*-hexane, and then the by-products were extracted with *n*-pentane, leaving behind an off-white powder that was recrystallized from THF/Et_2O to yield colorless crystals that were dried to a white powder (212 mg, 0.30 mmol, 52% yield). ^{1}H NMR (THF-d_8, 300 MHz, 20 °C): δ 6.27 (s, 6H, *o*-Ar), 6.11 (s, 3H, *p*-Ar), 4.36 (s, 6H, NCH_2), 1.91 (s,

18H, ArCH_3), 0.83 (s, 27H, ^{t}Bu) ppm. Elem. Anal. Calcd for $C_{39}H_{60}N_4NaNb$: C, 66.84; H, 8.63; N, 7.99. Found: C, 66.61, 8.64; H, 7.91.

4.4.8 Preparation of AsMo(N[^{t}Bu]Ar)$_3$ (48)

This synthesis was performed in collaboration with John Curley: A Schlenk flask containing yellow arsenic in toluene was prepared under argon at *ca*. –30 °C. Solid Mo(N[^{t}Bu]Ar)$_3$ (1.50 g, 2.4 mmol) was added to the mixture via a solid addition flask, forming a yellow-brown solution. The mixture was allowed to sit (with occasional swishing) in the absence of light for 2 h, over which time the mixture warmed to 20 °C. The Schlenk flask was then brought into a glovebox and the mixture was filtered through Celite atop a sintered glass frit to remove grey arsenic. The filtrate was concentrated to dryness under a dynamic vacuum and the remaining residue was taken up in Et_2O/*n*-pentane. The solution so-formed was allowed to stand at –35 °C to precipitate the product, which was collected via filtration atop a sintered-glass frit in several crops (550 mg, 35% yield). ^{1}H NMR (C_6D_6, 400 MHz, 20 °C): δ 6.62 (s, 3H, *p*-Ar), 5.83 (br s, 6H, *o*-Ar), 2.04 (s, 18 H, ArCH_3), 1.67 (s, 27H, C(CH_3)$_3$). ^{1}H NMR ($CDCl_3$, 400 MHz, 20 °C):δ 6.68 (s, 3H, *p*-Ar), 5.75 (s, 6H, *o*-Ar), 2.06 (s, 18H, ArCH_3), 1.43 (s, 27H, C(CH_3)$_3$). ^{13}C NMR ($CDCl_3$, 100 MHz, 20 °C): δ 149.6 (*ipso*-Ar), 138.6 (*m*-Ar), 136.5 (*p*-Ar), 127.4 (*o*-Ar), 59.7 (*C*(CH$_3$)$_3$), 33.9 (C(*C*H$_3$)$_3$), 21.5 (Ar*C*H$_3$) . Elem. Anal. Calcd for $C_{36}H_{54}N_3MoAs$: C, 61.80; H, 7.78; N, 6.01. Found: C, 60.96; H, 7.81; N, 6.07.

4.4.9 Preparation of (μ-As$_2$)[Nb(N[CH$_2$^{t}Bu]Ar)$_3$]$_2$ (49)[ii]

A toluene solution of yellow arsenic (15 mL), generated as described in the text, was added to toluene solution (1 mL) of HNb(η^2-^{t}BuCH=NAr)(N[CH$_2$^{t}Bu]Ar)$_2$ (177 mg, 0.27 mmol) The mixture was stirred in the absence of light for 2 h. After this time the mixture was concentrated to dryness under dynamic vacuum and then the residue was extracted with Et_2O and filtered through Celite to remove grey arsenic. The yellow-green filtrate was concentrated to dryness under a dynamic vacuum and the remaining residue was extracted with cold (–35 °C) *n*-hexane to reveal a dark green powder. The filtrate was extracted once more with $(Me_3Si)_2O$ to afford more green powder, and the two crops were combined (90 mg, 46% yield).^{1}H NMR (C_6D_6, 500 MHz, 20 °C): δ 6.95 (bs, 12H, *o*-Ar), 6.58 (s, 6H, *p*-Ar), 4.26 (s, 12H, NCH_2), 2.23 (s, 36H, ArCH_3), 0.99 (s, 54H, ^{t}Bu) ppm. ^{13}C NMR (C_6D_6, 125.8 MHz, 20 °C): δ 154.2 (*ipso*-Ar), 138.2 (*m*-Ar), 126.6 (*p*-Ar), 121.9 (*o*-Ar), 73.5 (br, N*C*H$_2$), 37.3 (*C*(CH$_3$)$_3$), 30.7 (C(*C*H$_3$)$_3$), 22.1 (Ar*C*H$_3$) ppm.

[ii]Optimized procedures will appear in an upcoming publication: Spinney, H. S.; Piro, N. A.; Cummins, C. C. **2009** *In preparation*.

4.4.10 Preparation of [(THF)Na][AsNb(N[$CH_2{}^tBu$]Ar)$_3$] (50)[ii]

A dark green THF (4 mL) solution of (μ-As$_2$)[Nb(N[$CH_2{}^tBu$]Ar)$_3$]$_2$ (48 mg, 0.032 mmol) was added to freshly prepared 1% Na/Hg (20 mg Na, 2 g Hg, 10 eq) at 22 °C and the mixture stirred vigorously for 2 h. The reaction remained green after this time, and so another 2 g of sodium amalgam was added. The solution quickly turned dark yellow and was stirred for 5 min before being decanted from the mercury and concentrated to dryness under dynamic vacuum. Extraction with Et_2O and filtration through Celite yielded a yellow solution which was dried to a foam. Crystallization from 2 mL of *n*-pentane at –35 °C overnight yielded orange crystals (a few of which were removed to screen for X-ray diffraction), which were isolated and dried (33 mg, 65% yield). ^{1}H NMR (C_6D_6, 500 MHz, 20 °C): δ 6.99 (s, 6H, *o*-Ar), 6.48 (s, 3H, *p*-Ar), 4.37 (s, 6H, NCH_2), 3.66 (THF), 2.24 (s, 18H, ArCH_3), 1.55 (THF), 1.13 (s, 27H, ^{t}Bu) ppm. ^{13}C NMR (C_6D_6, 75.8 MHz, 20 °C): δ 158.7 (*ipso*-Ar), 138.7 (*m*-Ar), 123.3 (*p*-Ar), 121.9 (*o*-Ar), 75.2 (NCH_2), 68.7 (THF), 36.6 (C(CH_3)$_3$), 30.2 (C(CH$_3$)$_3$), 26.1 (THF), 22.2 (ArCH$_3$) ppm.

4.4.11 Preparation of (Mes*NPN)Nb(N[$CH_2{}^tBu$]Ar)$_3$ (51)

To a thawing suspension of Na[NNb(N[$CH_2{}^tBu$]Ar)$_3$] (732 mg, 1.04 mmol) in Et_2O (15 mL) was added a thawing Et_2O solution (5 mL) of Mes*NPCl (340 mg, 1.04 mmol, 1 eq). The resulting mixture was stirred while warming to 22 °C over 1 h. After this time the NaCl was removed by filtration through Celite, and the red-orange filtrate was dried *in vacuo*. The resulting orange powder was extracted with *n*-pentane and then the solution was concentrated and stored at –35 °C to precipitate the product as an orange powder which was collected in two crops (789 mg, 0.815 mmol, 78% yield). ^{1}H NMR (C_6D_6, 500 MHz, 20 °C): δ 7.60 (s, 2H, Mes*), 6.53 (s, 3H, *p*-Ar), 6.50 (s, 6H, *o*-Ar), 4.09 (s, 6H, NCH_2), 2.08 (s, 18H, ArCH_3), 1.87 (s, 18H, *o*-Mes*), 1.45 (s, 9H, *p*-Mes*), 0.91 (s, 27H, ^{t}Bu) ppm. ^{31}P NMR (C_6D_6, 202.5 MHz, 20 °C): δ 243 ppm. ^{13}C NMR (C_6D_6, 75.8 MHz, 20 °C): δ 152.3 (*ipso*-Ar), 144.9 (d, J_{CP} = 21 Hz, *ipso*-Mes*), 141.7 (*m*-Mes*), 139.1 (*m*-Ar), 136.6 (d, J_{CP} = 10 Hz, *o*-Mes*), 126.6 (*p*-Ar), 122.5 (*o*-Ar), 122.1 (*p*-Mes*), 73.1 (NCH_2), 36.9 (Mes*), 36.2 (C(CH_3)$_3$), 32.7 (Mes*), 32.5 (Mes*), 29.5 (C(CH$_3$)$_3$), 21.9 (ArCH$_3$) ppm.

4.4.12 Preparation of (Mes*NPAs)Nb(N[$CH_2{}^tBu$]Ar)$_3$ (52)[ii]

To a thawing suspension of [(THF)Na][AsNb(N[$CH_2{}^tBu$]Ar)$_3$] (33 mg, 0.040 mmol) in Et_2O/THF (3 mL/1 mL) was added a thawing Et_2O solution (2 mL) of Mes*NPCl (1 eq). The resulting mixture was stirred while warming to 22 °C over 15 min. After this time the NaCl was removed by filtration through Celite, the filtrate was dried *in vacuo*, and the resulting residue was extracted with *n*-pentane. The extract was dried and then taken up in C_6D_6 for analysis by NMR spectroscopy, which revealed the desired product mixed with a small amount of Cl_2Nb(N[$CH_2{}^tBu$]Ar)$_3$. ^{1}H NMR (C_6D_6, 300 MHz, 20 °C): δ 7.76 (s, 2H, Mes*), 6.64 (s, 6H, *o*-Ar), 6.59 (s, 3H, *p*-Ar), 4.12 (s, 6H,

NCH_2), 2.13 (s, 18H, ArCH_3), 1.94 (s, 18H, *o*-Mes*), 1.48 (s, 9H, *p*-Mes*), 0.82 (s, 27H, ^{t}Bu) ppm. ^{31}P NMR (C_6D_6, 121.5 MHz, 20 °C): δ 348 ppm.

4.4.13 X-Ray Structure Determinations

Diffraction quality crystals of **45**, **48**, **50**, **51**, and **52** were grown from Et_2O at –35 °C. Crystals of **47** were grown from THF/Et_2O at –35 °C. Crystals were mounted in hydrocarbon oil on a nylon loop or a glass fiber. Low-temperature (100 K) data were collected on a Siemens Platform three-circle diffractometer coupled to a Bruker-AXS Smart Apex CCD detector with graphite-monochromated Mo Kα radiation (λ = 0.71073 Å) performing ϕ- and ω-scans. A semi-empirical absorption correction was applied to the diffraction data using SADABS.[49] All structures were solved by direct or Patterson methods using SHELXS[50,51] and refined against F^2 on all data by full-matrix least squares with SHELXL-97.[51,52] All non-hydrogen atoms were refined anisotropically. All hydrogen atoms were included in the model at geometrically calculated positions and refined using a riding model. The isotropic displacement parameters of all hydrogen atoms were fixed to 1.2 times the U_{eq} value of the atoms they are linked to (1.5 times for methyl groups). In structures where disorders were present, the disorders were refined within SHELXL with the help of rigid bond restraints as well as similarity restraints on the anisotropic displacement parameters for neighboring atoms and on 1,2- and 1,3-distances throughout the disordered components.[53] The relative occupancies of disordered components were refined freely within SHELXL. Further details are provided in Tables 4.1 – 4.2 and on Reciprocal Net.[54]

Table 4.1. Crystal Data for Niobium Trisamide Complexes Related to Nitrogen Chemistry

	47	**45**	**51**
Reciprocal Net code	05234	05230	06096
Empirical formula	$C_{82}H_{130}N_8Nb_2O$	$C_{36}H_{66}N_3Nb$	$C_{59}H_{94}N_5NbO_{0.5}P$
Formula weight	1429.76	633.83	1005.27
Temperature	100(2) K	100(2) K	100(2) K
Wavelength	0.71073 Å	0.71073 Å	0.71073 Å
Crystal system	Monoclinic	Triclinic	Monoclinic
Space group	$C2/c$	$P\bar{1}$	$P2_1/n$
Unit cell dimensions	$a = 20.451(3)$ Å, $\alpha = 90°$	$a = 9.7823(17)$ Å, $\alpha = 89.405(6)°$	$a = 14.6720(7)$ Å, $\alpha = 90°$
	$b = 11.8858(17)$ Å, $\beta = 97.009(6)°$	$b = 10.031(2)$ Å, $\beta = 86.813(6)°$	$b = 11.8806(6)$ Å, $\beta = 96.2920(10)°$
	$c = 34.635(5))$ Å, $\gamma = 90°$	$c = 18.947(4)$ Å, $\gamma = 74.978(6))°$	$c = 33.9384(16)$ Å, $\gamma = 90°$
Volume	8356(2) Å^3	1792.8(6) Å^3	5880.2(5) Å^3
Z	4	2	4
Density (calculated)	1.136 Mg/m^3	1.174 Mg/m^3	1.136 Mg/m^3
Absorption coefficient	0.319 mm^{-1}	0.362 mm^{-1}	0.272 mm^{-1}
$F(000)$	3072	688	2172
Crystal size	$0.25 \times 0.20 \times 0.10$ mm^3	$0.15 \times 0.15 \times 0.05$ mm^3	$0.45 \times 0.20 \times 0.10$ mm^3
Theta range for collection	1.99 to 29.58°	2.10 to 29.57°	2.10 to 30.03°
Index ranges	$-28 \le h \le 28$, $-16 \le k \le 16$,	$-13 \le h \le 13$, $-13 \le k \le 13$,	$-20 \le h \le 20$, $-16 \le k \le 16$,
	$-48 \le l \le 48$	$-26 \le l \le 26$	$-47 \le l \le 47$
Reflections collected	89779	36696	132570
Independent reflections	11759 [R(int) = 0.0506]	10025 [R(int) = 0.0624]	17196 [R(int) = 0.0394]
Completeness to θ_{max}	100.0%	99.6%	99.9%
Absorption correction	Semi-empirical from equivalents	Semi-empirical from equivalents	Semi-empirical from equivalents
Max. and min. transmission	0.9688 and 0.9244	0.9821 and 0.9477	0.9734 and 0.8876
Refinement method	Full-matrix least-squares on F^2	Full-matrix least-squares on F^2	Full-matrix least-squares on F^2
Data / restraints / parameters	11759 / 147 /470	10025/ 1 /9477	17196 / 34 /646
Goodness-of-fit[a]	1.135	1.033	1.049
Final R indices[b] [$I > 2\sigma(I)$]	$R_1 = 0.0525$, $wR_2 = 0.1162$	$R_1 = 0.0505$, $wR_2 = 0.1173$	$R_1 = 0.0328$, $wR_2 = 0.0802$
R indices[b] (all data)	$R_1 = 0.0657$, $wR_2 = 0.1224$	$R_1 = 0.0733$, $wR_2 = 0.1274$	$R_1 = 0.0408$, $wR_2 = 0.0846$
Largest diff. peak and hole	1.561 and -0.544 e Å^{-3}	2.769 and -0.411 e Å^{-3}	0.502 and -0.362 e Å^{-3}

[a] GooF = $\left[\frac{\Sigma[w(F_o^2-F_c^2)^2]}{(n-p)}\right]^{\frac{1}{2}}$ [b] $R_1 = \frac{\Sigma||F_o|-|F_c||}{\Sigma|F_o|}$; $wR_2 = \left[\frac{\Sigma[w(F_o^2-F_c^2)^2}{\Sigma[w(F_o^2)^2]}\right]^{\frac{1}{2}}$; $w = \frac{1}{\sigma^2(F_o^2)+(aP)^2+bP}$; $P = \frac{2F_c^2+\max(F_o^2,0)}{3}$

Table 4.2. Crystal Data for Complexes Containing Arsenic

	48	**50**	**52**
Reciprocal Net code	05201	06109	06112
Empirical formula	$C_{36}H_{54}N_3AsMo$	$C_{91}H_{148}As_2N_6Na_2Nb_2O_2$	$C_{61}H_{99}AsN_4NbOP$
Formula weight	699.68	1739.79	1103.24
Temperature	100(2) K	100(2) K	100(2) K
Wavelength	0.71073 Å	0.71073 Å	0.71073 Å
Crystal system	Monoclinic	Monoclinic	Triclinic
Space group	$P2_1$	$P2_1/n$	$P\bar{1}$
Unit cell dimensions	$a = 10.8545(8)$ Å, $\alpha = 90°$	$a = 20.6006(10)$ Å, $\alpha = 90°$	$a = 11.7490(5)$ Å, $\alpha = 69.8760(10)°$
	$b = 11.0354(8)$ Å, $\beta = 94.470(2)°$	$b = 11.2495(5)$ Å, $\beta = 115.8890(10)°$	$b = 16.4700(7)$ Å, $\beta = 78.4010(10)°$
	$c = 14.9320(11)$ Å, $\gamma = 90°$	$c = 22.3478(10)$ Å, $\gamma = 90°$	$c = 17.3444(7)$ Å, $\gamma = 87.0670(10)°$
Volume	1783.2(2) Å^3	4659.3(4) Å^3	3086.4(2) Å^3
Z	2	2	2
Density (calculated)	1.303Mg/m^3	1.240 Mg/m^3	1.187 Mg/m^3
Absorption coefficient	1.315 mm^{-1}	1.007 mm^{-1}	0.793 mm^{-1}
$F(000)$	732	1844	1180
Crystal size	$0.15 \times 0.11 \times 0.04$ mm^3	$0.30 \times 0.15 \times 0.05$ mm^3	$0.25 \times 0.08 \times 0.03$ mm^3
Theta range for collection	1.88 to 29.13°	2.03 to 29.57°	1.97 to 28.70°
Index ranges	$-14 \le h \le 14$, $-15 \le k \le 15$,	$-28 \le h \le 28$, $-15 \le k \le 15$,	$-15 \le h \le 15$, $-21 \le k \le 22$,
	$-20 \le l \le 19$	$-31 \le l \le 31$	$-23 \le l \le 23$
Reflections collected	32415	87526	60657
Independent reflections	9537 [R(int) = 0.0560]	13053 [R(int) = 0.0431]	15903 [R(int) = 0.0581]
Completeness to θ_{max}	99.9%	99.8%	99.6%
Absorption correction	Semi-empirical from equivalents	Semi-empirical from equivalents	Semi-empirical from equivalents
Max. and min. transmission	0.9493 and 0.8271	0.9514 and 0.7522	0.9766 and 0.8264
Refinement method	Full-matrix least-squares on F^2	Full-matrix least-squares on F^2	Full-matrix least-squares on F^2
Data / restraints / parameters	9537 / 1 / 376	13053 / 422 / 604	15903 / 19 / 673
Goodness-of-fit[a]	1.033	1.037	1.012
Final R indices[b] [$I > 2\sigma(I)$]	$R_1 = 0.0420$, $wR_2 = 0.0936$	$R_1 = 0.0344$, $wR_2 = 0.0803$	$R_1 = 0.0413$, $wR_2 = 0.0939$
R indices[b] (all data)	$R_1 = 0.0575$, $wR_2 = 0.0992$	$R_1 = 0.0492$, $wR_2 = 0.0886$	$R_1 = 0.0667$, $wR_2 = 0.1033$
Largest diff. peak and hole	0.864 and -0.582 e Å^{-3}	0.845 and -0.451 e Å^{-3}	0.943 and -0.561 e Å^{-3}

[a] GooF = $\left[\frac{\Sigma[w(F_o^2-F_c^2)^2]}{(n-p)}\right]^{\frac{1}{2}}$ [b] $R_1 = \frac{\Sigma||F_o|-|F_c||}{\Sigma|F_o|}$; $wR_2 = \left[\frac{\Sigma[w(F_o^2-F_c^2)^2}{\Sigma[w(F_o^2)^2]}\right]^{\frac{1}{2}}$; $w = \frac{1}{\sigma^2(F_o^2)+(aP)^2+bP}$; $P = \frac{2F_c^2+\max(F_o^2,0)}{3}$

4.5 REFERENCES

[1] Fryzuk, M. D.; Johnson, S. A. *Coord. Chem. Rev.* **2000**, *200-202*, 379–409.

[2] Shaver, M. P.; Fryzuk, M. D. *Adv. Synth. Catal.* **2003**, *345*, 1061–1076.

[3] MacKay, B. A.; Fryzuk, M. D. *Chem. Rev.* **2004**, *104*, 385–401.

[4] Clough, C. R.; Greco, J. B.; Figueroa, J. S.; Diaconescu, P. L.; Davis, W. M.; Cummins, C. C. *J. Am. Chem. Soc.* **2004**, *126*, 7742–7743.

[5] Curley, J. J.; Cook, T. R.; Reece, S. Y.; Müller, P.; Cummins, C. C. *J. Am. Chem. Soc.* **2008**, *130*, 9394–9405.

[6] Laplaza, C. E.; Cummins, C. C. *Science* **1995**, *268*, 861–863.

[7] Figueroa, J. S.; Piro, N. A.; Clough, C. R.; Cummins, C. C. *J. Am. Chem. Soc.* **2006**, *128*, 940–950.

[8] Curley, J. J.; Sceats, E. L.; Cummins, C. C. *J. Am. Chem. Soc.* **2006**, *128*, 14036–14037.

[9] Ferguson, R.; Solari, E.; Floriani, C.; Osella, D.; Ravera, M.; Re, N.; Chiesi-Villa, A.; Rizzoli, C. *J. Am. Chem. Soc.* **1997**, *119*, 10104–10115.

[10] Buijink, J. K. F.; Meetsma, A.; Teuben, J. H. *Organometallics* **1993**, *12*, 2004–2005.

[11] Song, J.-I.; Berno, P.; Gambarotta, S. *J. Am. Chem. Soc.* **1994**, *116*, 6927–6928.

[12] Berno, P.; Gambarotta, S. *Organometallics* **1995**, *14*, 2159–2161.

[13] Figueroa, J. S.; Cummins, C. C. *J. Am. Chem. Soc.* **2003**, *125*, 4020–4021.

[14] Figueroa, J. S.; Piro, N. A.; Mindiola, D. J.; Fickes, M. G.; Cummins, C. C. *Manuscript in preparation.* **2009**.

[15] Rocklage, S. M.; Schrock, R. R. *J. Am. Chem. Soc.* **1982**, *104*, 3077–81.

[16] Dilworth, J. R.; Henderson, R. A.; Hills, A.; Hughes, D. L.; Macdonald, C.; Stephens, A. N.; Walton, D. R. M. *J. Chem. Soc., Dalton Trans.* **1990**, 1077–1085.

[17] Hwu, J. R.; Wang, N. *Tetrahedron* **1988**, *44*, 4181–4196.

[18] Greenwood, N. N.; Earnshaw, A. *Chemistry of the Elements*, 2nd ed.; Butterworth-Heinemann: Oxford, 1997.

[19] Connelly, N. G.; Geiger, W. E. *Chem. Rev.* **1996**, *96*, 877–910.

[20] Johnson, B. P.; Balázs, G.; Scheer, M. *Coord. Chem. Rev.* **2006**, *250*, 1178–1195.

[21] Balázs, G.; Gregoriades, L. J.; Scheer, M. *Organometallics* **2007**, *26*, 3058–3075.

[22] Mösch-Zanetti, N. C.; Schrock, R. R.; Davis, W. M.; Wanninger, K.; Seidel, S. W.; O'Donoghue, M. B. *J. Am. Chem. Soc.* **1997**, *119*, 11037–11048.

[23] Scheer, M.; Müller, J.; Häser, M. *Angew. Chem., Int. Ed. Engl.* **1996**, *35*, 2492–2496.

[24] Gascoin, F.; Sevov, S. C. *Angew. Chem., Int. Ed.* **2002**, *41*, 1232–1234.

[25] Gascoin, F.; Sevov, S. C. *Inorg. Chem.* **2003**, *42*, 8567–8571.

[26] Rodionov, A.; Kalendarev, R.; Eiduss, J.; Zhukovskii, Y. *J. Molec. Struct.* **1996**, *380*, 257 – 266.

[27] Erdmann, H.; von Unruh, M. Z. *Z. Anorg. Chem.* **1902**, *32*, 437–452.

[28] Di Vaira, M.; Midollini, S.; Sacconi, L.; Zanobini, F. *Angew. Chem., Int. Ed. Engl.* **1978**, *17*, 676–677.

[29] Scherer, O. J.; Sitzmann, H.; Wolmershäuser, G. *J. Organomet. Chem.* **1986**, *309*, 77 – 86.

[30] Scherer, O. J.; Sitzmann, H.; Wolmershäuser, G. *Angew. Chem., Int. Ed. Engl.* **1989**, *28*, 212–213.

[31] Scherer, O. J.; Winter, R.; Heckmann, G.; Wolmershäuser, G. *Angew. Chem., Int. Ed. Engl.* **1991**, *30*, 850–852.

[32] Tan, R. B.; Comerlato, N. M.; Powell, D. R.; West, R. *Angew. Chem., Int. Ed. Engl.* **1992**, *31*, 1217–1218.

[33] Spinney, H. A.; Piro, N. A.; Cummins, C. C. *In preparation.* **2009**.

[34] A search of the Cambridge Structural Database on April 25, 2009, listed 2.240 Å as the shortest Mo–As distance; this distance is for the Mo–As bond in the terminal arsenide complex reported by Schrock.[22].

[35] Laplaza, C. E.; Johnson, M. J. A.; Peters, J. C.; Odom, A. L.; Kim, E.; Cummins, C. C.; George, G. N.; Pickering, I. J. *J. Am. Chem. Soc.* **1996**, *118*, 8623–8638.

[36] McDonough, J. E.; Mendiratta, A.; Curley, J. J.; Fortman, G. C.; Fantasia, S.; Cummins, C. C.; Rybak-Akimova, E. V.; Nolan, S. P.; Hoff, C. D. *Inorg. Chem.* **2008**, *47*, 2133–2141.

[37] Laplaza, C. E.; Davis, W. M.; Cummins, C. C. *Angew. Chem., Int. Ed. Engl.* **1995**, *34*, 2042–2044.

[38] Johnson, M. J. A.; Odom, A. L.; Cummins, C. C. *Chem. Commun.* **1997**, 1523–1524.

[39] Sidgwick, N. V. *Ann. Rep. Prog. Chem.* **1933**, *30*, 120–128.

[40] Drago, R. S. *J. Phys. Chem.* **1958**, *62*, 353–357.

[41] Figueroa, J. S.; Cummins, C. C. *Angew. Chem., Int. Ed.* **2004**, *43*, 984–988.

[42] Twamley, B.; Sofield, C. D.; Olmstead, M. M.; Power, P. P. *J. Am. Chem. Soc.* **1999**, *121*, 3357–3367.

[43] Brask, J. K.; Fickes, M. G.; Sangtrirutnugul, P.; Durà-Vilà, V.; Odom, A. L.; Cummins, C. C. *Chem. Commun.* **2001**, 1676–1677.

[44] Huber, K. P.; Herzberg, G. *Constants of Diatomic Molecules*; Linstrom, P. J.; Mallard, W. G., Eds.; NIST Chemistry WebBook, NIST Standard Reference Database Number 69; National Institute of Standards and Technology: Gaithersburg, MD, 2009.

[45] Regitz, M.; Scherer, O. J. *Multiple Bonds and Low Coordination in Phosphorus Chemistry*; Thieme: Stuttgart, 1990.

[46] Pangborn, A. B.; Giardello, M. A.; Grubbs, R. H.; Rosen, R. K.; Timmers, F. J. *Organometallics* **1996**, *15*, 1518–1520.

[47] Gibson, V. C.; Kee, T. P.; Shaw, A. *Polyhedron* **1988**, *7*, 2217–2219.

[48] Niecke, E.; Nieger, M.; Reichert, F. *Angew. Chem., Int. Ed. Engl.* **1988**, *27*, 1715.

[49] Sheldrick, G. M. *SHELXTL*; Bruker AXS, Inc.: Madison, WI (USA), 2005–2008.

[50] Sheldrick, G. M. *Acta Crystallogr., Sect. A: Fundam. Crystallogr.* **1990**, *46*, 467–473.

[51] Sheldrick, G. M. *Acta Crystallogr., Sect. A: Fundam. Crystallogr.* **2008**, *64*, 112–122.

[52] Sheldrick, G. M. *SHELXL-97: Program for crystal structure determination*; University of Göttingen, 1997.

[53] Müller, P.; Herbst-Irmer, R.; Spek, A. L.; Schneider, T. R.; Sawaya, M. R. *Crystal Structure Refinement: A Crystallographer's Guide to SHELXL*; Müller, P., Ed.; IUCr Texts on Crystallography; Oxford University Press: Oxford, 2006.

[54] The Reciprocal Net Site Network is a distributed database for crystallographic information, supported by the National Science Digital Library, and is run by participating crystallography labs across the world. Crystallographic data for complexes in this chapter are available under the identification codes listed in Tables 4.1 – 4.2 from the MIT Reciprocal Net site. `http://reciprocal.mit.edu/recipnet`.

APPENDIX A

A.1 STREAMLINED SYNTHESES OF NIOBIUM TRISANILIDE STARTING MATERIALS

The original synthesis of niobaziridine hydride **46** involved the introduction of three anilide ligands onto a niobium trichloride diphenylacetylene complex in *ca.* 50% yield.[1] Conversion of this molecule to the bisiodide complex with I_2, followed by reduction with magnesium anthracene yielded the desired complex in modest yield. It is has since been discovered that the oxoniobium trisanilide complex **21** can be converted cleanly to the bistriflate and then reduced down to niobaziridine hydride **46**.[2] A direct synthesis of $ONb(N[CH_2{}^tBu]Ar)_3$ was thus sought using the potential precursor $ONbCl_3(THF)_2$, a starting material which can be prepared easily in >90% yield from $NbCl_5$ and $(Me_3Si)_2O$.[3] Indeed, addition of solid lithium anilide, $(Et_2O)LiN[CH_2{}^tBu]Ar$, to a thawing Et_2O slurry of $ONbCl_3(THF)_2$ affords the desired oxoniobium complex **21** in roughly 65% yield after isolation. Moreover, addition of triflic anhydride to the crude reaction mixture, from which LiCl has been removed, precipitates $(TfO)_2Nb(N[CH_2{}^tBu]Ar)_3$ that can be filtered off and collected in up to 60% yield, Scheme A.1.

While it was previously believed that magnesium anthracene was a unique reductant in its ability to generate the niobaziridine hydride complex **46**, this was found not to be the case. Reduction of the bistriflate by 1% Na/Hg produces niobaziridine hydride **46** in >60% yield following recrystallization. The ease of sodium amalgam preparation relative to magnesium anthracene synthesis, and the preclusion of an anthracene removal step, make this a new route very attractive.

Moreover, the easy removal of Na/Hg and NaOTf from the reduction of **53** to **46** allows the ready formation of relatively clean solutions of **46** that can be used in further chemistry. This is exploited in a rapid synthesis of the niobium phosphide complex **3** in *ca.* 60% yield from **53** without the isolation of any intermediates, Scheme A.1 (dotted box).

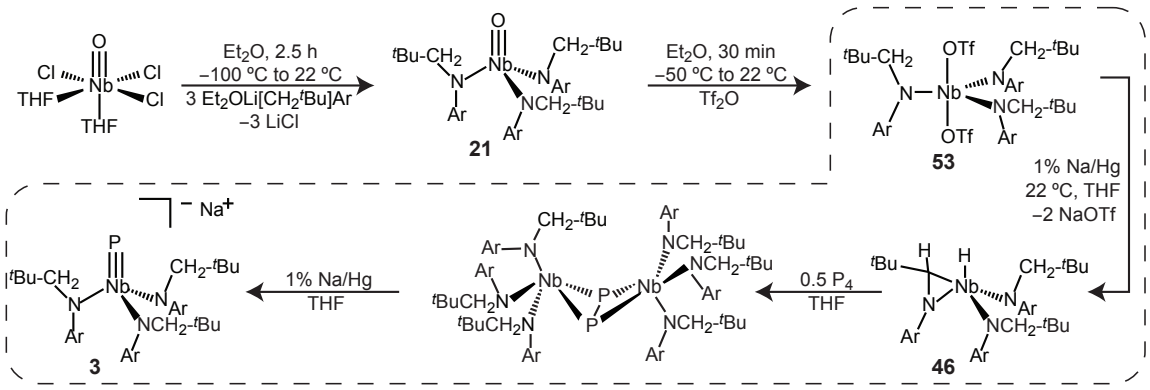

Scheme A.1. Concise syntheses of **53**, **46**, and **3** from $ONbCl_3(THF)_3$. The first two steps can be performed with out isolation of oxoniobium **21**. Similarly, the three steps in the dotted box can be carried out without any crystallization steps.

A.1.1 Preparation of $ONb(N[CH_2{}^tBu]Ar)_3$ and $(TfO)_2Nb(N[CH_2{}^tBu]Ar)_3$ from $ONbCl_3(THF)_2$

To a cold suspension of $ONbCl_3(THF)_2$ (9.15 g, 25.5 mol, 1 eq) in Et_2O (150 mL) was added solid $(Et_2O)LiN[CH_2{}^tBu]Ar$ (21.4 g, 78.9 mmol, 3.1 eq) in small portions with stirring and keeping the suspension cold. The color proceeded from colorless through blue to a final yellow-brown throughout the addition. The mixture was allowed to warm to room temperature and stir for 2 h before it was concentrated *in vacuo* and *n*-pentane was added to precipitate all LiCl. This was filtered through Celite to give a yellow-brown solution. (At this point the solution can be concentrated and cooled to afford crystals of **21**, if desired.) To isolate the bistriflate complex, the mixture was concentrated to 50 mL and cooled before triflic anhydride (8.2 g, 29.1 mmol, 1.15 eq) was added as a cooled Et_2O solution (20 mL). Immediate precipitation of an orange product occurred as the exothermic reaction proceeded. The mixture was concentrated down to 40 mL and put in the freezer to precipitate the product. The orange powder was then collected on a glass frit, washed with *n*-pentane, and dried *in vacuo* to afford $(TfO)_2Nb(N[CH_2{}^tBu]Ar)_3$ (16.6 g, 17.3 mmol, 68% yield).

A.1.2 Preparation of $[Et_2ONa][PNb(N[CH_2{}^tBu]Ar)_3]$ from $(TfO)_2Nb(N[CH_2{}^tBu]Ar)_3$

To freshly prepared Na/Hg (120 g Hg, 930 mg Na, 40 mmol, 3.5 eq) stirring under 200 mL of THF was added solid niobium bistriflate **53** (11.2 g, 11.6 mmol). The initially orange solution slowly turned brown and then brown yellow. After stirring for 1.5 h (an aliquot analyzed by NMR showed only **46**) the solution was decanted from the amalgam, filtered through Celite, and then the solvent was removed *in vacuo*. The solid residue was triturated with *n*-hexane twice to assist in the removal of THF. At this point the residue was extracted with *n*-pentane and filtered through Celite to remove NaOTf. The filter bed remained yellow, and so the Celite was washed with minimal benzene until the washings were colorless. The filtrate was then concentrated to

dryness under dynamic vacuum. This residue was then dissolved in THF (100 mL) and added to a stirring solution of white phosphorus (360 mg, 11.6 mmol, 1.0 eq) in THF (50 mL). This mixture took on a dark green hue from its initial yellow-brown color, and was allowed to stir for 1.75 h at RT. Meanwhile, the Na/Hg which was used in the first step was washed thoroughly with THF and then to it was added an additional 300 mg of Na. This regenerated sodium amalgam was then added to the green solution of $(P_2)[Nb(N[CH_2{}^tBu]Ar)_3]_2$. This solution was stirred for 2 h, losing the green color to give an orange-brown solution over this time. Decanting from the amalgam and filtering through Celite gave an orange-brown solution which was dried *in vacuo* and then extracted with *n*-pentane and filtered through Celite again. The filtrate was stripped to dryness and triturated with *n*-hexane several times. The desired niobium phosphide anion **3** was isolated from this residue by precipitation as its sodium salt from Et_2O/*n*-pentane and collected in several crops as a yellow powder by repeated concentration, collection atop a sintered glass frit, addition of Et_2O/pentane mixtures, and reconcentration. After the first large crop is collected the latter crops come more easily. The collected yellow solids were dried *in vacuo* to yield 5.5 g of $[(Et_2O)Na][PNb(N[CH_2{}^tBu]Ar)_3$ (6.95 mmol, 60% yield over two steps).

A.2 REFERENCES

[1] Figueroa, J. S.; Cummins, C. C. *J. Am. Chem. Soc.* **2003**, *125*, 4020–4021.

[2] Figueroa, J. S.; Cummins, C. C. *J. Am. Chem. Soc.* **2004**, *126*, 13916–13917.

[3] Gibson, V. C.; Kee, T. P.; Shaw, A. *Polyhedron* **1988**, *7*, 2217–2219.

APPENDIX B

This appendix contains observations made when the diphosphaazide complex (Mes*NPP)-Nb(N[$CH_2{}^tBu$]Ar)$_3$ was dissolved in certain samples of diene. In particular, a new species was observed, the identity of which has not been determined. As these observations turned out to be dependent on the exact batch of diene used, they are attributed to an impurity but are discussed here. Also discussed are some possible structures that could result from a direct reaction between (Mes*NPP)Nb(N[$CH_2{}^tBu$]Ar)$_3$ and dienes, but have been ruled out.

B.1 REACTIONS OF A DIPHOSPHAAZIDE COMPLEX IN DIENE SOLVENTS

Initial investigations of the (Mes*NPP)Nb(N[$CH_2{}^tBu$]Ar)$_3$/diene system revealed an unanticipated problem. Dissolution of **1** in certain solutions of neat 1,3-cyclohexadiene afforded a new product, **1x**, with a ^{31}P NMR spectrum consisting of doublets at 235 and 118 ppm (J_{PP} = 715 Hz). These chemical shifts are significantly different than those observed for **1** in C_6D_6. Moreover, removal of the diene under dynamic vacuum and re-dissolution in C_6D_6 regenerated **1**, with NMR properties identical to those prior to exposure to the diene. Upon varying the concentration of 1,3-cyclohexadiene in a C_6D_6 solution of **1**, the relative concentrations of **1** and **1x** were observed to change. Mixtures of **1** and 2,3-dimethylbutadiene or cyclopentadiene also generated new products with similar spectral features. The upfield ^{31}P resonances shifted by up to 20 ppm when other dienes were employed, while the downfield resonance remained relatively unchanged. The related arsenic compound, **52**, showed a similar change in spectrum upon dissolution in 1,3-cyclohexadiene, with its ^{31}P NMR singlet moving from 348 ppm to 263 ppm. These combined observations allow assignment of the resonance at 118 ppm to the phosphide-derived phosphorus, P_α, which does not bear the Mes*N substituent. They also suggest that this is the site of the reaction, based on the observation that this resonance shifts more as the diene is varied.

However, while these observations were made on more than one occasion, and with different diene samples, not all samples of these dienes afforded formation of **1x**. If the diene was carefully distilled from $NaBH_4$, discarding the first fraction, **1x** was not generated upon dissolving **1** in diene solvent—only **1** was identified in the ^{31}P NMR spectrum. These results suggest that the product observed in initial experiments resulted from a minor impurity in the diene.[1] This also explains why very large excesses of diene were required to observe formation of **1x**. It is noteworthy that formation of the diene trapping product $P_2(C_6H_8)_2$, **6**, is independent of the appearance of **1x**. All samples of diene, regardless of whether they lead to formation of **1x**, allow for the synthesis of **6**.

In an attempt to identify the structure of **1x**, crystals were grown from a cyclohexadiene solution in which **1** was dissolved and **1x** was observed to form. The structure obtained from such a crystal, however, revealed only **1** solvated by five equivalents of 1,3-cyclohexadiene, Figure B.1. We are thus left to speculate on the identity of the complex **1x**.

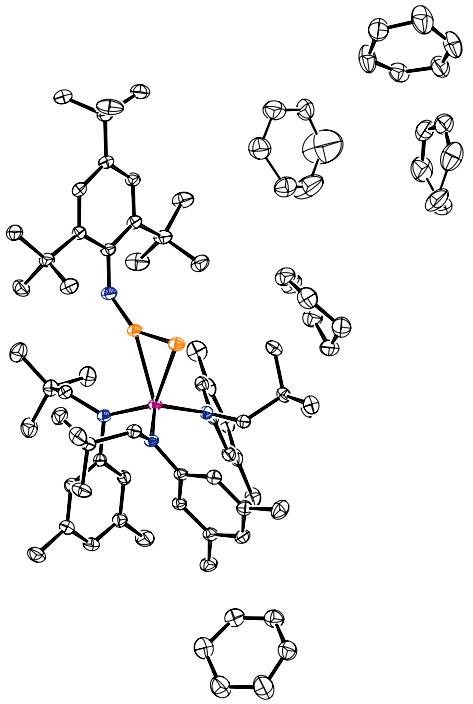

Figure B.1. The diphosphaazide complex crystallizes from 1,3-cyclohexadiene with five equivalents of diene.

B.2 Possible Products of Diene Addition to a Diphosphaazide Complex

The finding that diene solvents, or an impurity present in them, can lead to a direct reaction with **1** compelled a consideration of possible reaction products, Scheme B.1. Without knowing what

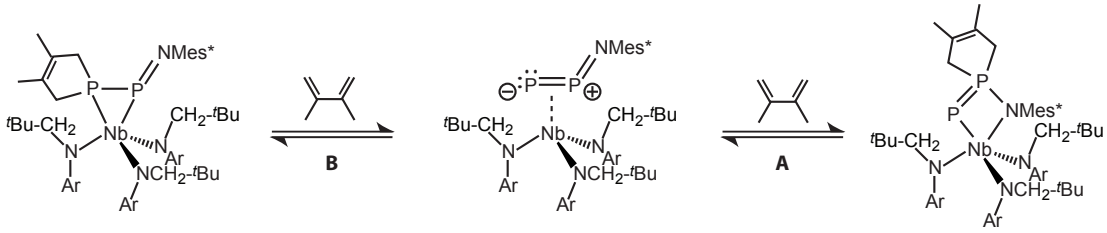

Scheme B.1. Two possibilities for a reaction between **1** and a diene.

impurities are present, a focus was made on reaction products that could result from reactions with diene itself. One such compound is a metallacycle-containing product of $[4+1]$-cycloaddition at the β phosphorus of **1**, as shown in reaction **A** of Scheme B.1. Such a product is similar to those for related NbPPO metallacycles bearing substituents at their β phosphorus (see Section 3.3). An independent synthesis of a $Mes^*NP(C_6H_{10})P$ ligand complexed to $Nb(N[CH_2{}^tBu]Ar)_3$ was thus sought. This was achieved in two steps from Mes^*NPCl and niobium phosphide **3**, Scheme B.2. This synthesis is based on the observation that iminophosphanes bearing bulky substituents at nitrogen will undergo $[4+1]$ cycloadditions with dienes at the phosphorus center.[2,3] This methodology was used to synthesize a chloroiminophosphorane for reaction with niobium phosphide **3**. This synthesis yielded a new product, **54**, with NMR features distinct from **1x**. The ^{31}P NMR of **54** displays a downfield doublet at 474 ppm and a second doublet at 10 ppm, $^1J_{PP}$ = 465 Hz. These parameters lead to the assignment of **54** as the terminal phosphinidene depicted in Scheme B.2. This independent synthesis argues further against a proposal wherein cycloaddition of 1,3-cyclohexadiene or 2,3-dimethylbutadiene at the β phosphorus of **1** is responsible for formation of **1x**.

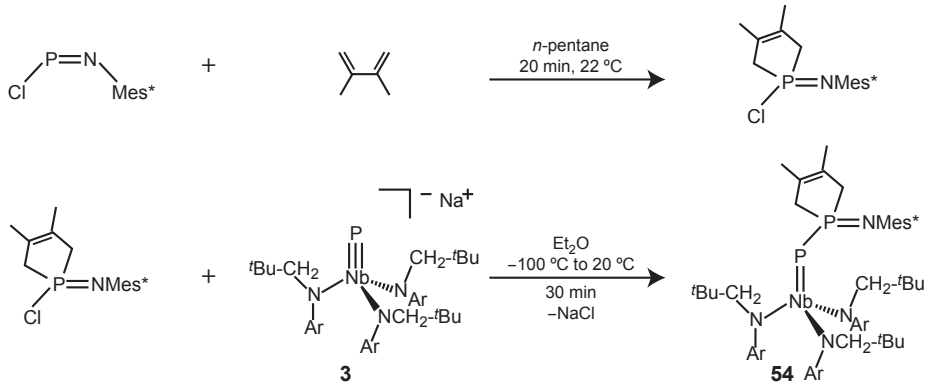

Scheme B.2. Independent synthesis of $Mes^*NP(C_6H_{10})PNb(N[CH_2{}^tBu]Ar)_3$ (**54**).

To rule out $[4+1]$ cycloaddition at the α phosphorus, a structure analogous to that on the left of Scheme B.1 was optimized using DFT calculations. This optimized structure is shown in Figure B.2. NMR chemical shielding values were calculated for such a structure and the chemical shift

values predicted are –90 ppm for P_α and +95 ppm for P_β. These values are in very poor agreement with the observed shifts for **1x**, and so a structure of this type can also be ruled out. Consequently, it again seems as though **1x** is in fact a product of reaction with an impurity, and not one of a cycloaddition reaction between **1** and a diene itself.

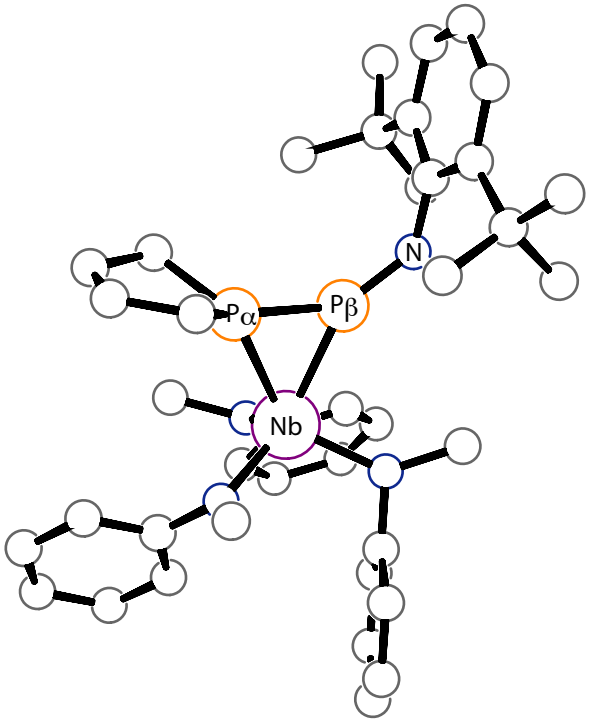

Figure B.2. Optimized structure of (2,6-^{t}BuC_6H_3NPP[C_4H_6])Nb(N[Me]Ph)$_3$.

Preparation of Mes*NP(C_6H_{10})NPCl

2,3-Dimethylbutadiene (150 μL, 1.3 mmol, 2.9 eq) was added via syringe to a red solution of Mes*NPCl (150 mg, 0.46 mmol) in *n*-pentane (7 mL). The solution was stirred for 20 min at 22 °C, fading to colorless over this time. The solution was concentrated to dryness under dynamic vacuum to afford the desired product as a white powder in quantitative yield. ^{1}H NMR (C_6D_6, 500 MHz, 20 °C): δ 7.63 (s, 2H, Mes*), 2.92 (dd, $^2J_{HH}$ = 17 Hz, $^2J_{HP}$ = 7 Hz, 2H, PCH_2), 2.70 (dm, $^2J_{HH}$ = 17 Hz, 2H, PCH_2), 1.62 (s, 18H, Mes*), 1.43 (s, 9H, Mes*), 1.34 (s, 6H, CH_3) ppm. ^{31}P{^{1}H} NMR (C_6D_6, 121.5 MHz, 20 °C): δ −1 (s) ppm.

Preparation of Mes*NP(C_6H_{10})PNb(N[$CH_2{}^t$Bu]Ar)$_3$ (54)

To a thawing solution of [(Et_2O)Na][PNb(N[$CH_2{}^t$Bu]Ar)$_3$] (70 mg, 0.088 mmol) in Et_2O (7 mL) was added Mes*NP(C_6H_{10})Cl (35 mg, 0.086 mmol, 0.98 eq) as a thawing Et_2O solution (3 mL). The solution was stirred for 20 min, and then 1 mL of THF was added and the mixture stirred another 5 min. After this time the solution was stripped to dryness to afford a red residue. This residue was

dissolved in C_6D_6 and analyzed by ^{31}P and ^{1}H NMR spectroscopy. ^{1}H NMR (C_6D_6, 300 MHz, 20 °C): δ 7.59 (d, J_{PH} = 2 Hz, 2H, *m*-Mes*), 6.50 (s, 3H, *p*-Ar), 6.45 (s, 6H, *o*-Ar), 4.30 (s, 6H, NCH_2), 3.47 (m, 2H, PCH_2), 3.26 (m, 2H, PCH_2),2.05 (s, 18H, ArCH_3), 1.80 (s,18H, *o*-Mes*), 1.63 (s, 6H, CH_3), 1.48 (s, 9H, *p*-Mes*), 0.81 (s, 27H, ^{t}Bu) ppm. $^{31}P\{^{1}H\}$ NMR (C_6D_6, 121.5 MHz, 20 °C): δ 474 (br d, J_{PP} = 460 Hz), 10 (d, J_{PP} = 460) ppm.

B.3 REFERENCES

[1] Mironov, V. A.; Fedorovich, A. D.; Akhrem, A. A. *Russ. Chem. Rev.* **1983**, *52*, 61–78; This review contains various techniquies for synthesizing cyclohexa-1,3-dienes and includes their common impurities.

[2] Niecke, E.; Lysek, M. *Tetrahedron Lett.* **1988**, *29*, 605–606.

[3] Niecke, E.; Gudat, D. *Angew. Chem., Int. Ed. Engl.* **1991**, *30*, 217–237.

APPENDIX C

This appendix describes the programs used to create this document.

C.1 LaTeX

The typesetting of this document was handled using LaTeX.[1] In particular, the MacTex-2008 distribution was employed.[2] This package includes the TeXShop program for file editing, processing and viewing, and BibDesk for reference handling.[3,4] The document was based on the *mitthesis* class and the template available from MIT's Athena network.[5] Certain minor modifications to the style of the template were made. Several LaTeX packages were employed to assist in stylistic adjustments and to aid in document creation. The *chemstyle* package was not used but may be found helpful.

The main .tex file used to process this document is included below. This includes comments to describe the useful packages and style changes that were used.

```
%\documentclass[12pt,vi,twoside]{mitthesis}
%%
%%  If you want your thesis copyright to you instead of MIT, use the
%%  ``vi'' option, as above.
%%
%\documentclass[12pt,twoside,leftblank]{mitthesis}
%%
%% If you want blank pages before new chapters to be labelled ``This
%% Page Intentionally Left Blank'', use the ``leftblank'' option, as
%% above.
```

```
\documentclass[11pt, twoside]{mitthesis} % Sets the class to mitthesis,
\usepackage{pslatex} %Sets the collection of fonts used
%\usepackage{newcent} % An alternate font selection
\onehalfspacing % Gives a line spacing of 1.5
%\doublespacing % Gives a double spaced document
%\setlength{\parskip}{6pt plus 1pt minus 1pt}  %This controls the spacing between
% paragraphs but should instead be included in each chapter.
%The plus/minus values allow for changes in the spacing to
% accommodate favorable page layouts.

\usepackage{pdfsync} % Allows for a clickable interface between pdf and tex documents
   %within TeXShop (and certain other editors)

%%%%% H Y P H E N A T I O N and J U S T I F I C A T I O N
%  Most of the options in this section deal with preferences regarding how hyphenation
%  is treated (more hyphenation or more variation in word spacings). Also, included
% are options on how page breaks and white space are handled.
\hyphenpenalty 8000
\tolerance 2000
\hfuzz 1pt
\raggedbottom
\widowpenalty 10000
\clubpenalty 10000

%%%%% S C H E M E S and F I G U R E S
\usepackage[margin=10pt, font={small}, labelfont={bf,sf}, justification=justified,%
    labelsep=period, singlelinecheck=true, skip=0pt]{caption}
    % Sets the format of captions
\usepackage{ctable} % A useful environment for tables that include footnotes
\usepackage[listofformat=simple]{subfig} % Allows for the use of subfloats
\usepackage{trivfloat} % A package that makes creating new floats very easy
\trivfloat{scheme} % Makes the Scheme float using the above package
\usepackage{graphicx} % Allows for inclusion of certain graphics directly
\usepackage{chngcntr} % Enables the option below to allow for numbering of figures
% properly within a chapter.
\counterwithin{figure}{chapter} % Sets desired behavior for figure label counters

%%%%% F O O T N O T E S,  C O N T E N T S,  T I T L E S  and L I S T S
\renewcommand{\thefootnote}{\roman{footnote}} % Sets footnotes to be numbered
```

```
     % with lowercase Roman numerals
\usepackage[stable]{footmisc}  % Allows for footnotes in section headings
\usepackage{minitoc} % Allows inclusion of Table of Contents for each chapter
\nomtcrule % Removes line below tables of contents in each chapter
\setcounter{tocdepth}{1} % Changes the front matter table of contents to only include
% chapters and sections, no subsections.
\renewcommand{\contentsname}{Table of Contents} % Renames  "Table of Contents"
\usepackage{enumitem} % Allows for more formatting control of lists within the text
\usepackage{multirow} % Allows tables to have entries that span rows
\usepackage{titlesec} % Allows for changing the formatting of chapter/section headings.
  % These are changed from the defaults on the next few lines.
\titleformat{\chapter}[display]%
{\sc\sffamily\Huge\bfseries} {\chaptertitlename\ \thechapter}%
 {20pt} {\normalfont\sffamily\bfseries\raggedleft\huge\parbox[b]{5.75in}}
\titleformat{\section} {\sc\sffamily\Large\bfseries}{\thesection}{1em}{}%
\titleformat{\subsection}{\sffamily\large\bfseries}{\thesubsection}{1em}{}%
\titleformat{\subsubsection}{\sffamily\normalsize\bfseries}{\thesubsubsection}{1em}{}
\titlespacing*{\subsubsection}{0pt}{3.25ex plus 1ex minus .2ex}{0ex plus .2ex}

%%%% B I B L I O G R A P H Y
\usepackage[super,sort&compress, sectionbib]{natbib} % Sets the ordering, etc
     % for the bibliography treatment
\usepackage{mciteplus} % Allows multiple references with one citation
\bibpunct{}{}{,}{s}{}{} % Sets up natbib options regarding punctuation
\usepackage{chapterbib} % Makes each chapter's bibliography separate
\renewcommand{\bibsection}{\section{References}} % Sets the name of the bibliography
% to "Referneces"
\setlength{\bibsep}{1pt} % Sets the spacing between references
\newcommand{\bibfont}{\footnotesize} % Makes the reference font smaller than the text
\usepackage{notes2bib} % Allows for notes to be included in the references section

%%%% C H E M I S T R Y
\usepackage{tikz} % Used by mhchem to make pretty arrows
\usepackage[version=3, arrows=pgf-filled]{mhchem} % Fantastic package for typesetting
% chemical formulas quickly and easily.
\usepackage{chemcompounds} % A package to handle compound numbering automatically

%%%% S H O R T C U T S
 % These are all simply shortcuts to allow less typing when writing your document.
```

```
 % \degc is probably the most useful.  20\degc\ typsets 20 C with a nice small
 % space between the number and the units. Other things to include here are chemical
 % formulae used a lot or other oft-used formated text that is cumbersome to type.
\newcommand{\molly}{\ce{Mo(N[$^t$Bu]Ar)3}}
\newcommand{\degc}{\,$^\circ$C}
\newcommand{\dzero}{\emph{d}$^0$}
\newcommand{\done}{\emph{d}$^1$}
\newcommand{\dtwo}{\emph{d}$^2$}
\newcommand{\dthree}{\emph{d}$^3$}
\newcommand{\Nb}{\ce{Nb(N[CH2$^t$Bu]Ar)3}}
\newcommand{\NbH}{\ce{HNb($\eta^2\hyphen^t$BuCH=NAr)}\-\ce{(N[CH2$^t$Bu]Ar)2$}}
\newcommand{\Elim}{\ce{(Mes$^*$NPP)}\-\ce{Nb(N[CH2$^t$Bu]Ar)3}}
\newcommand{\PtwoW}{(\ce{P2)W(CO)5}}
\newcommand{\PNb}{\ce{[PNb(N[CH2$^t$Bu]Ar)3]-}}
\newcommand{\WElim}{\ce{(OC)5W}\-\ce{(Mes$^*$NPP)}\-\ce{Nb(N[CH2$^t$Bu]Ar)3}}
\newcommand{\WPthree}{\ce{[\{(OC)5W\}2P3Nb(N[CH2$^t$Bu]Ar)3]-}}
\newcommand{\WP}{\ce{[(OC)5WPNb(N[CH2$^t$Bu]Ar)3]-}}
\newcommand{\cyclo}{\emph{cyclo}-\ce{P3}}
\newcommand{\ether}{\ce{Et2O}}
\newcommand{\insitu}{\emph{in situ}}
%space groups
\newcommand{\ptwooneonn}{$P2_1/n$}
\newcommand{\ptwooneonc}{$P2_1/c$}
\newcommand{\ponebar}{$P\bar{1}$}

%%%% P D F    D O C U M E N T
\usepackage[bookmarks, colorlinks,%
    citecolor=black,%
    filecolor=black,%
    linkcolor=black,%
    urlcolor=black, %
    pdfauthor={Nicholas A. Piro},%
    pdftitle={Niobium-Mediated Generation of P-P Multiply Bonded Intermediates},%
    pdfsubject={PhD Thesis in Inorganic Chemistry, MIT},%
    pdfkeywords={niobium, diphosphorus, cyclo-P3, reactive intermediates}]{hyperref}
    % Sets up hyperlinks within the pdf output to allow for clickable navigation,
    % Options include properties of the PDF file generated, color of links, etc.
\usepackage[all]{hypcap} % Sets proper behavior of pdf links to floats when %
% the captions are below the float.
```

```
\usepackage{url}  % Enables proper formatting of urls

% This is the end of all optional packages.  Things below set up the document.

\pagestyle{plain}  % Sets default pagestyle, can be changed if you want headers
    % or something else fancy on all the pages

%% This bit allows you to either specify only the files which you wish to
%% process, or 'all' to process all files which you \include.

\typein [\files]{Enter file names to process, (chap1,chap2 ...), or 'all' to
process all files:}
\def\all{all}
\ifx\files\all \typeout{Including all files.} \else \typeout{Including only \files.} %
\includeonly{\files} \fi

% Below here is included each part of the thesis document.
% They are broken into cover material, contents pages, chapters, and appendicies.
% See documentation on mitthesis class for more information
% and templates for each of these sections.

\begin{document}
\include{cover}
\pagestyle{plain} % Resets to default pagestyle after cover material
\include{contents}
%\include{changes}
\include{chap1}
\include{chap2}
\include{chap3}
\include{chap4}
\appendix
\include{appc}
\include{appd}
\include{appe}
\include{extra}
%\include{biblio} % This is commented out because references are included in each chapter.
\end{document}
```

C.2 GRAPHICS

Schemes and figures were made using Adobe Illustrator CS2.[6] Orbital pictures were made using VMD and rendered in POV-Ray.[7–9] Graphs were plotted in Gnuplot.[10] Thermal ellipsoid plots were made using Platon.[11] NMR spectra were processed in VNMR or gNMR, and exported as vector graphics.[12,13] All graphics were scaled, colorized, and exported as PDF files from Adobe Illustrator.

C.3 REFERENCES

[1] *LaTeX – A document preparation system*. http://www.latex-project.org/.

[2] TeX Users Group; *MacTex-2008*. http://www.tug.org/mactex/.

[3] Koch, R.; Olmes, D.; Wierda, G. *TeXShop*; v1.43; Eugene Algorithms, 2006. http://www.uoregon.edu/~koch/texshop.

[4] Hofman, C. M.; Maxwell, A. R.; McCracken, M. O. *BibDesk*; 1.2.11. http://bibdesk.sourceforge.net/.

[5] *More LaTeX on Athena: MIT Thesis*. http://web.mit.edu/olh/Latex/thes-latex.html.

[6] *Adobe Illustrator CS2*; v. 12.0.1; Adobe: San Jose, CA, 2005.

[7] *VMD–Visual Molecular Dynamics*; 1.8.4a22; University of Illinois at Urbana-Champaign. http://www.ks.uiuc.edu/Research/vmd/.

[8] Humphrey, W.; Dalke, A.; Schulten, K. *J. Mol. Graphics* **1996**, *14*, 33–38.

[9] *POV-Ray: Persistence of Vision Raytracer*; 3.6; Persistence of Vision Raytracer Pty. Ltd., 2005. http://www.povray.org/.

[10] Williams, T.; Kelley, C. *Gnuplot*; 3.8j, 2002. http://www.gnuplot.info.

[11] Spek, A. L. *PLATON, A Multipurpose Crystallographic Tool*; Utrecht University: Utrecht, Netherlands, 2008.

[12] *VNMR*; 6.1C; Varian, Inc., 1999.

[13] Budzelaar, P. H. *gNMR*; 5.1, 2005. http://home.cc.umanitoba.ca/~budzelaa/gNMR/gNMR.html.

Nicholas A. Piro

Phone: (857) 891-6867
E-mail: piro@mit.edu
napiro@gmail.com

Massachusetts Institute of Technology
Department of Chemistry
77 Massachusetts Avenue, Room 6-332
Cambridge, MA 02139

EDUCATION

Ph.D. in Inorganic Chemistry, Massachusetts Institute of Technology, Cambridge, MA, 2009.

B.S. with Honors in Chemistry, California Institute of Technology, Pasadena, CA, 2004.

RESEARCH EXPERIENCE

2005–2009 Niobium-Mediated Generation of P–P Multiply Bonded Intermediates
Advisor: Prof. Christopher C. Cummins, Massachusetts Institute of Technology

2002–2004 Metal *pseudo*-Carbene Complexes: Ligand Syntheses and Metallations
Advisor: Prof. John E. Bercaw, California Institute of Technology

2001 Conformational Analysis of Small Molecules via NMR Spectroscopy
Advisor: Prof. John D. Roberts, California Institute of Technology

AWARDS

- Miller Research Fellowship, University of California, Berkeley, 2009–
- NSF Graduate Research Fellowship, 2004–2008
- MIT Presidential Fellowship, 2004
- Richard P. Schuster Memorial Prize, Caltech Division of Chemistry and Chemical Engineering, 2003 and 2004
- Caltech Merck Index Award, 2004
- Caltech Upper Class Merit Award, 2003
- Summer Undergraduate Research Fellowships, Caltech, 2001, 2002, and 2003
- AIDS/Baltimore Research Scholar, Achievement Rewards for College Scientists Foundation, 2001

PUBLICATIONS

N. A. Piro, C. C. Cummins. An Unusual P=P Double Bond Formed via Phospha-Wittig Transformation of a Terminal PO Complex. **2009**, *Submitted*.

N. A. Piro, C. C. Cummins. Tetraphosphabenzenes Obtained via a Triphosphacyclobutadiene Intermediate. *Angew. Chem., Int. Ed.* **2008**, *48*, 934–938.

N. A. Piro, C. C. Cummins. P_2 Addition to Terminal Phosphide M≡P Triple Bonds: A Rational Synthesis of *cyclo*-P_3 Complexes. *J. Am. Chem. Soc.* **2008**, *130*, 9524–9535.

N. A. Piro, C. C. Cummins. Ethylenebis(triphenylphosphine)platinum as a Probe for Niobium-Mediated Diphosphorus Chemistry. *Inorg. Chem.* **2007**, *46*, 7387–7393.

P. Agarwal, **N. A. Piro**, K. Meyer, P. Muller, C. C. Cummins. An Isolable and Monomeric Phosphorus Radical that is Resonance-Stabilized by the Vanadium(IV/V) Redox Couple. *Angew. Chem., Int. Ed.* **2007**, *46*, 3111–3114.

A. R. Fox, C. R. Clough, **N. A. Piro**, C. C. Cummins. A Terminal Nitride-to-Phosphide Conversion Sequence Followed by Tungsten Phosphide Functionalization Using a Diphenylphosphenium Synthon. *Angew. Chem., Int. Ed.* **2007**, *46*, 973–976.

N. A. Piro, J. S. Figueroa, J. T. McKellar, C. C. Cummins. Triple-Bond Reactivity of Diphosphorus Molecules. *Science* **2006**, *313*, 1276–1279.

J. S. Figueroa, **N. A. Piro**, C. R. Clough, C. C. Cummins. A Nitridoniobium(V) Reagent That Effects Acid Chloride to Organic Nitrile Conversion: Synthesis via Heterodinuclear (Nb/Mo) Dinitrogen Cleavage, Mechanistic Insights, and Recycling. *J. Am. Chem. Soc.* **2006**, *128*, 940–950.

N. A. Piro, J. S. Owen, J. E. Bercaw. Pyridinium-derived *N*-Heterocyclic Carbene Ligands: Syntheses, Structures and Reactivity of *N*-(2'-pyridyl)pyridin-2-ylidene Complexes of Nickel(II), Palladium(II) and Platinum(II). *Polyhedron* **2004**, *23*, 2797–2804.

N. A. Piro, R. S. Stein, J. D. Roberts. Conformations of *N,N*-diethyl-β-alanine and β-alanine as a Function of Solvent. *J. Phys. Org. Chem.* **2004**, *17*, 418–422.

PRESENTATIONS

- Gordon Research Conference in Organometallic Chemistry, Newport, RI, July 2008 (Poster)
- MIT Inorganic Seminar Series, Cambridge, MA, May 2008
- American Chemical Society 235th National Meeting, New Orleans, LA, April 2008
- Bruker/MIT Symposium, Cambridge, MA, February 2008 (Poster)
- American Chemical Society 234th National Meeting, Boston, MA, August 2007
- Gordon-Keane Graduate Research Seminar in Organometallic Chemistry, Newport, RI, July 2007 (Poster)
- American Chemical Society 233rd National Meeting, Chicago, IL, March 2007
- Bruker/MIT Symposium, Cambridge, MA, February 2007 (Poster)
- American Chemical Society 232nd National Meeting, San Francisco, CA, September 2006

TEACHING EXPERIENCE

2005–2008	Mentoring of two undergraduate researchers in the Cummins Group
2005	5.301—Chemistry Laboratory Techniques Teaching Assistant with Dr. Kimberly Berkowski
2004, 2005	5.112—Principles of Chemical Science Teaching Assistant with Profs. Christopher C. Cummins and Sylvia T. Ceyer